

High-precision, personalized, and non-invasive brain decoding of upper limb movements

Sotirios Papadopoulos

▶ **To cite this version:**

Sotirios Papadopoulos. High-precision, personalized, and non-invasive brain decoding of upper limb movements. Neurons and Cognition [q-bio.NC]. Université Lyon 1 - Claude Bernard, 2025. English. ⟨NNT : ⟩. ⟨tel-05157747⟩

HAL Id: tel-05157747

https://theses.hal.science/tel-05157747v1

Submitted on 11 Jul 2025

HAL is a multi-disciplinary open access archive for the deposit and dissemination of scientific research documents, whether they are published or not. The documents may come from teaching and research institutions in France or abroad, or from public or private research centers.

L'archive ouverte pluridisciplinaire **HAL**, est destinée au dépôt et à la diffusion de documents scientifiques de niveau recherche, publiés ou non, émanant des établissements d'enseignement et de recherche français ou étrangers, des laboratoires publics ou privés.



Distributed under a Creative Commons CC BY-SA 4.0 - Attribution - ShareAlike - International License

Université Claude Bernard Lyon 1

THESE de DOCTORAT DE L'UNIVERSITE CLAUDE BERNARD LYON 1

Ecole Doctorale 476
L'École Doctorale Neurosciences et Cognition

Discipline : Neuroscience

Soutenue publiquement le 17/06/2025, par:

Sotirios Papadopoulos

High-precision, personalized, and non-invasive brain decoding of upper limb movements

Devant le jury composé de :

Yves Rossetti	Professor, Université Lyon 1	President du jury
Bernadette van Wijk	Associate Professor, Vrije Universiteit Amsterdam	Rapporteure
Elaine Åstrand	Associate Professor, Mälardalen University	Rapporteure
Reinhold Scherer	Professor, University of Essex	Rapporteur
Nathalie George	Research Director, ICM, INSERM Paris	Examinatrice
Suliann Ben Hamed	Research Director, ISC Marc Jeannerod	Examinatrice
James J. Bonaiuto	Research Director, ISC Marc Jeannerod	Co-directeur de thèse
Jérémie Mattout	Research Director, CRNL, INSERM Lyon	Co-directeur de thèse

“It is futile to reject general concepts. But this does not exhaust the dignity of universals. That which is common to many individuals or returns constantly in the individual does not have to be more stable, eternal, or deeper than the particular. The scale of types is not identical to the scale of significance.”

Theodor W. Adorno & Max Horkheimer, *Dialectic of Enlightenment*, 1944

I Abstract

Time-locked amplitude modulations of brain signals recorded from the sensorimotor cortex have long been shown to index various processes related to movement planning, execution and imagination (motor imagery). Relative to a baseline period, signal power in the mu (8 – 13 Hz) and beta (13 – 30 Hz) frequency bands decreases prior to the onset of a real, attempted or imagined movement and conversely increases following its completion. These reproducible findings can be used in order to decode motor-related brain activity and are leveraged by several applications.

Brain computer interface (BCI) technology refers to applications that allow a user to communicate with a computer through thought, by monitoring and inferring their mental state to issue an appropriate output. Motor imagery BCI (MI-BCI) constitutes a particular non-invasive BCI category that attempts to monitor and utilize signal changes due to the imagination of movements in order to produce commands, usually targeting the aforementioned signal modulations. MI-BCIs form the basis of non-invasive applications that attempt to decode motor intention in patients suffering from various deficits with the goal of restoring some level of communication with and/or control of their environment. However, they have so far been unable to live up to the high expectations and are consequently still far from widespread adoption out of research institutions.

Multiple factors have been suggested to affect BCI reliability. In this work, we hypothesize that one of these factors is related to the signal features used. Based on recent literature that highlights the importance of characterizing transient activity dynamics in Chapter 2 - Motivation we suggest that MI-BCI should exploit features other than signal power. Moving beyond many assumptions regarding brain activity and therefore the algorithms used to analyze it, we propose that an analysis of single-trial signal properties that do not conform to the idea of sustained, sinusoidal-like oscillations can provide novel insights in motor-related brain processes and concurrently improve BCI performance. Notably, we argue in favor of analyzing beta band burst activity and mu band non-sinusoidal oscillatory characteristics.

Focusing on the burst-like nature of the beta band activity in Chapter 3 – Beta bursts feasibility for BCI we show that like executed movements motor imagery too is characterized by beta bursts. We explore multiple ways to describe this burst activity showing that the burst rate of bursts with certain waveforms comprises the best representation among all in terms of classification accuracy and, importantly, that it is is more informative than signal power in a MI binary classification task.

Then, we propose a computationally efficient algorithm to compute waveform-resolved burst rates, suitable for real-time BCI applications. Assuming the existence of calibration data we find waveforms of beta bursts whose rate is expected to be modulated the most by a MI task. We use these waveforms to filter raw brain activity in time domain. The resulting signals can then be exploited by standard signal-processing and classification paradigms used in the field. Compared to signal power we show that these novel features increase classification accuracy and information transfer rate, thus further reinforcing their potential role for MI-BCI.

Finally, we address the question of waveform stability across recording sessions. We adopt a similar approach but focus on the impact of transferring waveforms learned in specific recording sessions to the decoding results of other sessions. We show that in contrast to power features classification accuracy is minimally impacted when using beta bursts in transfer learning.

Taken together, these results prove the advantages of analyzing transient activity features and establish the feasibility of beta bursts for offline as well as online MI-BCI applications.

II Résumé

Les modulations d'amplitude verrouillées dans le temps des signaux cérébraux enregistrés dans le cortex sensorimoteur indexent divers processus liés à la planification, à l'exécution et à l'imagination des mouvements. Par rapport à une période de référence la puissance du signal dans les bandes de fréquences mu (8 – 13 Hz) et bêta (13 – 30 Hz) diminue avant le début d'un mouvement réel, tenté ou imaginé et augmente après son achèvement. Ces résultats reproductibles peuvent être utilisés pour décoder l'activité cérébrale liée à la motricité et sont exploités par applications.

Les interfaces cerveau-ordinateur (BCI) se réfère aux applications qui permettent à un utilisateur de communiquer par la pensée avec un ordinateur en surveillant et en déduisant son état mental pour émettre une sortie appropriée. Les BCI par imagerie motrice (MI-BCI) constitue une catégorie de BCI qui utilise les changements de signaux dus à l'imagination de mouvements afin de produire des commandes, en ciblant généralement les modulations de signaux susmentionnées. Les MI-BCI sont la base des applications qui tentent de décoder l'intention motrice chez les patients souffrant de déficits divers afin de rétablir un certain niveau de communication avec leur environnement. Toutefois, ils sont encore loin d'une adoption généralisée en dehors des institutions de recherche.

De multiples facteurs affectent la fiabilité des BCI. Dans ce travail, nous supposons que l'un d'entre eux est lié aux caractéristiques du signal. Basés sur la littérature qui souligne l'importance de la caractérisation de l'activité transitoire dans le Chapitre 2 – Motivation nous suggérons que les MI-BCI devraient exploiter d'autres caractéristiques que la puissance du signal. Nous proposons qu'une analyse des propriétés du signal d'un seul essai qui ne se conforment pas à les oscillations soutenues, sinusoïdales peut fournir de nouvelles informations sur les processus cérébraux liés à la motricité et améliorer les performances des BCI. Notamment, nous plaidons en faveur de l'analyse de l'activité des beta bursts et des caractéristiques oscillatoires, non sinusoïdales de la bande mu.

En se concentrant sur la l'activité de la bande bêta qui s'apparente à bursts dans le Chapitre 3 – Faisabilité des beta bursts pour les BCI nous montrons que l'imagerie motrice est caractérisée par des beta bursts. Nous explorons de multiples façons de décrire cette activité en bursts, en montrant que le taux de bursts avec certaines formes d'onde (waveforms) constitue la meilleure représentation parmi toutes en termes de précision de classification et, surtout, qu'il est plus informatif que la puissance du signal dans une tâche de classification binaire de la MI.

Nous proposons ensuite un algorithme efficace pour calculer le taux de bursts résolu par le waveform. Nous trouvons les waveforms des beta bursts dont le taux devrait être le plus modulé par une tâche de MI dans des données d'étalonnage. Nous utilisons ces waveforms pour filtrer l'activité cérébrale brute. Les signaux résultants peuvent puis être exploités par les paradigmes de traitement du signal et de classification standard. Par rapport à la puissance du signal ces caractéristiques augmentent la précision de la classification et le taux de transfert de l'information renforçant ainsi leur rôle potentiel pour les MI-BCI.

Enfin nous abordons la question de la stabilité des waveforms entre les sessions d'enregistrement en nous concentrant sur l'impact du transfert des waveforms apprises lors de sessions d'enregistrement spécifiques sur les résultats de décodage d'autres sessions. Nous montrons que

contrairement aux caractéristiques de puissance la précision de la classification est très peu affectée par l'utilisation des beta bursts dans l'apprentissage par transfert.

En résumé, ces résultats prouvent les avantages de l'analyse des caractéristiques de l'activité transitoire et établissent la faisabilité des beta bursts pour les applications MI-BCI.

III Περίληψη

Χρονικά καθορισμένες (time-locked) μεταβολές του πλάτους κύματος εγκεφαλικών σημάτων του κινητικού και αισθητηριακού φλοιού έχει αποδειχθεί προ πολλού πως υποδεικνύουν διάφορες διαδικασίες που σχετίζονται με τον σχεδιασμό, την εκτέλεση και τη φαντασίωση εκτέλεσης (motor imagery) κινήσεων. Πιο συγκεκριμένα, σε σχέση με μια περίοδο αναφοράς η ενέργεια των σημάτων στο φάσμα συχνότητας μ (8 – 13 Hz) και β (13 – 30 Hz) ελαττώνεται πριν την έναρξη μίας κίνησης, μίας απόπειρας κίνησης ή μιας φαντασίωσης κίνησης, ενώ, αντιθέτως, αυξάνεται μετά το πέρας της κίνησης. Αυτές οι παρατηρήσεις μπορούν να αναπαραχθούν και δύναται να χρησιμοποιηθούν προκειμένου να αποκωδικοποιηθεί εγκεφαλική δραστηριότητα σχετιζόμενη με κινήσεις, γεγονός που τις καθιστά αξιοποιήσιμες από πολλαπλές εφαρμογές.

Η τεχνολογία διεπαφής εγκεφάλου – υπολογιστή (brain computer interface, BCI) αναφέρεται σε εφαρμογές που επιτρέπουν σε έναν χρήστη να επικοινωνήσει με έναν υπολογιστή η μηχάνημα αποκλειστικά διαμέσου της σκέψης. Οι BCI βασίζονται στην επεξεργασία εγκεφαλικής δραστηριότητας ούτως ώστε να παρακολουθήσουν και να συμπεράνουν τη νοητική κατάσταση ενός χρήστη και κατά συνέπεια να εκδώσουν ένα κατάλληλο σήμα εξόδου. Οι διεπαφές που στηρίζονται στην φαντασίωση κίνησης (MI-BCI) αποτελούν μία ειδική κατηγορία μη επεμβατικών BCI που επιχειρούν να παρακολουθήσουν και να χρησιμοποιήσουν τροποποιήσεις των σημάτων οφειλόμενες στη φαντασίωση διαφόρου τύπου κινήσεων ώστε να παράξουν εντολές, συνήθως αξιοποιώντας τις προαναφερθείσες μεταβολές. Εφαρμογές που στηρίζονται σε αυτές τις διεπαφές έχουν μελετηθεί εκτενώς σε υγιείς πληθυσμούς και αποτελούν την βάση των εφαρμογών που επιχειρούν να αποκωδικοποιήσουν την πρόθεση κίνησης ασθενών που πάσχουν από διάφορα ελλείμματα και έχουν ως στόχο την αποκατάσταση ενός βαθμού επικοινωνίας με ή/και ελέγχου του περιβάλλοντός τους. Ωστόσο, οι μη επεμβατικές διεπαφές εν γένει και πιο συγκεκριμένα οι MI-BCI δεν έχουν κατορθώσει έως σήμερα να επιβεβαιώσουν τις υψηλές προσδοκίες που τις συνοδεύουν και κατά συνέπεια απέχουν σημαντικά από το να υιοθετηθούν ευρέως πέραν ερευνητικών ινστιτούτων και πρωτοκόλλων.

Έχει προταθεί ότι η αξιοπιστία των BCI επηρεάζεται από πολλαπλούς παράγοντες. Στην παρούσα μελέτη υποθέτουμε πως ένας από αυτούς τους παράγοντες σχετίζεται με τα αξιοποιήσιμα χαρακτηριστικά των σημάτων. Βασιζόμενοι σε πρόσφατη βιβλιογραφία η οποία έχει υπογραμμίσει την σημασία της περιγραφής της παροδικής δυναμικής της εγκεφαλικής δραστηριότητας στο Κεφάλαιο 2 – Κίνητρο υποστηρίζουμε ό,τι οι MI-BCI θα πρέπει να αξιοποιήσουν εναλλακτικά χαρακτηριστικά των σημάτων πέραν της ενέργειάς τους. Προσπερνώντας πολλές υποθέσεις όσον αφορά την εγκεφαλική δραστηριότητα και συνεπώς τους αλγόριθμους που χρησιμοποιούνται για την ανάλυση αυτής της δραστηριότητας, προτείνουμε πως στο επίπεδο μονήρων δοκιμών η ανάλυση των χαρακτηριστικών των σημάτων μπορεί να προσφέρει νέες πληροφορίες σχετικά με εγκεφαλικές διαδικασίες που σχετίζονται με την παραγωγή κίνησης και ταυτόχρονα να βελτιώσει την αποδοτικότητα των διεπαφών, καθώς αυτά τα χαρακτηριστικά δεν συμμορφώνονται στην ιδέα μεγάλης διάρκειας ταλαντώσεων που ομοιάζουν με ημιτονοειδή. Ιδιαίτερα, επιχειρηματολογούμε υπέρ της ανάλυσης ξεσπασμάτων υψηλού πλάτους β δραστηριότητας (beta bursts) καθώς και χαρακτηριστικών των μη-ημιτονοειδών ταλαντώσεων στη συχνοτικό φάσμα μ.

Επικεντρωνόμενοι στη φύση της δραστηριότητας στο συχνοτικό φάσμα β, η οποία χαρακτηρίζεται από beta bursts, στο Κεφάλαιο 3 – Δυνατότητα εφαρμογής των beta bursts σε διεπαφές εγκεφάλου – υπολογιστή δείχνουμε ό,τι όπως και οι πραγματοποιηθείσες κινήσεις οι φαντασιακές

κινήσεις χαρακτηρίζονται από beta bursts. Εξερευνούμε πολλαπλούς, εναλλακτικούς τρόπους περιγραφής της δραστηριότητας αυτού του τύπου δείχνοντας ό,τι ο ρυθμός με τον οποίο συμβαίνουν bursts με συγκεκριμένα χαρακτηριστικά κυματομορφής (waveform) αποτελεί την καλύτερη εναλλακτική μεταξύ όλων ως προς την ακρίβεια αποκωδικοποίησης. Εξίσου σημαντικά, καταδεικνύουμε επίσης ό,τι η μελέτη του ρυθμού αυτού για επιλεγμένες κυματομορφές μας παρέχει περισσότερες πληροφορίες συγκριτικά με την ενέργεια σήματος σε δυαδικού τύπου ασκήσεις (task) ταξινόμησης (classification) της φαντασίωσης κίνησης.

Ακολούθως, προτείνουμε έναν υπολογιστικά αποτελεσματικό αλγόριθμο για τον υπολογισμό του ρυθμού εμφάνισης beta bursts με ορισμένες κυματομορφές ο οποίος είναι κατάλληλος για εφαρμογές πραγματικού χρόνου. Με την προϋπόθεση ύπαρξης ορισμένων δεδομένων προσαρμογής (calibration data) προσδιορίζουμε κυματομορφές των οποίων ο ρυθμός εμφάνισης αναμένεται να μεταβληθεί στο μέγιστο βαθμό εξαιτίας της άσκησης φαντασίωσης κίνησης. Χρησιμοποιούμε αυτές τις κυματομορφές προκειμένου να φιλτράρουμε την ακατέργαστη (raw) εγκεφαλική δραστηριότητα στο πεδίο του χρόνου με συνέπεια τα τροποποιημένα σήματα να είναι στη συνέχεια εκμεταλλεύσιμα από συμβατικές στο πεδίο μεθόδους ανάλυσης σήματος και ταξινόμησης. Δείχνουμε ότι συγκριτικά με την ενέργεια σήματος αυτά τα καινοτόμα χαρακτηριστικά αυξάνουν την ακρίβεια ταξινόμησης (classification accuracy) και τον ρυθμό μετάδοσης πληροφοριών (information transfer rate), ενισχύοντας συνεπώς ακόμη περισσότερο τον ενδεχόμενο ρόλο τους για τις διεπαφές που βασίζονται στην φαντασίωση κίνησης.

Τέλος, απαντούμε στο ερώτημα κατά πόσο αυτές οι κυματομορφές παραμένουν ή μη αμετάβλητες ανάμεσα σε διαφορετικές συνεδρίες καταγραφών. Υιοθετούμε μία παρόμοια προσέγγιση, αλλά εστιάζουμε στον αντίκτυπο που έχει η μεταφορά κυματομορφών που μαθαίνονται σε συγκεκριμένες συνεδρίες στα αποτελέσματα αποκωδικοποίησης σε άλλες συνεδρίες. Δείχνουμε ό,τι, σε αντίθεση με χαρακτηριστικά που στηρίζονται στην ενέργεια σήματος, η ακρίβεια ταξινόμησης επηρεάζεται ελάχιστα όταν τα beta bursts χρησιμοποιούνται σε πρωτόκολλα μεταφοράς μάθησης (transfer learning).

Συμπερασματικά, τα αποτελέσματα αυτής της διατριβής αποδεικνύουν τα πλεονεκτήματα που ενέχει η ανάλυση παροδικών χαρακτηριστικών της εγκεφαλικής δραστηριότητας και καταδεικνύουν την δυνατότητα αξιοποίησης των beta bursts σε εφαρμογές BCI σε πραγματικό ή μη χρόνο.

IV Acknowledgments / Remerciements / Ευχαριστίες

I wish to take a moment and attempt to express my gratitude to everyone that in their way have helped me traverse the long and winding road of the PhD.

I would like to thank Camille Jeunet and Charlie Wilson both of whom have regularly followed up on this work as it was evolving and provided insightful feedback that is hopefully reflected in parts of this thesis. I would also like to thank all the members of my jury for accepting to carefully read this work and for their critical suggestions to improve the manuscript: Bernadette van Wijk, Elaine Astrand, Nathalie George, Reinhold Scherer, Suliann Ben Hamed and Yves Rossetti. Any remaining weak points in this thesis rest solely on my shoulders.

I want to thank Jimmy for giving me the opportunity to work with him, for being so open to listen, discuss, provide help, and for transmitting his passion for work and scientific rigor. Merci également à Jérémie pour la opportunité de travailler avec lui, les discussions, l'encouragement, le soutien apporté à tous les aspects du travail, de me pousser à partager ce travail. I really appreciate the time working with both of you and hope that our paths will cross again in the future.

It goes without saying that this work would have been impossible for me to realize outside the welcoming and stimulating environment of the DANC lab and COPHY team, but also the rest of the teams at the INSERM building. Thanks to all members, present and past, for the discussions (scientific or not), coffee breaks, table tennis matches, lab dinners or drinks. Merci à Christina pour son aide indispensable pendant les trois premières années du doctorat. A special thanks to those of you with whom we have shared the same office and therefore had to put up with me the most: Hamed, Stefano, Tommy's aura, Thomas, Uliana, Ludovic, Danila, Antonella, Divyanshi, Marine.

Ευχαριστώ πολύ όλους τους φίλους μου που με ανέχονται τόσα χρόνια και είναι πάντα εκεί όποτε μετράει. Φίλοι από διαφορετικές φάσεις της ζωής μου που συνέβαλαν και συνεχίζουν να συμβάλλουν στο να είμαι αυτός που είμαι – καλώς ή κακώς! Ελπίζω πως και θα προσπαθήσω να έχω περισσότερες ευκαιρίες να σας βλέπω από 'δω και πέρα.

Το μεγαλύτερο ευχαριστώ, φυσικά, πάει στην οικογένειά μου. Ιδιαίτερα στους γονείς μου, Μαρία και Ηλία, και τον αδερφό μου, Κώστα, χωρίς την αμέριστη αγάπη και πολύπλευρη συμπαράσταση των οποίων τίποτα από όσα έχω καταφέρει δεν θα ήταν πραγματικότητα. Ό,τι και να πω θα είναι λίγο.

Enfin, je souhaite remercier Carla d'avoir été là pour moi, d'être ma meilleure amie.

V Table of contents

I Abstract..... v
II Résumé..... vii
III Περίληψη..... ix
IV Acknowledgments / Remerciements / Ευχαριστίες..... xi
V Table of contents..... xiii
VI List of figures..... xvii
VII List of tables..... xix
Chapter 1 - Introduction..... 1
1.1 Neurophysiology of upper limb movements: from anatomy to signals..... 3
1.1.1. Elements of macro- and micro-scopic anatomy of the central nervous system..... 3
1.1.2. Sensorimotor transformations pertaining to upper limb movements..... 6
1.1.2.1. The role of cortical areas..... 6
1.1.2.2. The role of subcortical areas..... 10
1.1.3. Basic principles of inter-neuronal and inter-areal brain communication..... 11
1.1.3.1. The action potential..... 11
1.1.3.2. From action potentials to local field potentials and oscillations..... 12
1.1.3.3. Sensorimotor activity during movements is characterized by frequency-specific amplitude modulation of oscillations..... 13
1.1.4. Extracranial recordings of brain activity: electroencephalography and magnetoencephalography principles..... 14
1.2 Brain-computer interfaces..... 17
1.2.1. Definition & overview..... 17
1.2.2. Motor imagery BCI..... 18
1.2.2.1. Motor imagery..... 18
1.2.2.2. State-of-the art in signal processing and classification for MI-BCI..... 19
1.3 A change in perspective: from beta oscillations to bursts..... 23
Chapter 2 - Motivation..... 27
2.1 Contribution 1 – An impeding paradigm shift in motor imagery based brain computer interfaces..... 29
2.1.1. Abstract..... 29
2.1.2. Introduction..... 30
2.1.3. Current approaches to non-invasive, motor imagery based brain-computer interfaces..... 31
2.1.3.1. Electroencephalography and magnetoencephalography overview..... 32
2.1.3.2. Motor imagery in electroencephalography and magnetoencephalography..... 32
2.1.3.3. Common techniques in motor imagery based brain-computer interfaces..... 33
2.1.4. Proposed alternative..... 34
2.1.4.1. The quest for refined neurophysiological markers..... 34
2.1.4.2. Subject-specific, forward models of dynamic activity..... 36

2.1.4.3. A paradigm shift toward motor rehabilitation....37
2.1.5. Conclusion....37
2.1.6. Data availability statement....38
2.1.7. Author contributions....38
2.1.8. Funding....38
2.1.9. Acknowledgments....38
Chapter 3 - Beta bursts feasibility for BCI....41
3.1 Contribution 2 – Beta bursts question the ruling power for brain computer interfaces....43
3.1.1. Abstract....43
3.1.2. Objective....44
3.1.3. Approach....47
3.1.3.1. Datasets....47
3.1.3.2. Data pre-processing....47
3.1.3.3. Identification of channel-specific beta band and burst detection....48
3.1.3.4. Feature extraction based on patterns of burst rate modulation....49
3.1.4. Classification....50
3.1.5. Main results....54
3.1.5.1. Beta bursts with distinct waveforms are characterized by different modulation patterns…54
3.1.5.2. Beta band burst features outperform beta band power in binary classification tasks....57
3.1.6. Significance....58
3.1.7. Data availability statements....60
3.1.8. Acknowledgments....61
3.1.9. Author contributions....61
3.1.10. Conflict of interest....61
3.2 Contribution 3 – Surfing beta burst waveforms to improve motor imagery-based BCI....63
3.2.1. Abstract....63
3.2.2. Introduction....64
3.2.3. Methods....65
3.2.3.1. Datasets....65
3.2.3.2. Pre-processing....66
3.2.3.3. Burst detection and kernel selection....66
3.2.3.4. Feature extraction....68
3.2.3.5. Classification....70
3.2.3.6. Information transfer rate....70
3.2.3.7. Statistical analysis....70
3.2.4. Results....71
3.2.4.1. Classification....71
3.2.4.2. Information transfer rate....73
3.2.4.3. Statistical analysis....75
3.2.5. Discussion....77

3.2.6. Data and code availability....80
3.2.7. Author contributions....80
3.2.8. Funding....80
3.2.9. Declaration of competing interests....80
3.3 Contribution 4 – Improved motor imagery decoding with spatiotemporal filtering based on beta burst kernels....81
3.3.1. Abstract....81
3.3.2. Introduction....82
3.3.3. Materials and Methods....83
3.3.3.1. Datasets....83
3.3.3.2. Pre-processing....83
3.3.3.3. Burst-detection....83
3.3.3.4. Kernel selection....84
3.3.3.5. Feature selection....84
3.3.3.6. Classification....85
3.3.3.7. Statistical analysis....85
3.3.4. Results....86
3.3.5. Discussion....88
3.3.6. Conclusion....89
Chapter 4 - Discussion....91
4.1 Summary of contributions....93
4.2 Limitations....97
4.2.1. Data selection and pre-processing....97
4.2.2. Data processing....97
4.2.3. Classification results....99
4.3 Future directions....101
4.3.1. Experiment of executed and imagined wrist movements....101
4.3.2. Other prospects....102
4.3.2.1. Analysis and combination of alternative features....102
4.3.2.2. Feasibility of approach in patient populations....103
Chapter 5 - References....107
Chapter 6 - Appendix....137
6.1 List of abbreviations....139
6.2 Supplementary material....141
6.3 List of contributions....155
6.3.1. Peer-reviewed articles....155
6.3.2. Peer-reviewed conference articles....155
6.3.3. Pre-prints....156
6.3.4. Peer-reviewed conference abstracts with oral presentation....156
6.3.5. Peer-reviewed conference abstracts with poster presentation....157

VI List of figures

Figure 1.1.1 4
Figure 1.1.2 5
Figure 1.1.3 7
Figure 1.1.4 9
Figure 1.1.5 13
Figure 1.1.6 14
Figure 1.3.1 24
Figure 2.1.1 35
Figure 2.1.2 36
Figure 3.1.1 50
Figure 3.1.2 51
Figure 3.1.3 53
Figure 3.1.4 55
Figure 3.1.5 56
Figure 3.1.6 58
Figure 3.2.1 69
Figure 3.2.2 72
Figure 3.2.3 74
Figure 3.2.4 76
Figure 3.3.1 86
Figure 3.3.2 87
Sup. Figure 3.1.1 141
Sup. Figure 3.1.2 142
Sup. Figure 3.2.1 143
Sup. Figure 3.2.2 144
Sup. Figure 3.2.3 146
Sup. Figure 3.2.4 147
Sup. Figure 3.2.5 148
Sup. Figure 3.2.6 149
Sup. Figure 3.2.7 150
Sup. Figure 3.3.1 151
Sup. Figure 4.3.1 152

VII List of tables

Table 3.1.1 48
Table 3.2.1 67
Table 3.3.1 84

Chapter 1 - Introduction

1.1 Neurophysiology of upper limb movements: from anatomy to signals

1.1.1. Elements of macro- and micro-scopic anatomy of the central nervous system

The mammalian central nervous system (CNS) constitutes the most elaborate biological system known to us. Part of the human CNS, the human brain comprises a complex network of approximately 100 billion nerve cells, termed neurons, and an estimated 10- to 50-fold more glial cells, the cells that are responsible for the support, the oxygen and nutrients supply, and the protection of neurons (Kandel, 2013; Purves, 2017). Neurons form the substrate of behavior. They are responsible for integrating interoceptive and exteroceptive sensory inputs and for generating a suitable output, often translated to a suitable action which allows us to meaningfully shape our environment according to our needs.

The cerebrum constitutes the largest part of the human brain. In its outer part, the highly-folded gray matter, the cerebral cortex, forms gyri that are separated by sulci (Campbell and Barohn, 2020). Below the cortex, large bundles of ascending and descending tracts constitute the brain's white mater (Campbell and Barohn, 2020). The white mater forms the corona radiata which further converges to the internal capsule and connects the cortex to the basal ganglia and brainstem (Campbell and Barohn, 2020).

The cerebral cortex can be divided in two cerebral hemispheres that are separated by the medial longitudinal fissure (Figure 1.1.1). Each hemisphere is anatomically discretized into four lobes (Campbell and Barohn, 2020). The frontal lobe is located fronto-rostrally with its caudal border being the central (Rolandic) sulcus. This lobe can be further subdivided in the prefrontal cortex and several motor-related areas such as the premotor cortex (PM), the supplementary motor area (SMA) and the primary motor cortex (M1) (Campbell and Barohn, 2020). The parietal lobe lies posterior to the central fissure and anterior to the occipital lobe. It contains the primary (S1) and secondary (S2) somatosensory cortices and associational areas responsible for sensorimotor transformations (Kandel, 2013; Purves, 2017) and visuospatial attention (Kandel, 2013; Purves, 2017). The occipital lobe, located posteriorly and caudally, is specialized in visual information processing. Deep within the lobe the primary visual (striate) cortex is organized along the banks of the calcarine sulcus (Campbell and Barohn, 2020). The extrastriate visual cortex covers the rest of this lobe and transfers visual information to the parietal and occipital lobes via distinct pathways (Kandel, 2013). Finally, the temporal lobe forms the base of the cerebrum laterally to the diencephalon. It is separated from the frontal lobe by the lateral fissure of Sylvious. It houses higher-order visual areas as well as the auditory cortex. The angular gyrus at the posterior bank of the Sylvian fissure connects this lobe to the parietal lobe (Campbell and Barohn, 2020).

Neurons of the CNS are characterized by a set of features relating to their anatomy and function, conserved across areas and species. Depending on the direction of information flow neurons can be divided in three categories (Kandel, 2013). Sensory or afferent neurons subserve perception by carrying information from the body's peripheral sensors to the spinal cord and then to the brain-

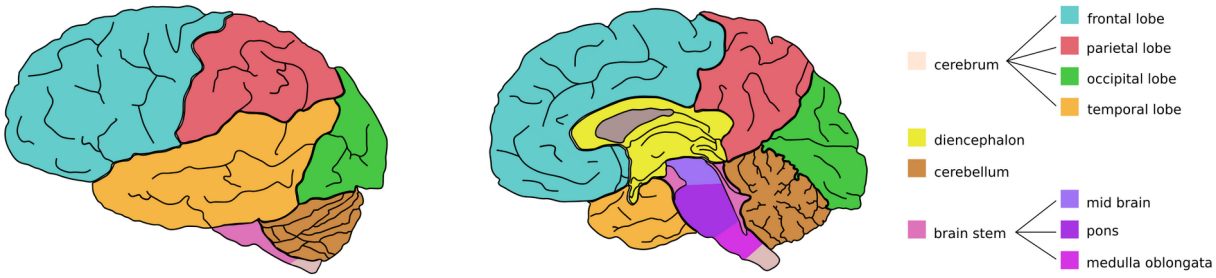


Figure 1.1.1: Schematic representation of a lateral and a medial view of the human brain. The human brain can be divided in the cerebrum, the diencephalon, the cerebellum and the brain stem. The cerebrum can be anatomically further sub-divided in the frontal, parietal, occipital and temporal lobes. The brain stem consists of the mid brain, the pons and the medulla oblongata.

stem, thalamus and the sensory cortices via the ascending spinocerebellar and spinothamalamic tracts (Campbell and Barohn, 2020; Kandel, 2013). Motor or efferent neurons carry information from the brain and/or spinal cord to muscles (and glands) (Campbell and Barohn, 2020; Kandel, 2013). Interneurons, greater in numbers than the previous categories, act as relay neurons transmitting signals over longer distances with their long axons, or as local interneurons forming connections with adjacent neurons in local circuits (Kandel, 2013).

A typical neuron has four morphologically and functionally distinct areas (Figure 1.1.2). The soma forms the body of the cell containing the nucleus and the critical structures that control the metabolic procedures of the cell (Kandel, 2013; Purves, 2017). The axon is a process stemming from the soma and targeting other neurons in order to allow inter-neuronal communication. It emerges from the axon hillock, a structure involved in the generation of the most prominent electrical activity of neurons, the action potential (AP) (Kandel, 2013; Purves, 2017) (see section 1.1.3 Basic principles of inter-neuronal and inter-areal brain communication). At its end the axon branches off (axon terminal) giving rise to numerous synaptic buttons (Mohan et al., 2015; Spruston, 2008). The axon is covered by a myelin sheath, that acts as an insulating material allowing for faster and longer-range inter-neuronal communication (Kandel, 2013; Purves, 2017). The axon constitutes the main cell structure involved in propagating information to other neurons (Kandel, 2013; Purves, 2017).

The dendritic tree constitutes a collection of fine cellular processes with extensive branches (dendrites). It is the main structure that is involved in receiving inputs from other neurons, as it is the principal target of axons of other neurons (Kandel, 2013; Purves, 2017). Axons and dendrites communicate via synapses. In pyramidal neurons a distinction can be made between basal and apical dendrites (Spruston, 2008). Although differences exist, in the majority of the pyramidal neurons a single main apical trunk sprouts from the soma which lies in cortical layers II-VI and may extend up to the cortical surface (Mohan et al., 2015). The trunk gives rise to the apical tuft, a collection of relatively short dendrites with a few branches each, while, also, some oblique dendrites may stem from the trunk. On the other hand, basal dendrites tend to have greater lengths and branch more extensively compared to the apical tuft (Mohan et al., 2015). This morphology is especially maintained in the pyramidal neurons found in layers II and III of the cortex (Mohan et al., 2015). Finally, the synapses comprise the communication zones between nerve cells transmitting a signal, called pre-synaptic neurons, and nerve cells receiving the signal, the

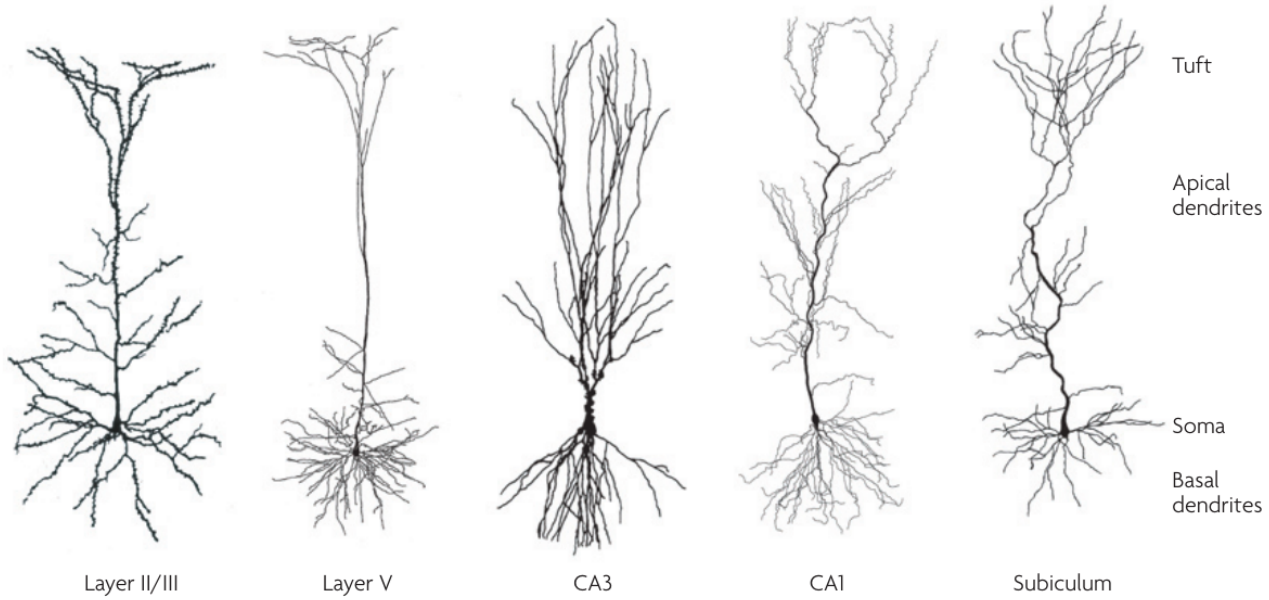


Figure 1.1.2.: Structure of pyramidal cells from different brain areas. Reproduced from Spruston, 2008.

post-synaptic neurons (Segev and Rall, 1998). The pre- and post-synaptic cells are separated by a narrow space, termed the synaptic cleft (Kandel, 2013; Purves, 2017).

The cerebral cortex is organized in cortical columns (Kandel, 2013; Purves, 2017). Each column consists of millions of neurons arranged in six layers, cortical layer (L) I being the outermost and layer VI the innermost. Cortical L IV is a relatively thin layer of stellate cells; it is the main input layer of the cortex, as it constitutes the target of afferent axons originating from first-order thalamic nuclei. Its cells form synapses to cortical L II and III pyramidal cells, whose axons project horizontally either locally within these layers or more distally via the thin L I. Moreover, L II/III neurons project to nearby pyramidal cells of layers V and VI, most of which in turn target subcortical structures like the thalamus, the basal ganglia and the brain stem.

This canonical organization of the cerebral cortex has pronounced differences between distinct areas. In fact, these differences serve the disparate functional roles of each area; as an example, the somatosensory cortex has an enlarged cortical L IV but diminished L V and VI because of the massive inputs it receives from the thalamus, whereas the motor cortex is characterized by thick L V and VI. These cytoarchitectonic distinctions allowed Brodmann to divide the cortex in fifty two discrete functional areas more than a century ago (Campbell and Barohn, 2020). His schema for the organization of the cerebral cortex has been so influential that, despite the vast revisions is has gone through over the years, it still remains pertinent and is extensively used in many neuroscience fields, especially in clinical settings.

1.1.2. Sensorimotor transformations pertaining to upper limb movements

1.1.2.1. The role of cortical areas

As already alluded to, behavior is tightly linked to movement planning and execution. Movement planning is based on spatial maps that are distributed in the parietal and frontal cortices, each of which is dynamically tuned to the requirements of different effectors. The mapping from sensory inputs, like for example the visual properties of an object, to potential or intended motor actions, termed sensorimotor transformation, is the foundation of a great number of actions in our daily lives. This process is supported by a broad network of interconnected brain areas located in the parietal, temporal and frontal lobes that constantly exchange information and update the motor plan (Kandel, 2013).

A significant portion of this network is tasked with controlling upper extremities. For simplification purposes a classic approach to study the interactions of the relevant cortical areas has been to bisect this complex network into two core components that function in parallel, the dorsomedial network for reaching and the dorsolateral network for grasping (Figure 1.1.3). These two streams connect the “hubs” of the whole network that is, distinct parietal associational areas (mainly Brodmann areas 5 and 7) projecting to different divisions of the premotor cortex (PM, Brodmann area 6) before eventually converging to the primary motor cortex (M1, Brodmann area 4) (Davare et al., 2011; Grafton, 2010).

The dorsomedial reaching network mainly consists of the areas V6A of the parieto-occipital sulcus, the premotor dorsal (PMd) area and M1 (Galletti and Fattori, 2018; Janssen and Scherberger, 2015). Studies in non-human primates have shown that in area V6A space is represented in a viewer-centered coordinate frame. Many of the neurons in this area are considered “reach-related” as their activity is modulated while preparing or performing a reaching movement towards a specific visual receptive field as well as by eye-position signals (Battaglia-Mayer et al., 2000; Fattori et al., 2005). Serving as an evidence of the complexity of the whole system and the fact that reaching and grasping are intermingled, the activity of this area’s neurons has also been shown to be modulated by the hand orientation and the grip type that is planned, with the placement of the index finger serving as the critical factor to allow for grip distinction (Fattori et al., 2010, 2009).

At the next hub of this network, the PMd, a shift in information coding is observed. Whereas V6A encodes spatial information in viewer centric coordinates, this area’s population code preferentially mirrors horizontal rotations of the shoulder joint and visual stimuli are encoded in relative arm-centric coordinates (Caminiti et al., 1991). The neuronal activity is maximally modulated in accordance with the spatial location of the arm, however visual information is still crucial as the spatial location of the arm is determined not based on proprioceptive mechanisms but rather as the visually perceived location with respect to the shoulder (Graziano, 1999). Moreover, neuronal activity in PMd has been shown to be modulated by grasp components too. Viewing a target object raises specific affordances relating to grip size and type and wrist orientation all of which affect the firing activity of PMd neurons (Raos et al., 2004).

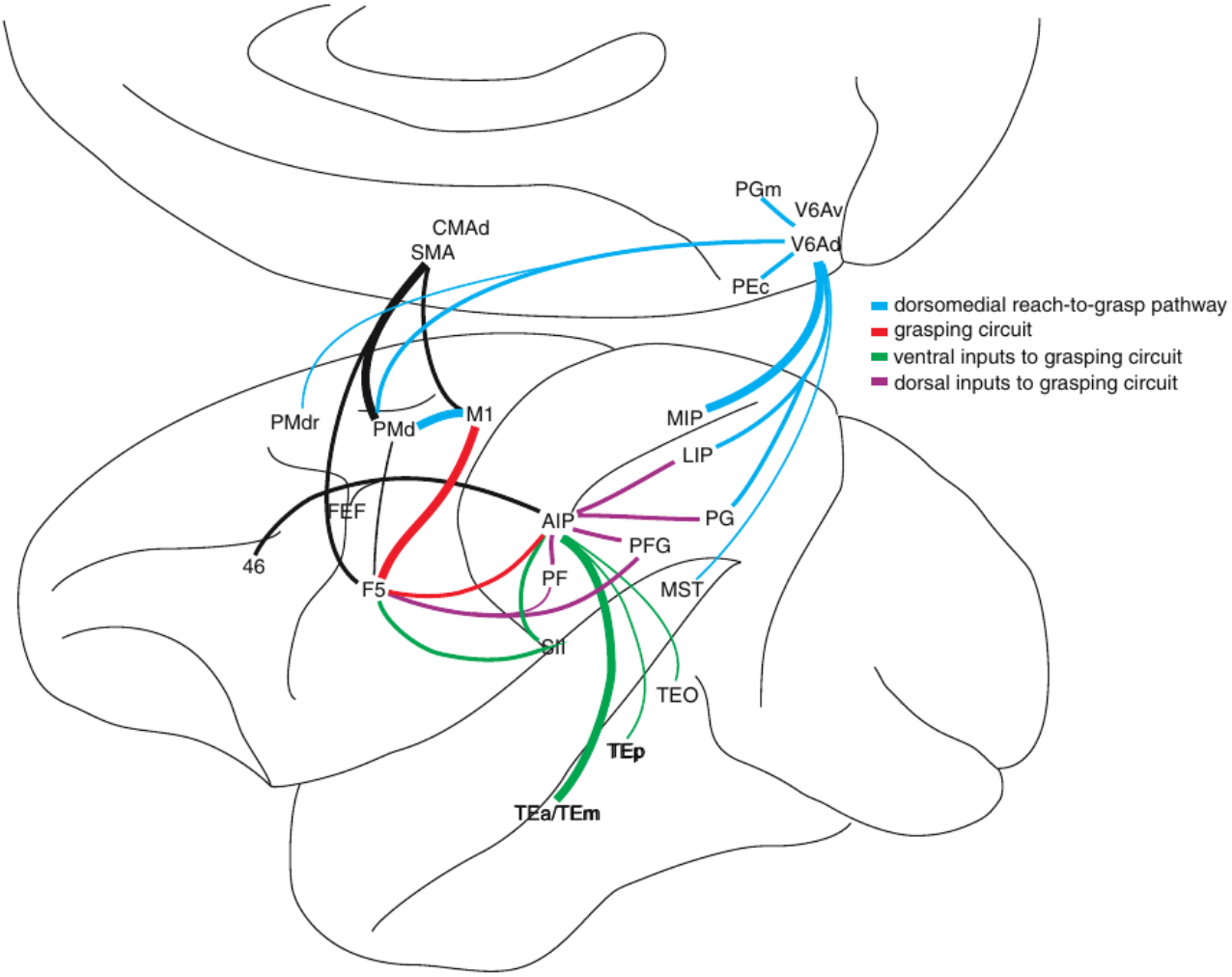


Figure 1.1.3: Depiction of the cortical areas involved in the dorsomedial and dorsolateral networks for reaching and grasping in non-human primates. Also depicted are the anatomical connections of the areas involved. Network originally proposed in Grafton et al, 2010 and reproduced from Davare et al., 2011.

The dorsolateral grasping network mainly consists of the areas AIP, located in the intraparietal sulcus, the premotor ventral (PMv) area and M1. Like area V6A, AIP consists of neurons sensitive to components of an action, but which are primarily visual neurons, and is tightly connected to the hand preshaping that takes place during the reach component (Gallese, 1994; Murata et al., 2000; Townsend et al., 2011). Some neurons' activity is modulated while fixating at an object while others' not. Some neurons respond during object manipulation irrespective of the ability to see the object, whereas other do so only in the light, and yet another subpopulation is characterized by a response somewhere in-between the previous two, preferentially responding, but not only, under light (Murata et al., 2000). Accordingly, motor-dominant neurons are characterized by grip type selectivity, meaning that the activity of different neurons is tied to the execution of different grips, while visual neurons demonstrate 3D shape selectivity (Murata et al., 2000).

Area PMv is considered to host the motor prototypes, a dictionary of hand movements that when combined appropriately allow for the generation of different grip types (Brochier et al., 2004; Davare et al., 2006; Shimazu et al., 2004; Townsend et al., 2011). PMv associates the affordances

extracted by AIP with appropriate motor actions. Neuronal activity in this area is correlated to the goal of the motor plan; this area's neuronal activity is grasp-specific and this specificity is mainly dependent upon thumb use (Raos et al., 2006). Neuronal activity has been shown to be modulated not just during but even before movement onset, and has a facilitatory role with regard to efferent signals of M1 to the spinal cord (Umilta et al., 2007).

It is important to note, again, that this distinction in parallel streams is only a simplification that has helped us study the motor system. All areas of the dorsolateral stream encode arm and hand joint kinematics with the hand representation being more prevalent while moving rostrally (Menz et al., 2015) and the reference frame changing preferentially from extrinsic to intrinsic (Blohm et al., 2024). Additionally, both the premotor dorsal and premotor ventral areas contain neurons that preferentially encode information either regarding the hand and the reach component simultaneously, or the arm and the grasp component (Takahashi et al., 2017). These mixed representations at the neuronal level form the substrate of the population coding at the network level (Michaels et al., 2020; Scherberger, 2021). At this level spiking and oscillatory activity (see section 1.1.3 Basic principles of inter-neuronal and inter-areal brain communication) controls reaching movements through computations performed on preserved, low-dimensional neuronal manifolds (Gallego-Carracedo et al., 2022; Gallego et al., 2017, 2020; Ottenhoff et al., 2023; Safaie et al., 2023). Upper limb movements requiring more fine-grained control, like individual finger movements or grasp formations, are controlled by movement-specific sub-manifolds of low frequency oscillatory activity (Natraj et al., 2022).

Within the frontal lobe distinct cortical structures are responsible for different aspects of the motor plan generation. The prefrontal cortex has the role of making a perceptual decision about the action to be taken, while in the premotor cortex this decision is converted to a movement plan. There, neuronal activity encodes the extrinsic spatial kinematics of a movement, with some evidence indicating that this encoding is independent of the arm that will perform it (Kandel, 2013). This activity is transmitted to the primary motor cortex, which is in turn responsible for controlling the execution of movements of the contralateral limb (Campbell and Barohn, 2020).

Neurons in the primary motor cortex control both movement kinematics and kinetics, or put differently what movement to perform and how to do so (Branco et al., 2019; Scott, 2003; Sergio et al., 2005). Through feedback and feed-forward connections with sensory areas the interplay between the control of ongoing and intended movements adjusts behavior. The primary motor cortex is organized roughly in somatotopic manner (Campbell and Barohn, 2020; Penfield and Rasmussen, 1950). Different body parts are represented in different locations of the cortex, although overlap exists. This motor map also has a specific structure, a concentric one (Gordon et al., 2023; Park et al., 2001). Distal parts of a given body area are represented by neuronal populations within the central zone of the cortex, whereas proximal parts are represented around this zone, with significant overlap of the two populations between the two zones (Figure 1.1.4). The somatotopic organization of M1 leads to the convergence of multiple primary motor neurons on the same spinal motor neuron (Campbell and Barohn, 2020). As each single neuron of this area generates signals pertaining to movements of specific body parts, the emerging population code is generated as the vectorial sum of single neuron contributions to a specific spinal motor neuron and therefore controls the activation of the appropriate muscle synergies for performing a specific action (Georgopoulos et al., 1982; Todorov, 2000). Moreover, motor learning takes place in two time scales in a reinforcement and a supervised manner respectively, by computing and trying to

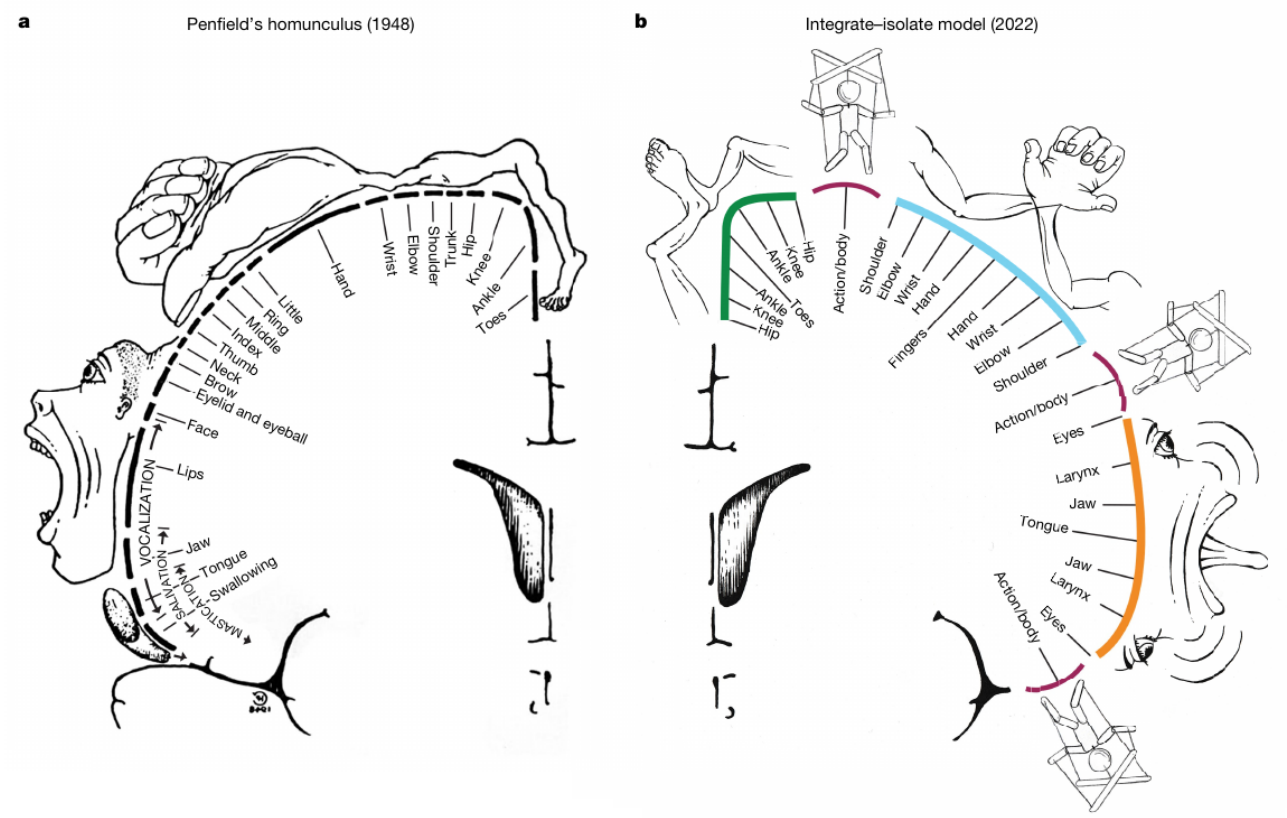


Figure 1.1.4: Somatotopic organization of the motor cortex. **(a)** Penfield's classical homunculus. **(b)** Revised homunculus model that emphasizes the concentric organization of effector-specific regions (feet, hands and mouth) and the presence of inter-effector regions between them. Reproduced from Gordon et al., 2023.

minimize the motor error signal via the adjustment of the tuning curve of individual neurons and the internal models of actions (Li et al., 2001).

Together the premotor and the motor cortex contribute approximately 2/3 to 4/5 of the total number of fibers that constitute the pyramidal system (corticospinal tract) (Campbell and Barohn, 2020). The rest of the fibers mainly arise from the primary somatosensory cortex, the supplementary motor area and, to a much lesser extent, from the occipital, parietal and temporal cortices as well as some subcortical structures (Campbell and Barohn, 2020).

The supplementary motor cortex is located in the medial surface of each hemisphere, anterior to the primary motor cortex. It plays an important role in selecting and executing complex, voluntary impending and ongoing movements (Kandel, 2013). It can be subdivided in two parts. The supplementary motor area proper (SMA) is responsible for coordinating acquired-through-training sequences of movements that involve the hands, arms, head and trunk (Kandel, 2013). The pre-SMA, on the other hand, contains neurons whose activity is correlated to impending movements, particularly depending on whether or not specific objects can be acted upon or not (Kandel, 2013).

The primary somatosensory cortex is also somatotopically organized. It contains four strips (Brodmann areas 3a, 3b, 2, 1) that process exteroceptive information from the skin and proprioceptive information regarding limb positions (Campbell and Barohn, 2020; Kandel, 2013; Purves, 2017). It receives information via the thalamocortical tract and relays it to the secondary

and the primary visual and auditory cortices, sensory areas of the parietal cortex and the motor cortex (Borich et al., 2016; Campbell and Barohn, 2020). The direct projections of S1 to M1 and the spinal cord help modulate the activity of spinal motor neurons (Kandel, 2013).

1.1.2.2. The role of subcortical areas

The basal ganglia form a complex network of interconnected nuclei that control the balance between competing movements thus promoting certain motor plans over other. Their main role is believed to be action selection and motor learning, but they have also been implicated in the control and sequencing of movements (Campbell and Barohn, 2020; Kandel, 2013; Purves, 2017). Simplistically, all their connections can be broken down to two pathways that connect the striatum to the substantia nigra and the globus pallidus (GP); the direct (inhibitory) pathway and the indirect (excitatory) pathway via relays at GPe and STN (Campbell and Barohn, 2020; Kandel, 2013; Purves, 2017). The cortex forms excitatory connections with the striatum, while the substantia nigra is connected to the thalamus by inhibitory projections, and the thalamus in turn projects back to the cortex via excitatory neurons. This closed loop results, at rest, in thalamic inhibition that suppresses movement production (Campbell and Barohn, 2020; Kandel, 2013; Purves, 2017). Following excitatory input flow from the cortex, the activation of the direct pathway results in thalamic disinhibition therefore facilitating the production of selected and/or anticipated movements (Campbell and Barohn, 2020; Kandel, 2013; Purves, 2017). Meanwhile, concurrent activation of the indirect pathway can inhibit GPe inhibitory output to the STN and suppress competing movements (Campbell and Barohn, 2020; Kandel, 2013; Purves, 2017).

The role of the cerebellum in motor control is rather complicated. However, cerebellar disorders lead to consistent symptomatology that helps us understand the contribution of this part of the CNS to motor control. Hypotonia, astasia, ataxia in the form of dysmetria and dysdiadochokinesia, and action and intention tremor reveal that this structure is responsible for the unconscious fine-tuning of movements, especially for actions consisting of multiple movements leading to distal muscles' control, and also for the control of balance and posture via axial muscles (Campbell and Barohn, 2020). It is thought that the cerebellum is the primary locus of motor learning and adjustment of an ongoing motor plan (Kandel, 2013). Regarding body and limb movements, the dorsal spinocerebellar tract collects sensory information from muscle and joint receptors, which is compared to the efference copy of spinal motor neuron activity collected via the ventral spinocerebellar tract (Kandel, 2013). The computed motor error is signaled by cells of the inferior olivary nucleus and leads to an alteration of the excitation - inhibition balance of different cerebellar neurons, mainly by inducing long-term depression between granule and Purkinje cells that are activated concurrently with the inferior olivary nucleus cells (Kandel, 2013). Via its projections to the midbrain, thalamus and the spinal cord (Campbell and Barohn, 2020) the cerebellum adjusts movement plans accordingly.

Finally, cortical and subcotrical motor-related signals converge at the brainstem or the spinal cord level and regulate the activity of cranial nerve nuclei and spinal motor neurons located at the ventral horn of the spinal cord's gray matter respectively (Campbell and Barohn, 2020). Located in the interior of the spinal cord, and arranged in a butterfly-like shape, the gray matter consists primarily of the bodies of spinal nerve cells. The spinal nerve cells are organized in thin layers

called laminae; the dorsal horn laminae (I-VI) host projection and relay interneurons that are important for sensory signals transmission, the ventral horn laminae (VII-IX) host spinal motor neurons as well as interneurons important for motor coordination, and the intermediate zone (VI, VII) interneurons that connect the dorsal and ventral horns ipsilaterally and contralaterally (Campbell and Barohn, 2020). Moreover, dorsal horn neurons connect directly to ventral horn neurons ipsilaterally, and indirectly via interneurons both ipsi- and contralaterally forming local spinal reflexes arcs (Campbell and Barohn, 2020).

Descending axons in the corticospinal tracts of the spinal cord's white matter form synapses with numerous spinal motor neurons that innervate different muscles, thus activating complex muscle activation patterns (Campbell and Barohn, 2020; Kandel, 2013). The ventral horn spinal motor neurons are arranged in a somatotopic fashion with neurons that innervate proximal muscles of the limbs lying centrally and cells targeting distal muscles laterally; e.g. in the cervical spinal cord section upper limb posture and power progressively transitions to fine motor skills of the fingers (Campbell and Barohn, 2020; Kandel, 2013). The emerging muscle synergies result in the production of coordinated, goal-directed behavior thanks to the spinal reflex arcs that adjust the contraction of synergistic and antagonistic muscles (Campbell and Barohn, 2020).

1.1.3. Basic principles of inter-neuronal and inter-areal brain communication

1.1.3.1. The action potential

The principle of dynamic polarization by Ramón y Cajal (Kandel, 2013; Purves, 2017), suggests that the stereotypical structure of neurons serves a specific functional role. Dendrites act as an input component for signals, the body and the axon hillock integrate the inputs in order to "decide" whether or not an output should be produced, axons convey the output to the axon terminal, and the synaptic buttons secrete neurotransmitter molecules in the synaptic cleft transmitting a signal to the postsynaptic cell (Kandel, 2013; Purves, 2017).

Every neuron is equipped with passive as well as active mechanisms called pumps, most importantly the Na^+ - K^+ pump, that create a difference in ion concentration on either side of the plasma membrane. Na^+ concentration is low inside the cell, whereas K^+ concentration is low outside the membrane, thus creating also a difference in electrical potential on either side of the membrane. This is called the membrane potential (Kandel, 2013; Purves, 2017). In a resting neuron i.e., a neuron not actively involved in signal transmission, the membrane potential voltage inside the cell is more negative than the voltage outside. Considering the voltage outside as an equivalent of an electrical circuit's ground, the resting potential inside the membrane is usually about -65 mV (Kandel, 2013; Purves, 2017). The membrane potential can be modulated due to its cell type specific or non-specific electrochemical properties (Lee et al., 2024) and this forms the substrate of inter-neuronal communication (Kandel, 2013; Purves, 2017).

The difference in ion concentrations creates an electrochemical gradient. Ionic flux should in theory be such that a stability between different concentrations and charges is achieved, if no mechanisms to control this process where present (Kandel, 2013; Purves, 2017). Passive leaking

mechanisms controlled by protein pores, the ion channels, are selectively permeable to different ions. In the resting state the active channels allow K^+ to pass through, creating the negative net charge inside the membrane. However, if for some reason the membrane potential becomes more positive by about 10 mV, a process termed depolarization, the open ion channels become much more permeable to Na^+ compared to K^+. In turn, this causes an influx of positively charged ions inside the cell, thus leading to a brief and great change in the potential to +40 mV (Kandel, 2013; Purves, 2017). This is the action potential, and it is the result of a positive feedback loop between open Na^+ channels and further depolarization that increases the probability of Na^+ channels being open (Kandel, 2013; Purves, 2017).

1.1.3.2. From action potentials to local field potentials and oscillations

The generation of an action potential in the axon hillock is followed by its transmission to the synaptic buttons due to the cellular membrane's active properties (Kandel, 2013; Purves, 2017). There, the membrane depolarization leads to the release of neurotransmitters in the synaptic cleft which bind on receptors of the post-synaptic dendrites (Kandel, 2013; Purves, 2017). Depending on the type of neurotransmitter released by the pre-synaptic neuron and the receptors of the post-synaptic neuron, an excitatory (EPSP) or inhibitory (IPSP) post-synaptic potential is generated in the dendritic tree of the post-synaptic neuron which, in turn, depolarizes or hyperpolarizes, respectively, the cellular membrane (Kandel, 2013; Purves, 2017). Multiple PSPs are spatially and temporally integrated in the dendritic trees and the net resulting polarization of the soma’s membrane determines whether an AP will be generated or not (Spruston and Kath, 2004).

All intracellular ionic processes are mirrored by extracellular changes in potential. This constitutes the basis of the local field potential (LFP) that is, voltage changes in the extracellular matrix that reflect co-occurring neuronal activity in a brain area (Buzsáki et al., 2012; Gallego-Carracedo et al., 2022; van Bree et al., 2025). The properties of measured extracellular potentials depend on the architecture of a brain area and the distance of an electrode to each current source (Buzsáki et al., 2012; van Bree et al., 2025) (Figure 1.1.5). The further an electrode is placed from the current source the more the electrical signal is dissipated according to the brain tissue conductance, while also more sources are being mixed (Buzsáki et al., 2012; van Bree et al., 2025). As such, LFPs constitute measures of detailed activity within a small brain area, whereas electrocorticography, electroencephalography and magnetoencephalography measure aggregate i.e., less informative, activity of much larger areas (Buzsáki et al., 2012; van Bree et al., 2025). This aggregate activity reflects synchronized neuronal activity of intra- and/or inter-areal communication which macroscopically appears as high or low frequency oscillations respectively (Buzsáki and Draguhn, 2004; Lisman and Buzsáki, 2008; van Bree et al., 2025).

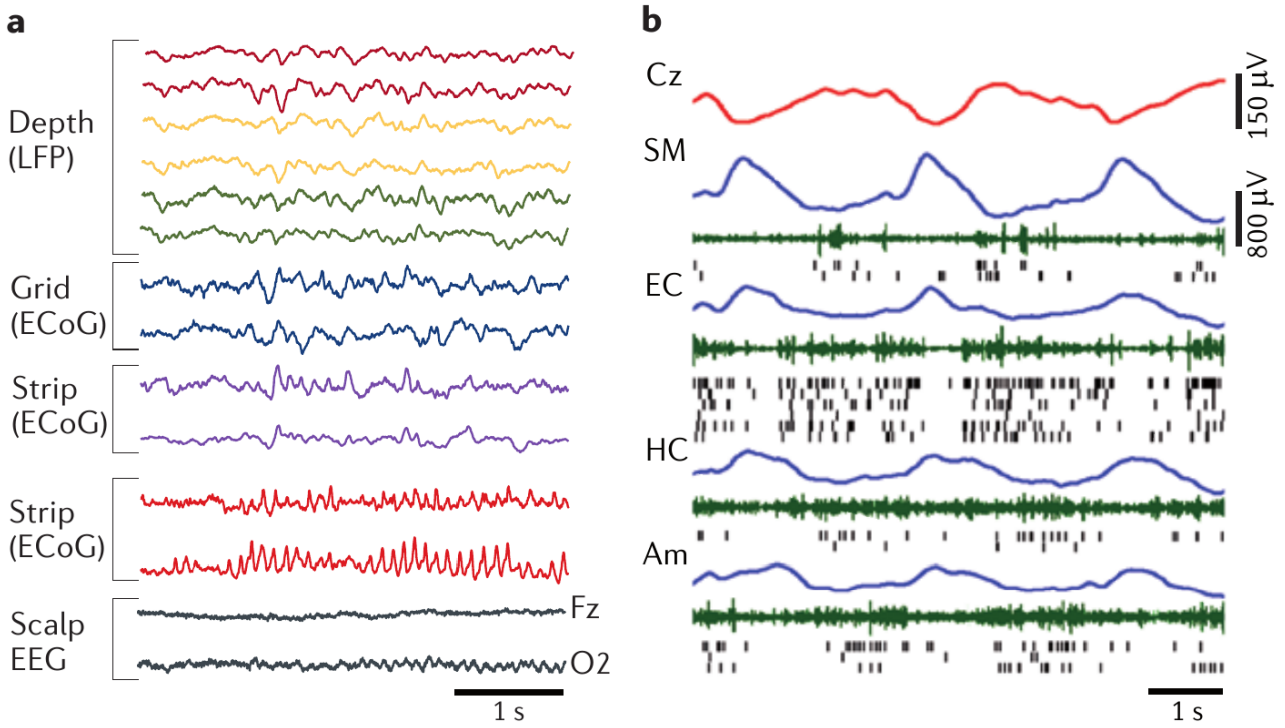


Figure 1.1.5: Extracellular activity recorded in parallel from various areas using different recording techniques. **(a)** The dynamics of signals recorded in parallel from deep structures (LFP), the cortical surface (ECoG) and the scalp (EEG) are similar. The amplitude of the signals and the high-frequency resolution diminishes the further a sensor is placed from the source of interest. **(b)** Slow oscillatory activity recorded with scalp electroencephalography (red trace) and LFPs (blue traces) across different sites is similar despite the differences in signal amplitude. Also depicted are the multi-unit activity (green traces) and single neuron spiking activity (raster plots). Reproduced from Buzsáki et al., 2012.

1.1.3.3. Sensorimotor activity during movements is characterized by frequency-specific amplitude modulation of oscillations

The temporal and spectral features of brain signals recorded during a movement correspond to time-locked, band-limited amplitude modulation of brain signals before the start of the movement and shortly following its completion (Friston et al., 2006; Pfurtscheller and Lopes da Silva, 1999; Ramadan and Vasilakos, 2017). These amplitude modulations refer to the event-related desynchronization (ERD) and the event-related synchronization (ERS) phenomena which are pronounced in the mu (~ 8 – 12 Hz) and beta (~ 13 – 30 Hz) frequency bands (Kilavik et al., 2013; Neuper et al., 2006; Pfurtscheller et al., 2006, 1997; Pfurtscheller and Lopes da Silva, 1999; Tam et al., 2019; Unterweger et al., 2020) (Figure 1.1.6), but have also been described in the theta (4 – 8 Hz) (Putzolu et al., 2024) and gamma (~ 30 – 120 Hz) (Ball et al., 2008; Cheyne and Ferrari, 2013; Darvas et al., 2010) bands.

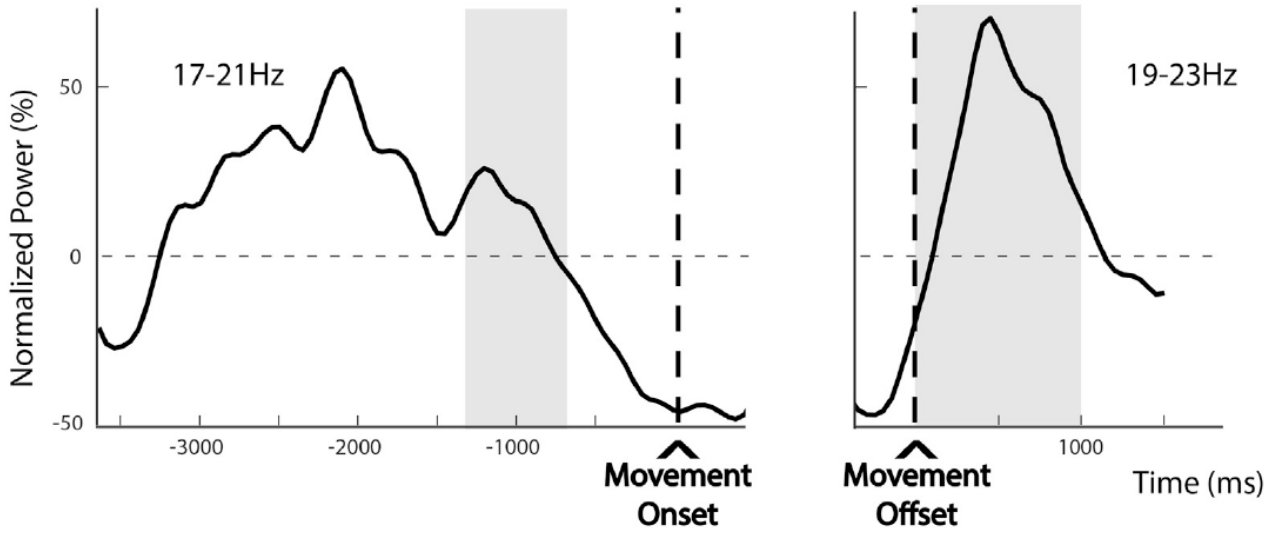


Figure 1.1.6: Beta band desynchronization and synchronization recorded with electroencephalography during a unimanual reaching task. Depicted on the left hand side is the pre-movement power decrease corresponding to the beta band (averaged in the 17-21 Hz frequency range). The ERD is observed starting approximately half a second before the movement onset and is sustained during the movement. Depicted on the right hand side is the beta ERS (averaged in the 19-23 Hz frequency range) that occurs following the movement completion. Reproduced from Alayrangues et al., 2019.

The ERD is a decrease in signal power compared to a baseline period (Neuper et al., 2006; Pfurtscheller et al., 2006; Pfurtscheller and Lopes da Silva, 1999) attributed to a reduced synchronization of neuronal firing that disinhibits the motor cortex in preparation of executing a motor plan (Kilavik et al., 2013; Pfurtscheller and Lopes da Silva, 1999; Pfurtscheller and Neuper, 1997). Conversely, the ERS is an increase in power compared to the baseline (Alayrangues et al., 2019; Neuper et al., 2006; Pfurtscheller et al., 1996; Rhodes et al., 2024) considered to reflect synchronized firing of the neurons that reestablishes the inhibition necessary to prevent competing motor plans from interfering with the ongoing one (Brovelli et al., 2005; Cheyne and Ferrari, 2013; Gaetz et al., 2013; Kilavik et al., 2013; Rhodes et al., 2024). The ERD and ERS phenomena have been described to occur before, during (ERD) and following (ERS) an executed, attempted or imagined movement for recordings of the sensorimotor cortex bilaterally, ipsilaterally and contralaterally to the movement across multiple brain areas including the premotor cortex, the primary motor and sensory areas and secondary sensory areas of the parietal lobe (Kobler et al., 2020; Little et al., 2019; Makeig et al., 2000; Pfurtscheller et al., 1996; Pfurtscheller and Berghold, 1989; Pfurtscheller and Neuper, 1997; Seeber et al., 2016; Zich et al., 2023).

1.1.4. Extracranial recordings of brain activity: electroencephalography and magnetoencephalography principles

Electroencephalography, invented by Hans Berger in 1929, comprises one of the most studied and widely adopted techniques to record brain activity (Wolpaw, 2002). EEG setups are safe, portable and low-cost compared to other neuroimaging techniques. As such, EEG is extensively used in

various clinical and research settings (Baniqued et al., 2021; Bhattacharyya et al., 2014; Chaudhary et al., 2016; Coscia et al., 2019; Crell and Müller-Putz, 2024; Daly and Wolpaw, 2008; Jochumsen et al., 2015; Karabanov et al., 2021; Koles, 1991; Lennon et al., 2020; Muralidharan et al., 2011; Pichiorri and Mattia, 2020; Schwarz et al., 2018; Seeber et al., 2015), while during the past years its use at home has been steadily increasing with affordable, wearable devices (Anders and Arnrich, 2022; Kaongoen et al., 2023; Sabio and Lucia, 2022).

As its name suggests, EEG measures electrical brain activity. This activity corresponds to the aggregate extracellular activity, mainly post-synaptic potentials, of millions of cortical neurons over a broad brain area (Buzsáki et al., 2012; Krusienski et al., 2011). To achieve this, a number of electrodes connected to an amplifier is placed on the scalp surface and the voltage measured at each site is compared to the voltage of a ground electrode (Buzsáki et al., 2012; van Bree et al., 2025). This relative difference in potential corresponds to the measured signal. Because the amplifier circuit is contaminated by large amplitude noise an additional (or more) reference electrode(s), usually placed on the earlobe(s) or the mastoid(s), is (are) used in order to remove the noise from brain activity (Nicolas-Alonso and Gomez-Gil, 2012).

Magnetoencephalography too measures the post-synaptic activity of neurons of a brain patch but, unlike EEG, MEG sensors capture weak magnetic fields that are generated by the aforementioned electrical activity (da Silva, 2010; Hämäläinen and Hari, 2002; Lecaignard and Mattout, 2015). To achieve this, classical MEG systems utilizing superconducting quantum interference devices (SQUIDs) place an array of actively cooled sensors above the head (Hämäläinen and Hari, 2002; Kim and Davis, 2021). These sensors comprise the pick-up coils, which can be either magnetometers or gradiometers, and the SQUID that translates magnetic fields to voltage (Hämäläinen and Hari, 2002; Kim and Davis, 2021).

Both EEG and MEG can measure brain activity with a high temporal resolution in the order of milliseconds, however each technique faces different limitations. On the one hand, EEG signals suffer from significant attenuation from their source to the electrode as they traverse the skull and other tissues (Nicolas-Alonso and Gomez-Gil, 2012), leading to poor spatial resolution (Lopes da Silva, 2013). Additionally, they are often contaminated by electrical noise originating either from muscle activity, especially from the scalp, neck and the eyes, or the environment (Chavarriaga et al., 2016; Iturrate et al., 2020; Ronca et al., 2024; Wallstrom et al., 2004). On the other hand, the fact that MEG sensors are placed much further from the brain compared to EEG electrodes in conjunction with the fact that they are not fixed with respect to the skull practically limit the spatial resolution of this recording technique too (Hillebrand and Barnes, 2011; Medvedovsky et al., 2007). However, high-precision MEG based on headcasts (Bonaiuto et al., 2021; Little et al., 2019; Meyer et al., 2017) and a new type of MEG using optimally-pumped magnetometer (OPM) sensors (Borna et al., 2020; Boto et al., 2021, 2019; Hill et al., 2020; Iivanainen et al., 2019; Paek et al., 2020; Roberts et al., 2019; Wittevrongel et al., 2021) hold the promise to overcome some of these limitations. Finally, both types of recordings may be characterized by significant variability across long recording periods, different recording sessions and individuals due to neurophysiological and experimental differences (Gallego et al., 2018, 2017; Lotte et al., 2018a; Xu et al., 2020).

1.2 Brain-computer interfaces

1.2.1. Definition & overview

A survey of numerous parties involved in brain-computer interface technology, conducted by the BCI Society in 2024[1], led to the adoption the following definition for brain-computer interfaces:

> *"A brain-computer interface is a system that measures brain activity and converts it in (nearly) real-time into functionally useful outputs to replace, restore, enhance, supplement, and/or improve the natural outputs of the brain, thereby changing the ongoing interactions between the brain and its external or internal environments. It may additionally modify brain activity using targeted delivery of stimuli to create functionally useful inputs to the brain."*

Moreover, it is clarified that the term "brain" stands for the cerebrum, the diencephalon, the brainstem, and the cerebellum, whereas "computer" might mean a computer as the term is commonly used, but also computerized devices like robots or stimulation devices.

The first key notion in this definition is the measurement of brain activity. This can be achieved using several recording techniques which can be invasive or non-invasive and may rely on electrical or hemodynamic signals (Kawala-Sterniuk et al., 2021; Nicolas-Alonso and Gomez-Gil, 2012). Invasive techniques rely on electrical signals and normally include single- and multi-unit activity and/or local field potentials. These signals are recorded either from neurons in a small patch of the cortex following implantation of recording electrodes or arrays, or from larger neuronal populations using electrocorticography (Abiri et al., 2019; Kawala-Sterniuk et al., 2021; Nicolas-Alonso and Gomez-Gil, 2012). Non-invasive techniques may rely on either electrical signals, as is the case with electroencephalography, or hemodynamic signals with the use of functional magnetic resonance imaging (fMRI) and functional near-infrared spectroscopy (fNIRS) (Allison et al., 2010; Banville and Falk, 2016; Kawala-Sterniuk et al., 2021; Naseer and Hong, 2015; Wolpaw et al., 2020). In this category, the inclusion of magnetic signals could also be envisioned as an alternative with techniques like magnetoencephalography (Corsi et al., 2019; Wittevrongel et al., 2021).

Focusing on EEG and MEG, different brain signals can be recorded based on different experimental paradigms. On the one hand, exogenous paradigms rely on evoked potentials, like auditory evoked potentials (Mladenović, 2021; Séguin et al., 2024) or visually evoked potentials (Arslan and Sinha, 2024; Choi and Jo, 2013; Farwell and Donchin, 1988; Lin et al., 2006), which comprise brain patterns that are spontaneously elicited following a stimulation. They can index the detection of a stimulus or the allocation of attentional resources on specific stimuli and are usually utilized to establish a switch-like communication or to control spellers (Pfurtscheller, 2010; Wolpaw, 2002). A special case of evoked potentials that is used in BCI is the error-related potential (Bhattacharyya et al., 2014; Chavarriaga et al., 2014; Van Schie et al., 2004), which can be recorded from prefrontal areas following an unexpected or erroneous feedback.

1 BCI Society: https://bcisociety.org/bci-definition/

On the other hand, self-paced BCI paradigms rely on voluntarily induced modulations of brain activity, usually referred to as event-related potentials. These include movement-related cortical potentials (Jochumsen et al., 2015), the event-related desynchronization (ERD) (Neuper et al., 2006; Pfurtscheller et al., 1997, 1996) and the event-related synchronization (ERS) (Neuper et al., 2006; Pfurtscheller et al., 1997). These phenomena are related to movement planning, attempt, execution and imagination and are typically used in applications that involve control of virtual or mechanical devices. They can be exploited during rehabilitation protocols with exoskeletons (Hatsopoulos and Donoghue, 2009; Vilela and Hochberg, 2020) and/or virtual or augmented reality in order to promote healthy plasticity following stroke (Ceradini et al., 2024). Other application examples include the decoding of movement intention of patients with severe motor deficits (Coscia et al., 2019; Hatem et al., 2016; Jeunet et al., 2019) or in locked-in states (Freudenburg et al., 2019).

The second key notion in the BCI definition is that of output. Natural brain output refers to observable behavior controlled via the cranial or peripheral nerves. Cranial nerve output corresponds to occulomotricity, control of facial muscles and modulation of rhythms like respiration or heart rate. Peripheral nerve outputs control muscles of the limbs and the trunk. Via these two output pathways the brain can interact with both its internal and external environments. BCI systems alter these natural outputs in various ways depending on the application. For example, they can by-pass a motor deficit due to spinal cord injury and provide a subject with an alternative way to control an actuator (Hochberg et al., 2012) or write text on a computer (Willett et al., 2021).

The third key notion is the delivery of stimuli to the brain. Usually this refers to neurofeedback (Alkoby et al., 2018; Jeunet et al., 2018) that is, a feedback that reflects (or at least is expected to reflect) how a user’s mental state is changing during the course of a mental task. Neurofeedback can be indicative of various cognitive processes, therefore it can be used in order to enhance or restore several cognitive abilities (Alkoby et al., 2018). A different type of stimuli could be direct peripheral or central electrical stimulation that potentially alters ongoing processes, e.g. the alleviation of Parkinson’s disease symptoms with deep brain stimulation of STN (Lozano et al., 2019) using a closed-loop system (Schmidt et al., 2020; Tinkhauser et al., 2017b).

The last important point of the definition of a brain computer-interface is that is needs to operate in real time. Although a significant portion of the research on BCI involves offline analysis (Carrara and Papadopoulo, 2024; Lotte et al., 2018a), BCI systems should be able to function in online settings if the goal is the deployment of such technology in the everyday life of people.

1.2.2. Motor imagery BCI

1.2.2.1. Motor imagery

Motor imagery refers to the mental activity of imagination of a moving body part (Bach et al., 2021; Hanakawa et al., 2008; Jeannerod, 1995). It is normally considered to encompass two subtypes according to whether it is exercised in a third- or first-person perspective (Decety, 1996; Sisti et al., 2022). It can involve the mental visualization of a movement, in which case it is termed visual MI (Malouin et al., 2007; Van Caenegem et al., 2022), or an attempt to reproduce the cutaneous and

proprioceptive sensations elicited during a movement, that is kinesthetic MI (Pfurtscheller and Lopes da Silva, 1999).

Motor imagery recruits similar cortical networks to executed or attempted movements. This has been indicated by some studies that have demonstrated on the one hand elevated autonomic responses due to imagery compared to rest (Decety, 1996), and on the other the diminished MI capabilities of patients suffering from Parkinson's disease and stroke in contrast to people suffering from spinal cord injuries or amputations (Decety, 1996; Rienzo et al., 2014). Additionally, studies that contrasted measurements of cerebral blood flow during motor imagery and action execution tasks have shown a significant increase in frontal and premotor activity compared to M1 (including SMA when the imagery is kinesthetic rather than visual), and also increased activity in the cerebellum and the basal ganglia (Decety, 1996). Visual motor imagery has been shown to involve increased occipital and superior parietal lobule activity, whereas kinesthetic imagery is linked to increased activity in the inferior parietal lobule, the cerebellum and subcortical structures (Guillot et al., 2009). Therefore, it has been suggested that MI is more closely linked to movement planning (Bach et al., 2021; Hanakawa et al., 2008, 2003; Jeannerod, 1995; Meng et al., 2018; Raffin et al., 2012) and that global as well as task-specific inhibitory mechanisms, realized by the posterior parietal cortex and the primary and supplementary motor cortices respectively, are involved in restraining motor output (Nalborczyk et al., 2025; Rieger et al., 2017; Yoo et al., 2020).

The practice of motor imagery elicits amplitude modulations similar to those of executed movements that is, the aforementioned ERD and ERS patterns. These well-studied features of the brain signals recorded during MI, which can efficiently be extracted using several algorithms and can often guarantee the replicability of experimental findings, have made motor imagery one of the most widely adopted BCI paradigms. An additional reason contributing to this is the fact that motor imagery-based experimental paradigms are easy to design and test with both healthy individuals and patients (Bhattacharyya et al., 2014; Horki et al., 2014; Liu et al., 2024; Pfurtscheller and Neuper, 1997), despite the fact that extensive training may be required before subjects can efficiently perform MI (Roc et al., 2021). Finally, due to its similarities to executed and attempted movements, MI can also be used to test hypotheses only on healthy populations, which can then be translated to similar paradigms for applications targeting certain patient populations (Benaroch et al., 2021; Blokland et al., 2015, 2014).

1.2.2.2. State-of-the art in signal processing and classification for MI-BCI

Brain-computer interfaces rely on measuring brain activity and making an inference of the mental state of a user in order to issue a command. In the case of MI-BCI the target brain activity is very often signal power modulations like those which are described by the ERD or ERS (Camargo-Vargas et al., 2021; Kawala-Sterniuk et al., 2021; Lotte et al., 2018a; Tam et al., 2019), although alternative features describing connectivity properties of relevant neuronal networks have also been recently explored (Corsi et al., 2022, 2021, 2024). To reliably uncover relevant signal modulations, while at the same time avoiding the limitations of EEG and MEG recordings, a principled pre-processing and processing of the signals is necessary (Wolpaw, 2002).

Pre-processing refers mainly to the process of removing artifacts from the signals. This is an important step while analyzing brain recordings because artifacts can mask relevant signal

features or, alternatively, bias the classification procedure (Fatourechi et al., 2007; McDermott et al., 2022). Common sources of artifacts include power line noise, eye movements and muscle activity of the neck or limbs (Fatourechi et al., 2007; McDermott et al., 2022) and can be dealt with using a combination of band-pass and band-stop filtering, regression, amplitude thresholds, independent component analysis, and more sophisticated techniques like artifact subspace reconstruction (de Cheveigné, 2020; Fatourechi et al., 2007; Jas et al., 2017; Kachenoura et al., 2008; Kotte and Kumar Dabbakuti, 2020; McDermott et al., 2022; Medeiros de Freitas et al., 2020; Mumtaz et al., 2021; Wallstrom et al., 2004). The impact of these techniques on signal quality is often validated offline, as they are often unsuitable for real-time BCI applications (Kotte and Kumar Dabbakuti, 2020; Mumtaz et al., 2021).

After cleaning the signals, the next goal is to extract relevant signal features. This is achieved during the processing step. In MI-BCI a standard analysis involves filtering in the mu and beta bands in order to amplify the signal-to-noise ratio of the signals (Iturrate et al., 2020; Lotte et al., 2018a). Then, the amplitude envelope or the power of a time-frequency decomposition can be directly computed from the signals (Brodu et al., 2011; Bruns, 2004; Herman et al., 2008; Wang et al., 2008) for a given time window of interest per task trial and condition. Alternatively, a widely adopted strategy is to first use some version of spatial filtering, most notably implementing the common spatial pattern (CSP) algorithm (Blankertz et al., 2008, 2007; Koles, 1991; Müller-Gerking et al., 1999), which aims to uncover signal sources that maximize the topographic disparity between different conditions. Similar to this workflow, the estimation of the covariance matrix of the recordings transforms the signals of different electrodes/sensors in a way that succinctly describes how their amplitude and phase co-vary during each task condition (Barachant et al., 2013; Congedo et al., 2017). An alternative approach to signal processing is based on extracting graph-theoretic metrics which describe how connectivity patterns between the areas of the sensorimotor cortex alter according to different task demands (Corsi et al., 2022, 2021, 2024). In contrast to these approaches, deep learning approaches do not usually require hand-crafted features as inputs but rather rely on architectures that are specifically designed to extract equivalent features as part of the transformations they apply on raw signals (Chiarelli et al., 2018; Eder et al., 2024; Kwon et al., 2020; Roy, 2022; Roy et al., 2019; Schirrmeister et al., 2017; Tayeb et al., 2019).

The final step in any BCI pipeline is classification. Following the processing step, the features extracted from the transformed signals are used in order to train a classifier that can distinguish between different task conditions e.g., “let hand MI”, “right hand MI” or “rest”. In its simplest form, the signal power estimation, usually represented in vector format, comprises the input to any standard machine learning algorithm like linear discriminant analysis or support vector machine (Iturrate et al., 2020; Lemm et al., 2011; Llera et al., 2014; Pfurtscheller and Neuper, 2001; Song et al., 2013; Vidaurre et al., 2011). The classifier is usually trained in a supervised manner on a subset of the data and learns the mapping that maximally separates the different task classes, before being tested on a different data sample. In an analogous way, covariance matrices or graph-theoretic measures can be used as inputs to similar or specialized classifiers (Congedo et al., 2017; Corsi et al., 2019), whereas regarding deep learning approaches, the classification step forms part of their design. To get an accurate estimation of the classification results during offline evaluations this process is usually repeated multiple times using different train and validation data subsets, a procedure termed cross validation (Iturrate et al., 2020; Lemm et al., 2011). These evaluations serve as a benchmark in order to select the appropriate processing algorithm and

classifier for online analyses (Iturrate et al., 2020), although discrepancies between offline and online paradigms may be significant (Carrara and Papadopoulo, 2024).

1.3 A change in perspective: from beta oscillations to bursts

The importance of measurements of changes in continuous signals like the event-related (de)synchronization are implicitly based on the assumption that brain activity is characterized by sustained oscillations whose phase and amplitude are modulated according to specific cognitive demands (Neuper et al., 2006; Pfurtscheller and Berghold, 1989). This assumption seems to be corroborated by the findings of numerous studies that, in an attempt to study the relationship between specific task demands and brain signals modulations, rely on averaging power over multiple trials in order to overcome the inherently low signal-to-noise ratio of extracranially recorded signals (Alayrangues et al., 2019; Hervault et al., 2021; Horki et al., 2014; Lotte and Rimbert, 2022; Müller-Putz et al., 2007; Neuper et al., 2006; Pfurtscheller et al., 1997, 1996; Pfurtscheller, 1981; Pfurtscheller et al., 2006; Pfurtscheller and Berghold, 1989; Pfurtscheller and Lopes da Silva, 1999). However, a significant amount of studies have shown that the notion of sustained, oscillatory activity may be erroneous and point towards a different direction.

Instead of oscillations, beta frequency band (among others) is now thought to be characterized by transient activity in single trials (Anderson et al., 2020; Coleman et al., 2024; Feingold et al., 2015; Jones, 2016; Khawaldeh et al., 2020; Little et al., 2019; Lofredi et al., 2018; Lundqvist et al., 2018, 2016; Seedat et al., 2020; Sherman et al., 2016; Shin et al., 2017; Tinkhauser et al., 2017a; Torrecillos et al., 2018; Wessel, 2020; West et al., 2022; Yeh et al., 2020). This activity is defined by high-amplitude events that last a few milliseconds and which are termed bursts (Figure 1.3.1). According to modeling approaches, beta bursts arise from the (nearly) synchronous arrival of inputs to the apical and basal dendrites of pyramidal neurons in a cortical patch (Jones, 2016; Szul et al., 2023). In practice, beta bursts have been studied usually by applying some form of amplitude threshold to recordings filtered within the target frequency band (Feingold et al., 2015; Little et al., 2019; Lundqvist et al., 2024, 2016; Shin et al., 2017; Wessel, 2020), and can be described by numerous features depending on the exact technique used to compute signal amplitude/power. These features may correspond to the peak amplitude, the central time point of occurrence and the time duration, the peak frequency and the frequency span (Lundqvist et al., 2024; Zich et al., 2023), or taken together by the shape of the signal waveform in specific time windows (Donoghue et al., 2021; Szul et al., 2023).

The implications of conceiving brain activity in terms of bursts rather than oscillations may be far reaching. Rather than relying on amplitude and phase modulation of slowly evolving processes, local and inter-areal brain communication may instead be more flexible by instantaneously adjusting transient activity (Lundqvist et al., 2024). This can be achieved by adopting and possibly combining more strategies, like changing the bursts' amplitude, duration and rate relative to an event (Lundqvist et al., 2024). Looking at brain activity through this lens also has the potential of disentangling distinct but co-occurring processes. Brain communication is an incessant integration of multiple processes that adjust the excitation-inhibition equilibrium in different brain areas (Buzsáki and Draguhn, 2004). By analyzing transient activity instead of power, brain activity can be disentangled in bursts that are involved in a specific process related to a task and bursts that occur in the background, thus amplifying the signal-to-noise ratio and allowing us to make better inferences about the cognitive processes involved in specific tasks.

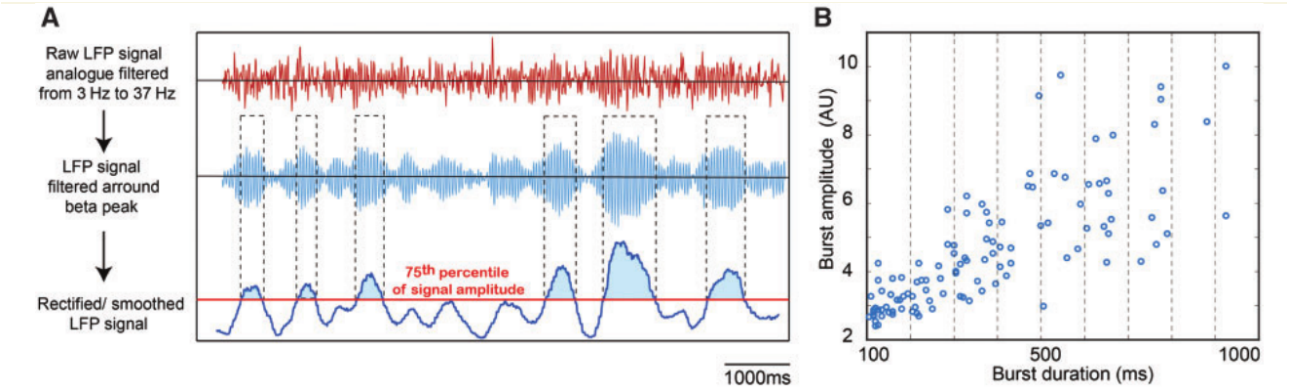


Figure 1.3.1: Beta band activity is characterized by transient events. **(A)** The raw LFP signal (red trace) is characterized by transient amplitude modulations (blue trace) when filtered in the beta frequency band. The onset and offset of each burst are defined as the time points when the amplitude crosses a predefined threshold. **(B)** Scatter plot of beta burst durations and amplitudes shows that longer lasting events tend to have higher amplitude than shorter lasting events. Reproduced from Tinkhauser et al., 2017a.

Based on these principles, beta burst activity modulations in healthy and patient populations have been shown to correlate with working memory, attention, action selection and execution, action error processing and movement inhibition (Lundqvist et al., 2024). Focusing on the relationship between beta bursts and actions, prior to movement onset changes in burst rate in motor areas can predict response times, while following the completion of a movement burst rate has been correlated to behavioral error (Little et al., 2019). In prefrontal and frontal areas burst timing, rate and volume are indicative of successful movement cancellation (Enz et al., 2021; Hannah et al., 2020; Soh et al., 2021; Wessel, 2020). Additionally, on the motor unit level activity can be characterized too in terms of bursts that are time-locked to cortical beta bursts in the sensorimotor cortex (Bräcklein et al., 2022; Echeverria-Altuna et al., 2022). In one study it has been suggested that the beta burst rate can be modulated through neurofeedback training (He et al., 2020), while a few studies point towards the different contributions of bursts with distinct waveform shapes to movement execution through rate modulations (Rayson et al., 2023; Szul et al., 2023). Taken together, the spatial and temporal distribution of beta bursts pose as a promising candidate feature to enhance MI-BCI by offering complementary information to the features normally used.

Chapter 2 - Motivation

So far we have examined the role of the sensorimotor cortex in integrating sensory input and producing a suitable motor output. Sensorimotor transformations depend on a wide network of interconnected areas, each of which is composed of functionally distinct neuronal populations. The orchestrated communication of these populations is, on a macroscopic level, mediated by oscillations, whose modulation of frequency content is classically thought to reflect ongoing processes on the neuronal level. Under normal circumstances information is transmitted from the sensorimotor cortex to subcortical structures, the brainstem and the spinal cord mainly via the pyramidal tract, and behavior is produced by recruiting neurons of the appropriate brainstem and spinal cord nuclei. However, various lesions of the CNS can interrupt the communication network and result in altered, diminished or even complete loss of motor output.

Brain computer interfaces hold the promise of alleviating such deficits. Non-invasive, motor-related BCI applications rely on recordings of brain activity (typically using electroencephalography) from intact brain areas in order to establish communication with a machine. We have already seen that in principle BCI applications aim to reliably uncover task-dependent, oscillatory changes during movement imagination (MI) or attempt. The detected differences in signal properties are attributed to different movement intentions or attempts e.g. movement of the left or right hand, and are translated into commands. In turn, these commands are used to control a range of devices like spellers, wheelchairs or robotic actuators.

Finally, we have introduced the notion of transient activity, and particularly beta burst activity. Bursts are transient, generally high-power events whose probability to occur is affected by task conditions. Bursts occurring within distinct frequency bands have been characterized in several brain areas and the motor-unit level in the periphery. Of more interest to us are bursts in the beta frequency band i.e., beta bursts, recorded from sensorimotor areas in relation to executed movements. In this chapter we discuss how and under which settings transient activity could prove to be a viable alternative to standard motor-related BCI features, and what are the possible advantages for applications that take into account this activity.

2.1 Contribution 1 – An impeding paradigm shift in motor imagery based brain computer interfaces

Sotirios Papadopoulos[1,2,3,*], James Bonaiuto[1,3,†] and Jérémie Mattout[1,2,†]

[1] University Lyon 1, Lyon, France

[2] Lyon Neuroscience Research Center, CRNL, INSERM, U1028, CNRS, UMR5292, Lyon, France

[3] Institut des Sciences Cognitives Marc Jeannerod, CNRS, UMR5229, Bron, France

[†] These authors have contributed equally to this work.

[*] **Correspondence:** Sotirios Papadopoulos

email: sotirios.papadopoulos@univ-lyon1.fr

2.1.1. Abstract

The development of reliable assistive devices for patients that suffer from motor impairments following central nervous system lesions remains a major challenge in the field of non-invasive Brain-Computer Interfaces (BCIs). These approaches are predominated by electroencephalography and rely on advanced signal processing and machine learning methods to extract neural correlates of motor activity. However despite tremendous and still ongoing efforts, their value as effective clinical tools remains limited. We advocate that a rather overlooked research avenue lies in efforts to question neurophysiological markers traditionally targeted in non-invasive motor BCIs. We propose an alternative approach grounded by recent fundamental advances in non-invasive neurophysiology, specifically subject-specific feature extraction of sensorimotor bursts of activity recorded via (possibly magnetoencephalography-optimized) electroencephalography. This path holds promise in overcoming a significant proportion of existing limitations, and could foster the wider adoption of online BCIs in rehabilitation protocols.

Keywords: beta bursts, Brain-Computer Interface (BCI), EEG, magnetoencephalography (MEG), motor imagery (MI), neurological rehabilitation, upper limb

2.1.2. Introduction

Central nervous system (CNS) lesions have a major socioeconomic impact on modern societies (World Health Organization, 2011). A grave manifestation involves upper limb motor deficits that affect the quality of life of patients to various degrees depending on both the extent and the exact nature of the lesions. Emerging medical technologies may alleviate these deficits and therefore improve the lives of millions of patients in several ways, diminishing the psychological burden and societal discrimination against people with disabilities.

A prominent direction lies in the development of Brain-Computer Interfaces (BCIs) whose output can be translated into motor commands for rehabilitation protocols (Coscia et al., 2019; Raffin and Hummel, 2017), or devices such as wheelchairs, spellers, exoskeletons, and prostheses (Rosenfeld and Wong, 2017), in order to assist patients in overcoming motor disabilities following stroke, spinal cord injuries, and other CNS pathologies or peripheral deficits, respectively. However, despite the attention that such devices have attracted over the last few years and the fact that numerous research teams are actively working on improving them, to date BCIs have not delivered on their promises. The reasons for this span multiple axes (Chavarriaga et al., 2016) including issues specific to the brain-signal acquisition techniques used, the underlying assumptions about the extracted signals and the targeted mental states, as well as the specific signal processing and feature extraction methods employed.

Broadly, BCIs can be categorized as invasive or non-invasive based on the techniques used to extract relevant brain signals (Daly and Wolpaw, 2008; Hatsopoulos and Donoghue, 2009). Typically, the former require surgery and enable the recording of single- or multi-unit activity, or local field potentials, with depth electrodes or electrocorticography (Hatsopoulos and Donoghue, 2009). The advantages of these techniques are that (a) they allow for close and precise intra- or supracortical placement of the electrodes and thus high spatial resolution and signal-to-noise ratio (SNR), and (b) they can avoid certain sources of noise while still recording high-frequency signals such as neural spiking or high-frequency gamma activity.

Nonetheless, these advantages are blunted by potential risks. As is the case for surgical implantation of electrodes in patients suffering from pharmacoresistant epilepsy or other diseases treated via deep-brain stimulation protocols, invasive techniques are inherently accompanied by risk of complications such as infections, subdural and intracerebral bleeding, and brain edema (Hariz, 2002; Wellmer et al., 2012). Moreover, invasive methods based on electrode implantation are characterized by instability over large periods of time due to extensive tissue scaring around the implantation site and electrode drift, which often reduce the numbers of recorded units (Hatsopoulos and Donoghue, 2009). In practice, these drawbacks often require the implanted electrodes to be removed after a fairly short amount of time [although see (Hochberg et al., 2012)].

Considering the risks inherent to surgically implanted electrodes, it is evident that at least for certain applications, non-invasive BCIs seem to be a more viable option for widespread adoption in the foreseeable future, a fact reflected in the predominance of EEG in most BCI applications. Despite the lower SNR and the lower frequency and spatial resolution of extracranially recorded brain signals, advanced signal processing and feature extraction methods (Blankertz et al., 2008; Iturrate et al., 2020), often paired with sophisticated machine and deep learning algorithms (Lotte et al., 2018a; Mladenović et al., 2019; Roy et al., 2019), or hybrid BCI designs (Hong and Khan,

2017; Müller-Putz et al., 2015) have steadily improved the decoding capabilities of non-invasive BCIs.

However, most efforts have focused on the development of agent-agnostic algorithms, while only a few studies have focused on refining the neural correlates that are thought to be relevant for a given motor task. We propose that future efforts for online extraction of pertinent brain signals and features should instead concentrate on (a) redefining the neurophysiological markers and features to be extracted and, (b) adopting an individualized and neurophysiologically informed paradigm (Chavarriaga et al., 2016; Mladenović et al., 2019) specifically targeting these markers and features.

Taking advantage of recent work that emphasizes the pitfalls of indiscriminately performing time-frequency analyzes of neural signals (Cole and Voytek, 2017; Cole et al., 2017; Donoghue et al., 2021; Jones, 2016), the importance of transient bursts of frequency-specific activity for behavior (Anderson et al., 2020; Jones, 2016; Khawaldeh et al., 2020; Little et al., 2019; Lofredi et al., 2018; Lundqvist et al., 2018, 2016; Seedat et al., 2020; Sherman et al., 2016; Shin et al., 2017; Torrecillos et al., 2018; Yeh et al., 2020), and the ability to precisely localize these bursts (Bonaiuto et al., 2021), this line of research could vastly improve the decoding capabilities of BCIs and serve as a basis for a wide range of applications that leverage motor-related signals. As a final note, we discuss why we believe non-invasive BCIs should primarily target rehabilitation rather than restoration of control and list a few outstanding questions that remain to be answered.

2.1.3. Current approaches to non-invasive, motor imagery based brain-computer interfaces

State-of-the-art non-invasive BCI paradigms vary greatly according to the techniques used to extract signals that are potentially informative for a task. Depending on the goal they aim to attain, several setups can exploit different brain signals sometimes even mixed with other, non-brain signals like eye movements and muscle activity (Choi et al., 2017). The recorded brain signals can be electrical, or hemodynamic, measured using electroencephalography (EEG) possibly magnetoencephalography (MEG)[2], or functional near-infrared spectroscopy (fNIRS), respectively.

Contrary to hemodynamic signals (Nicolas-Alonso and Gomez-Gil, 2012), EEG and MEG signals provide direct measures of neuronal activity and are characterized by high temporal resolution. They are therefore privileged candidates for real-time applications. In this section we will briefly discuss these two techniques as well as the common physiological markers of motor-related cortical activity they record, highlighting the steps usually taken to analyze these signals and their respective shortcomings.

2 The emergence of optically-pumped magnetometers (OPMs) could, unlike currently available systems, render MEG portable and, thus, a very attractive platform for BCI applications in the future.

2.1.3.1. Electroencephalography and magnetoencephalography overview

Electroencephalography measures the electrical activity due to variations of post-synaptic potentials synchronized across large populations of cortical neurons (Buzsáki et al., 2012). The signal is measured as the difference in electric potentials recorded from electrodes relative to a reference (ground) electrode (Nicolas-Alonso and Gomez-Gil, 2012). These post-synaptic potentials also generate weak magnetic fields which are measured by MEG sensors (da Silva, 2010; Hämäläinen and Hari, 2002; Lecaignard and Mattout, 2015).

The major goal of any BCI application is to ultimately enhance and improve the everyday lives of its users. Hence, EEG is frequently the recording technique of choice for BCIs because EEG setups have the advantage of being portable and inexpensive compared to other signal acquisition technologies, thus making them suitable for a wide range of environments from the laboratory to the medical office, or even at home. On the contrary, current SQUID-based MEG systems are more expensive and inherently constrained to magnetic-shielded laboratory environments because of technical limitations imposed by the small amplitude of the measured fields in comparison to multiple sources of noise.

Electroencephalography electrodes are placed on the scalp surface and, as a result, must contend with two main challenges. Firstly, the recorded signals are significantly attenuated and contaminated by physiological and non-physiological noise as they have to traverse multiple layers such as the meninges, cerebrospinal fluid, skull, and muscle tissue before reaching the scalp (Nicolas-Alonso and Gomez-Gil, 2012). Secondly, each electrode samples the activity, distorted by the skull (Lopes da Silva, 2013), of a relatively large cortical area (Krusienski et al., 2011), therefore leading to poor spatial resolution (Lopes da Silva, 2013). Conversely, MEG is not affected to the same extent by either challenge. Although MEG sensors sample magnetic fields from an equivalent cortical area, these fields are only attenuated with distance and not distorted by the presence of layers of tissue and skull between the neural sources and the MEG sensors. As a consequence, MEG offers a higher spatial resolution than EEG. However, in practice it is limited by the head movements that subjects make while performing a task (Medvedovsky et al., 2007), as well as by co-registration errors with anatomical images (Hillebrand and Barnes, 2011). Finally, due to the dynamic nature of brain signals, both EEG and MEG recordings are characterized by great variability, both between individuals, and within recordings of the same individual over long periods of time or different recording sessions.

2.1.3.2. Motor imagery in electroencephalography and magnetoencephalography

Brain-Computer Interfaces that aim to leverage motor-related brain activity usually depend on two types of signals. For patients, the signal of interest is occasionally recorded during an attempted movement (Muralidharan et al., 2011). The other common strategy for healthy subjects and patients involves asking subjects to imagine producing movements, known as (kinesthetic) motor imagery (MI) (Pfurtscheller and Lopes da Silva, 1999), on which we will focus hereafter. Whereas a signal recorded while a patient is attempting to perform a movement despite their disability is

thought to reflect purely motor functions, MI may also implicate other cognitive processes like mental rotation or conscious access to the motor plan (Hanakawa et al., 2008, 2003; Jeannerod, 1995; Meng et al., 2018; Raffin et al., 2012).

Traditionally, both movement execution and MI have been linked to time-locked changes in induced power within various frequency bands recorded from the sensorimotor cortex (Friston et al., 2006; Pfurtscheller and Lopes da Silva, 1999; Ramadan and Vasilakos, 2017). In the beta (~13–30 Hz) and mu (~8–12 Hz) frequency bands, these signals are marked by a gradual reduction in power prior to a real or imagined movement, named event-related desynchronization (ERD), followed by a post-movement increase called event-related synchronization (ERS) in the beta band (Neuper et al., 2006; Pfurtscheller et al., 2006, 1996; Pfurtscheller and Neuper, 1997; Tam et al., 2019). In the mu and beta bands, pre-movement ERD has long been considered to reflect neural processes related to movement preparation, initiation and realization, while post-movement ERS was related to the re-establishment of inhibition after the execution of a motor plan (Pfurtscheller et al., 1997; Pfurtscheller and Lopes da Silva, 1999). An ERS is also typically observed in the gamma band (30–120 Hz) around the time of movement onset (Ball et al., 2008; Darvas et al., 2010; Miller et al., 2010), and is thought to reflect movement execution or monitoring (Brovelli et al., 2005; Cheyne and Ferrari, 2013; Gaetz et al., 2013).

2.1.3.3. Common techniques in motor imagery based brain-computer interfaces

Most approaches for MI signal analysis utilize a similar pipeline (Wolpaw, 2002) that involves pre-processing and time-frequency decomposition to extract movement-related ERD and ERS signals, and classification of these signals to predict some aspect of an imagined movement. A great repertoire of signal processing and feature extraction methods have been developed or adapted to particularly address the low SNR and source localization problems inherent in EEG and MEG (Iturrate et al., 2020; Lotte et al., 2018a). Signal processing methods aim to improve the quality of the recorded signals by means of artifact rejection, frequency filtering, or spatial filtering. Such methods increase SNR by rejecting non-brain signals, filtering out irrelevant aspects of the signals, and reducing the contribution of non-pertinent areas in the feature extraction step. Dimensionality reduction techniques such as principal component analysis (Zarei et al., 2017) or independent component analysis (Kachenoura et al., 2008) are typically used to select artefactual sources to be removed, or relevant components to be further analyzed (Medeiros de Freitas et al., 2020). Feature extraction refers to the process of extracting the metrics of a signal that is most informative of the imagined movement. Standard procedures include channel selection, and time or spectral feature estimation. For analyzes of frequency-specific changes in power, time-frequency decomposition techniques such as the fast Fourier transform (Brodu et al., 2011; Herman et al., 2008), Hilbert–Huang transform (Wang et al., 2008), or Morlet wavelets (Brodu et al., 2011; Herman et al., 2008) are commonly used.

As the goal of MI based BCI applications is usually to decode aspects of the intended movement from recorded neural activity, the extracted features are used as input to some sort of classifier. Classifiers are trained offline on the sampled activity, yielding a model that maps the underlying features to a set of outputs (e.g., left vs. right imagined movement), and are then employed online

to map the recorded activity to an output in real time (Iturrate et al., 2020). Common machine learning algorithms used in BCI applications for decoding a subject's imagined movement include neural networks (Hazrati and Erfanian, 2010; Pfurtscheller and Neuper, 2001), linear discriminant analysis (Llera et al., 2014; Pfurtscheller and Neuper, 2001; Vidaurre et al., 2011), and support vector machines (Song et al., 2013), while during the last few years the field has experienced a steady shift of interest toward more elaborate deep learning architectures (Roy et al., 2019).

This general BCI pipeline has been widely adopted, but important limitations still exist. Most MI based applications are limited to binary classifications (e.g., left vs. right), or classifications among a few classes at best, and achieve modest results even when continuous paradigms are used, as classification accuracies steeply decrease with an increasing number of output classes (Hong and Khan, 2017). Notably, only a few studies have involved patients, and therefore the real value of BCIs for patients is still unproven. Additionally, despite the sophisticated methods employed, still about a third of subjects have great difficulty or are totally unable to control BCIs, a phenomenon known as BCI illiteracy (Vidaurre and Blankertz, 2010). We argue that this focus on advanced signal-processing and feature extraction techniques for MI based BCIs has effectively rendered ERD and ERS the only signals of interest, creating a gap between the BCI community and recent advances in neurophysiology.

2.1.4. Proposed alternative

In light of these considerations we believe that significant progress toward the development of high-fidelity non-invasive BCIs, suitable for online motor decoding, will be achieved only if we attempt to bridge the gap between basic neuroscience and applied neuroengineering. To this end we propose a reassessment of the neurophysiological features of interest for the decoding of motor related activity, and a novel methodology that exploits the advantages of both MEG and EEG in order to take advantage of subtle, individualized physiological markers of motor processing.

2.1.4.1. The quest for refined neurophysiological markers

While standard non-invasive BCI features such as changes in frequency band power are somewhat informative of movement, these approaches discard potentially valuable information in the temporal domain. Time-frequency analyzes rarely take into account the temporal variability and waveform shape of the signals of interest (Donoghue et al., 2021), potentially overlooking the fact that neural activity can occur as bursts rather than oscillations (Anderson et al., 2020; Jones, 2016; Khawaldeh et al., 2020; Little et al., 2019; Lofredi et al., 2018; Lundqvist et al., 2018, 2016; Seedat et al., 2020; Sherman et al., 2016; Shin et al., 2017; Torrecillos et al., 2018; Yeh et al., 2020) and that oscillations can have non-sinusoidal waveform shapes (Cole and Voytek, 2017; Cole et al., 2017). Both of these potentially rich sources of information are lost in typical time frequency analyzes.

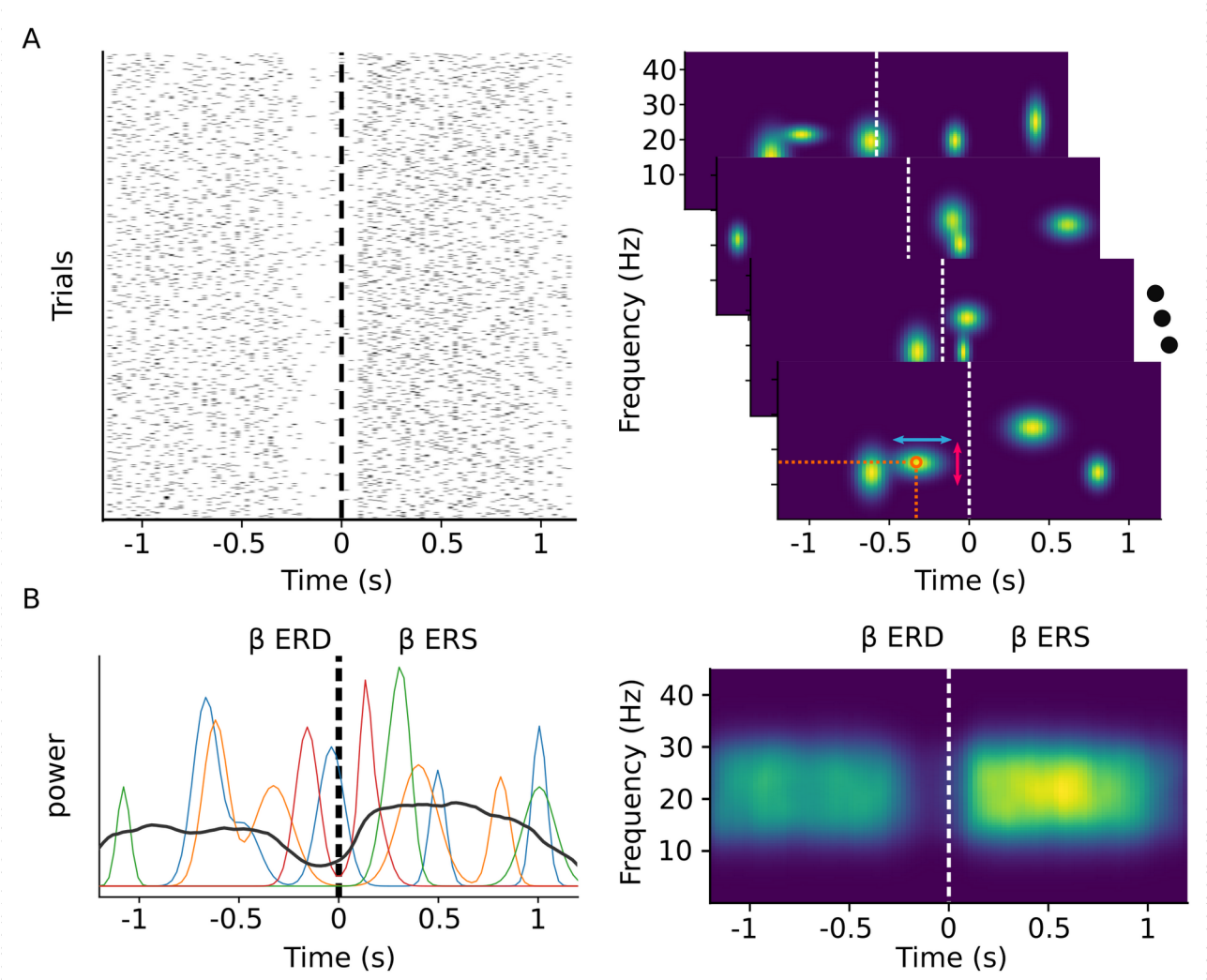


Figure 2.1.1: Trial-averaged discrete bursts can appear to be sustained oscillations. Simulated beta burst activity from multivariate Gaussian distributions with a time varying probability and random peak frequency, frequency span, and time duration. **(a)** Left: The timing of simulated bursts in each trial (N = 1,000). Right: Time-frequency decomposition analysis of each single trial level (shown for four random ones) allows for the extraction of features such as the exact timing and peak frequency (orange circle), the time duration (red vertical arrows) and the frequency span (light blue horizontal arrows) of each burst. **(b)** Beta band power of the same four random trials from the right panel of (A) (colored lines) depicted along with the average beta band power over all trials (black line). During each trial, beta power appears as transient peaks at varying time points. The classically described ERD and ERS phenomena emerge as a consequence of averaging over multiple trials.

In the case of beta activity, it has recently been demonstrated that the majority of sensorimotor activity within this band occurs as discrete transient bursts (Jones, 2016; Little et al., 2019; Lundqvist et al., 2018, 2016; Sherman et al., 2016; Shin et al., 2017) (Figure 2.1.1 a), and that the patterns of pre-movement beta ERD and post-movement beta rebound are a result of averaging these bursts over multiple trials (Little et al., 2019; Wessel, 2020) (Figure 2.1.1 b). Indeed, it has been shown that the timing of beta bursts in the motor cortex are, before movement, predictive of response times, and after movement, informative of behavioral errors, more so than changes in be-

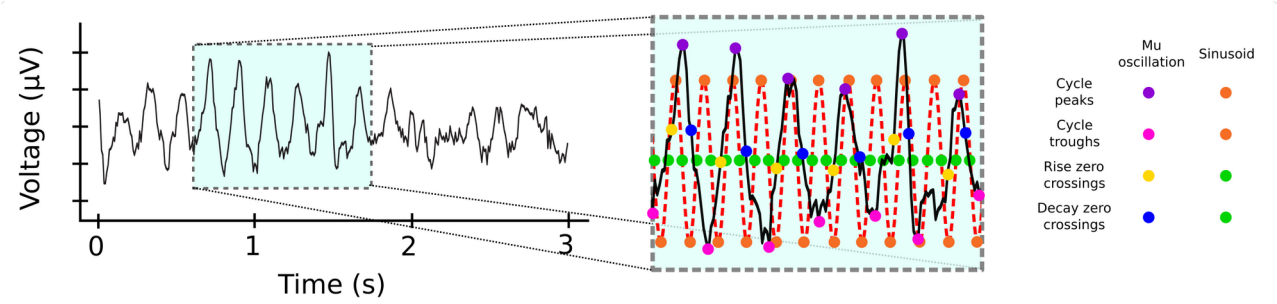


Figure 2.1.2: Frequency specific activity can be non-sinusoidal. Mu activity from EEG electrode C4. Inset: Cycle-by-cycle analysis (Cole and Voytek, 2019) of the activity reveals that mu occurs in bursts with significant variability for measures such as peaks (magenta dots) and troughs (pink dots), or rise (yellow dots) and decay (blue dots) duration between cycles, unlike the corresponding measures of a pure 10 Hz sinusoid (orange and green dots). EEG data from BCI Competition IV (Leeb et al., 2007) https://www.bbci.de/competition/iv.

ta amplitude (Little et al., 2019). In the right inferior frontal cortex, beta burst timing is related to electromyography correlates of movement cancellation (Hannah et al., 2020), and may coordinate bursts in the sensorimotor cortex following successful movement cancellation (Wessel, 2020). Beta burst activity can also be modulated through neurofeedback training (He et al., 2020), making beta burst timing and spatial distribution a potential rich source of information for MI decoding.

In contrast to beta, activity in the mu frequency band is oscillatory even in single trials (Y. Y. Chen et al., 2021). This activity is typically analyzed using time-frequency decomposition techniques, which assume that the underlying signal is sinusoidal. However, there is now growing consensus that oscillatory neural activity is often non-sinusoidal (Cole and Voytek, 2019, 2017; Donoghue et al., 2021; Fabus et al., 2021), and that the raw waveform shape can be informative of movement (Quinn et al., 2021) (Figure 2.1.2). Future efforts could take advantage of this possibility by using recently developed non-parametric cycle-by-cycle analyzes (Cole and Voytek, 2019).

2.1.4.2. Subject-specific, forward models of dynamic activity

The major challenges for non-invasive BCIs are to deal with highly variable and noisy single trial activity, and to overcome the low SNR and limited spatial resolution in order to improve online feature extraction and decoding. We anticipate that these challenges will be even more acute when targeting short-lasting, potentially non-sinusoidal bursts of frequency specific activity. To overcome these challenges, we propose that MEG could be used to complement EEG. Hybrid designs (Allison et al., 2010; Pfurtscheller, 2010) that combine the two techniques yield superior results compared to either technique used alone in certain applications (Corsi et al., 2019; Lecaignard et al., 2021), however such designs are limited to laboratory settings. To deploy a system under more naturalistic settings, one alternative is to use MEG to develop personalized forward models that can subsequently be used to improve the decoding efficacy of online EEG-based BCI applications.

The spatial precision of MEG is traditionally limited by within-session subject movement and between-session co-registration error. However, recently developed high-precision MEG (hpMEG) techniques based on the use of 3D printed individualized head-casts (Meyer et al., 2017), have

allowed for fine-grained analyzes of movement-related signals at the level of cortical laminae (Bonaiuto et al., 2018a, 2018b, 2021; Troebinger et al., 2014a, 2014b). Customized forward models based on offline hpMEG analysis could be used to identify the neural features most informative of imaged movements and isolate these features to subsequently optimize EEG-based real-time decoding. In the near future, optically-pumped magnetometers (OPMs) may be able to replace hybrid M/EEG (Borna et al., 2020; Boto et al., 2021, 2019; Hill et al., 2020; Iivanainen et al., 2019; Paek et al., 2020; Roberts et al., 2019; Wittevrongel et al., 2021), as they promise to be more portable and cheaper while also improving SNR.

2.1.4.3. A paradigm shift toward motor rehabilitation

Lately the BCI community has been drifting away from the restoration of motor control to target motor rehabilitation instead (Coscia et al., 2019; Lennon et al., 2020; MacEira-Elvira et al., 2019; McFarland et al., 2017; Micera et al., 2020; Raffin and Hummel, 2017). Motor rehabilitation is a challenging yet more attainable goal compared to motor restoration, simply because of the amount of complexity that the control of multiple-degrees-of-freedom devices introduces both for the BCI designers and users. Moreover, BCI-assisted rehabilitation protocols are relevant for a wider group of patients beyond those that need to overcome a peripheral handicap; from stroke patients with motor impairments to patients suffering from Parkinson's disease. The features extracted through bursts analysis could revolutionize these protocols.

As an example, the coupling of this design with mirror therapy based on virtual or augmented reality could be important for a number of reasons. Visual feedback is known to reduce movement errors due to impaired proprioception (Ghez et al., 1995), while it has, also, long been shown in experiments with non-human primates that the role of vision is crucial for the formation of the internal representation of upper limb position, more so than proprioceptive feedback (Graziano, 1999). Additionally, it is established that erroneous visual feedback ultimately results in inaccurate movements being regarded as accurate representations of a subject's movement intentions (Preston and Newport, 2014). Therefore, hpMEG-optimized BCI training accompanied by digital mirror or camera therapy may soon provide clinicians and, importantly, patients with novel therapeutic solutions.

2.1.5. Conclusion

Despite the significant effort toward the development of sophisticated algorithms and design paradigms, state-of-the-art EEG-based BCI applications exploiting MI face many limitations. To overcome these limitations, we propose that more subtle neurophysiological markers such as burst timing and waveform shape be explored, and techniques with high temporal and spatial resolution such as hpMEG and OPMs be adopted.

2.1.6. Data availability statement

The original contributions presented in the study are included in the article/supplementary material, further inquiries can be directed to the corresponding author/s.

2.1.7. Author contributions

J B and J M contributed to the conception of the manuscript. S P drafted the manuscript. All authors contributed to manuscript revision, read, and approved the submitted version.

2.1.8. Funding

S P, J B, and J M are supported by the French National Research Agency (ANR) project HiFi (2020–2024). J B is supported by the European Research Council (ERC) under the European Union's Horizon 2020 Research and Innovation Program (ERC consolidator grant 864550 to J B).

2.1.9. Acknowledgments

This work was performed within the framework of the LABEX CORTEX (ANR-11-LABX-0042) of Université de Lyon, within the program "Investissements d'Avenir" (decision n◦ 2019-ANR-LABX-02) operated by the French National Research Agency (ANR).

Chapter 3 - Beta bursts feasibility for BCI

In the previous chapter we presented the basic principles behind non-invasive, motor-related BCI applications. We emphasized that there are still significant limitations for a wider adoption of such applications, and therefore we offered an alternative way to tackle some of these limitations. Particularly, we argued that signal properties which describe transient, spatially and temporally limited modulations could serve as complementary features that are potentially more informative of single trial dynamics. As such, we contrasted beta bursts and mu band oscillatory peak-to-peak variations to sinusoidal amplitude modulations.

In this chapter we focus on the feasibility of using beta bursts as alternative features for classification in binary, motor imagery paradigms by analyzing electroencephalography recordings of numerous, benchmark, freely accessible datasets. In the first subchapter we explore multiple representations of the beta band activity, including beta power, beta burst amplitude and volume and a recently proposed analysis that characterizes beta band activity in terms of the burst rate of bursts with distinct waveform shapes. We adopt a nested cross validation approach in order to identify beta burst waveforms whose rate modulation is the most informative of the ongoing MI task and we show that this representation is superior to any other in terms of classification accuracy, thus providing the first evidence for the feasibility of waveform-resolved burst features for BCI.

Next, in the second subchapter, we attempt to tackle the major limitation of the previous study that is, its computational complexity. We propose a simple algorithm to identify waveform shapes whose rate is expected to be modulated due to the MI task using a small set of calibration data. Upon finding these waveforms we use them as kernels and we filter the signals in time domain by applying convolution. The resulting signals comprise a proxy for burst rate with an increased signal-to-noise ratio with respect to the selected waveforms that can be utilized by many machine learning, classification pipelines. Here, we show that these beta burst features increase classification accuracy and information transfer rate compared to signal power, thus validating the feasibility and significance of analyzing transient beta band activity for BCI.

Finally, in the last subchapter we take advantage of the same algorithm and we investigate the stability of beta burst waveforms across different recording sessions. We use data from one recording session to establish the waveforms and assess the classification score using the same features on other sessions. We compare these results to results obtained without transferring features across sessions and we show that beta burst waveforms minimize the across-session score loss compared to signal power. This study, therefore, suggests that task-dependent beta

burst rate modulations are sustained across trials and sessions because specific burst waveforms are systematically linked to processes pertaining to the MI task.

3.1 Contribution 2 – Beta bursts question the ruling power for brain computer interfaces

Sotirios Papadopoulos[1,2,3,*], Maciej J Szul[1,3], Marco Congedo[4], James J Bonaiuto[1,3,5] and Jérémie Mattout[1,2,5]

[1] University Lyon 1, Lyon, France

[2] Lyon Neuroscience Research Center, CRNL, INSERM U1028, CNRS, UMR5292, Lyon, France

[3] Institut de Sciences Cognitives Marc Jeannerod, CNRS, UMR5229, Lyon, France

[4] GIPSA-lab, University Grenoble Alpes, CNRS, Grenoble-INP, Grenoble, France

[5] These two authors contributed equally.

[*] Author to whom any correspondence should be addressed.

email: sotirios.papadopoulos@univ-lyon1.fr

3.1.1. Abstract

Current efforts to build reliable brain–computer interfaces (BCI) span multiple axes from hardware, to software, to more sophisticated experimental protocols, and personalized approaches. However, despite these abundant efforts, there is still room for significant improvement. We argue that a rather overlooked direction lies in linking BCI protocols with recent advances in fundamental neuroscience. In light of these advances, and particularly the characterization of the burst-like nature of beta frequency band activity and the diversity of beta bursts, we revisit the role of beta activity in “left vs. right hand” motor imagery (MI) tasks. Current decoding approaches for such tasks take advantage of the fact that MI generates time-locked changes in induced power in the sensorimotor cortex and rely on band-passed power changes in single or multiple channels. Although little is known about the dynamics of beta burst activity during MI, we hypothesized that beta bursts should be modulated in a way analogous to their activity during performance of real upper limb movements. We show that classification features based on patterns of beta burst modulations yield decoding results that are equivalent to or better than typically used beta power across multiple open electroencephalography datasets, thus providing insights into the specificity of these bio-markers.

Keywords: beta bursts, brain–computer interface (BCI), decoding, electroencephalography (EEG), motor imagery (MI)

3.1.2. Objective

Neural interfaces, and in particular brain–computer interfaces (BCI), have long been conceptualized as effective means of surmounting disabilities for patients suffering from various diseases and traumas, while transhumanist philosophy sees BCI (Kurzweil, 2014) as a way to enhance the capabilities of our bodies and brains. To achieve such goals, a multidisciplinary approach is crucial. Over the past few decades, an increasing number of research groups from diverse fields have been striving towards several objectives, from laying the foundations of BCI (Hatsopoulos and Donoghue, 2009; Lotte et al., 2018c; Ramadan and Vasilakos, 2017; Wolpaw, 2002; Wolpaw et al., 2020) to improving their reliability (Mueller-Putz et al., 2008; Vidaurre and Blankertz, 2010) and applicability under more naturalistic settings (Chavarriaga et al., 2016; Hughes et al., 2020; Iturrate et al., 2020).

Although we are still far from achieving goals like those portrayed in science fiction, a few real-world BCI applications are currently deployed. Most applications revolve around selected groups of patients improving their ability to interact with their environment (McFarland et al., 2017) via diverse protocols like post-stroke rehabilitation for improving motor function and cognitive deficits (Bai et al., 2020; Baniqued et al., 2021; Luauté et al., 2015; Mane et al., 2022), or devices offering communication options or switch control to locked-in and tetraplegic patients (Benaroch et al., 2021; Blokland et al., 2014; Chaudhary et al., 2016; Mcfarland, 2021; Saeedi et al., 2017). Such applications usually form part of studies that employ invasive recording techniques in an attempt to acquire high-quality brain signals (Tam et al., 2019; Willett et al., 2021). Invasive techniques provide higher signal-to-noise ratio, spatial specificity and frequency resolution compared to non-invasive techniques, trading off the availability of the subjects, and the necessity of medical interventions. However, non-invasive techniques attract a significant portion of BCI research due to their safety, the lower equipment cost, and the ability to collect large amount of data from patients and healthy participants. Specifically in the case of electroencephalography (EEG), the added advantage of portability allows for the inclusion of more subjects under more diverse and ecologically valid scenarios, therefore making it currently one of the most attractive platforms.

Non-invasive BCI emerged in the early 90’s (Farwell and Donchin, 1988; Pfurtscheller et al., 1993; Wolpaw et al., 1991), along with the first spatial filtering algorithms. The Laplacian filter (Lu et al., 2013; McFarland et al., 1997) allowed for improved signal-to-noise ratio, while the common spatial pattern algorithm (Blankertz et al., 2007; Koles, 1991; Müller-Gerking et al., 1999) provided a way to weight the contribution of each channel in order to optimize classification. Around the same time, a reliable, reproducible signature of brain activity was demonstrated for the first time, at least on a trial-averaged level. Studies in motor neuroscience involving healthy subjects revealed time-locked changes in induced power within specific frequency bands (Cheyne and Ferrari, 2013; Makeig et al., 2000; Pfurtscheller and Berghold, 1989; Pfurtscheller and Lopes da Silva, 1999). Brain recordings were shown to exhibit a gradual reduction in signal power, relative to baseline, in the mu (~8–12 Hz) (Neuper et al., 2006; Pfurtscheller et al., 2006, 1997; Pfurtscheller and Berghold, 1989) and beta (~13–30 Hz) (Kilavik et al., 2013; Neuper et al., 2006; Pfurtscheller et al., 1997) frequency bands during an action or during motor imagery (MI): the so-called event-related desynchronization (ERD). This phenomenon is considered to reflect processes related to movement preparation and execution, and is particularly pronounced in the contralateral sensorimotor cortex (Makeig et al., 2000; Pfurtscheller and Berghold, 1989; Pfurtscheller and

Neuper, 1997). Moreover, shortly following the completion of the task a relative increase in power, the event-related synchronization (ERS) (also referred to as the beta rebound), could be observed in the beta band (Alayrangues et al., 2019; Neuper et al., 2006; Pfurtscheller et al., 1996). ERS is thought to reflect the re-establishment of inhibition in the same area (Neuper et al., 2006; Pfurtscheller et al., 1996).

In the following years, the field witnessed the introduction of more advanced signal processing methods (Makeig et al., 2000), alternative non-invasive recording techniques (Naseer and Hong, 2015; Waldert et al., 2008) and hybrid BCI paradigms (Allison et al., 2010; Buccino et al., 2016; Choi et al., 2017; Corsi et al., 2019; Sadeghi and Maleki, 2018). During the past decade, attempts have been made to place more emphasis on the user by studying individual traits that correlate with performance (Lotte and Rimbert, 2022), or adapting BCI protocols to the user (Lotte et al., 2018b; Mladenović, 2021; Mladenović et al., 2022) in an effort to better understand and mitigate the problem of BCI illiteracy (Vidaurre and Blankertz, 2010): the inability of approximately 1/3 of the users to control a motor-imagery based BCI system. Directly linked to this problem, there are significant efforts being made towards creating more informative neurofeedback paradigms by studying the influence of feedback modality (Pillette et al., 2021) and factors not directly linked to the experimental task (Jeunet et al., 2018). This multifaceted endeavor holds the potential of considerably improving existing rehabilitation protocols (Jeunet et al., 2019).

Meanwhile, a great body of work has developed an arsenal of advanced pre-processing, feature extraction, and classification algorithms dedicated specifically or adapted to the particular characteristics and limitations of EEG signals (Iturrate et al., 2020; Lotte et al., 2018a). As a first step, a standard BCI pipeline includes dimensionality reduction techniques for channel selection and noise removal (Kachenoura et al., 2008; Medeiros de Freitas et al., 2020; Zarei et al., 2017). Subsequently, a common practice for signals recorded during MI or attempted movements is to use a time-frequency (TF) transformation such as the short-time Fourier, Hilbert, or wavelet transform (Brodu et al., 2011; Bruns, 2004; Herman et al., 2008) and extract the power of the signal in specific time windows and frequency bands of interest. Finally, any of a large range of machine learning algorithms like linear discriminant analysis (LDA) (Llera et al., 2014; Pfurtscheller and Neuper, 2001; Vidaurre et al., 2011), support vector machines (Song et al., 2013), random forests (Steyrl et al., 2016, 2014) or neural networks (Hazrati and Erfanian, 2010) can be trained in order to establish a mapping between the features and labels, and assess the performance of the whole pipeline.

This archetypical analysis is, to a significant extent, based on the idea that signal power is the most informative signature of non-invasively recorded neural activity for motor-related tasks. Ever since the characterization of the ERD and ERS phenomena, there has been little to no discussion in the non-invasive BCI field as to whether these features accurately capture the task-related modulations of brain activity. Recent studies in neurophysiology have challenged this view and have demonstrated that the ERD and ERS patterns only emerge as a result of averaging signal power over multiple trials (Jones, 2016; Little et al., 2019). On a single trial level, beta band activity occurs in short, transient events, termed bursts, rather than as sustained oscillations (Jones, 2016; Little et al., 2019; Lundqvist et al., 2016; Shin et al., 2017; Torrecillos et al., 2018; Wessel, 2020). This indicates that the ERD and ERS patterns reflect accumulated, time-varying changes in the burst probability during each trial. Thus, beta bursts may carry more behaviorally relevant information than averaged beta band power. Indeed, studies in humans involving arm movements have established a link between the timing of sensorimotor beta bursts and response times prior to

movement, as well as behavioral errors post-movement (Little et al., 2019). Beta burst activity in frontal areas has also been shown to correlate with movement cancellation (Enz et al., 2021; Hannah et al., 2020; Wessel, 2020) and recent studies show that activity at the motor unit level also occurs in a transient manner, which is time-locked to sensorimotor beta bursts (Bräcklein et al., 2022; Echeverria-Altuna et al., 2022).

Although beta burst rate has been shown to carry significant information, it still comprises a rather simplistic representation of the underlying activity. Every burst can be characterized by a set of TF-based features: the burst peak time and peak frequency, as well as its duration and its span in the frequency axis (Zich et al., 2023). In turn, all these descriptors are extracted using a particular TF transformation and constitute simpler representations of the more complex burst waveform that is embedded in the raw signals, and which is characterized by a stereotypical average shape with large variability around it (Szul et al., 2023). The waveform features are neglected in standard BCI approaches, because conventional signal processing methods generally presuppose sustained, oscillatory and stationary signals, and are thus inherently unsuitable for analyzing transient activity (Donoghue et al., 2021).

In line with the classically described ERD and ERS phenomena, the non-invasive BCI community still heavily relies on signal power as the target feature for classification, although, notably, state of the art Riemannian classifiers (Barachant et al., 2013, 2012; Congedo et al., 2017) and some deep learning approaches (Kwon et al., 2020; Roy et al., 2019) have independently moved on from explicitly using frequency-specific power features. In this article we propose a shift in perspective, by demonstrating how beta band activity during MI tasks is modulated in terms of patterns of distinctly shaped bursts that are better descriptors of transient activity changes.

We have previously argued that analyzing beta burst activity should enable us to gain access to classification features that are at least as sensitive as beta band power (Papadopoulos et al., 2022). If this hypothesis is valid, then we should be able to test it and verify it using publicly available datasets. Here, we attempt to understand which features of the beta band activity are most informative of MI and how they can improve BCI decoding. These two goals are tightly connected because the long-term objective of improving decoding requires a good understanding of the targeted brain markers. However, since there exist multiple, possibly complementary representations of the beta band activity, we choose to adopt a BCI-first approach so as to assess the relevance of the different representations.

We show that our approach allows us to achieve better classification results than those obtained when assessing signal power in binary MI classification tasks, when comparing burst features to signal power from EEG. To do so, we explore multiple beta burst activity representations and validate our approach against six open EEG BCI datasets analyzing only the activity of channels C3 and C4. This choice allows us to reduce the computational complexity of the analysis and instead to focus on examining these representations, providing links between the decoding performance and the modulation of the different features considered for classification across datasets and subjects. Although our results obtained by using beta burst features are in most cases inferior to state-of-the-art, namely because our analysis only included two channels and focused solely on the beta frequency band, they are, conversely, superior to those obtained using only beta band power in these channels. This analysis demonstrates the utility of beta burst analysis for BCI and paves the way to improve classification performance in the near future.

3.1.3. Approach

3.1.3.1. Datasets

We used six open EEG MI datasets: BNCI 2014-001 (Tangermann et al., 2012), BNCI 2014-004 (Leeb et al., 2007), Cho 2017 (Cho et al., 2017), MunichMI (Grosse-Wentrup 2009) (Grosse-Wentrup et al., 2009), Weibo 2014 (Yi et al., 2014) and Zhou 2016 (Zhou et al., 2016), all available through the MOABB project (Jayaram and Barachant, 2018). Briefly, all datasets contain recordings of subjects who were required to perform sustained MI following the appearance of a visual cue on a screen. During the task corresponding to the BNCI 2014-001 dataset one of four cues instructing to perform “left hand”, “right hand”, “foot” or “tongue” imagery was randomly presented in succession over multiple blocks of trials. In the experimental paradigms corresponding to the BNCI 2014-004, Cho 2017 and MunichMI (Grosse-Wentrup 2009) datasets only two imagery instructions (“left hand” and “right hand”) were randomly presented during each block of trials. Six kinds of MI tasks were performed in the paradigm of Weibo 2014 dataset, that is “left hand”, “right hand”, “feet”, “both hands”, “left hand combined with right foot” and “right hand combined with left foot”, randomly presented during the course of multiple blocks of trials. Finally, “left hand”, “right hand” and “foot” were the randomly interleaved instructions over multiple blocks of trials in the paradigm corresponding to the Zhou 2016 dataset. For our analysis we only considered trials corresponding to the “left hand” or “right hand” classes.

3.1.3.2. Data pre-processing

For each dataset, recordings were loaded per subject using the MOABB python package (v0.4.6) MotorImagery class, and were filtered with a low pass cutoff of 120 Hz (zero-phase FIR filter designed with the windowed approach and transition bandwidth of 25% of the low pass frequency). The low pass cutoff was set to 95 Hz for the Weibo 2014 dataset, which is below the Nyquist frequency for this dataset, as the corresponding sampling frequency of the recordings is 200 Hz. For most of these datasets numerous channels are available, so we defined a subset of channels over the sensorimotor cortex that we deemed relevant for the task and applied pre-processing (Table 3.1.1). Then, in this work, we only analyzed data from channels C3 and C4. Each trial was aligned to the cue onset, and the task period was defined as the time between cue onset and the end of the MI task. We used the time window within one second prior to the cue onset as the baseline period (Table 3.1.1). In the case of the Cho 2017 and MunichMI (Grosse-Wentrup 2009) datasets we noted the presence of noise at approximately 25 – 30 Hz that interferes with the burst detection step. We therefore included an extra pre-processing step involving a custom implementation of the meegkit python package (v0.1.3, dss_line function) (de Cheveigné, 2020) to remove these artifacts. Considering only this subset of sensorimotor channels and all recording periods, we rejected trials using the autoreject python package (0.4.0) (Jas et al., 2017) (Table 3.1.1).

Dataset	# Subjects	(# total channels) Channels used for pre-processing	min – max # trials over subjects (# after trial rejection)	Baseline period (s)	Task period (s)	Post-task period (s)	References
BNCI 2014-001	9	(22) "FC3", "FCz", "FC4", "C3", "Cz", "C4", "CP3", "CPz", "CP4"	288 (207 – 287)	-1.0 – 0.0	0.0 – 4.0	4.0 – 5.5	Tangermann et al., 2012
BNCI 2014-004	9	(3) "C3", "Cz", "C4"	680 – 760 (269 – 621)	-1.0 – 0.0	0.0 – 4.5	4.5 – 6.5	Leeb et al., 2007
Cho 2017	49	(64) "FC3", "FCz", "FC4", "C3", "Cz", "C4", "CP3", "CPz", "CP4"	200 – 240 (77 – 240)	-1.0 – 0.0	0.0 – 3.0	3.0 – 5.0	Cho et al., 2017
MunichMI (Grosse-Wentrup 2009)	10	(13) “111”, “112”, “113”, “114”, “43”, “21”, “63”, “22”, “44”, “119”, “120”, “121”, “122”	300 (167 – 299)	-1.0 – 0.0	0.0 – 7.0	7.0 – 9.0	Grosse-Wentrup et al., 2009
Weibo 2014	10	(60) "FC3", "FCz", "FC4", "C3", "Cz", "C4", "CP3", "CPz", "CP4"	140 – 160 (32 – 160)	-1.0 – 0.0	0.0 – 4.0	4.0 – 5.0	Yi et al., 2014
Zhou 2016	4	(64) "FC3", "FCz", "FC4", "C3", "Cz", "C4", "CP3", "CPz", "CP4"	290 – 319 (167 – 289)	-1.0 – 0.0	0.0 – 5.0	5.0 – 7.0	Zhou et al., 2016

Table 3.1.1: Attributes of the datasets used in the study.

3.1.3.3. Identification of channel-specific beta band and burst detection

Each subject’s full recordings (from the beginning of the baseline period to the end of the post-task period as indicated in table 1) were first transformed in the TF domain from 1 to 43 Hz using the superlets algorithm (parameters: o_min = 1, o_max = 40, c = 4) (Moca et al., 2021) with a frequency resolution of 0.5 Hz. We selected the superlets algorithm over other more commonly used methods as it allows us to obtain a more optimal trade-off between temporal and spectral resolution, and because it has been shown to yield better classification results compared to other approaches (Bârzan et al., 2022). Before proceeding with any further analysis we trimmed 200 to

250 ms from the beginning and end of the epoched data in order to exclude any edge effects introduced by the TF transform.

The power spectral density (PSD) of the baseline period was then computed by averaging the resulting TF matrices over the temporal dimension for each trial and channel of a given subject. Based on the distributions of the PSD peaks we attributed the peaks of the power spectra to either the mu (peaks below 15 Hz) or beta (peaks between 15 and 30 Hz) frequency band and proceeded by analyzing activity in the beta band.

Using a previously published iterative, adaptive procedure, we identified bursts within the beta frequency range from each TF matrix. Briefly, this procedure identifies the highest amplitude of the TF matrix as a burst and models this burst by a 2D Gaussian. The Gaussian is then subtracted from the TF matrix, and the procedure is repeated using the residual until no peak in the TF matrix exceeds the noise floor (2 SDs across all time and frequency bins). Finally, the algorithm extracts the waveforms of the detected bursts from the ‘raw’ time series (after low pass filtering as pre-processing) within a fixed time window of 260 ms, centered on the burst peak (Szul et al., 2023) (figure 1 of the referenced article). Due to inability to parameterize spectra from all datasets we subtracted twice the standard deviation of the TF before fitting each peak as a 2D Gaussian instead of subtracting the aperiodic activity from the TF matrices (Brady and Bardouille, 2022; Rodriguez-Larios and Haegens, 2023; Szul et al., 2023), before detecting beta bursts.

3.1.3.4. Feature extraction based on patterns of burst rate modulation

Beta burst waveform analysis was performed for each dataset by aggregating detected bursts across subjects and experimental conditions (“left hand” or “right hand”) (Figure 3.1.1). This allowed us to create a matrix of burst waveforms by combining all detected bursts per subject, after robust scaling (scikit-learn package (Pedregosa et al., 2011), v1.0.2), a normalization technique robust to the presence of outliers, based on removing the median and scaling according to the quartile range. This representation of burst waveforms is suitable for applying a dimensionality reduction technique in order to better understand the variability in the recorded beta burst shapes. For the remaining of the analysis, we only considered channels C3 and C4, or equivalently channels 43 and 44 for the MunichMI (Grosse-Wentrup 2009) dataset whose naming convention for the recording channels is not based on the 10–20 system.

Previous work from our group has demonstrated that principal component analysis (PCA) (Shlens, 2014) (scikit-learn package, v1.0.2) can be used to understand how the rates of bursts with different waveforms are modulated during reaching movements (Rayson et al., 2023; Szul et al., 2023). In order to construct features suitable for classification, we projected the detected bursts along each principal component. As such, each burst was associated with a specific score along each dimension of the C-dimensional space, representing the distance of the burst’s waveform from the average waveform of all bursts, along this dimension. Because of the scarcity of bursts with extreme scores, we winsorized scores outside of the 2nd and 98th percentile of their distribution. For each component, we then discretized the bursts into groups of bursts within equally spaced score ranges, thus grouping bursts with similar waveforms along that dimension. Since each burst occurs in a specific point in time, following this procedure all bursts were represented in a subspace spanned by the dimensions of scores and time. In other words, for each

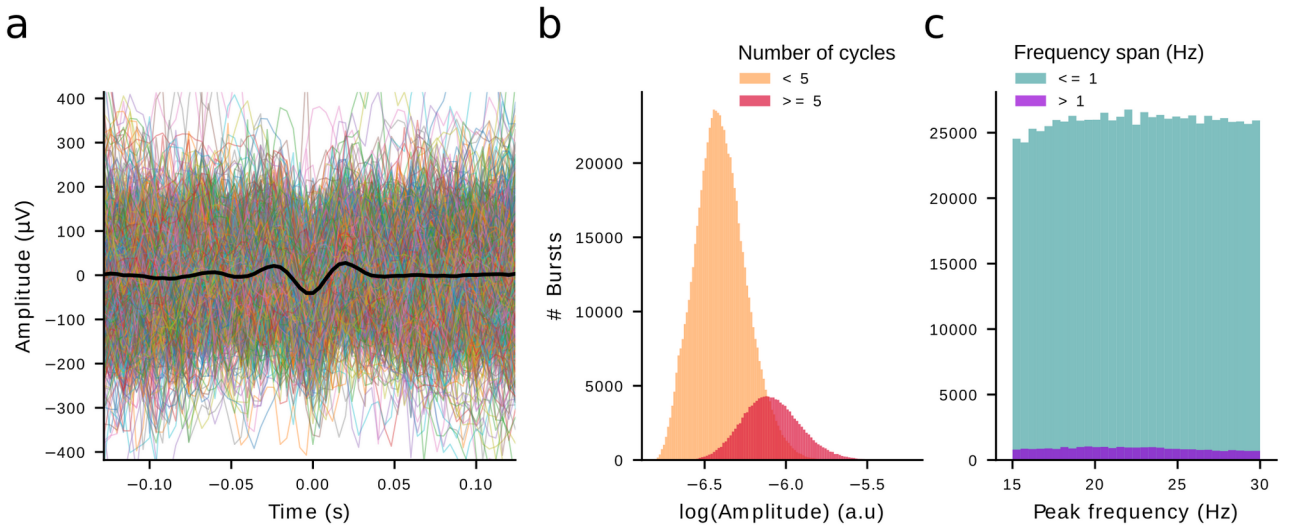


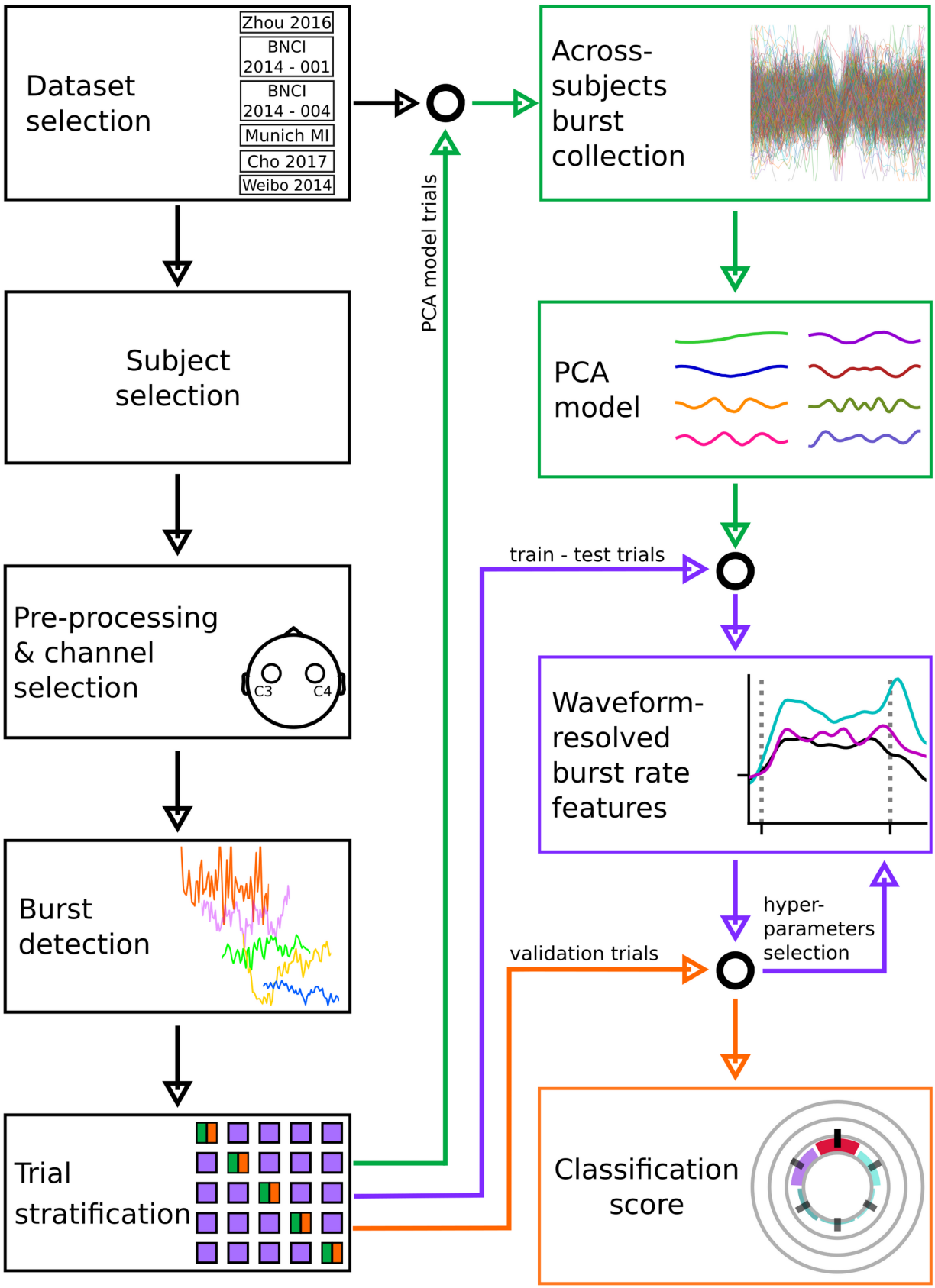
Figure 3.1.1: Burst waveforms corresponding to the recordings of all subjects of the Zhou 2016 dataset. **(a)** This collection of bursts contains raw, aligned signal waveforms of 260 ms duration. The black trace represents the average waveform over all beta bursts. Colored traces correspond to a randomly drawn subset of waveforms (0.2% of all bursts). **(b)** Distribution of the TF amplitude of bursts as computed by the superlets transform, grouped according to burst duration in terms of cycles. The burst detection algorithm identifies a wide range of bursts with amplitudes spanning more than one order of magnitude. The majority of detected beta bursts are low-power, short lasting events. **(c)** Distribution of the peak frequency grouped by the frequency span of each burst. Most of the beta bursts have a narrow frequency span, and are uniformly distributed across the analyzed range of frequencies.

principal component we generated a representation of burst rate as a function of waveform shape.

3.1.4. Classification

We performed the classification per subject of each dataset by examining six representations of the beta band activity: the waveform-resolved burst rate, the overall burst rate, a combination of the TF-based characteristics that describe bursts in terms of the modeled 2D Gaussians, the TF-based burst peak amplitude, the TF-based burst volume and finally the beta band power. In all cases, we only analyzed the activity of channels C3 and C4 during the task period.

In order to select an appropriate number of components C and burst groups G that would allow us to have unbiased classification results for the beta burst waveform-based features, we used a nested cross validation approach. For each subject, we first randomized the trials' order and split the available trials in m = 5 strata. Then, in every iteration of the nested cross validation procedure, one stratum was split in half. The first half was used to sample detected bursts, create the waveform matrix and apply PCA (Figure 3.1.2, green arrows and boxes). Then, the remaining four strata were used as train and test sets to explore the hyper-parameter space of C and G and find the configuration that would maximize the expected decoding accuracy (Figure 3.1.2, purple arrows and boxes). We did so by computing the waveform-resolved burst rate of each trial in non-overlapping 100 ms windows using a repeated (n = 100), 5-fold cross validation approach,


Dataset selection
Zhou 2016
BNCI 2014 - 001
BNCI 2014 - 004
Munich MI
Cho 2017
Weibo 2014
Subject selection
Pre-processing & channel selection
C3
C4
Burst detection
Trial stratification
PCA model trials
Across-subjects burst collection
PCA model
train - test trials
Waveform-resolved burst rate features
hyper-parameters selection
validation trials
Classification score

(← continues from previous page) **Figure 3.1.2:** Flowchart illustrating the steps of the proposed, waveform-resolved burst rate analysis. For each dataset, we iteratively pre-processed the data of each subject, rejecting trials and keeping only channels C3 and C4. The burst detection algorithm was run on the raw signals of these two channels. We then split the remaining trials of each subject in three sets using a nested, 5-fold cross validation approach. The first set was used only to sample bursts and create the corresponding PCA model combining data from all subjects of any given dataset (PCA model trials, indicated by the green boxes and arrows). The second set was used as the training and testing set of trials, in order to select the best model of waveform-resolved features, in terms of decoding score, through a repeated cross validation procedure (train-test trials, purple boxes and arrows). Finally, the third set of trials served the role of the validation trials for the previously selected model (validation trials, orange boxes and arrows), based on which the classification scores were computed.

shuffling the trials during each repetition. In order to avoid configurations with imbalanced trial-to-features ratio that could lead to overfitting, we restricted our analysis by iterating over a number of principal components (from 1 to 8) and groups (from 2 to 9). Finally, after estimating the optimal C and G hyper-parameters, we tested this configuration on the remaining half of the originally mentioned stratum, which constituted the validation trials (Figure 3.1.2, orange arrows and boxes). The reported results in the Main results section reflect the average score obtained after iterating over all strata.

In order to compute the overall beta burst rate we only considered bursts with an amplitude equal to or higher than the 75th percentile of the TF amplitude distribution of all bursts, a threshold commonly used when detecting beta bursts with alternative methods (Khawaldeh et al., 2020; Lofredi et al., 2018; Tinkhauser et al., 2017a, 2017b; Torrecillos et al., 2018). Beta bursts were treated as point processes and the burst rate for each subject and trial was computed by counting the number of bursts occurring in non-overlapping 100 ms long time windows.

The classification features of the combination of the TF-based characteristics, TF-based burst peak amplitude and TF-based burst volume were based on the distributions of the corresponding values as returned by the burst detection method. We explored various possible ways to group burst waveforms and compute the corresponding burst rate of each group in a way analogous to the waveform-resolved burst rate, but this time based on the distributions of TF characteristics (Sup. Figure 3.1.1).

Finally, beta band power was computed per subject and trial. Raw recordings were first band-pass filtered using the same beta frequency range (15 – 30 Hz) used for selecting beta bursts. Then, the squared envelope of the Hilbert transform of the filtered signals was computed and used as classification feature, using a repeated (n = 100), 5-fold cross validation approach.

All classification results were obtained by using LDA as a classifier (scikit-learn, v1.0.2). We estimated the classification score based on the area under the curve (AUC) of the receiver operating characteristic (scikit-learn, v1.0.2). All numeric computations were based on the numpy python package (v1.21.6; (Harris et al., 2020)), an environment running python (v3.10). We compared trial-level classification results of the waveform-resolved burst features to the beta band power features using a generalized linear mixed model with a binomial distribution and logit link function with correct classification of each trial as the dependent variable, the type of classification feature as a fixed effect, and the subject nested within the dataset as random intercepts. We also compared classification results of the waveform-resolved burst features to the rest of the burst

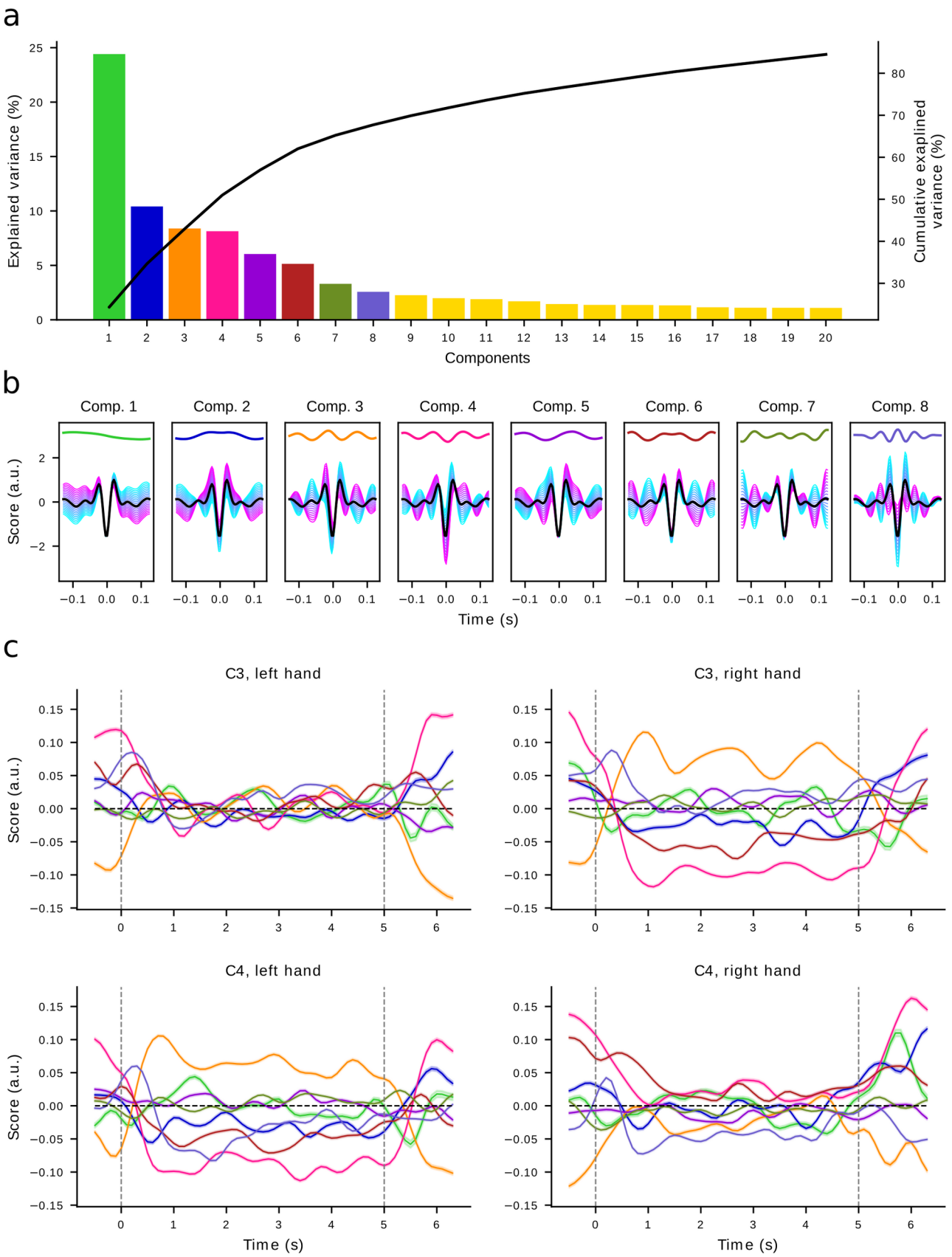


Figure 3.1.3: PCA applied on all detected bursts of the Zhou 2016 dataset. Principal components describe the variability of burst waveforms. **(a)** Ratio of explained variance and cumulative explained variance for the

(← continues from previous page) first 20 components. **(b)** The first 8 components define orthogonal axes of waveform shape alteration with respect to the average waveform (black trace). Each subplot depicts one component (color code as in a), the mean waveform (black trace), and simulated waveform alterations along each component, spanning a continuous space from negative (cyan traces) to positive (magenta traces) scores. **(c)** Average score and standard error of all waveforms along each component during the three periods of the epoched data for the first 8 components (color code as in **a**) for each condition and channel. During the baseline and post-task periods (signified by the vertical dashed lines), waveforms deviate from the average waveform (score equal to 0) mainly along the third and fourth dimension ipsilaterally, while contralaterally the deviation is more pronounced during the task period.

features using a similar model. Statistical analyses were conducted using R (v4.1.2) and lme4 (v1.1-31; (Bates et al., 2015)). Fixed effects were assessed using type II Wald X^2 tests using car (v3.1-1; (Fox and Weisberg, 2019)). Pairwise Tukey-corrected follow-up tests and effect size computations were carried out using estimated marginal means from the emmeans package (v.1,8,7; (Lenth, 2023)).

3.1.5. Main results

We used six open MI EEG datasets for the purpose of examining the explanatory value of beta burst activity as a feature for BCI classification. For each dataset, we detected beta bursts in a subset of channels over the sensorimotor cortex under two conditions, “left hand” and “right hand” MI. Based on the bursts detected in channels C3 and C4 of each subject, we built dataset-specific burst representations which capture the variability of the burst waveforms (Figure 3.1.1) (see 3.1.3 Approach).

3.1.5.1. Beta bursts with distinct waveforms are characterized by different modulation patterns

We used PCA to explain the variability of the burst waveforms of each dataset (number of components explaining 99% of variance). This method allowed us to reduce the dimensionality of the burst waveform space, with each resulting dimension being a linear combination of the burst waveforms that emphasizes specific time points that best describe the waveform variability (Figure 3.1.3 a) and along which the waveforms vary. The projection of a burst waveform along each component, associates this waveform with a score, a value that indicates its similarity to the average waveform of all bursts along that dimension.

We simulated how each component alters the waveform with respect to the average by varying the score along each dimension, adding the weighted eigenvector to the mean waveform (Figure 3.1.3 b) in order to understand how the burst waveform is modulated by the first 8 components. For example, the first component represents a trend that describes how the waveforms are temporally skewed. Components 5, 6 and 7 mainly capture the variability along the flanks of the waveform, whereas components 2, 3 and 4 describe changes of the central negative deflection.

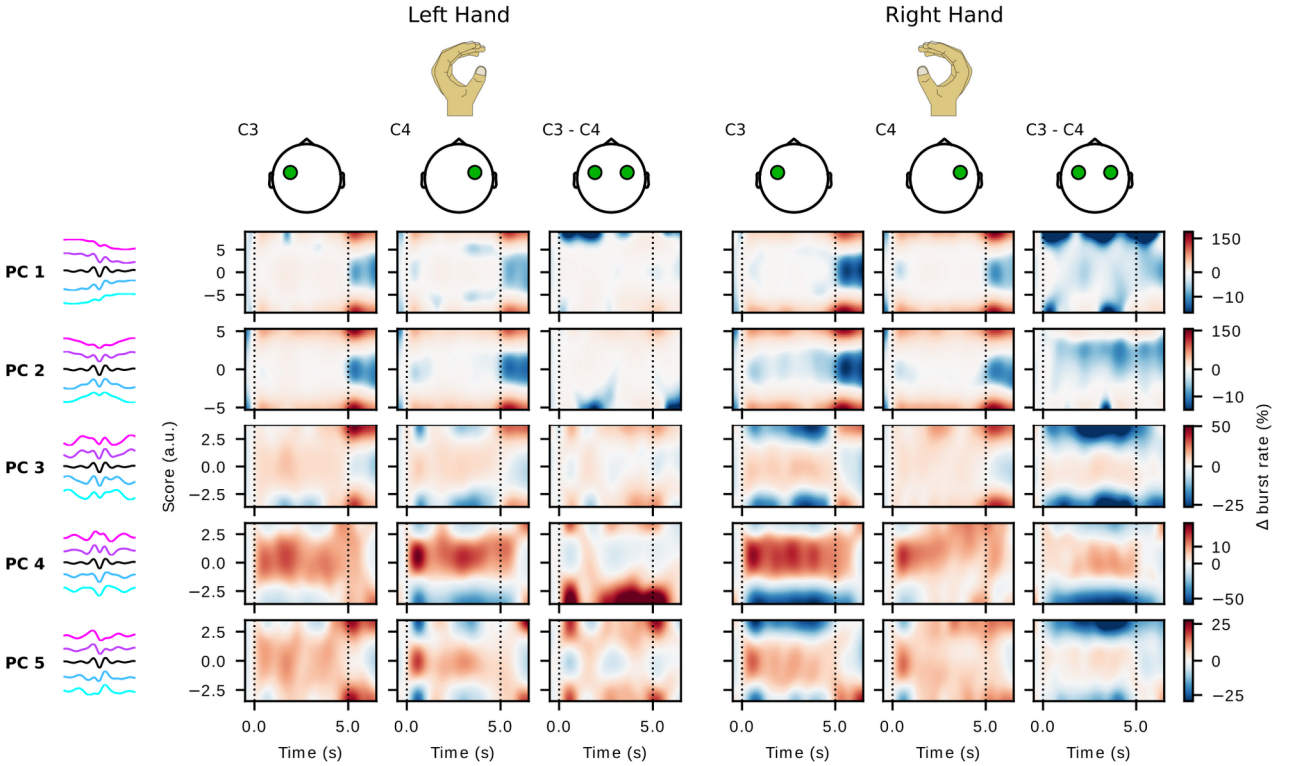


Figure 3.1.4: Trial-averaged, baseline-corrected burst rate along different components for a representative subject (Zhou 2016, S1). The first column depicts how burst waveforms vary independently along each component (components as depicted in Figure 3.1.3). Negative scores correspond to the cyan traces, and positive to the magenta traces. The average waveform is represented by the black trace. During “left hand” trials, burst rate varies per component for channels C3 and C4 and the difference of the two channels. During the task period, both channels exhibit various degrees of burst rate increase for bursts whose waveforms resemble the average along any principal component. Waveforms lying further from the average along component 3 and more prominently 4 are characterized by a reduction of burst rate contralaterally, in channel C4. Similar patterns arise for the “right hand” trials. Component 5 is characterized by an ipsilateral increase and a contralateral decrease of ‘positive outlier’ waveforms. During the post-task period a burst rate increase for specific waveforms is observed, mainly seen along components 1 and 2.

For each condition, channel and component we computed the average score of all bursts from the baseline to the post-task period using non-overlapping 100 ms windows, and applied a Gaussian smoothing kernel with a standard deviation of 2 windows (scipy package (Virtanen et al., 2020), v1.11.3, ndimage.gaussian_filter1d function). Burst scores in specific components were modulated to different extents within the three trial periods: baseline, task and post-task period (Figure 3.1.3 c). This means that, on average, bursts with different waveforms occurred more or less frequently within specific trial periods (e.g. component 4). However, a change in mean waveform shape is ambiguous with respect to the underlying mechanism: e.g. over the contralateral motor cortex there was a pronounced decrease in score along component 4 during the task, but this could be due to a reduction in the rate of bursts with positive scores, an increase in the rate of bursts with negative scores, or a combination of the two.

To better understand the rate modulation of bursts with distinct waveforms along each component over all experimental periods, we visualized the trial-averaged, baseline-corrected burst rate as a

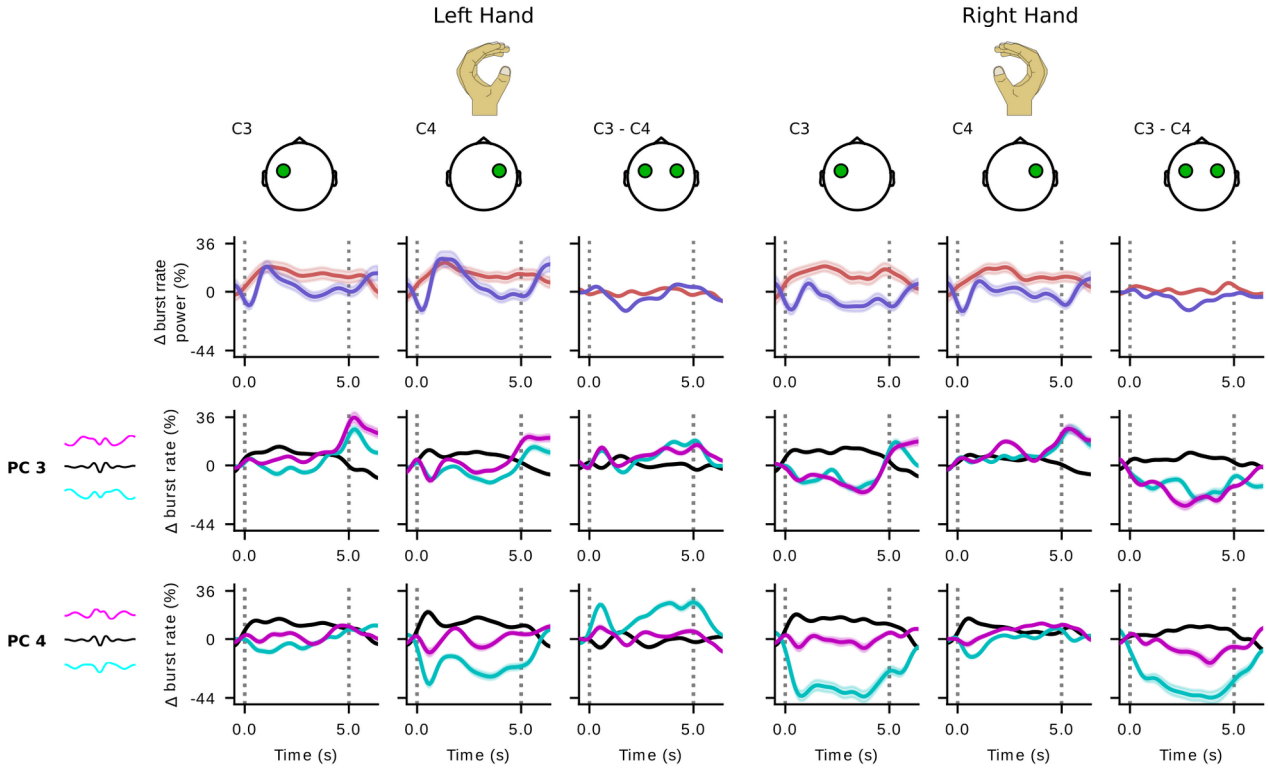


Figure 3.1.5: Trial-averaged, baseline-corrected overall burst rate, beta band power and overall burst rate modulation of three burst groups along components 3 and 4 for a representative subject (Zhou 2016 dataset, S1). For both conditions and channels, beta band power changes (purple trace) roughly track the overall burst rate modulation (red trace). Burst rate modulation for different burst groups varies per condition, channel and component. The differential modulation of burst rate is particularly pronounced contralaterally, in channel C4 during “left hand” trials and channel C3 during “right hand” trials along the fourth component. A clear distinction between conditions is evident when comparing the difference of rate modulation of the two channels for each waveform group.

function of time and component score, for the first five components of a representative subject (Figure 3.1.4; Zhou 2016 dataset, S1). In this particular case there were differences in burst rate modulation between channels C3 and C4, as well as between the two experimental conditions.

During the task period there was a decrease in the rate of bursts with large positive or negative scores along component 4 on the contralateral channel for either condition. These patterns correspond to bursts whose waveforms resemble the corresponding magenta and cyan traces. The lateralization of beta burst rate modulation is further exemplified when visualizing the difference between the two channels. The comparison of these differences across the two conditions, reveals that all components and especially components 3, 4 and 5 encode disparities between the “left hand” and “right hand” conditions, and could therefore constitute informative features for a classifier. Interestingly, some components define axes along which the waveform-resolved burst rates describe post-task period modulations, as is particularly evident for either condition in components 1 and 2.

3.1.5.2. Beta band burst features outperform beta band power in binary classification tasks

After establishing the lower dimensional space for projecting the burst waveforms, we binned the scores axis into several groups per component (Figure 3.1.5) using a nested cross validation procedure, and analyzed the average burst rate per group (see 3.1.3 Approach). The average burst rate for each group during the task period within each of the two channels was then used as a feature for an LDA classifier, resulting in C × G × 2 features per experimental condition, where C is the number of components and G is the number of groups, and, e.g. in the two bottom lines of figure 5 we visualize what would correspond to C = 2 and G = 3 when averaging over trials. In order to validate our hypothesis, we compared classification results based on this method against results based on alternative features: the overall beta burst rate for bursts detected in channels C3 and C4 and whose amplitude is greater than a threshold (the 75th percentile of the dictionary's TF amplitude distribution); TF-derived descriptions of bursts, and band power in the beta frequency (see 3.1.3 Approach).

For each dataset we present the across-subject average results estimated with each method, as well as the results for each participant (Figure 3.1.6 a, Sup. Figure 3.1.2). At the dataset level, the waveform-resolved burst rate features yield decoding results that are equivalent or better than the results obtained by analyzing beta band power, or alternative beta band representations. These representations bear analogous results in each dataset. We emphasize, though, that the results are highly variable across subjects. For example, for subject S1 of the Zhou 2016 dataset beta power does not hold much explanatory value, unlike beta burst rate, beta burst amplitude or the waveform-resolved burst rate. This is not true for subject S4 of the BNCI 2014-004 dataset: all representations yield similarly good results, except for the waveform-resolved burst rate that outperforms the rest (Sup. Figure 3.1.2).

After obtaining these results we proceeded to quantify the statistical significance of the observed differences for each classification feature set. In order to test the explanatory value of the waveform-resolved burst rate against beta band power we analyzed the decoding results using a generalized linear mixed model (see 3.1.3 Approach). The waveform-resolved burst rate features are significantly better than beta band power features ($X^2(1) = 21.384$, $p < 0.001$) (Figure 3.1.6 b). We also compared the waveform-resolved burst rate against the rest of the examined beta band representations and verified that it yields the highest classification accuracy ($X^2(4) = 242.95$, all pairwise $p < 0.001$) (Figure 3.1.6 b). Finally, we estimated the effect size for all pairwise comparisons using Cohen's d as a metric. We found a small effect size for the contrast between waveform-resolved burst rate and beta band power ($d = 0.10$) as well as beta burst rate ($d = 0.18$), and moderate effect sizes for the rest of the comparisons ($d = 0.25$ for TF-based burst peak amplitude and TF-based burst characteristics, $d = 0.30$ for TF-based burst volume) (Figure 3.1.6 b). In conclusion, we confirmed our hypothesis that waveform-resolved beta burst activity holds promise to improve BCI performance, especially if further optimized so that it can be analyzed online and take into account multiple recording channels.

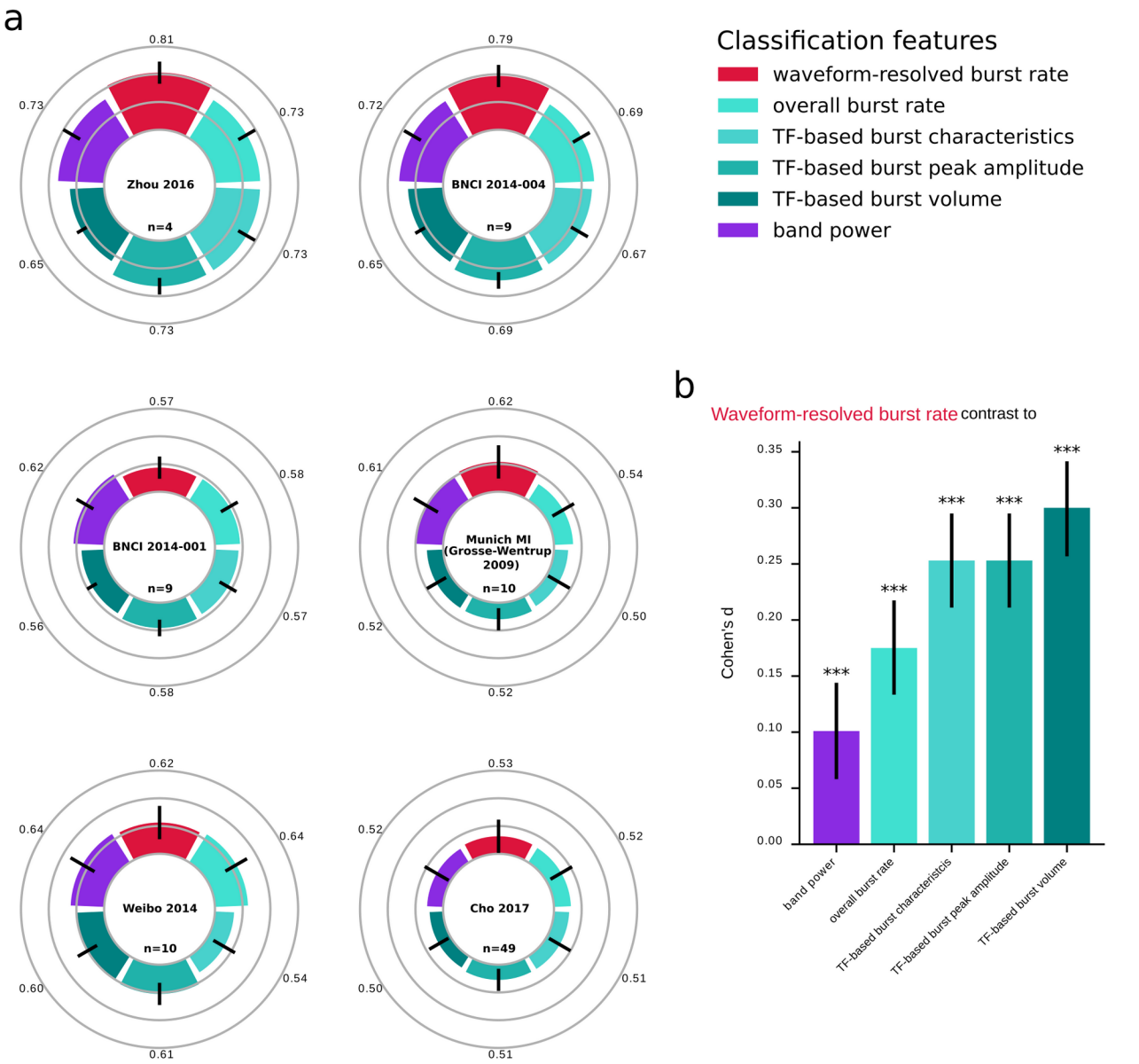


Figure 3.1.6: (a) Population average results for binary “left hand” vs “right hand” classification per dataset included in the analysis. The waveform-resolved burst rate features outperform or are on par with beta band signal power and all alternative beta burst representations across datasets. **(b)** Classification features based on burst waveform-resolved burst rate yield, on the population level across all datasets, significantly better results that those obtained using TF-derived burst features, or beta power from channels C3 and C4 (all pairwise $p < 0.001$, indicated by $***$). Small ($d < 0.2$) or moderate effect sizes ($d < 0.5$), as measured by Cohen’s d, characterize all pairwise comparisons of the waveform-resolved burst rate to the rest of the beta band representations.

3.1.6. Significance

In this study, we showed for the first time that the waveform-specific beta burst rate is a representation comparable to beta power within a framework of binary classification MI tasks. In

order to understand which beta burst characteristics are the most informative, we compared multiple representations of beta activity modulation during the MI task. We restricted our analysis to recordings from channels C3 and C4, considering that this activity is representative of modulations happening during such tasks, and showed that bursts of different shapes are selectively modulated following task onset, with distinct waveforms occurring with different probability during different points in time (Szul et al., 2023) (Figures 3.1.4 and 3.1.5). This modulation can be encoded either by TF-derived features, or alternatively, burst waveforms. All of the TF-derived features were equally informative when used as classification features but, like the overall burst rate, they yielded lower decoding performance than waveform-based features, across all datasets.

Previous work has demonstrated that TF-based descriptions of beta bursts fail to explain the full variability of detected burst waveforms (Szul et al., 2023), but unveiled waveform-resolved burst rate modulations during a motor adaptation task in adults and reaching movements in infants and adults alike (Rayson et al., 2023; Szul et al., 2023). Therefore, we hypothesize that beta band activity carries important task-specific information and does not simply reflect inhibitory processes of motor areas, and that waveform-resolved burst rate modulations during either real movements or MI constitute more sensitive markers of cortical patch- and/or laminar-specific brain activity than other beta band representations.

The results presented in this article are based on features of beta bursts detected from only two channels, and are therefore not directly comparable to results of previous studies that have implemented standard designs within the BCI literature (Jayaram and Barachant, 2018; Luiz et al., 2019) and incorporate all available recording channels, do not perform trial rejection, and utilize spatial filtering. However, waveform-based burst rate features are more informative about imagined movements than beta power in channels C3 and C4, in spite of our choice to constrain the analysis to only a few principal components in an attempt to ensure a balanced trial-to-feature ratio when performing the waveform-resolved analysis. In this regard, our analysis is a first step in the direction of establishing a neurophysiologically informed alternative to currently existing methodologies of feature extraction.

Our results rely on aggregating bursts from all subjects across a dataset and using PCA in order to analyze them. By doing so, the dimensionality reduction step is less susceptible to noise and results in the same components for all subjects within a dataset, thus rendering the classification features and decoding results easier to interpret. It is worth noticing that the resulting principal components are quite similar to a Fourier decomposition of the time series, because of the enforced orthogonality between PCA dimensions. This property of PCA imposes restrictions on the resulting components, which makes them also more likely to be similar across datasets, provided that the bursts are similar. In the context of BCI, this decomposition may be suboptimal in the sense that it is unsupervised and does not take into account the class labels. In other words, it ignores potential disparities in burst shapes due to task demands and/or recording sites. However, it can also be seen as an advantage for transfer learning approaches or offline calibration sessions. Indeed, if burst waveforms are stable across participants, datasets and recording sessions, a single PCA model that describes the variability of waveforms should suffice.

An important question is whether this procedure would be suitable for online, real-time decoding. The superlets algorithm, and to a lesser extent the burst detection algorithm, are computationally expensive and increasing the number of recording channels, task duration, and frequency

resolution would make it difficult to employ this analysis online. However, our results show that the burst rate modulations of beta bursts with certain waveforms are more informative of underlying activity changes during MI tasks than those of bursts with other waveforms. These waveforms could be used as kernels and convolved with online recordings to efficiently detect bursts directly in the time domain. If burst waveforms are maintained across recording sessions, the superlets-based burst analysis could be performed during an offline session and its results used for online burst detection during follow-up, online sessions.

Tremendous efforts to improve the reliability of non-invasive BCI have been so far unable to provide solutions that would be acceptable for widely-adopted applications. Ever since the characterization of the event-related synchronization and desynchronization phenomena of mu and beta activity, little effort has been put into revisiting the features that are considered to best capture the underlying brain activity in these BCI paradigms. Growing evidence suggests that beta activity modulations are best described in terms of bursts (Jones, 2016; Little et al., 2019; Lundqvist et al., 2016; Rayson et al., 2023; Shin et al., 2017; Torrecillos et al., 2018; Wessel, 2020). The analysis presented in this study serves as a proof of concept for the proposed methodology, but there is significant potential for improvement in the burst detection and feature creation procedures. Future directions of interest lie in incorporating more advanced spatial filtering with the burst detection technique, and possibly the use of state-of-the-art Riemannian methods, so that we can leverage the activity of more channels within this framework. Finally, another future direction lies in the incorporation of novel neurophysiological markers for the mu frequency band in our framework. A growing number of studies have shown that the activity in this band can occur as longer-lasting bursts (Vigué-Guix and Soto-Faraco, 2023), or non-sinusoidal oscillations (Y. Y. Chen et al., 2021). We believe that by adapting our approach to the characteristics of this frequency band, or by adopting alternative frameworks such as cycle-by-cycle analysis (Cole and Voytek, 2019) we can uncover features that will further help us attain the goal of improving BCI robustness. We believe all these goals to be particularly interesting because they hold the promise of further improving current results and rendering them comparable to state-of-the-art approaches.

Waveform-resolved patterns of burst rate constitute a new way of analyzing beta band activity during MI tasks. The assessment of this method against multiple open EEG datasets shows that this representation is better than conventional power features in terms of classification. This work serves as a first step and opens up numerous directions for further improvements that can potentially ameliorate the reliability of existing, non-invasive BCI technology.

3.1.7. Data availability statements

All data are available via the MOABB project. All scripts necessary for reproducing the results of this article are available at the following public repository: https://gitlab.com/sotpapad/bebopbci. No new data were created or analyzed in this study.

3.1.8. Acknowledgments

This work was performed within the framework of the LABEX CORTEX (ANR-11LABX-0042) of Université de Lyon, within the program ‘Investissements d’Avenir’ (decision n◦ 2019-ANR- LABX-02) operated by the French National Research Agency (ANR). S P, M C, J B and J M are supported by the French National Research Agency (ANR) project HiFi (2020–2024). M S and J B are supported by the European Research Council (ERC) under the European Union’s Horizon 2020 Research and Innovation Programme (ERC consolidator Grant 864550 to J B).

3.1.9. Author contributions

S P, J B and J M conceptualized the manuscript. S P drafted the manuscript and performed the analysis. All authors contributed to manuscript revision, read, and approved the submitted version.

3.1.10. Conflict of interest

All authors declare no competing interests.

3.2 Contribution 3 – Surfing beta burst waveforms to improve motor imagery-based BCI

S. Papadopoulos[1,2,3,*], L. Darmet[1,2,3], M.J. Szul[1,3], M. Congedo[4], J.J. Bonaiuto[1,3,†], J. Mattout[1,2,†]

[1] University Lyon 1, Lyon, France

[2] Lyon Neuroscience Research Center, CRNL, INSERM, U1028, CNRS, UMR5292, Lyon, France

[3] Institut des Sciences Cognitives Marc Jeannerod, CNRS, UMR5229, Lyon, France

[4] GIPSA-lab, University Grenoble Alpes, CNRS, Grenoble-INP, Grenoble, France

[†] These authors contributed equally.

[*] Corresponding author: Sotirios Papadopoulos

E-mail: sotirios.papadopoulos@univ-lyon1.fr

3.2.1. Abstract

Our understanding of motor-related, macroscale brain processes has been significantly shaped by the description of the event-related desynchronization (ERD) and synchronization (ERS) phenomena in the mu and beta frequency bands prior to, during and following movement. The demonstration of reproducible, spatially- and band-limited signal power changes has, consequently, attracted the interest of non-invasive brain-computer interface (BCI) research for a long time. BCIs often rely on motor imagery (MI) experimental paradigms that are expected to generate brain signal modulations analogous to movement-related ERD and ERS. However, a number of recent neuroscience studies has questioned the nature of these phenomena. Beta band activity has been shown to occur, on a single-trial level, in short, transient and heterogeneous events termed bursts rather than sustained oscillations. In a previous study, we established that an analysis of hand MI binary classification tasks based on beta bursts can be superior to beta power in terms of classification score. In this article we elaborate on this idea, proposing a signal processing algorithm that is comparable to- and compatible with state-of-the-art techniques. Our pipeline filters brain recordings by convolving them with kernels extracted from beta bursts and then applies spatial filtering before classification. This data-driven filtering allowed for a simple and efficient analysis of signals from multiple sensors thus being suitable for online applications. By adopting a time-resolved decoding approach we explored MI dynamics and showed the specificity of the new classification features. In accordance with previous results, beta bursts improved classification performance compared to beta band power, while often increasing information transfer rate compared to state-of-the-art approaches.

Keywords: beta bursts, brain–computer interface (BCI), decoding, electro-encephalography (EEG), motor imagery (MI)

3.2.2. Introduction

Time-locked changes in induced power within specific frequency bands, originally described in a number of seminal studies in motor neuroscience (Pfurtscheller, 1981; Pfurtscheller and Berghold, 1989; Pfurtscheller and Lopes da Silva, 1999), have long influenced the way in which we interpret macroscale recordings of brain activity such as those provided by electroencephalography (EEG). These studies have revealed a gradual reduction in brain signal power during an ongoing movement or motor imagery (MI) task in the mu (~ 8 – 12 Hz) (Neuper et al., 2006; Pfurtscheller et al., 2006, 1997; Pfurtscheller and Lopes da Silva, 1999) and beta (~ 13 – 30 Hz) (Pfurtscheller et al., 1997; Pfurtscheller and Lopes da Silva, 1999) frequency bands relative to baseline activity. This phenomenon is termed event-related desynchronization (ERD). The same studies have, moreover, described a relative-to-baseline increase in power in the beta band shortly following the end of the movement or MI (Alayrangues et al., 2019; Neuper et al., 2006; Pfurtscheller et al., 1996), known as event-related synchronization (ERS). These phenomena are especially marked over cortical areas contralateral to the real or imagined movement (Kobler et al., 2020; Little et al., 2019; Makeig et al., 2000; Pfurtscheller and Berghold, 1989; Pfurtscheller and Neuper, 1997; Seeber et al., 2016; Zich et al., 2023) and their topographies approximately match the somatotopic organization of the sensorimotor cortices (Gordon et al., 2023; Natraj et al., 2022; Penfield and Rasmussen, 1950). Taken together, these observations have given rise to the hypothesis that the ERD is an indication of brain processes pertaining to movement preparation and execution while the ERS is an indication of processes related to movement completion (Kilavik et al., 2013).

Given the reproducibility of the spatial and frequency specificity of the ERD and ERS, these neural markers are often exploited by non-invasive BCI applications, especially those that are based on MI paradigms (Jayaram and Barachant, 2018; Tangermann et al., 2012). Such paradigms, designed to reproduce consistent time-locked signal modulations, normally rely on transforming the recordings in the time-frequency domain (TF) (Brodu et al., 2011; Bruns, 2004; Herman et al., 2008) and then applying spatial filtering, most commonly using the common spatial pattern algorithm (CSP) (Blankertz et al., 2007; Koles, 1991; Müller-Gerking et al., 1999). This chain of signal transformations is expected to increase signal-to-noise ratio by extracting signal power in specific time windows and frequency bands of interest, and also to maximize the spatial disparity among different MI classes (e.g. “left” or “right” hand, or “feet”), thus improving classification results and/or allowing for decoding of multiple commands with distinct signal features (Lotte, 2014; Lotte et al., 2018a).

Although the ERD and ERS are consistently observed across subjects and recording modalities, their nature is not clear. Based on the assumption of amplitude modulation of sustained oscillations, these patterns are the result of signal power averaging in the TF domain over multiple trials. However, converging evidence suggests that, on the contrary, beta band activity occurs in short events termed bursts (Coleman et al., 2024; Jones, 2016; Little et al., 2019; Lundqvist et al., 2024, 2016; Shin et al., 2017; Torrecillos et al., 2018; Wessel, 2020; West et al., 2023) on the single trial level, therefore questioning the functional role of ERD and ERS altogether, at least within the beta band. Beta burst rate has been shown to be more behaviorally relevant in motor processes (Enz et al., 2021; Hannah et al., 2020; Little et al., 2019; Rayson et al., 2023; Soh et al., 2021; Szul et al., 2023; Wessel, 2020) than averaged beta band power. Additionally, recent studies have shown that beta bursts are not a unitary phenomenon but rather constitute heterogeneous

events (Szul et al., 2023) with different functions, alluded to by the differential modulation of their rate and shape depending on task conditions (Langford et al., 2023; Papadopoulos et al., 2024) or movement phase (Rayson et al., 2023; Szul et al., 2023). As such, beta bursts have the potential to be a more sensitive marker of brain processes during real or imagined movements on the single trial level.

To test this hypothesis, in a previous study we examined six open, benchmark MI EEG datasets, which we also analyzed here. In that study, we analyzed the activity of channels C3 and C4 during binary classification tasks of hand MI i.e., “left” vs “right” hand under the assumption that beta burst activity modulations during MI should resemble those observed during real movements of the upper limbs. We demonstrated that the waveform-resolved beta burst rate is superior to beta band power changes and alternative beta burst representations in terms of classification (Papadopoulos et al., 2024). Briefly, we adopted a nested cross validation approach in order to identify the optimal waveforms for maximizing classification score. This was done by first iterating over different data samples, finding multiple beta burst waveforms from each sample, then treating each distinct waveform as a point process and computing the corresponding burst rate. The best (in terms of classification score) combination of waveform-specific burst rates was then selected based on cross validation, before being tested on a previously unseen validation sample in each iteration of the nested cross validation. The major limitation of that study was the algorithm’s computational complexity, which was unsuitable to be potentially translated to real-time implementations, and also compelled us to restrict the analysis only to channels C3 and C4 assuming that they capture brain signal modulations that are relevant to the task.

In this article we streamline our approach. We develop an algorithm that is computationally efficient and can analyze an arbitrary number of recorded signals thus being comparable to state-of-the-art techniques. Beta burst waveforms, whose rate is expected to be maximally modulated during the trial period compared to baseline, are identified in calibration data. These bursts are used as data-driven kernels that filter the signals from all recording channels in the time domain. The convolved signals are then spatially filtered with CSP and the spatial features are used as classification features. We re-analyze the activity during “left” and “right” hand MI of the same open EEG datasets and also a recently-published composite EEG dataset, now in a time-resolved fashion. We show that classification features based on waveform-resolved beta burst rate offer better decoding performance and improve the decoding speed versus accuracy trade-off when compared to standard band-limited, power-based classification features.

3.2.3. Methods

3.2.3.1. Datasets

We analyzed the recordings of six open EEG MI benchmark datasets available through the MOABB (Aristimunha et al., 2023; Jayaram and Barachant, 2018) project: BNCI 2014-001 (Tangermann et al., 2012), BNCI 2014-004 (Leeb et al., 2007), Cho 2017 (Cho et al., 2017), Munich MI (Grosse-Wentrup 2009) (Grosse-Wentrup et al., 2009), Weibo 2014 (Yi et al., 2014) and Zhou 2016 (Zhou et al., 2016), and the recordings of a composite open EEG dataset that became

recently available (Dreyer et al., 2023) referred to hereafter as Dreyer 2023. All datasets comprise a number of subjects with recordings corresponding to multiple trials of two or more randomly chosen, sustained kinesthetic MI commands, each performed following the appearance of a visual cue on a screen (Table 3.2.1). For our analysis we only considered trials corresponding to the “left hand” or “right hand” classes.

3.2.3.2. Pre-processing

The epoched recordings of each subject were loaded using the MOABB python package (v0.4.6, class LeftRightImagery; parameters: tmin and tmax as indicated in Table 3.2.1), and were filtered with a low pass cutoff of 120 Hz (parameters: fmin = 0, fmax = 120; default MNE (Gramfort et al., 2013) zero-phase FIR filter designed with the windowed approach and transition bandwidth of 25% of the low pass frequency). Because the sampling frequency of the Weibo 2014 recordings is 200 Hz, we set the low pass cutoff to 95 Hz for this dataset. Finally, we used the autoreject python package (Jas et al., 2017) (v0.4.0, function get_rejection_threshold, default parameters) in order to remove noisy trials.

3.2.3.3. Burst detection and kernel selection

In order to select kernels for convolving the data from all channels we first detected bursts, after applying the pre-processing steps described above within a dataset-specific cluster of channels above the sensorimotor cortex (Papadopoulos et al., 2024). We applied a time-frequency (TF) decomposition in the 1 – 43 Hz range on each selected channel separately, using the superlets algorithm (Moca et al., 2021) (parameters: o_min = 1, o_max = 40, c = 4) with a frequency resolution of 0.5 Hz. We noted narrow-band, high-power artifacts at approximately 25 – 30 Hz when inspecting the TF of the Cho 2017, Dreyer 2023 and Munich MI (Grosse-Wentrup 2009) datasets, possibly attributable to power-line sub-harmonics or some other source of electronic interference. This noise interferes with the burst detection step, therefore, we included an extra pre-processing step, prior to trial rejection, based on a custom implementation of the ZapLine algorithm (de Cheveigné, 2020) from the meegkit python package (v0.1.3, dss_line function) to remove these artifacts (Sup. Figure 3.2.1).

Then, we detected bursts within the beta frequency range (15 – 30 Hz) from each TF matrix channel and used their temporal location to extract their waveforms from the raw time series within a fixed time window of 260 ms as described in detail in Szul et al. (2023) and adapted for the analyzed datasets in Papadopoulos et al. (2024). In summary, the burst detection algorithm iteratively identifies the highest amplitude of a TF matrix and models it as a two-dimensional Gaussian taking into account the full-width at half-maximum (FWHM) of the peak amplitude along the dimensions of time and frequency. Then, the time point of the burst’s peak amplitude is used to look for the centering point of each waveform in the low-passed EEG signal. This corresponds to the signal’s minimum phase point around the peak provided that it occurs within 30 ms prior to or following this peak. Based on the FHWM of the average lagged coherence value across the beta frequency band, a time window of 260 ms is used to extract the burst waveform. Finally, the 2D

Dataset	# Subjects	# Channels	# Trials	Baseline period (s)	Task period (s)	Post-task period (s)
BNCI 2014-001	9	22	288 217 – 288 (243)	-1.0 – 0.0	0.0 – 4.0	4.0 – 5.5
BNCI 2014-004	9	3	680 – 760 (720) 269 – 621 (411)	-1.0 – 0.0	0.0 – 4.5	4.5 – 6.5
Cho 2017	49	64	200 – 240 (200) 38 – 237 (159)	-1.0 – 0.0	0.0 – 3.0	3.0 – 5.0
Dreyer 2023	87	27	160 – 240 (240) 23 – 240 (192)	-1.0 – 0.0	0.0 – 5.0	5.0 – 6.0
Munich MI (Grosse-Wentrup 2009)	10	128	300 109 – 278 (200)	-1.0 – 0.0	0.0 – 7.0	7.0 – 9.0
Weibo 2014	10	64	140 – 160 (160) 31 – 160 (132)	-1.0 – 0.0	0.0 – 4.0	4.0 – 5.0
Zhou 2016	4	14	290 – 319 (295) 114 – 280 (150)	-1.0 – 0.0	0.0 – 5.0	5.0 – 7.0

Table 3.2.1: Dataset attributes. The lines in the fourth column indicate the original number of trials per subject (or the range in case this number was different between subjects), and the range of remaining trials across all subjects following trial rejection. Numbers in parentheses indicate the median number of trials.

Gaussian is subtracted from the TF matrix and the TF residual is used in the next algorithm iteration. The process stops when no amplitude peak exceeds the noise floor of two standard deviations across the whole TF matrix. For more details regarding the burst detection step we refer the readers to previous work from our group (Szul et al., 2023).

As the number of detected bursts per subject is large, we randomly sampled 10% of the trials of each participant per dataset and created a matrix that contained the waveforms of all detected bursts regardless of the trial class (“left” or “right” hand) for a given dataset, corresponding to approximately 100,000 to 2,000,000 bursts depending on the dataset. Due to the large number of subjects of the Dreyer 2023 dataset we restricted the random sample to 5% of each subject’s trials. The sample sizes were selected such that enough data was provided to the PCA in order for the selected kernels to be stable over multiple iterations of the random sampling (see below), while as many data as possible were retained for performing the rest of the analysis. Then, after robust scaling (scikit-learn package (Pedregosa et al., 2011), v1.0.2), we reduced the time dimension of the waveforms using principal component analysis (PCA) (Shlens, 2014) (scikit-learn package, v1.0.2).

We used the PCA score of each waveform detected from electrodes C3 and C4 (or equivalently channels 43 and 44 for the Munich MI (Grosse-Wentrup 2009) dataset), which is a metric of the difference between any waveform and the average shape of all bursts contained in the matrix provided as input to PCA. We defined an index of lateralized modulation of the average-per-axis PCA score I_m :

$$I_m = \left| \left(u_{ipsi}^{C3} - u_{contra}^{C4} \right) - \left(u_{ipsi}^{C4} - u_{contra}^{C3} \right) \right|, m \in \{2, \ldots, 9\}$$

$$u = \left| \widehat{score}_{trial\ \ period} - \widehat{score}_{baseline} \right|$$

where ipsi (contra) refers to bursts recorded from channels C3 / C4 during a left / right (right / left) hand MI (Figure 3.2.1 a).

This index measures the inter-hemispheric difference of the average waveform shape between the baseline and trial periods. Its values span the range $[0, \infty)$ and higher values indicate greater discrepancies between hemispheres and the two recording periods.

Based on observations from our previous study (Papadopoulos et al., 2024), we computed I_m among components 2 to 9 in order to find three PCA axes that maximized this metric. We did not take into account the first component because it likely describes the temporal skew of the bursts (Papadopoulos et al., 2024; Szul et al., 2023). Finally, we divided the score range of each of the three selected axes in seven equally spaced groups, each group corresponding to a set of “similarly shaped” bursts. We kept the two groups per axis that lie further away from the origin (score equal to 0) and, by computing the Euclidean-average waveform of bursts within each group, we identified two kernels per axis. As such, we identified six kernels per dataset corresponding to burst waveforms whose rates were expected to be maximally modulated during the task, compared to baseline.

3.2.3.4. Feature extraction

For each subject we applied the pre-processing, burst detection and kernel selection steps described above (pre-processing was applied to all available recording channels). Then, we convolved the EEG recordings with the corresponding kernels thus computing a proxy of the waveform-resolved burst rate per kernel. The temporally convolved, epoched data was then spatially filtered using the CSP algorithm (MNE package, v1.5.1, function CSP, parameters: n_components = 4, transform_into = “average_power”). Finally, we concatenated all 24 spatial features into a single vector for each trial (Figure 3.2.1 b).

To compare with, we also used standard approaches to compute spatial features of band-limited power modulations. After pre-processing, we independently filtered the epoched data in the mu (6 – 15 Hz), beta (15 – 30 Hz) or both the mu and beta (6 – 30 Hz) bands, using either a single filter or a filter bank approach. Then, the filtered data served as inputs to the CSP algorithm (using the already described parameters) resulting in four spatial features per filter in the former case. For the filter bank approach, we split either frequency range in non-overlapping filter banks with a frequency span of 3 Hz per filter. As such, we defined three filters for the mu band (6 – 9 Hz, 9 – 12 Hz, 12 – 15 Hz), five filters for the beta band (15 – 18 Hz, 18 – 21 Hz, 21 – 24 Hz, 24 – 27 Hz, 27 – 30 Hz) and eight filters for the mu-beta band (6 – 9 Hz, 9 – 12 Hz, 12 – 15 Hz, 15 – 18 Hz, 18 – 21 Hz, 21 – 24 Hz, 24 – 27 Hz, 27 – 30 Hz). Then, we again used CSP and concatenated all spatial features of each filter bank, resulting in 12, 20 and 32 spatial features respectively per trial.

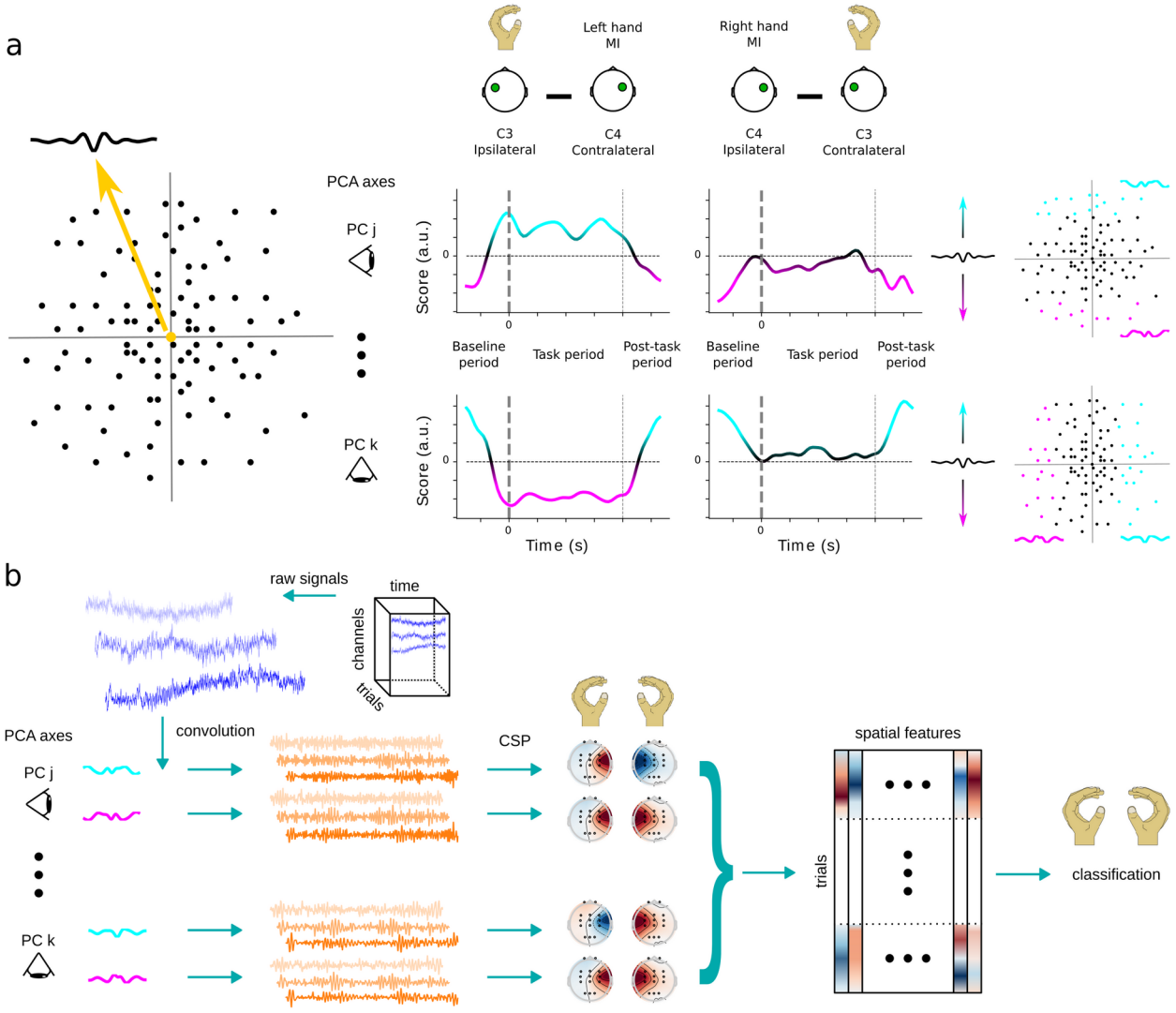


Figure 3.2.1: Illustration of methodology for computing classification features based on the convolution of raw signals with beta burst waveform kernels. **(a)** After randomly sampling the recording trials of all subjects within any dataset the beta burst waveforms are analyzed using PCA. This constructs a high-dimensional space whose origin corresponds to the shape of the average waveform or equivalently a score equal to 0, and each axis defines a different axis of waveform variation. By only considering the beta bursts of channels C3 and C4 that occur at any point in time, the lateralization modulation index I_m dynamically identifies the expected deviation of the average waveform shape from the overall average shape for each PCA axis. The axes that maximize I_m are identified, the bursts are projected on these axes, split in groups of similarly shaped waveforms and the average waveform shapes of the two extrema are computed. **(b)** The raw signals of all recording channels of each dataset are independently convolved with each selected waveform from **a** resulting in distinctly temporally filtered copies of the signals. Each copy is then spatially filtered using the CSP algorithm, and finally all spatial features are concatenated in a single matrix that is provided as input to the classifier.

3.2.3.5. Classification

We used a repeated (n = 10), 5-fold cross validation procedure to estimate the decoding score using linear discriminant analysis (LDA) (Tharwat et al., 2017; Vidaurre et al., 2011) (scikit-learn, v1.0.2) as a classifier. We adopted a time-resolved decoding paradigm, using both an incremental and a sliding time window. In the first case we started with a 100 ms time window and repeated the classification procedure by incrementing this window by 100 ms at a time. The baseline period was considered separately from the trial period. In the latter case we used 1 s long sliding time windows which moved in 50 ms increments. Decoding scores were based on the area under the curve (AUC) of the receiver operating characteristic (scikit-learn, v1.0.2). All numeric computations were based on the numpy python package (v1.21.6; (Harris et al., 2020)) and an environment running python (v3.10).

3.2.3.6. Information transfer rate

Information transfer rate (Arslan and Sinha, 2024; Sadeghi and Maleki, 2019) was defined as:

$$ITR = \frac{1-H}{T}$$

$$H = -p(t)\log_2 p(t) - (1-p(t))\log_2(1-p(t))$$

where the binary entropy function H depends on the average accuracy probability at any time window $p(t)$, and T corresponds to the maximum recording time required by each time window in seconds. T was shifted such that all time values are positive, *i.e.* using the absolute time starting from the beginning of the baseline period (Table 3.2.1) when using a sliding window and when considering the baseline period using an incremental time window. The values of this metric span the range $[0,10]$ when using an incremental window decoding approach and $[0,20]$ when using a sliding window. Large values indicate a better trade-off between decoding accuracy and decoding speed.

3.2.3.7. Statistical analysis

On the dataset level, we performed pairwise comparisons of the across-subject average decoding score corresponding to the beta burst convolution spatial features and each of the spatial features of the band-limited power modulations. These comparisons were based on threshold-free cluster-based permutation (n = 2^{13}) tests (MNE package, v1.5.1, function permutation_cluster_test, parameters: threshold = dict(start = 0, step = 0.2), tail = 1) that were subsequently thresholded at significance level of a = 0.05 for visualization purposes.

To estimate, on the population level, any statistical differences between the maximum classification scores obtained using different feature extraction pipelines during the trial period, we compared the scores of the beta burst convolution pipeline against those based on classical filtering pipelines.

We used a linear mixed model with across-trials average classification score as the dependent variable setting the number of trials as prior weights, the type of classification feature as a fixed effect, and subject nested within dataset as random intercepts. We implemented similar models to compare the time required to achieve the maximum classification score per feature extraction pipeline, and also the maximum ITR and time needed to reach it. In the latter two cases we first transformed the values to logarithmic scale in order to ensure normality of the residuals. Statistical analyses were conducted using R (v4.1.2) and lme4 (v1.1-31; (Bates et al., 2015)). Fixed effects were assessed using type II Wald X^2 tests using car (v3.1-1; (Fox and Weisberg, 2019)). Pairwise Tukey-corrected follow-up tests were carried out using estimated marginal means from the emmeans package (v.1,8,7; (Lenth, 2023)).

3.2.4. Results

3.2.4.1. Classification

In summary, we have employed seven freely available datasets of EEG recordings from subjects performing left and right hand MI. Within each dataset, we detected beta bursts for each subject within electrode clusters over the left and right sensorimotor cortex and then randomly sampled 10% of the trials containing these bursts (the sample size was limited to 5% for the Dreyer 2023 dataset). We applied PCA to the matrix of all burst waveforms and defined a modulation index I_m in order to find burst waveform shapes whose lateralized rates were expected to be maximally modulated between the baseline and trial periods. These waveforms were then employed as kernels for convolving the EEG data in time domain before applying spatial filtering with CSP. Finally all spatial features were combined and served as input for LDA, in order to classify “left” versus “right” hand MI. We also performed classification by applying standard temporal filtering techniques before applying spatial filtering with CSP, using either a single filter or a filter bank in the mu (6 – 15 Hz), beta (15 – 30 Hz) and mu-beta (6 – 30 Hz) frequency bands. We estimated the time-resolved decoding score per subject of each dataset for each classification feature using both an incremental and a sliding decoding window (see 3.2.3 Methods for details).

Across all datasets, the average decoding accuracy obtained using the proposed methodology based on beta bursts outperformed the results based on standard beta band filtering irrespective of the filtering (single filter or filter bank) or the windowing (incremental or sliding) technique during most of the recording time (Figure 3.2.2 a, Sup. Figure 3.2.3 a). Within each dataset, the across-subject average score obtained by beta bursts was higher than that of any beta band filtering technique, usually shortly after the beginning of the trial or towards its end (Figure 3.2.2 b-h, Sup. Figure 3.2.3 b-h). Exceptions to this finding when using an incremental window were the BNCI 2014-001 dataset, for which all features produced equivalent results (Figure 3.2.2 c, Sup. Figure 3.2.3 c), and the Weibo 2014 dataset, for which mu-beta filtering outperformed beta bursts (Figure 3.2.2 g, Sup. Figure 3.2.3 g). Threshold-free cluster-based permutation tests (see 3.2.3 Methods) revealed a significant cluster of increased accuracy for beta bursts compared to either beta filtering technique during most of the recording time or following the trial onset for each windowing (incre-

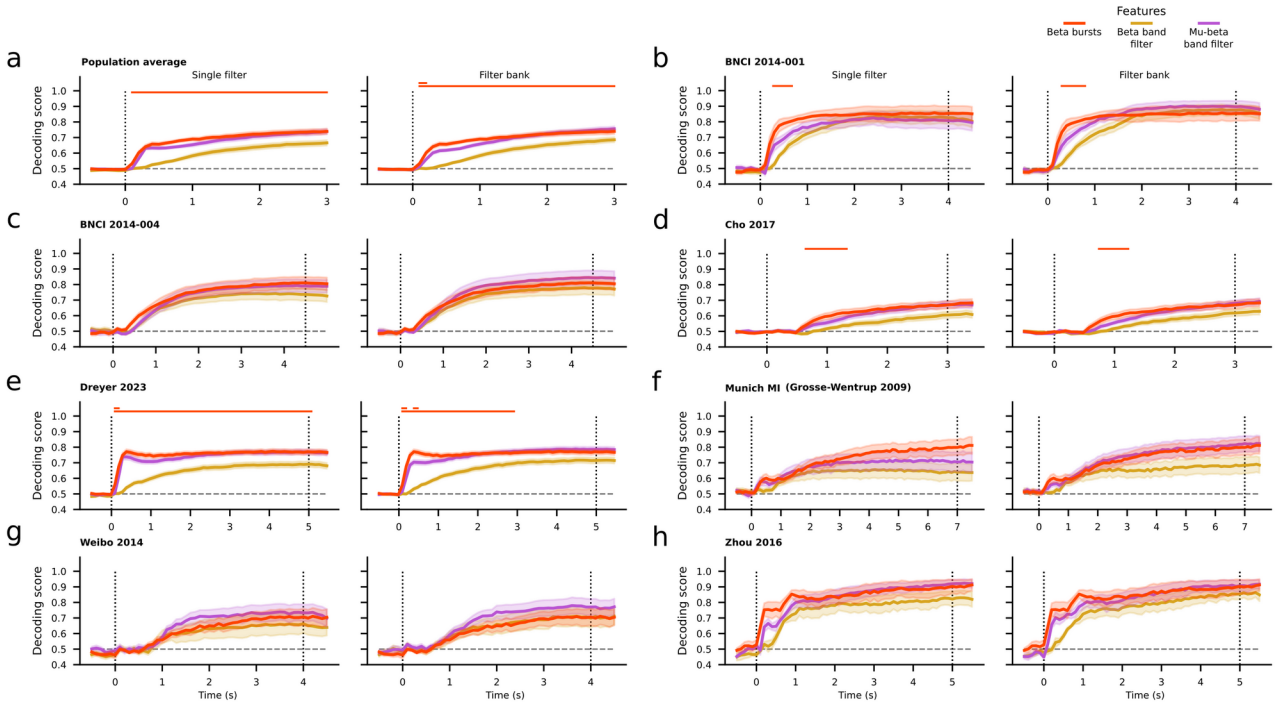


Figure 3.2.2: (a) Population average, time-resolved decoding score and standard error for the beta burst convolution (red), beta band (yellow) and mu-beta band (purple) filtering pipelines using an incremental window. Due to the different duration of the task per dataset we restricted the time to the minimum trial period corresponding to 3 seconds. **(b – h)** Average, time-resolved decoding score and standard error per dataset of the same features using an incremental window. For each panel, the left subplot depicts the decoding results obtained using a single filter, while the right subplot depicts the results based on a filter bank technique. The beta burst results are the same for the pair of each panel. The horizontal dashed line corresponds to the expected chance level. Vertical dotted lines represent the onset and end of the trial period of each dataset. The two horizontal lines on the top of each subplot show the results of the two pair-wise permutation cluster tests, that is, between the beta bursts and the beta band (bottom line) or mu-beta band (top line) filtering technique respectively, with correction for multiple comparisons at significance level of 0.05. At any time point, each line is color-coded so as to indicate which feature produces, on average, better results. A lack of color at any given time point indicates no statistically significant differences between the compared features.

mental or sliding) technique respectively (Figure 3.2.2 a, Sup. Figure 3.2.3 a). Within each dataset, we found clusters similar to those of the population average for the Dreyer 2023 dataset (Figure 3.2.2 e, Sup. Figure 3.2.3 e). The across-subject average score obtained by beta bursts was higher than that of any beta band filtering technique shortly after the beginning of the trial for the BNCI 2014-001 and Cho 2017 datasets (Figure 3.2.2 b, d, Sup. Figure 3.2.3 b, d). For the rest of the datasets (BNCI 2014-004, Munich MI (Grosse-Wentrup 2009), Weibo 2014, Zhou 2016) no differences were observed among the beta bursts and either beta band filtering method. Overall, in terms of classification accuracy, we observed an improvement with beta bursts over beta power on the population level and in 5/7 (4/7) datasets, with clusters of statistically significant differences arising on the population level and in 3/7 (2/7) datasets when using an incremental (sliding) window.

We did not observe such clear differences when comparing the beta bursts and mu-beta filtering decoding scores. On the population level, when using an incremental time window, average beta burst convolution results outperformed the single filter and filter bank techniques early after the beginning of a trial (Figure 3.2.2 a). On the dataset level, this was true for the BNCI 2014-001 and Dreyer datasets (Figure 3.2.2 b, e). For the rest of the datasets, differences varied depending on the filtering technique. Notably, in the mu-beta band, both filtering techniques produced higher decoding scores than beta bursts for the Weibo 2014 dataset (Figure 3.2.2 g). A similar pattern was also observed when using a sliding window (Sup. Figure 3.2.3 a-h). The permutation tests between the beta burst features and the mu-beta filtering techniques revealed only small clusters on the population level, as well for the Dreyer 2023 dataset. We found that beta bursts improve classification scores over the mu-band filtering techniques on the population level and 4/7 (2/7) datasets when using an incremental (sliding) window, with small clusters of statistically significant differences on the population level and one dataset only when using an incremental window.

Finally, comparisons between beta burst convolution and mu filtering results showed an improvement when using an incremental window. No clusters of statistically significant differences were revealed when comparing beta bursts to single-filter mu band power on the population level, but beta bursts slightly improved decoding on the population level and for datasets BNCI 2014-001, BNCI 2014-004 and Zhoud 2016 (Sup. Figure 3.2.4 a-c). No differences were found on the population level when comparing beta bursts to the filter bank technique, but on the dataset level the beta bursts score was better for the BNCI 2014-001 dataset (Sup. Figure 3.2.4 b) and conversely worse for the Weibo 2014 dataset (Sup. Figure 3.2.4 g) based on cluster permutation tests. Comparisons of results when using a sliding window approach did not reveal any differences (Sup. Figure 3.2.5).

3.2.4.2. Information transfer rate

For all datasets we computed the information transfer rate (ITR) in order to quantify the difference between all classification features in terms of the decoding speed-accuracy trade-off (see 3.2.3 Methods). On the population level, beta bursts provided a higher ITR than either beta band filtering technique across the whole trial (Figure 3.2.3 a). On the dataset level, the same pattern was observed for the Dreyer 2023 dataset (Figure 3.2.3 e). Moreover, beta bursts ITR was higher than any beta band filtering early after trial onset for the BNCI 2014-001, Munich MI (Grosse-Wentrup 2009) and Zhou 2016 datasets, and later for the Cho 2017 dataset. No differences between the features were observed in the case of BNCI 2014-004 dataset, whereas beta bursts resulted in the lowest ITR for the Weibo 2014 dataset (Figure 3.2.3 b-h). Permutation cluster tests revealed a significant difference between beta bursts and either filtering technique in the beta band on the population level, and for most of the time for the Dreyer 2023 dataset. A cluster after the trial onset was found for the BNCI 2014-001 dataset, and no clusters were found for the rest of the datasets. When using a sliding window approach, beta bursts provided a higher ITR than either beta band filtering technique on the population level early after the beginning of the trial and towards its end highlighted by the presence of a cluster (Sup. Figure 3.2.6 a). A significant difference was also found for the Dreyer 2023 dataset after the trial onset (Sup. Figure 3.2.6 e). For datasets BNCI 2014-001, Cho 2017, Dreyer 2023 and Zhou 2016 we observed a higher ITR for beta bursts

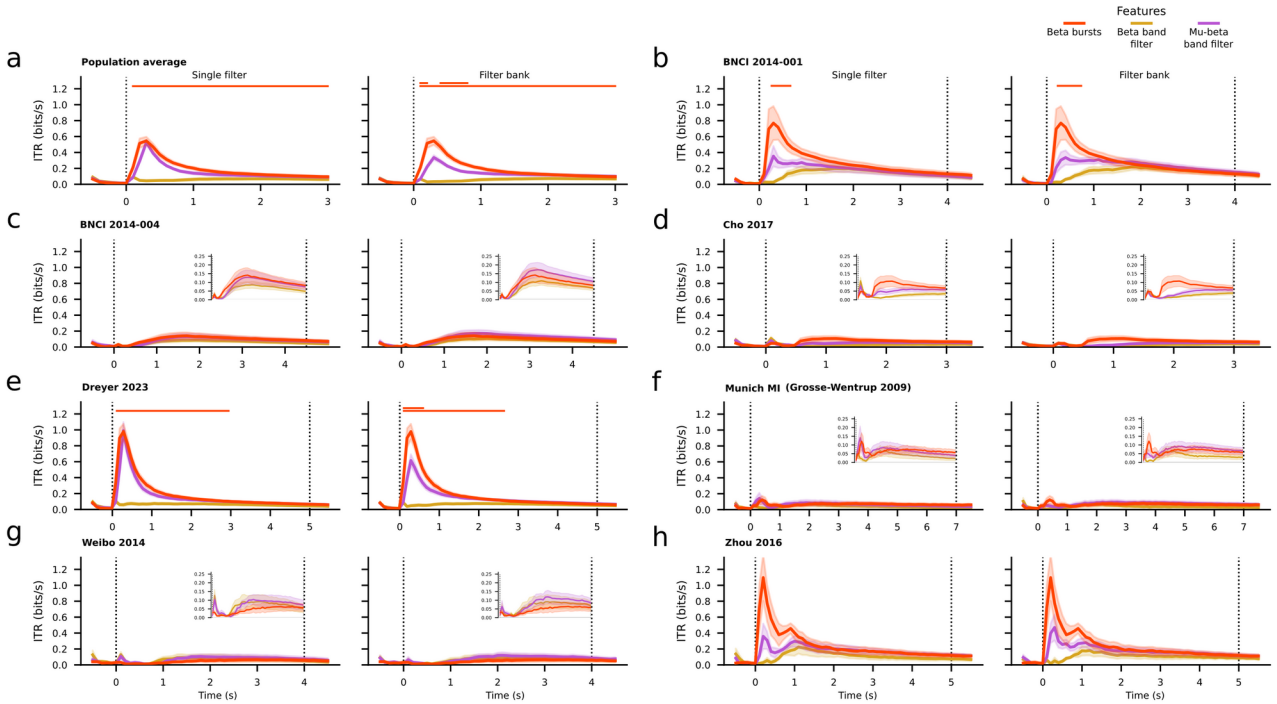


Figure 3.2.3: (a) Population average, time-resolved information transfer rate (ITR) and standard error for the beta burst convolution (red), beta band (yellow) and mu-beta band (purple) filtering pipelines using an incremental window. Due to the different duration of the task per dataset we restricted the time to the minimum trial period corresponding to 3 seconds. **(b – h)** Average, time-resolved information transfer rate (ITR) and standard error per dataset of the same features using an incremental window. For each panel, the left subplot depicts the ITR results obtained using a single filter, while the right subplot depicts the results based on a filter bank technique. The beta burst results are the same for the pair of each panel. Vertical dotted lines represent the onset and end of the trial period of each dataset. The two horizontal lines on the top of each subplot show the results of the two pair-wise permutation cluster tests, that is, between the beta bursts and the beta band (bottom line) or mu-beta band (top line) filtering technique respectively, with correction for multiple comparisons at significance level of 0.05. At any time point, each line is color-coded so as to indicate which feature produces, on average, better results. A lack of color at any given time point indicates no statistically significant differences between the compared features.

compared to beta band filtering mainly after the trial onset, whereas for the rest of the datasets either feature resulted in equivalent ITRs (Sup. Figure 3.2.6 b-h). No significant clusters were found for any of these datasets. In summary, irrespective of the windowing method beta bursts resulted in higher ITR than beta power on the population level and for 5/7 datasets with clusters arising on the population level and 2/7 datasets.

Regarding the comparison between beta bursts and the mu-beta filtering techniques, ITR was higher for the former on the population level as well as datasets BNCI 2014-001, Cho 2017, Dreyer 2023, Munich MI (Grosse-Wentrup 2009) and Zhou 2016 shortly after the trial onset, especially when adopting the filter bank method. No differences were observed for the BNCI 2014-004 dataset. The mu-band filter bank technique produced higher ITR than beta bursts during the trial period in the case of the Weibo 2014 dataset (Figure 3.2.3 a-h). The results were similar when using a sliding window (Sup. Figure 3.2.6 a-h). On the population level, cluster-based permutations tests revealed a significant difference between the beta bursts features and the filter bank in the

mu-beta band using either an incremental or a sliding window approach, but no significant clusters when comparing the beta bursts to the single filter in the mu-beta band (Figure 3.2.3 a, Sup. Figure 3.2.6 a). Similar clusters of significant differences between the features were found only for the Dreyer 2023 dataset with an incremental window (Figure 3.2.3 e, Sup. Figure 3.2.6 e). Overall, beta bursts yielded higher ITR than mu-beta power on the population level and 4/7 datasets regardless of the windowing technique. Permutation cluster tests revealed improvements attributable to beta bursts compared to the filter bank technique on the population level, and for one dataset when using an incremental time window.

3.2.4.3. Statistical analysis

We used linear mixed models to quantify the differences in maximum decoding score, latency to achieve the maximum score, maximum ITR and latency to the maximum ITR per feature (see 3.2.3 Methods) using both the incremental and sliding windows (Figure 3.2.4, Sup. Figure 3.2.7).

On the population level, the maximum classification scores for the beta bursts technique, filtering in the beta band using a single filter, filtering in the mu-beta band using a single filter, and filter bank in the beta or mu-beta bands using an incremental time window were 0.832 ± 0.066, 0.755 ± 0.065, 0.827 ± 0.066, 0.734 ± 0.066 and 0.819 ± 0.066 (Figure 3.2.4 a). The time required to reach each of these decoding scores (latency) was 2.26 ± 0.91, 3.04 ± 0.90, 2.96 ± 0.90, 2.50 ± 0.90 and 2.44 ± 0.91 seconds (Figure 3.2.4 c), respectively. The maxima of the ITR before applying the logarithmic transformation (see 3.2.3 Methods) per feature were 0.6443 ± 0.207, 0.0554 ± 0.207, 0.3531 ± 0.206, 0.0667 ± 0.206, 0.5241 ± 0.207 bits per second (Figure 3.2.4 b). The corresponding average latencies before the logarithmic transformation were 0.827 ± 0.203, 1.316 ± 0.204, 1.182 ± 0.203, 1.064 ± 0.201, 0.945 ± 0.203 seconds (Figure 3.2.4 d). Regarding the analysis based on a sliding window, the maximum classification scores were 0.816 ± 0.050, 0.753 ± 0.050, 0.810 ± 0.050, 0.753 ± 0.050 and 0.818 ± 0.050 respectively (Sup. Figure 3.2.7 a). The latencies were 2.03 ± 0.23, 2.45 ± 0.22, 2.19 ± 0.23, 2.49 ± 0.24 and 2.22 ± 0.23 seconds (Sup. Figure 3.2.7 c). Before applying the logarithmic transformation, the ITR maxima were 0.694 ± 0.180, 0.170 ± 0.178, 0.413 ± 0.177, 0.206 ± 0.182, 0.533 ± 0.179 bits per second (Sup. Figure 3.2.7 b), and the corresponding latencies 0.575 ± 0.162, 0.840 ± 0.161, 0.796 ± 0.160, 0.743 ± 0.161, 0.701 ± 0.162 seconds (Sup. Figure 3.2.7 d).

Across all datasets the maximum classification accuracy of the beta bursts technique when using an incremental window was significantly higher than that of the beta band single filter and filter bank pipelines ($X^2(4) = 326.81$, $t(24587436) = 10.697$, $p < 0.001$ and $t(24548972) = 13.705$, $p < 0.001$ respectively), but did not differ significantly from either technique exploiting both the mu and beta bands ($t(24904394) = 0.637$, $p = 0.9691$ and $t(24049399) = 1.777$, $p = 0.3873$). The latency to achieve the maximum score was significantly lower for the beta burst convolution pipeline compared to both the single filtering techniques in the beta and mu-beta bands ($X^2(4) = 62.508$, $t(24698263) = -6.361$, $p < 0.001$ and $t(25032435) = -5.769$, $p < 0.001$), but did not differ significantly compared to the corresponding filter bank techniques ($t(24649522) = -1.926$, $p = 0.3034$ and $t(24151454) = -1.488$, $p = 0.5703$). The logarithmic transform of the maximum ITR for the beta bursts technique was significantly higher than the single filtering and filter bank techniques in both the beta and mu-beta bands ($X^2(4) = 309.58$, $t(24722157) = 14.0967$, $p < 0.001$,

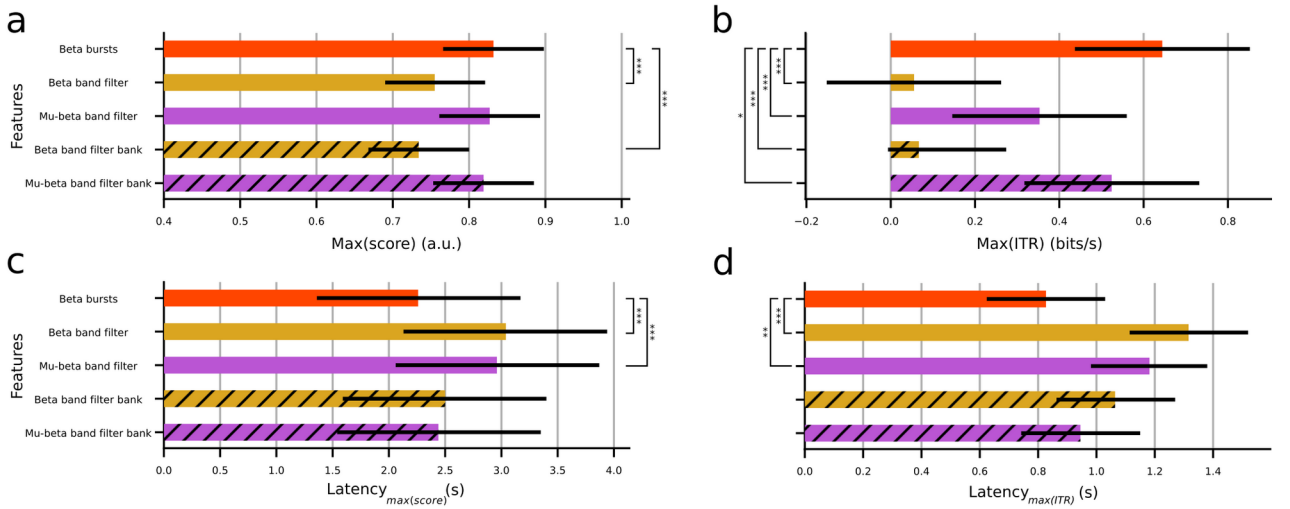


Figure 3.2.4: Population-level statistical analysis based on linear mixed models when using an incremental window per feature. **(a)** Average maximum decoding score. **(b)** Average maximum ITR. **(c)** Average latency to reach the maximum decoding score. **(d)** Average latency to reach the maximum ITR. Error bars show 95% confidence intervals. Hatches indicate the use of a filter bank technique. Asterisks indicate statistically significant differences among pairwise comparisons of the beta bursts and the rest of the features (* : $p < 0.05$, ** : $p < 0.01$, *** : $p < 0.001$). A lack of asterisks implies no statistically significant differences. Note that the log transform of the maximum ITR and latency to maximum ITR were used for the statistical analysis (see 3.2.3 Methods), but panels **b** and **d** depict results before applying the transformation for ease of comparisons with panels **a** and **c** respectively.

t(24671284) = 12.904, p < 0.001 and t(25060057) = 5.127, p < 0.001, t(24173608) = 2.909, p = 0.0298). The logarithmic transform of the latency to achieve maximum ITR was significantly lower for the beta bursts technique compared to either single filtering pipeline in the beta and mu-beta bands ($X^2(4) = 40.75$, t(24777354) = -5.863, p < 0.001 and t(25130735) = -3.885, p = 0.001), but did not significantly differ compared to the filter bank method in either band (t(24721433) = -2.071, p = 0.2329 and t(24227058) = -1.545, p = 0.5329).

When using a sliding window, across all datasets the maximum classification accuracy of the beta bursts technique was significantly higher than that of the beta band single filter and filter bank pipelines ($X^2(4) = 237.95$, t(24582761) = 10.072, p < 0.001 and t(24544732) = 10.055, p < 0.001 respectively), but did not differ significantly from either technique exploiting both the mu and beta bands (t(24898964) = 0.956, p = 0.8748 and t(24045211) = -0.418, p = 0.9936). Similarly, the latency to achieve the maximum score was significantly lower for the beta burst convolution pipeline compared to either filtering technique in the beta band ($X^2(4) = 25.552$, t(24736767) = -3.890, p < 0.001 and t(24684274) = -4.281, p < 0.001), but did not differ significantly compared to the mu-beta band (t(25086359) = -1.467, p = 0.5840 and t(24189739) = -1.762, p = 0.3961). The logarithmic transform of the maximum ITR for the beta bursts technique was significantly higher than both filtering techniques in the beta band and the single filtering in the mu-beta band ($X^2(4) = 162.26$, t(24732475) = 10.236, p < 0.001, t(24680636) = 9.172, p < 0.001 and t(25072582) = 4.499, p < 0.001) but did not significantly differ from the mu-beta filter bank (t(24183763) = 1.665, p = 0.4559). The logarithmic transform of the latency to achieve maximum ITR was significantly lower for the beta bursts technique compared to either single filtering pipeline in the beta and mu-

beta bands ($X^2(4)$ = 13.151, t(24808114) = -3.069, p = 0.0183 and t(25164334) = -3.029, p = 0.0207), but did not significantly differ compared to the filter bank method in either band (t(24749694) = -1.796, p = 0.3756 and t(24255336) = -1.296, p = 0.6937).

3.2.5. Discussion

Standard techniques for analyzing meso- and macro-scale neural signals recorded during the execution or imagination of movements typically rely on signal power metrics assuming that relevant changes in brain signals are reflected in amplitude modulations (Alayrangues et al., 2019; Kilavik et al., 2013; Pfurtscheller, 1981; Pfurtscheller et al., 1997, 1996; Pfurtscheller and Lopes da Silva, 1999). However, there has recently been a considerable paradigm shift towards considering transient signal features on the single trial level (Y. Y. Chen et al., 2021; Coleman et al., 2024; Jones, 2016; Little et al., 2019; Lundqvist et al., 2024, 2016; Rayson et al., 2023; Shin et al., 2017; Soh et al., 2021; Szul et al., 2023; Torrecillos et al., 2018; Vigué-Guix and Soto-Faraco, 2023; Wessel, 2020). Therefore, considering that computational models describing the neuronal generators of specific burst waveform shapes (Bonaiuto et al., 2021; Sherman et al., 2016; Szul et al., 2023) offer an improved theoretical interpretability of the observed signal modulations, applications leveraging such signal characteristics, like beta bursts, could potentially benefit from incorporating recent neuroscience findings (Papadopoulos et al., 2022).

In this work we analyzed the activity of seven open EEG MI datasets and focused on developing a streamlined process for incorporating beta bursts into a BCI pipeline. We used a simple pre-processing algorithm in order to reject noisy trials based on amplitude thresholds before detecting beta bursts, but the impact of more sophisticated algorithms like independent component analysis on burst detection could be explored in the future. Then, we defined a modulation index I_m which allowed us to identify beta burst waveforms whose rate is expected to be modulated due to task demands. This was based on the assumption that maximal modulations of the average waveform shape along specific PCA components are the result of a net imbalance of the rates of bursts with different shapes driven by task demands. PCA constitutes a mathematically tractable and interpretable way of analyzing the diversity of beta burst waveform shapes. However, by definition it imposes to some extent orthogonality in the frequency content of the kernels, a property which may not be desirable. Other supervised dimensionality reduction algorithms, especially those designed for analyzing time series, could better disentangle the waveforms by imposing different constraints, e.g. taking into account trial labels, and their potential advantages remain to be studied. We also note that this index only used beta burst waveforms originating from channels C3 and C4 (or equivalent). Our assumption was that the channels localization should allow for signals which are sufficiently informative of the binary “left hand” vs “right hand” MI task. Future work can explore a more principled way to include data from multiple channels.

We used these waveforms as kernels to convolve the raw signals in the time domain. We chose to keep the number of kernels and the method for extracting them fixed based on insights from a previous study (Papadopoulos et al., 2024), but future work could employ a formal hyper-parameter search so as to maximize classification accuracy. Similarly, we did not check for any redundancy in the convolved signals due to selection of similarly shaped kernels, a point which could be addressed by another dimensionality reduction algorithm. The implementation of the

convolution is virtually as computationally efficient as any filtering technique. However, we note that the proposed methodology assumes the existence of data that can be analyzed offline in order to first find the relevant beta burst waveforms to use as kernels. Moreover, this data needs to be clean of artifacts as the beta burst detection algorithm may fail to detect transient activity in the presence of high-power oscillations, instead detecting only the latter. For this reason, we believe that the superlets algorithm is the only time-frequency decomposition technique providing adequate time and frequency resolution in order to determine if the data is clean and to extract burst waveforms.

This data-driven, neurophysiology-informed filtering of the signals resulted in a proxy of the waveform-resolved burst rate per kernel. We also performed a standard filtering in the mu (6 – 15 Hz) band, beta (15 – 30 Hz) band, or a wider frequency range encompassing both the mu and beta (6 – 30 Hz) bands. Finally, we used CSP to extract spatial features for classification. We showed that classification scores can be improved compared to a standard power-based analysis of the beta band activity, requiring briefer recordings to do so and that, without explicitly considering the mu (6 – 15 Hz) band activity in our beta bursts pipeline, the corresponding classification scores are equivalent to scores of state-of-the-art approaches again needing shorter recordings. Further, the filter bank-based analysis allowed us to verify that the decoding improvements where not simply the result of an increase in number of spatial features used for classification. Instead, beta burst waveforms are more informative of the underlying MI task on the population level than beta band power, and equally informative to standard power-based techniques that take into account mu activity modulations.

A possible explanation for this result is that beta burst kernels also capture slower modulations of the underlying activity. Beta and mu band modulations during MI tasks involve overlapping cortical networks and have equivalent time horizons (Neuper et al., 2006; Pfurtscheller and Neuper, 2001; Seeber et al., 2016). The actual signal properties and/or underlying mechanisms that would explain why beta burst waveforms perform similarly to oscillatory mu band power remain to be studied. As such, we have opted not to perform a formal comparison of the beta burst features to mu band power. However, one hypothesis is that our definition of the mu band frequency range overlaps -at least partially- with what has been described as lower beta frequency (Kilavik et al., 2012; Lotte, 2014; Lotte and Rimbert, 2022; Schmidt et al., 2019). Future work could explore the incorporation of novel mu band features that characterize time-resolved oscillatory waveform changes (Cole and Voytek, 2019; Giehl and Siegel, 2024; Vigué-Guix and Soto-Faraco, 2023), or a combination of mu power and beta burst features using more sophisticated classifiers or ensemble methods. We also note that the use of alternative classifiers can potentially affect the beta burst results reported here. Although the combination of CSP and LDA is known to produce reliable results (Carrara and Papadopoulo, 2024; Jayaram and Barachant, 2018), a formal comparison of multiple classifiers would be necessary in order to optimize performance and/or ITR, especially for online applications.

By employing both an incremental and a sliding window strategy for classification we can speculate on the observed differences of decoding scores across classification features and datasets. First, it appears that MI does not begin right after the go cue in all datasets but can be delayed possibly due to differences in the task design or the instructions given to the participants. Second, relatively sustained decoding performances when using a sliding window were translated into slow increases of those performances when using an incremental window. In contrast, a drop in performance when using a sliding window was reflected in a plateau when using an incremental window. Taken together these observations imply that finding an optimal decoding time window, especially for

online paradigms, is not trivial and depends not only on the selected classification features or algorithm but also on experimental design variables.

In order to assess the trade-off between decoding accuracy and speed, we used the classification scores obtained by implementing each pipeline and computed the corresponding ITR. By definition, given a fixed number of classes ITR increases either by reducing recording time or by increasing decoding score (or a combination of the two). This means that when comparing different features and/or algorithms, ITR will indicate which one is faster assuming equivalent classification scores, or which one performs best assuming equivalent recording times. We showed a statistically significant increase of the maximum ITR achieved using the beta burst kernel filtering compared to any other method, and a statistically significant decrease of the time needed to achieve this value compared to single filters. These results are in accordance with previous studies that have showed the specificity of the waveform-resolved burst rate which captures subtle changes on the single-trial level not necessarily reflected in signal power and overall burst rate (Papadopoulos et al., 2024; Rayson et al., 2023; Szul et al., 2023), due to slower amplitude modulation and averaging over distinct processes respectively. The results suggest that, by retaining or improving the precision of command issuing while increasing its speed, beta bursts could be particularly relevant for BCI applications that aim to minimize the recording time required before issuing a command like in the case of real-time decoding of a switch control, although the self-paced nature of such applications still poses a considerable challenge (Carrara and Papadopoulo, 2024).

Among the datasets analyzed in this study decoding and ITR results of the Weibo 2014 were noticeably different. This dataset is to some degree contaminated by high-frequency noise even following pre-processing and, compared to what we have observed for the rest of the datasets, is characterized by a smaller number of detected bursts the majority of which last longer (more than 5 cycles) and have higher amplitude. The reduced variability in the detected bursts is also reflected in the smaller number of PCA components that explain at least 90% of the variance. We presume that these recordings are mostly composed of oscillatory rather than burst activity. Therefore, the proposed, burst-based approach, despite being able to capture and quantify modulations of signal amplitude, is sub-optimal for this dataset.

This study focused on incorporating recent neurophysiology insights, specifically task dependent waveform-specific modulation of beta burst rates, in a pipeline for decoding EEG signals during imagined movements. We proposed a simple and computationally efficient algorithm that leverages beta burst waveforms and transforms brain recordings in a way that is compatible with other widely adopted algorithms. We demonstrated that classification results based on beta bursts are superior to results based on beta band power alone, and are on-par with power-based results that take into account the mu band. By computing the information transfer rate we showed that, often, features based on beta bursts significantly improve the decoding speed-accuracy trade-off. We also verified this finding using a sliding window decoding technique, a fact which further suggests the feasibility for online decoding with this approach. Taking everything into account, we believe that these findings can serve as an important step in the direction of improving online BCI decoding paradigms.

3.2.6. Data and code availability

All data are freely available via the MOABB project and the open access repository Zenodo at https://zenodo.org/records/8089820. All scripts necessary for reproducing the results of this article are available at the following public repository: https://gitlab.com/sotpapad/bebopbci.

3.2.7. Author contributions

S P, J B and J M conceptualized the manuscript. S P drafted the manuscript and performed the analysis. All authors contributed to manuscript revision, read, and approved the submitted version.

3.2.8. Funding

S P, L D, M C, J B and J M are supported by the French National Research Agency (ANR) project HiFi (2020–2024, ANR-20-CE17-0023). M S and J B are supported by the European Research Council (ERC) under the European Union's Horizon 2020 Research and Innovation Programme (ERC consolidator Grant 864550 to J B). This work was performed within the framework of the LABEX CORTEX (ANR-11LABX-0042) of Université de Lyon, within the program 'Investissements d'Avenir' (decision n◦ 2019-ANR-LABX-02) operated by the French National Research Agency (ANR).

3.2.9. Declaration of competing interests

All authors declare no competing interests.

3.3 Contribution 4 – Improved motor imagery decoding with spatiotemporal filtering based on beta burst kernels

S. Papadopoulos[1,2,3,*], L. Darmet[1,2,3], M.J. Szul[1,3], M. Congedo[4], J.J. Bonaiuto[1,3,†], J. Mattout[1,2,†]

[1] University Lyon 1, Lyon, France

[2] Lyon Neuroscience Research Center, CRNL, INSERM, U1028, CNRS, UMR5292, Lyon, France

[3] Institut des Sciences Cognitives Marc Jeannerod, CNRS, UMR5229, Lyon, France

[4] GIPSA-lab, University Grenoble Alpes, CNRS, Grenoble-INP, Grenoble, France

[†] These authors contributed equally.

[*] Corresponding author: Sotirios Papadopoulos

E-mail: sotirios.papadopoulos@univ-lyon1.fr

3.3.1. Abstract

The description of the event-related desynchronization and synchronization phenomena in the mu and beta frequency bands has to a significant extent shaped our understanding of motor-related brain processes. Accordingly, Brain-Computer Interface applications leveraging attempted or imagined movements usually depend on spatially- and band-limited power changes as the brain markers of interest. Yet, converging neuroscience evidence question the idea that signal power best describes the movement-related modulation of brain activity. On a single-trial level, beta band activity is characterized by short, transient and heterogeneous events termed bursts rather than sustained oscillations. In a recent study we demonstrated that a beta burst analysis of hand motor imagery binary classification tasks is often superior to beta power in terms of classification score. Here we expand upon this idea proposing a comparable to state-of-the-art algorithm. We confirm our previous results by using convolution kernels extracted from beta bursts. Moreover, we show that these kernels can effectively be used in inter-session transfer learning strategies.

3.3.2. Introduction

Three decades ago a number of seminal studies in motor neuroscience revealed for the first time time-locked changes in induced power within specific frequency bands (Pfurtscheller, 1981; Pfurtscheller and Berghold, 1989; Pfurtscheller and Lopes da Silva, 1999). These studies described a relative-to-baseline gradual reduction in the power of brain signals recorded during an ongoing movement or motor imagery (MI) task in the mu (~ 8 – 12 Hz) (Neuper et al., 2006; Pfurtscheller et al., 2006, 1997; Pfurtscheller and Lopes da Silva, 1999) and beta (~ 13 – 30 Hz) (Pfurtscheller et al., 2006, 1997; Pfurtscheller and Lopes da Silva, 1999) frequency bands, termed event-related desynchronization (ERD). They, also, demonstrated a relative increase in power in the beta band shortly after the end of the task, known as event-related synchronization (ERS) (Alayrangues et al., 2019; Neuper et al., 2006; Pfurtscheller et al., 1996). The ERD is considered to be a high-level indication of brain processes pertaining to movement preparation and execution, and is particularly prominent in the contralateral sensorimotor cortex (Little et al., 2019; Makeig et al., 2000; Pfurtscheller and Berghold, 1989; Pfurtscheller and Neuper, 1997; Zich et al., 2023).

Because of this spatial and frequency specificity, ERD is the main marker of interest for motor-related and especially MI-based, non-invasive BCI applications (Jayaram and Barachant, 2018; Tangermann et al., 2012). Typically, signals recorded during MI are transformed in the time-frequency domain (TF) (Brodu et al., 2011; Bruns, 2004; Herman et al., 2008), and are then spatially filtered using the common spatial pattern algorithm (CSP) (Blankertz et al., 2007; Koles, 1991; Müller-Gerking et al., 1999). This results in an increase of signal-to-noise ratio and extracts the signal power in specific time windows and frequency bands of interest, while also maximizing the spatial disparity among different MI classes (e.g.”left” or “right” hand).

The hypothesized reliability and reproducibility of these signal characteristics has also served as the basis for a range of transfer-learning attempts. Transfer learning refers to the exploitation of specific signal features extracted from past recording sessions, different subjects and/or experiments to guide decoding during future sessions (Lotte et al., 2018a).

Despite the fact that the ERD and ERS are widely observed, their nature is not well-understood and converging neurophysiology evidence puts these phenomena into question. The ERD and ERS are typically revealed by averaging signal power in the TF domain over multiple trials, especially in the beta frequency band (Jones, 2016; Little et al., 2019), under the assumption of sustained oscillations. However, this evidence points out that, on the contrary, on a single trial level, beta band activity occurs in short events, termed bursts (Jones, 2016; Little et al., 2019; Lundqvist et al., 2016; Shin et al., 2017; Torrecillos et al., 2018; Wessel, 2020). The rate of these beta bursts is more behaviorally relevant in motor processes (Enz et al., 2021; Hannah et al., 2020; Little et al., 2019; Rayson et al., 2023; Szul et al., 2023; Wessel, 2020) than averaged beta band power. Moreover, it has been shown that beta bursts comprise heterogeneous events (Szul et al., 2023) with different functions, alluded to by their differential modulation during different task conditions (Langford et al., 2023; Papadopoulos et al., 2024) or phases (Rayson et al., 2023; Szul et al., 2023).

In a recent study we showed that the analysis of beta bursts from channels C3 and C4 during hand motor imagery can be advantageous to beta power in terms of classification, confirming the hypothesis that on the single-trial level beta burst rate modulations are more behaviorally relevant

than beta band power changes (Papadopoulos et al., 2024). In this article we expand upon that study. We introduce an algorithm that exploits beta bursts in order to transform brain signals into measures of waveform-resolved burst rate. Moreover this algorithm can take advantage of an arbitrary number of recorded signals while being computationally efficient, thus constructing decoding features that are comparable to state-of-the-art in BCI. We analyze the activity during “left” and “right” hand MI of three open EEG datasets and show that the use of beta bursts instead of beta band power can improve classification results. Finally, we adopt a transfer learning approach and show that beta bursts detected in one recorded session can be exploited to guide the decoding in other sessions.

3.3.3. Materials and Methods

3.3.3.1. Datasets

We analyzed three open EEG MI datasets: BNCI 2014-001 (Tangermann et al., 2012), BNCI 2014-004 (Leeb et al., 2007) and Zhou 2016 (Zhou et al., 2016), all available through the MOABB project (Jayaram and Barachant, 2018) (Table 3.3.1). These datasets are composed of recordings of numerous subjects who were required to perform sustained MI following the appearance of a visual cue on a screen. For our analysis we only considered trials corresponding to the “left hand” or “right hand” classes even though two experimental paradigms consisted of more MI classes.

3.3.3.2. Pre-processing

Each subject’s epoched recordings were loaded with the MOABB python package (v0.4.6) LeftRightImagery class, and were filtered with a low pass cutoff of 120 Hz (zero-phase FIR filter designed with the windowed approach and transition bandwidth of 25% of the low pass frequency). Then, we rejected trials using the autoreject python package (Jas et al., 2017) (v0.4.0, function get_rejection_threshold).

3.3.3.3. Burst-detection

Following pre-processing, a subset of channels above the sensorimotor cortex was defined. The corresponding recordings were first transformed in the time-frequency (TF) domain from 1 to 43 Hz using the superlets algorithm (Moca et al., 2021) (parameters: o_min = 1, o_max = 40, c = 4) with a frequency resolution of 0.5 Hz. Then, we identified bursts within the beta frequency range (15 – 30 Hz) from each TF matrix using a previously published procedure that allowed us to extract the waveforms of the beta bursts within a fixed time window (Papadopoulos et al., 2024; Szul et al., 2023).

Dataset	BNCI 2014-001	BNCI 2014-004	Zhou 2016
# Subjects	9	9	4
# Channels	3	22	64
# Sessions	2	5	3
Min - Max # trials across subjects	288	680 - 760	290 - 319
Min - Max # trials (after trial rejection)	217 - 287	269 - 621	114 - 280
Trial duration (s)	4.0	4.5	5.0
Reference	Tangermann et al., 2012	Leeb et al., 2007	Zhou et al., 2016

Table 3.3.1: Dataset attributes.

3.3.3.4. Kernel selection

For each dataset and subject we randomly sampled 10% of the recording trials (or all trials corresponding to a recording session when assessing transfer learning) of each participant after trial rejection and aggregated all detected bursts within these trials in a matrix (irrespective of the trial class, i.e. “left hand” or “right hand”) after robust scaling (scikit-learn package (Pedregosa et al., 2011), v1.0.2). Then, we used principal component analysis (PCA) (Shlens, 2014) (scikit-learn package, v1.0.2) in order to reduce the time dimension of the waveforms. We defined an index of lateralized modulation of the average-per-axis PCA score I_m (a metric of the difference between any burst waveform and the average shape) from the baseline to the trial periods of the recordings as using electrodes C3 and C4:

$$I_m = \left| \left(u_{ipsi}^{C3} - u_{contra}^{C4} \right) - \left(u_{ipsi}^{C4} - u_{contra}^{C3} \right) \right|, m \in \{2, \ldots, 9\}$$

$$u = \left| \widehat{score}_{trial\ \ period} - \widehat{score}_{baseline} \right|$$

where ipsi (contra) refers to bursts recorded from channels C3 / C4 during a left / right (right / left) hand MI. Using this index we identified the three PCA axes that maximized I_m among components 2 to 9. We did not consider the first PCA component as it simply describes the temporal skew of the burst waveforms (Papadopoulos et al., 2024; Szul et al., 2023). Finally, based on our previous study (Papadopoulos et al., 2024), we split the computed score range of each of the three selected axes in seven equally spaced groups. We considered the two groups that lie further away from the origin (score equal to 0), grouped similarly shaped bursts together and defined 2 kernels per PCA axis by computing the average waveform of all bursts within these two groups. As a result, we ended up with 6 kernels that describe the burst waveforms that were expected to be maximally rate-modulated during the task, compared to baseline, for each participant of each dataset separately.

3.3.3.5. Feature selection

We used these kernels in order to transform the available EEG recordings, not considering the subset of trials that were used for defining the kernels. Specifically, a copy of each subject’s

epoched data was convolved with one kernel, resulting in a proxy of the waveform-resolved burst rate. Then, each of the temporally filtered epoched data was spatially filtered using the CSP algorithm (MNE package (Gramfort et al., 2013), v 1.5.1, function CSP, parameters: n_components = 4, transform_into = “average_power”).

We also created band-limited spatial features with a standard filtering technique. Specifically, we computed the envelope of the epoched data Hilbert transform (MNE package, v 1.5.1, function apply_hilbert) after independently applying a single filter in the beta frequency band (15 – 30 Hz) and a wider frequency range encompassing both the mu and beta bands (6 – 30 Hz). Then, these signals served as inputs to the CSP algorithm (we kept the parameters unchanged).

In order to assess whether the number of spatial features used for classification (24 for the beta burst kernel approach versus 4 for the Hilbert power approach) affected the observed results, we also adopted a filter bank approach. We split either frequency range in non-overlapping filter banks of 3 Hz range; this resulted in 5 filters for the beta band (15 – 18 Hz, 18 – 21 Hz, 21 – 24 Hz, 24 – 27 Hz, 27 – 30 Hz) and 8 filters for the mu-beta band (6 – 9 Hz, 9 – 12 Hz, 12 – 15 Hz, 15 – 18 Hz, 18 – 21 Hz, 21 – 24 Hz, 24 – 27 Hz, 27 – 30 Hz) corresponding to 20 and 32 spatial features respectively.

We also estimated kernel-specific CSP filters on one session and used these filters in the remaining sessions. For comparison, we estimated the CSP filters of a session and used them to transform the signals of the other sessions for each of the previously described filtering techniques.

3.3.3.6. Classification

The resulting spatially filtered data were concatenated in a single matrix. Using a repeated (n = 10), 5-fold cross validation procedure we estimated the decoding score using LDA (scikit-learn, v1.0.2) as a classifier using the whole trial recordings. The decoding scores were based on the area under the curve (AUC) of the receiver operating characteristic (scikit-learn, v1.0.2). All numeric computations were based on the numpy python package (v1.21.6; (Harris et al., 2020)) and an environment running python (v3.10).

3.3.3.7. Statistical analysis

To estimate, at the population level, any statistical difference between methods, we compared classification results of the waveform-resolved burst features against multiple band-limited power features. We used a generalized linear mixed model with a binomial distribution and logit link function with across-trials average classification score as the dependent variable setting the number of trials as prior weights, the type of classification feature as a fixed effect, and the subject nested within the dataset as random intercepts. We also compared the across-session average difference in classification score between a transfer learning approach and an across-session,

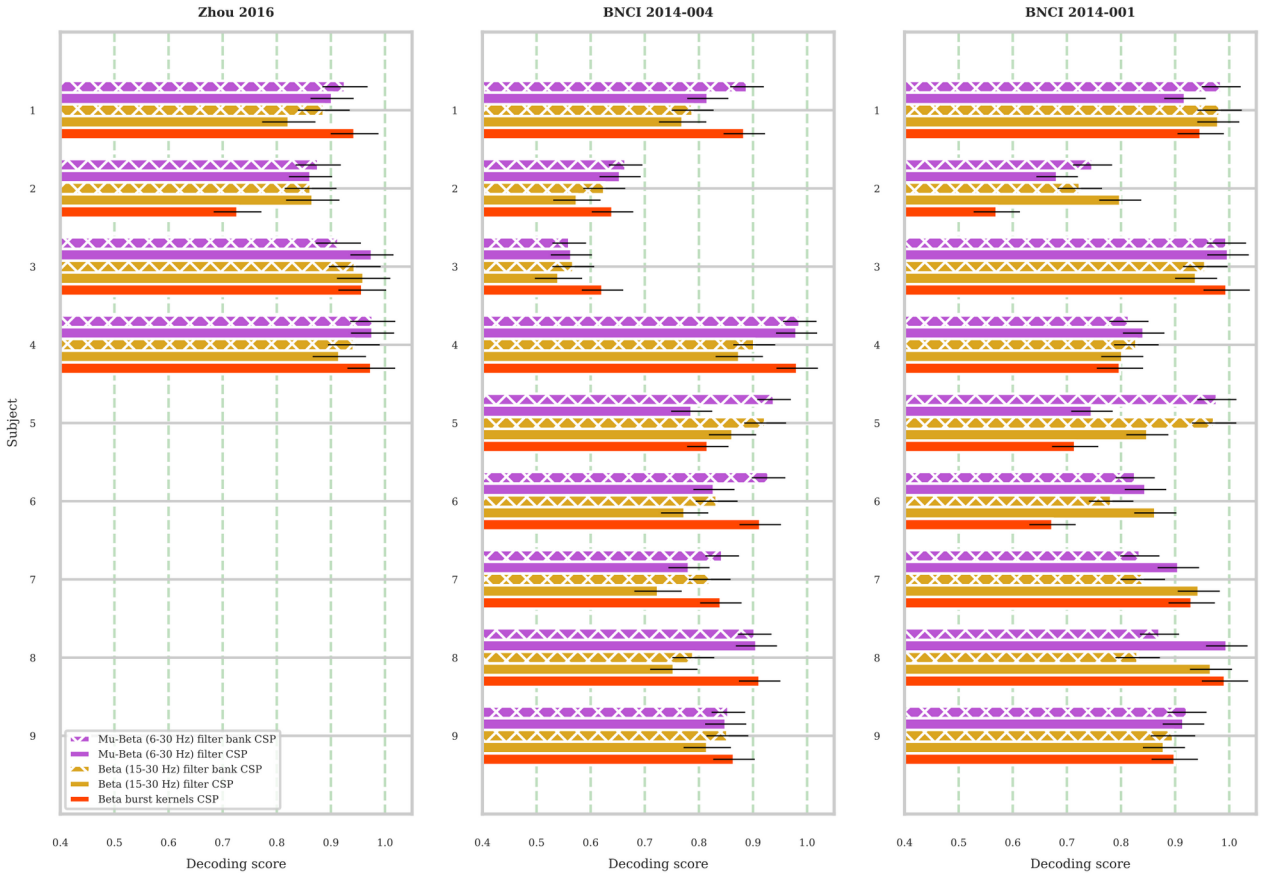


Figure 3.3.1: Average decoding score and standard deviation per dataset, subject and classification feature.

global classification, using a similar model but with a Gaussian distribution. Statistical analyses were conducted using R (v4.1.2) and lme4 (v1.1-31; (Bates et al., 2015)). Fixed effects were assessed using type II Wald X^2 tests using car (v3.1-1; (Fox and Weisberg, 2019)). Pairwise Tukey-corrected follow-up tests were carried out using estimated marginal means from the emmeans package (v.1,8,7; (Lenth, 2023)).

3.3.4. Results

We estimated the across-session decoding score per subject of each dataset using the waveform-resolved approach. In order to assess the significance of the waveform-resolved burst rate features we also computed classification features based on signal power and compared the different decoding results. We used a filter bank approach to assess whether the number of spatial features used for classification affected the decoding scores (Figure 3.3.1).

Across all datasets, the waveform-resolved burst rate features resulted in statistically significant improvement in decoding performance compared to beta band power estimated using a single filter ($X^2(5) = 97.081$, $p < 0.001$), non-significant differences compared to the beta band filter bank and mu-beta band single filter approaches ($p = 0.1047$ and $p = 0.9987$ respectively), and significant



Figure 3.3.2: Average difference in decoding score between classification scores of a transfer learning session and classification scores obtained using all available trials per subject. A value of 0 indicates no difference in decoding between the two approaches. Positive values or negative values indicate a performance gain or loss respectively when adopting a transfer learning approach.

decoding score decrease compared to mu-beta band filter bank approach (p = 0.004) (Sup. Figure 3.3.1).

Moreover, we assessed whether the beta burst kernels can be exploited in a transfer learning approach. To do so we iteratively estimated the kernels based on the recordings of one session and used them for transforming the recordings of the remaining sessions. We also examined whether we can use kernel-specific CSP filters for transfer learning. We compared these approaches to transfer learning of CSP filters after applying the standard filtering techniques.

The difference between the results depicted in Figure 3.3.1. and the transfer learning approach results per subject of each dataset are depicted in Figure 3.3.2. Negative values indicate greater decoding performance when estimating the results based on all available recordings, whereas positive values indicate an improvement in decoding score using transfer learning. Interestingly, transfer learning based on the beta burst kernels not only maintained the overall decoding score, but was also the only method that had the potential to improve decoding for some of the subjects.

The two kernel-based transfer learning approaches yielded statistically non-significant discrepancies in decoding score difference ($X^2(6) = 28.8$, p = 0.93). Transfer learning based only

on the kernels yielded significantly smaller reduction in decoding score difference compared to all filtering methods ($p = 0.013$ vs beta band filter; $p < 0.001$ vs beta band filter bank; $p = 0.0237$ vs mu-beta band filter; $p = 0.0011$ vs mu-beta band filter bank) (Sup. Figure 3.3.1). Transfer learning based on kernel-specific CSP patterns resulted in significantly smaller decoding score differences in all comparisons except for filtering in the mu-beta band using a single filter ($p = 0.0392$ vs beta band filter; $p = 0.0161$ vs beta band filter bank; $p = 0.3061$ vs mu-beta band filter; $p = 0.034$ vs mu-beta band filter bank) (Sup. Figure 3.3.1).

3.3.5. Discussion

Recently, the fields of neurophysiology and systems neuroscience have been experiencing a surge in the development of novel methods for analyzing neural recordings. An increasing number of articles are concerned with unveiling traditionally disregarded signal characteristics (Jones, 2016; Little et al., 2019; Lundqvist et al., 2016; Rayson et al., 2023; Shin et al., 2017; Szul et al., 2023; Torrecillos et al., 2018; Wessel, 2020) with several important implications for BCI. Particularly, the description of beta bursts has put into question the importance of band-limited power modulations in motor or MI tasks.

BCI applications often rely on signal power under the assumption of sustained and/or oscillatory signals. However, the description of waveform-specific beta burst modulations opens up new possibilities and holds the potential of improving decoding (Papadopoulos et al., 2024). In this article we verified that waveform-resolved burst rate features can be informative markers of the underlying brain activity during MI tasks. In line with previous results we showed that indeed waveform-resolved burst rate features can be more informative than beta band power. We also showed that the information content of these features is comparable to that of filtering within a wider frequency band encompassing the mu band, although the mu-beta filter bank approach still yielded the best decoding results. A possible explanation for this finding is that beta burst kernels also capture slower modulations of the underlying activity and, thus, by adapting the waveform-resolved burst rate features to the mu band characteristics (Y. Y. Chen et al., 2021; Vigué-Guix and Soto-Faraco, 2023) we may be able to further improve decoding.

Additionally, we adopted an inter-session transfer learning approach, and showed that the waveform-resolved features are stable over recording sessions. We demonstrated that the reduction in classification score can be minimal and that these features can even contribute in improving decoding for subjects with low classification score. This finding is important because it proves that, despite the difficulty of exploiting spatial features learned during previous sessions, there is potential in improving how previously acquired data can be leveraged during offline calibration or even online decoding sessions. In the future, an assessment of the across-subject kernel similarity may open the path for more reliable inter-subject transfer learning.

3.3.6. Conclusion

The waveform-resolved burst rate analysis is a promising, neurophysiology-grounded alternative to classic descriptions of beta band activity in motor and MI tasks. The results of this work reaffirm that classification features based on beta bursts can efficiently decode MI binary classification tasks and suggest that beta burst kernels are stable across recording sessions, thus potentially serving as an interesting feature inter-session transfer learning.

Chapter 4 - Discussion

4.1 Summary of contributions

State-of-the-art, non-invasive, MI-BCI pipelines, most notably those based on the combination of spatial filtering (Blankertz et al., 2007; Koles, 1991; Lu et al., 2013; McFarland et al., 1997; Müller-Gerking et al., 1999) or Riemannian techniques (Barachant et al., 2013, 2012; Congedo et al., 2017) with linear or non-linear classifiers, and more recently some deep learning approaches (Chiarelli et al., 2018; Eder et al., 2024; Kwon et al., 2020; Roy, 2022; Schirrmeister et al., 2017; Tayeb et al., 2019), rely on band-passed power features in order to decode user intentions. The employed band-passed filters are either broadband filters or filter banks that especially focus on the mu (~ 8 – 13 Hz), beta (~ 13 – 30 Hz) and low gamma (~ 30 – 40 Hz) frequency bands. This design choice is based on the findings of several studies that relate spatially and frequency limited signal amplitude modulations to specific changes of ongoing (Alayrangues et al., 2019; Cheyne and Ferrari, 2013; Kobler et al., 2020; Makeig et al., 2000; Neuper et al., 2006; Pfurtscheller, 1981; Pfurtscheller et al., 2006; Pfurtscheller and Berghold, 1989), attempted (Blokland et al., 2015; S. Chen et al., 2021; Horki et al., 2014; Müller-Putz et al., 2007) and imagined (Jeannerod, 1995; Pfurtscheller and Lopes da Silva, 1999) movements.

However, recent literature has placed emphasis on the fact that these signal changes are unveiled when averaging multiple trials in the frequency or time-frequency domain (Jones, 2016; Little et al., 2019) under the assumption of sustained, sinusoidal brain activity. There is now consensus that on the single trial level brain signals exhibit transient dynamics (Cole and Voytek, 2019; Coleman et al., 2024; Giehl and Siegel, 2024; Jones, 2016; Little et al., 2019; Lundqvist et al., 2024, 2016; Rayson et al., 2023; Shin et al., 2017; Szul et al., 2023; Torrecillos et al., 2018; Vigué-Guix and Soto-Faraco, 2023; Wessel, 2020; West et al., 2023) and that these signal features cannot be captured by standard techniques designed to analyze amplitude modulations of oscillatory activity. Inspired by this literature and motivated by the fact that non-invasive BCIs still face major limitations for wider adoption outside the lab (Jeunet et al., 2019, 2018; Lotte et al., 2018b; Mladenović, 2021; Mladenović et al., 2022; Pillette et al., 2021; Vidaurre and Blankertz, 2010), in this work we examined the feasibility of incorporating transient activity features in non-invasive, motor imagery brain computer interface pipelines in order to improve the reliability of relevant applications. We reasoned that, since transient activity is more informative of ongoing motor tasks on the single trial level, this could also be the case for motor imagery given the similarities of the recruited cortical networks and recorded signal features (Meng et al., 2018; Miller et al., 2010; Pfurtscheller and Lopes da Silva, 1999; Raffin et al., 2012; Sugata et al., 2016) among the two tasks.

Specifically, we focused on the analysis of beta burst activity and, first, we explored if and which signal features can be used in order to reliably decode motor intention under a binary classification setting. To do so, we took advantage of numerous, publicly available benchmark MI EEG datasets (Aristimunha et al., 2023; Jayaram and Barachant, 2018). We detected beta bursts in the frequency range of 15 – 30 Hz in time-frequency domain using a recently introduced algorithm (Szul et al., 2023) and then analyzed the activity of channels C3 and C4 in terms of the overall burst rate i.e., treating all beta bursts as a unitary phenomenon, and several beta burst features like amplitude, volume and frequency content. Moreover, we explored whether a combination of these features could further enhance classification results. An alternative way that succinctly

conveys all this information is the description of the bursts' waveform shape. Based on previous findings which have shown that the rate of bursts with specific shapes is differentially modulated during a joystrick task that required rapid upper limb movements (Szul et al., 2023), we also analyzed the waveform-resolved burst rate of the EEG recordings. All these classification features were benchmarked against the power modulation of the signals filtered within the beta band. This preliminary analysis revealed that MI indeed induces waveform-specific burst rate changes, which when used as classification features improved decoding accuracy compared to any other representation of the beta frequency band activity on the population level.

Having shown that BCI could benefit from evaluating beta burst activity recorded from the sensorimotor cortex we set out to improve our approach to analyzing waveform-resolved activity. The major limitation of the aforementioned study was the need to explore a large hyper-parameter space in order to identify which beta burst waveform shapes were relevant to the execution of the MI task. This computationally expensive processing step, that scales with the number of included channels, was not justifiable for offline – much less online – analyses which use multiple recording sensors. To circumvent this problem, first we defined a metric that identifies beta burst waveforms whose burst rate is expected to be modulated during a MI task based on a small set of calibration data. These waveforms' shapes are approximated by computing the euclidean average of subsets of detected bursts and as such they can be directly utilized in order to compute their rate in the EEG recordings. Therefore, these waveforms can be used as filters in the time domain by convolving the raw signals with them. The resulting signals measure the similarity between the raw signals and any selected waveform and hence and constitute a proxy to each waveforms' rate. The proxy burst rates can be efficiently estimated for an arbitrary number of recording channels, thus making waveform-resolved burst rate analysis suitable for common BCI pipelines.

In a subsequent study we used our refined approach to compute the waveform-resolved burst rate and analyzed again the same benchmark datasets along with a composite MI dataset that was made available in the meantime (Dreyer et al., 2023). Unlike our previous study, we used all available recording sensors and assessed the potential advantages of these features for BCI applications by combining them with spatial filtering and a linear classifier. We investigated the time-resolved classification accuracy and information transfer rate achieved by these features and contrasted them to results obtained using broadband filtering and filter banks to estimate power modulations in the mu and beta frequency bands. Our results demonstrated that the waveform-resolved burst rate increased maximum classification score and information transfer rate by achieving equivalent or superior decoding results in a shorter amount of time compared to beta band and mu-beta band power. This was compelling evidence that beta bursts are a good descriptor of single trial beta band activity that can improve the reliability of non-invasive, MI-BCI paradigms.

Additionally, we attempted to shed more light on the neurophysiological mechanisms that allowed waveform-resolved burst rate to improve classification and information transfer rate of motor imagery decoding. To tackle this point we used an indirect approach. We investigated if waveform-specific burst rate changes constitute a signal property that is better preserved across different recording sessions compared to amplitude modulations. If so, this would attest to beta band activity being a composite of heterogeneous processes co-occurring in time and space, and that by disentangling the contribution of specific processes that occur within this frequency band we can identify those that are most relevant to the ongoing motor imagery task.

To answer this question, in our final study we re-used three of the already analyzed datasets that specifically comprised recordings from multiple sessions. We computed the difference between classification results estimated when combining data from all sessions against results based on the transfer of learned features from a specific session to all other sessions. In more detail, we computed the relevant for the MI task beta burst waveforms in one session and estimated the classification score in all other sessions either by transferring and utilizing the learned waveforms or the spatial filters corresponding to them. Then, we computed the across-session average classification score difference between the “non-transfer” and “transfer” conditions. We, also, conducted a similar analysis for spatial features of mu and beta band power modulations, and again compared the results between the different features. We showed that, when using beta bursts, classification score loss during transfer learning was minimized compared to standard band power features. These results imply that beta band power constitutes an aggregate measure of the underlying neurophysiological processes which are better characterized in terms of bursts, therefore positing the modulation of the rate of specific beta bursts as a more informative descriptor of these processes.

4.2 Limitations

4.2.1. Data selection and pre-processing

Despite the promising insights we gained from our contributions, the analysis conducted in this work is characterized by several limitations. First of all, we want to emphasize that our main motivation for this work was to compare beta bursts to power modulations because the latter are the standard features used in MI-BCI applications. To our knowledge, there exists no literature describing beta burst activity modulations during motor imagery prior to this work. Motor-related beta burst activity in healthy adults has been traditionally studied in experiments involving upper limb movements (Bonaiuto et al., 2021; Coleman et al., 2024; Feingold et al., 2015; Little et al., 2019; Lofredi et al., 2018; Rayson et al., 2023; Torrecillos et al., 2018; West et al., 2023). As such, we needed to analyze a large number of datasets so that we could hopefully reproduce a consistent finding across all of them. Fortunately, a big amount of MI data is available online. However, the spatial resolution limitations of EEG signals are well-known and introducing multiple classes with overlapping spatial patterns would most likely hamper our analysis. This is the reason why for the purposes of this work we have constrained our analysis to binary classification tasks.

Further, in this work we have opted for a simple pre-processing step which may have not been able to remove all artifacts that may be present in the highly heterogeneous recordings of all subjects included in the seven datasets we have analyzed. To that effect more sophisticated pre-processing algorithms could be investigated. In the context of electroencephalography, and BCI specifically, independent component analysis (ICA) (Chaumon et al., 2015; Kachenoura et al., 2008; Onton et al., 2006) may be good for removing stereotyped physiological artifacts e.g., ocular artifacts (Fatourechi et al., 2007), that have been shown to affect BCI classification (Mcdermott et al., 2021). However, it is generally recommended to use ICA on data with a large number of channels (Onton et al., 2006), which is not the case for four of the datasets studied here. Also, ICA requires calibration data and often manual component selection, both, and particularly the latter, posing as major limitations for BCI applications. Alternatively, it has been proposed that simpler techniques like regression can achieve comparable results (Ronca et al., 2024; Wallstrom et al., 2004). On the contrary, non-stereotyped artifacts like muscle activity pose a more significant challenge and algorithms like artifact subspace reconstruction (ASR) (Chang et al., 2020) have been shown to yield better results (Medeiros de Freitas et al., 2020). Given that a more sophisticated pre-processing pipeline may lead to more distortions of the recordings (Wallstrom et al., 2004) which would, at least in theory, be an undesirable corollary for the burst detection technique and the characterization of beta burst waveforms' shapes, in this work we decided to minimize the impact of pre-processing on the signals.

4.2.2. Data processing

Another point that is related to the signals has to do with the degree of oscillatory activity that is present in the EEG recordings and the suitability of our algorithm to analyze such recordings. For

example, we can speculate that oscillations rather than bursts are prevalent in the case of the Weibo 2014 dataset based on three facts: a) the smaller number of detected burst waveforms (Sup. Figure 3.2.2 b-e), b) the prevalence of (high-power) long lasting “bursts” that is, bursts lasting at least 5 cycles, partially attributable to the presence of high-frequency noise despite pre-processing (Sup. Figure 3.2.2 a), iii) the significantly reduced number of PCA components explaining at least 90% of the data variance. Although it seems that, taking into account the supplementary material (Sup. Figures 3.2.4 and 3.2.5), power-based decoding for this dataset is mainly driven by mu activity modulations, we should note that it is likely that our methodology simply cannot uncover features that differ drastically from those detected using a power analysis and is thus sub-optimal for such datasets.

Moreover, the waveform-resolved analysis of beta burst activity presented in this work relies on several methodological choices whose impact on the reported results remains to be studied. First, the burst detection method used here is by design lenient and may be more prone to labeling noise fluctuations as bursts compared to other amplitude thresholds described in the literature (Little et al., 2019; Lundqvist et al., 2016; Wessel, 2020). On the one hand, this is an undesirable consequence that is expected to resolved by the dimensionality reduction step discussed next. On the other hand, standard amplitude thresholds are strict and discard a significant portion of the activity with no real justification since the ground truth is in any case unknown. A comparative analysis between the properties of bursts detected using several thresholding techniques should provide a clearer picture of the impact of this choice to the results.

Second, in order to characterize waveforms that are relevant to the MI task we have used principal component analysis (PCA). The selection of PCA to reduce the dimensionality of the detected burst waveforms follows the methodology described in previous work from our group (Szul et al., 2023), but this choice is not mandatory. PCA helps us interpret the modulation of different waveforms, however it may not be the best algorithm to maximize decoding accuracy or information transfer rate. We believe that the use of alternative techniques could potentially allow us to better understand waveform modulations and improve decoding. At the same time, we feel that a formal examination of multiple candidate algorithms would be required in order to get a clear understanding of the advantages and disadvantages of each choice, but we believe that undertaking such a task was out of this work’s scope.

Third, a major part of this work relies on exploiting burst activity from channels C3 and C4 specifically, in order to define an index that can help us identify waveform shapes that are relevant to the MI task. This approach is based on the assumption that these channels capture task-related modulations due to their localization. However, this assumption may be violated under several circumstances, like for example poor positioning of EEG electrodes, electrode drifting, execution of movements during the task and poor, or absent discernible lateralization of EEG activity owing to the MI. A possible way to circumvent these problems could be to first estimate on the user level a cluster of electrodes which exhibit significantly different activity from baseline in terms of signal amplitude. Then, after assigning the selected electrodes to distinct brain areas, a more general implementation of the modulation index I_m described in this work could be used to characterize the differential modulation of beta burst activity.

The last methodological choice concerns the need to perform a hyper-parameter search to identify which waveforms’ burst rate modulation (either directly or indirectly using the convolution method) should be selected for the analysis. Here, we have selected to restrain our hyper-parameter grid

search in an attempt to reduce computational complexity. A formal exploration of a much larger hyper-parameter space through greedy search or alternative approaches should be considered if the aim of a study is to attain the best possible decoding results based on the waveform-resolved burst rate. Such an approach could be based on the adaption of previously described algorithms that attempt to identify the optimal time window and filtering frequency band for motor imagery decoding (Lotte and Jeunet, 2018; Schaworonkow and Voytek, 2021; Singh Malan and Sharma, 2021; Xu et al., 2014).

4.2.3. Classification results

Another limitation that is linked to the previous point is the selection of classifiers to assess the decoding results (and consequently information transfer rate) based on the different features examined in this work. Here we have opted for a simple linear classifier, namely linear discriminant analysis (LDA) (Tharwat et al., 2017), but any of numerous (linear or non-linear) classifiers could be used instead. Our choice was motivated by the fact that the combination of common spatial pattern (CSP) and LDA for classification of motor imagery signals in BCI applications is the benchmark algorithm against which new algorithms are usually measured. This is because the applied signal transformations are tractable, computationally efficient and often give very good results especially in offline evaluations (Carrara and Papadopoulo, 2024; Jayaram and Barachant, 2018). This is also why we have selected to use the combination of these algorithms as the benchmark pipeline for a major part of this work. Since the goal for this study has been to compare the burst waveform features to standard signal power features, we feel that the use of alternative processing steps and/or classifiers (e.g., a Riemannian classifier of the covariance of the waveform-resolved burst rate) in an attempt to optimize results would be an interesting avenue to pursue in another study. An implementation of an artificial neural network or deep learning architecture that could take advantage of these novel features could also be an interesting option to consider.

As already stated, the main goal of this study has been to provide a clear comparison between different beta band (15 – 30 Hz) features that is, beta bursts and beta power. However, BCI decoding algorithms usually rely both on mu (8 – 13 Hz) and beta band activity. Thus, following the first study which established the feasibility of using beta burst for BCI, we deemed it important to also formally compare our results to a gold-standard approach. Moreover, having provided these comparisons to the reader, we decided to also include a comparison to the mu band power features for transparency. Literature has shown that activity in the upper mu – lower beta band (~ 10 – 20 Hz) is usually the most important for motor and motor imagery tasks involving the upper limbs (Kilavik et al., 2012; Lotte, 2014; Lotte and Rimbert, 2022; Schmidt et al., 2019). This is also suggested by the results presented in parts of this work, although when using a filter bank approach to decode power modulations we have not examined which sub-band contributes the most to decoding. Likewise, we did not attempt to find individualized spectral peaks and adjust the filter limits when assessing power-based classification results assuming that the filter bank approach would suffice.

Finally, we have not put emphasis on and did not provide any statistical analysis regarding the comparison between the waveform-resolved burst rate and mu band power because, although

complementary, the information provided by the mu and beta bands is distinct. Indeed, the information of the two bands could be combined in several ways, however exploring the different options (e.g. feature fusion, use of ensemble classifiers and/or alternative classifiers) would require a comprehensive study that was outside this work's scope. We are currently in the process of investigating novel features that better describe the non-sinusoidal mu oscillations on the single trial level (Cole and Voytek, 2019; Giehl and Siegel, 2024; Vigué-Guix and Soto-Faraco, 2023), and we believe that this will be of great interest to many readers in a future study (see section 4.3.2.1).

4.3 Future directions

4.3.1. Experiment of executed and imagined wrist movements

This work has served as a proof of concept for the feasibility of incorporating features of transient brain activity in classification paradigms, particularly focusing on the characterization of waveform-specific beta burst rate modulation during motor imagery tasks. The analyses performed here are restricted to binary classifications for reasons already discussed, but the question still remains whether beta bursts and more generally transient brain activity could be taken advantage of in order to bolster the reliability of more complicated BCI paradigms like multi-class or even continuous decoding problems.

To tackle this question we have designed an experiment that involves execution and imagination of wrist flexion and extension movements. In this experiment a group of healthy participants undergoes two recording sessions, one using EEG and another using hpMEG with personalized headcasts. Each session comprises two runs, one focusing on left hand and the other on right hand movements and imagery. On the population level, all runs have been organized in a counter-balanced fashion. During each run, participants are asked to perform a series of short trials of real or imagined wrist movements in a pseudo-randomly determined sequence of trial blocks (Sup. Figure 4.3.1 a).

Before the first run, participants are asked to perform a short training session that familiarizes them with the paradigm. Unlike the actual experiment, during training participants are initially presented with online feedback of executed movements which is progressively diminished in consecutive blocks of trials. The rationale behind this design choice is for participants to learn the mapping between wrist rotation and the cursor movement on the screen (see below).

To monitor hand movements, in each run participants place their hand in a custom-built contraption on top of a wooden base. The contraption is designed so as to rotate around a fixed point corresponding to a participants' radiocarpal (wrist) joint. In front of the hand a magneto-encephalography compatible mouse which records wrist movements is placed. The hand view is occluded by a box in order to motivate the participants to pay attention on the kinesthetic experience of the executed and imagined movements. The participants are comfortably seated on a chair. Instructions and stimuli are presented on a screen placed approximately at a distance of 60 cm.

Each trial starts with the participant placing their hand in neutral position that is, at 0° wrist flexion. A fixation cross appears in the middle of the screen along with a semi-circular path around it for a variable period of 2 to 4 seconds. Then, a red triangle cursor representing the participant's hand position and a blue circle representing the target of the movement to be executed or imagined appear on the screen for a period of 2 seconds, after which the circle color changes to magenta indicating the go cue. The target positions can correspond to 30° or 60° flexion or extension of the wrist and their pseudo-random order is predetermined per block of trials.

During action trials the red cursor disappears when a participant starts moving their hand. During imagery trials the cursor disappears automatically when the target changes color serving as the go

cue. Participants are given 1.5 seconds to start moving their hand in the action condition. Failing to do so will result in a canceled trial followed by a message to begin performing their movements earlier during subsequent trials. A premature hand movement that is, before the go cue onset, in either condition results in aborting the trial and is followed by a message to wait for the go cue during subsequent trials. In total the participants are given 4.5 seconds to complete a trial during both the real and imagined movements conditions. In the case of real movements a trial is terminated earlier if a participant stops moving their wrist for 1 second. Then, in both conditions the target disappears for 2 seconds during which the participants are asked to not move. After the completion of a real movement trial the fixation cross disappears and a new target corresponding to the 0° flexion appears asking the participant to place their hand in neutral position before the next trial starts. The subjects can indicate that they have repositioned their hand by pressing a button using the other hand. After that, the arc stays on for a total of 2 seconds before the next trial starts, as is also the case for imagery trials (Sup. Figure 4.3.1 b, c). Each block of executed movements is composed of 20 trials and each block of imagined movements is composed of 22 trials.

During a block of imagery trials some trials correspond to catch trials. In these trials, after a variable delay following the cue onset, the participants are asked to evaluate the quality of their motor imagery by indicating the extent of flexion or extension that they believe they have achieved in the time window they were given. To do so, they are asked to press a button with their “free” hand in order to move the cursor around the arc by increments of 15° (Sup. Figure 4.3.1 d). The reported amplitudes are compared to the real movements performed during the training session and participants are asked to adjust the speed of their imagery if necessary.

The design of this experiment is expected to provide us with a reach dataset. As far as the utilization of the recordings modalities is concerned, we believe that the higher quality of signals recorded with hpMEG will allow us to study in detail the neurophysiological differences between action execution and imagination at a first step. Then, we will attempt to further disentangle signal properties in relation to the multiple design levels, i.e., left or right hand, wrist flexion or extension, discretized amplitude of wrist flexion or extension and possibly continuous wrist angle trajectory. As discussed in Chapter 2 - Motivation, we hope that hpMEG forward models can then been used to guide EEG decoding analyses of real and imagined movements serving as another step towards improving existing MI-BCI paradigms.

Finally, a small cohort of post-stroke patients in the subacute phase will also participate in one EEG session. Following training, participants will be asked to attempt and/or perform a number of trials in blocks as described above. This way we will be able to conduct a preliminary analysis on the feasibility of using features like beta bursts in rehabilitation paradigms.

4.3.2. Other prospects

4.3.2.1. Analysis and combination of alternative features

A notable direction following this work would be the combination of multiple features in an attempt to maximize classification scores for each participant performing motor imagery. A simple first step

could be the fusion of waveform-resolved burst rate and signal power in the mu and beta frequency bands. Using these two sources of information complementarily should in theory guarantee that we can achieve the best possible decoding on the subject level and possibly offer a slightly increased classification performance. Another possibility is the incorporation of additional features in such an analysis. Two outstanding candidates are the aperiodic activity and an alternative analysis of the mu band activity.

Recently there is an increasing interest in disentangling the contributions of aperiodic and periodic (oscillations and bursts) components in the recorded signals (Barry and De Blasio, 2021; Brady and Bardouille, 2022; Bush et al., 2023; Donoghue, 2024; Donoghue et al., 2021, 2020; Gerster et al., 2022; Wilson et al., 2024). Aperiodic activity, also referred to as 1/f, pink noise or scale-free activity, is a broadband activity that is considered to reflect background processes relating to the integration of electrical currents and has been linked to the excitation-inhibition balance of neural circuits (Gao et al., 2017). Studies which have proposed algorithms to differentiate periodic and aperiodic activity in neural recordings have linked it to aging and behavior (Donoghue et al., 2020; Wilson et al., 2024). We speculate that a robust estimation of aperiodic activity could be interesting target feature for BCI in general, possibly indexing different brain states or tracking changes across recording sessions and different populations.

Regarding the mu frequency band activity we know that activity in this frequency band is more sustained compared to that in the beta band (Szul et al., 2023; Zhang et al., 2024), thus an alternative approach is required to characterize non-sinusoidal, oscillatory signals that are modulated due to a motor imagery task. To do so, we could take advantage of bicoherence and bispectrum to characterize and recreate mu band oscillations. Briefly, bispectrum and it’s normalized variant, bicoherence, measure the phase-amplitude coupling of a signal with respect to itself at several frequencies (Giehl et al., 2021; Giehl and Siegel, 2024; Hagihira et al., 2001; Sigl and Chamoun, 1994). It has been shown that these methods can be used in order to identify the fundamental frequency of a signal, its harmonics and the corresponding frequency-specific amplitude and phase shifts, measures which suffice to reconstruct any non-sinusoidal oscillation using Fourier series (Giehl and Siegel, 2024). By applying this methodology when analyzing signals recorded from the sensorimotor cortex during different task conditions the goal is to examine whether there is a task-dependent, waveform specific modulation of signals within the mu frequency band that could be leveraged in order to provide additional information to amplitude modulation and, as such, improve BCI performance.

4.3.2.2. Feasibility of approach in patient populations

A main motivation behind this project has been the wider adoption of non-invasive BCI paradigms by populations of individuals that could significantly benefit from establishing novel communication routes with their environment. A prime example of such populations corresponds to selected groups of patients suffering from motor deficits following central nervous system lesions. In clinical settings BCI could serve as assistive technology to guide rehabilitation protocols when attempting to restore motor deficits (Bai et al., 2020; Cervera et al., 2018; Coscia et al., 2019; McFarland et al., 2017; Raffin and Hummel, 2017). Also, a bedside diagnosis of conscious but unable to respond individuals could potentially be envisioned (Horki et al., 2014; Luauté et al., 2015). In other

settings, individuals suffering from permanent motor deficits, like for example following a spinal cord injury, could use BCI in order to gain reliable control of applications requiring a small number of degrees of freedom (Mondini et al., 2024; Scherer et al., 2015; Séguin et al., 2024). To test the hypothesis that transient activity can improve non-invasive decoding for these populations a large sample of people with heterogeneous pathologies and clinical phenotypes needs to be studied.

In such studies a great variability of observations is expected to be found, not only attributing to the distinct pathophysiological mechanisms underlying each type of lesion, but also to the lesions varying phase since they were established, their extent and localization. However, there is potential to uncover systematic relationships between these factors and specific signal features. The characterization of pathology-dependent transient and oscillatory activity brain signal changes would greatly enhance our understanding of the re-organization of cortical networks and could greatly improve the ability to monitor rehabilitation progress, or establish reliable communication protocols for people suffering from speech impairments, major motor deficits or even patients in a locked-in state. Currently existing literature has already shown differences in beta burst activity recorded from the subthalamic nucleus in patients with Parkinson's disease (Anderson et al., 2020; Kehnemouyi et al., 2021; Khawaldeh et al., 2020; Lofredi et al., 2018; Torrecillos et al., 2018; Yeh et al., 2020) compared to normal populations.

In our group we have already conducted a preliminary study with an individual who, following a brainstem lesion, is suffering from tetraparesis. After extensive training the participant managed to control a virtual wheelchair in a video-game like environment of the Cybathlon competition using three motor imagery commands, namely "feet" to "move forward", "left forearm flexion" to "turn left" and "right forearm flexion" to "turn right". What is important in the context of this work, is the fact that the latter two commands were triggered by an online classifier that assessed the waveform-resolved burst rate modulations using the convolution method. Waveform shapes that were modulated by left and right forearm flexion MI had been identified in advance by an offline analysis of data collected in the course of several calibration sessions. Then, during online sessions the detection of upper limb motor imagery triggered the classifier that assessed whether the participant was attempting to "turn left" or "turn right". This experiment serves as a proof-of-concept for the feasibility of analyzing transient activity to perform MI decoding in groups of patients.

Chapter 5 - References

Abiri R, Borhani S, Sellers EW, Jiang Y, Zhao X. 2019. A comprehensive review of EEG-based brain-computer interface paradigms. *J Neural Eng* **16**. doi:10.1088/1741-2552/aaf12e

Alayrangues J, Torrecillos F, Jahani A, Malfait N. 2019. Error-related modulations of the sensorimotor post-movement and foreperiod beta-band activities arise from distinct neural substrates and do not reflect efferent signal processing. *Neuroimage* **184**:10–24. doi:10.1016/j.neuroimage.2018.09.013

Alkoby O, Abu-Rmileh A, Shriki O, Todder D. 2018. Can We Predict Who Will Respond to Neurofeedback? A Review of the Inefficacy Problem and Existing Predictors for Successful EEG Neurofeedback Learning. *Neuroscience* **378**:155–164. doi:https://doi.org/10.1016/j.neuroscience.2016.12.050

Allison BZ, Brunner C, Kaiser V, Müller-Putz GR, Neuper C, Pfurtscheller G. 2010. Toward a hybrid brain-computer interface based on imagined movement and visual attention. *J Neural Eng* **7**. doi:10.1088/1741-2560/7/2/026007

Anders C, Arnrich B. 2022. Wearable electroencephalography and multi-modal mental state classification: A systematic literature review. *Comput Biol Med* **150**:106088. doi:https://doi.org/10.1016/j.compbiomed.2022.106088

Anderson RW, Kehnemouyi YM, Neuville RS, Wilkins KB, Anidi CM, Petrucci MN, Parker JE, Velisar A, Brontë-Stewart HM. 2020. A novel method for calculating beta band burst durations in Parkinson's disease using a physiological baseline. *J Neurosci Methods* **343**:1–29. doi:10.1016/j.jneumeth.2020.108811

Aristimunha B, Carrara I, Guetschel P, Sedlar S, Rodrigues P, Sosulski J, Narayanan D, Bjareholt E, Quentin B, Schirrmeister RT, Kalunga E, Darmet L, Gregoire C, Abdul Hussain A, Gatti R, Goncharenko V, Thielen J, Moreau T, Roy Y, Jayaram V, Barachant A, Chevallier S. 2023. Mother of all BCI Benchmarks. doi:10.5281/zenodo.10034224

Arslan SS, Sinha P. 2024. Information transfer rate in BCIs: Towards tightly integrated symbiosis. *Biomed Signal Process Control* **87**. doi:10.1016/j.bspc.2023.105466

Bach P, Frank C, Kunde W. 2021. Why motor imagery isn't really motoric: Towards a reconceptualization in terms of effect-based action control. doi:10.15900/j.cnki.zylf1995.2018.02.001

Bai Z, Fong KNK, Zhang JJ, Chan J, Ting KH. 2020. Immediate and long-term effects of BCI-based rehabilitation of the upper extremity after stroke: A systematic review and meta-analysis. *J Neuroeng Rehabil* **17**:1–20. doi:10.1186/s12984-020-00686-2

Ball T, Demandt E, Mutschler I, Neitzel E, Mehring C, Vogt K, Aertsen A, Schulze-Bonhage A. 2008. Movement related activity in the high gamma range of the human EEG. *Neuroimage* **41**:302–310. doi:10.1016/j.neuroimage.2008.02.032

Baniqued PDE, Stanyer EC, Awais M, Alazmani A, Jackson AE, Mon-Williams MA, Mushtaq F, Holt RJ. 2021. Brain–computer interface robotics for hand rehabilitation after stroke: a systematic review. *J Neuroeng Rehabil* **18**:1–25. doi:10.1186/s12984-021-00820-8

Banville H, Falk TH. 2016. Recent advances and open challenges in hybrid brain-computer interfacing: a technological review of non-invasive human research. *Brain-Computer Interfaces* **3**:9–46. doi:10.1080/2326263X.2015.1134958

Barachant A, Bonnet S, Congedo M, Jutten C. 2013. Classification of covariance matrices using a Riemannian-based kernel for BCI applications. *Neurocomputing* **112**:172–178. doi:10.1016/j.neucom.2012.12.039

Barachant A, Bonnet S, Congedo M, Jutten C. 2012. Multiclass Brain-Computer Interface Classification by Riemannian Geometry. *IEEE Trans Biomed Eng* **59**:920–928. doi:10.1109/TBME.2011.2172210

Barry RJ, De Blasio FM. 2021. Characterizing pink and white noise in the human electroencephalogram. *J Neural Eng* **18**. doi:10.1088/1741-2552/abe399

Bârzan H, Ichim AM, Moca VV, Mureşan RC. 2022. Time-Frequency Representations of Brain Oscillations: Which One Is Better? *Front Neuroinform* **16**:1–14. doi:10.3389/fninf.2022.871904

Bates D, Mächler M, Bolker BM, Walker SC. 2015. Fitting linear mixed-effects models using lme4. *J Stat Softw* **67**. doi:10.18637/jss.v067.i01

Battaglia-Mayer A, Ferraina S, Mitsuda T, Marconi B, Genovesio A, Onorati P, Lacquaniti F, Caminiti R. 2000. Early coding of reaching in the parietooccipital cortex. *J Neurophysiol* **83**:2374–2391. doi:10.1152/jn.2000.83.4.2374

Benaroch C, Sadatnejad K, Roc A, Appriou A, Monseigne T, Pramij S, Mladenovic J, Pillette L, Jeunet C, Lotte F. 2021. Long-Term BCI Training of a Tetraplegic User: Adaptive Riemannian Classifiers and User Training. *Front Hum Neurosci* **15**:1–22. doi:10.3389/fnhum.2021.635653

Bhattacharyya S, Konar A, Tibarewala DN. 2014. Motor imagery, P300 and error-related EEG-based robot arm movement control for rehabilitation purpose. *Med Biol Eng Comput* **52**:1007–1017. doi:10.1007/s11517-014-1204-4

Blankertz B, Kawanabe M, Tomioka R, Hohlefeld FU, Nikulin V, Müller KR. 2007. Invariant common spatial patterns: Alleviating nonstationarities in Brain-Computer InterfacingAdvances in Neural Information Processing Systems.

Blankertz B, Tomioka R, Lemn S, Kawanabe M, Muller K-R. 2008. Optimizing Spatial Filters for Robust EEG Single-Trial Analysis. *IEEE Signal Process Mag* 41–56.

Blohm G, Cheyne DO, Crawford JD. 2024. MEG signals reveal arm posture coding and intrinsic movement plans in parietofrontal cortex.

Blokland Y, Spyrou L, Lerou J, Mourisse J, Jan Scheffer G, Geffen GJ Van, Farquhar J, Bruhn J. 2015. Detection of attempted movement from the EEG during neuromuscular block: Proof of principle study in awake volunteers. *Sci Rep* **5**:1–10. doi:10.1038/srep12815

Blokland Y, Spyrou L, Thijssen D, Eijsvogels T, Colier W, Floor-Westerdijk M, Vlek R, Bruhn J, Farquhar J. 2014. Combined EEG-fNIRS decoding of motor attempt and imagery for brain switch control: An offline study in patients with tetraplegia. *IEEE Trans Neural Syst Rehabil Eng* **22**:222–229. doi:10.1109/TNSRE.2013.2292995

Bonaiuto J, Little S, Neymotin SA, Jones SR, Barnes GR, Bestmann S. 2021. Laminar dynamics of high amplitude beta bursts in human motor cortex. *Neuroimage* **242**:118479. doi:10.1016/j.neuroimage.2021.118479

Bonaiuto JJ, Meyer SS, Little S, Rossiter H, Callaghan MF, Dick F, Barnes GR, Bestmann S. 2018a. Laminar-specific cortical dynamics in human visual and sensorimotor cortices. *Elife* **7**. doi:10.7554/eLife.33977

Bonaiuto JJ, Rossiter HE, Meyer SS, Adams N, Little S, Callaghan MF, Dick F, Bestmann S, Barnes GR. 2018b. Non-invasive laminar inference with MEG: Comparison of methods and source inversion algorithms. *Neuroimage* **167**:372–383. doi:10.1016/j.neuroimage.2017.11.068

Borich MR, Brodie SM, Gray WA, Ionta S, Boyd LA. 2016. Understanding the role of the primary somatosensory cortex: Opportunities for rehabilitation. *Neuropsychologia* **176**:139–148. doi:10.1016/j.neuropsychologia.2015.07.007

Borna A, Carter TR, Colombo AP, Jau YY, McKay J, Weisend M, Taulu S, Stephen JM, Schwindt PDD. 2020. Non-invasive functional-brain-imaging with an OPM-based magnetoencephalography system. *PLoS One* **15**:1–24. doi:10.1371/journal.pone.0227684

Boto E, Hill RM, Rea M, Holmes N, Seedat ZA, Leggett J, Shah V, Osborne J, Bowtell R, Brookes MJ. 2021. Measuring functional connectivity with wearable MEG. *Neuroimage* **230**. doi:10.1016/j.neuroimage.2021.117815

Boto E, Seedat ZA, Holmes N, Leggett J, Hill RM, Roberts G, Shah V, Fromhold M, Mullinger KJ, Tierney TM, Barnes GR, Bowtell R, Brookes MJ. 2019. Wearable neuroimaging: Combining and contrasting magnetoencephalography and electroencephalography. *Neuroimage*. doi:10.1016/j.neuroimage.2019.116099

Bräcklein M, Barsakcioglu DY, Vecchio A Del, Ibáñez J. 2022. Reading and Modulating Cortical b Bursts from Motor Unit Spiking Activity **42**:3611–3621.

Brady B, Bardouille T. 2022. Periodic/Aperiodic parameterization of transient oscillations (PAPTO)–Implications for healthy ageing. *Neuroimage* **251**:118974. doi:10.1016/j.neuroimage.2022.118974

Branco MP, de Boer LM, Ramsey NF, Vansteensel MJ. 2019. Encoding of kinetic and kinematic movement parameters in the sensorimotor cortex: A Brain-Computer Interface perspective. *Eur J Neurosci* **50**:2755–2772. doi:10.1111/ejn.14342

Brochier T, Spinks RL, Umilta MA, Lemon RN. 2004. Patterns of muscle activity underlying object-specific grasp by the Macaque monkey. *J Neurophysiol* **92**:1770–1782. doi:10.1152/jn.00976.2003

Brodu N, Lotte F, Lécuyer A. 2011. Comparative study of band-power extraction techniques for Motor Imagery classification. *IEEE SSCI 2011 - Symp Ser Comput Intell - CCMB 2011 2011 IEEE Symp Comput Intell Cogn Algorithms, Mind, Brain* 95–100. doi:10.1109/CCMB.2011.5952105

Brovelli A, Lachaux JP, Kahane P, Boussaoud D. 2005. High gamma frequency oscillatory activity dissociates attention from intention in the human premotor cortex. *Neuroimage* **28**:154–164. doi:10.1016/j.neuroimage.2005.05.045

Bruns A. 2004. Fourier-, Hilbert- and wavelet-based signal analysis: Are they really different approaches? *J Neurosci Methods* **137**:321–332. doi:10.1016/j.jneumeth.2004.03.002

Buccino AP, Keles HO, Omurtag A. 2016. Hybrid EEG-fNIRS asynchronous brain-computer interface for multiple motor tasks. *PLoS One* **11**:1–16. doi:10.1371/journal.pone.0146610

Bush A, Zou J, Lipski WJ, Kokkinos V, Richardson RM. 2023. Broadband aperiodic components of local field potentials reflect inherent differences between cortical and subcortical activity. *bioRxiv* 2023.02.08.527719.

Buzsáki G, Anastassiou CA, Koch C. 2012. The origin of extracellular fields and currents-EEG, ECoG, LFP and spikes. *Nat Rev Neurosci* **13**:407–420. doi:10.1038/nrn3241

Buzsáki G, Draguhn A. 2004. Neuronal olscillations in cortical networks. *Science (80-)* **304**:1926–1929. doi:10.1126/science.1099745

Camargo-Vargas D, Callejas-Cuervo M, Mazzoleni S. 2021. Brain-computer interfaces systems for upper and lower limb rehabilitation: A systematic review. *Sensors* **21**:1–22. doi:10.3390/s21134312

Caminiti R, Johnson PB, Galli C, Ferraina S, Burnod Y. 1991. Making arm movements within different parts of space: The premotor and motor cortical representation of a coordinate system for reaching to visual targets. *J Neurosci* **11**:1182–1197. doi:10.1523/jneurosci.11-05-01182.1991

Campbell WW, Barohn RJ. 2020. DeJong's The Neurologic Examination, 8e. Lippincott Williams & Wilkins, a Wolters Kluwer business.

Carrara I, Papadopoulo T. 2024. Pseudo-online framework for BCI evaluation: a MOABB perspective using various MI and SSVEP datasets. *J Neural Eng* **21**. doi:10.1088/1741-2552/ad171a

Ceradini M, Losanno E, Micera S, Bandini A, Orlandi S. 2024. Immersive VR for upper-extremity rehabilitation in patients with neurological disorders: a scoping review. *J Neuroeng Rehabil* **21**:1–20. doi:10.1186/s12984-024-01367-0

Cervera MA, Soekadar SR, Ushiba J, Millán J del R, Liu M, Birbaumer N, Garipelli G. 2018. Brain-computer interfaces for post-stroke motor rehabilitation: a meta-analysis. *Ann Clin Transl Neurol* **5**:651–663. doi:10.1002/acn3.544

Chang CY, Hsu SH, Pion-Tonachini L, Jung TP. 2020. Evaluation of Artifact Subspace Reconstruction for Automatic Artifact Components Removal in Multi-Channel EEG Recordings. *IEEE Trans Biomed Eng* **67**:1114–1121. doi:10.1109/TBME.2019.2930186

Chaudhary U, Birbaumer N, Ramos-Murguialday A. 2016. Brain–computer interfaces in the completely locked-in state and chronic stroke, 1st ed, Progress in Brain Research. Elsevier B.V. doi:10.1016/bs.pbr.2016.04.019

Chaumon M, Bishop DVM, Busch NA. 2015. A practical guide to the selection of independent components of the electroencephalogram for artifact correction. *J Neurosci Methods* **250**:47–63. doi:10.1016/j.jneumeth.2015.02.025

Chavarriaga R, Fried-Oken M, Kleih S, Lotte F, Scherer R. 2016. Heading for new shores! Overcoming pitfalls in BCI design. *Brain-Computer Interfaces* **4**:60–73. doi:10.1080/2326263X.2016.1263916

Chavarriaga R, Sobolewski A, Millán J del R. 2014. Errare machinale est: The use of error-related potentials in brain-machine interfaces. *Front Neurosci* **8**:1–13. doi:10.3389/fnins.2014.00208

Chen S, Shu X, Wang H, Ding L, Fu J, Jia J. 2021. The Differences Between Motor Attempt and Motor Imagery in Brain-Computer Interface Accuracy and Event-Related Desynchronization of Patients With Hemiplegia. *Front Neurorobot* **15**:1–13. doi:10.3389/fnbot.2021.706630

Chen YY, Lambert KJM, Madan CR, Singhal A. 2021. Mu oscillations and motor imagery performance: A reflection of intra-individual success, not inter-individual ability. *Hum Mov Sci* **78**:1–12. doi:10.1016/j.humov.2021.102819

Cheyne D, Ferrari P. 2013. MEG studies of motor cortex gamma oscillations: Evidence for a gamma “fingerprint” in the brain? *Front Hum Neurosci* **7**:1–7. doi:10.3389/fnhum.2013.00575

Chiarelli AM, Croce P, Merla A, Zappasodi F. 2018. Deep learning for hybrid EEG-fNIRS brain-computer interface: Application to motor imagery classification. *J Neural Eng* **15**. doi:10.1088/1741-2552/aaaf82

Cho H, Ahn M, Ahn S, Kwon M, Jun SC. 2017. EEG datasets for motor imagery brain-computer interface. *Gigascience* **6**:1–8. doi:10.1093/gigascience/gix034

Choi B, Jo S. 2013. A Low-Cost EEG System-Based Hybrid Brain-Computer Interface for Humanoid Robot Navigation and Recognition. *PLoS One* **8**. doi:10.1371/journal.pone.0074583

Choi I, Rhiu I, Lee Y, Yun MH, Nam CS. 2017. A systematic review of hybrid brain-computer interfaces: Taxonomy and usability perspectives. *PLoS One* **12**. doi:10.1371/journal.pone.0176674

Cole S, Voytek B. 2019. Cycle-by-cycle analysis of neural oscillations. *J Neurophysiol* **122**:849–861. doi:10.1152/JN.00273.2019

Cole SR, Voytek B. 2017. Brain Oscillations and the Importance of Waveform Shape. *Trends Cogn Sci* **21**:137–149. doi:10.1016/j.tics.2016.12.008

Cole XSR, Meij R Van Der, Peterson EJ, Hemptinne C De, Starr XA, Voytek XB. 2017. Nonsinusoidal Beta Oscillations Reflect Cortical Pathophysiology in Parkinson ’ s Disease **37**:4830–4840. doi:10.1523/JNEUROSCI.2208-16.2017

Coleman SC, Seedat ZA, Pakenham DO, Quinn AJ, Brookes MJ, Woolrich MW, Mullinger KJ. 2024. Post-task responses following working memory and movement are driven by transient spectral bursts with similar characteristics 1–14. doi:10.1002/hbm.26700

Congedo M, Barachant A, Bhatia R. 2017. Riemannian geometry for EEG-based brain-computer interfaces; a primer and a review. *Brain-Computer Interfaces* **4**:155–174. doi:10.1080/2326263X.2017.1297192

Corsi M-C, Chevallier S, Fallani FDV, Yger F. 2022. Functional Connectivity Ensemble Method to Enhance BCI Performance (FUCONE). *IEEE Trans Biomed Eng* **69**:2826–2838. doi:10.1109/TBME.2022.3154885

Corsi M, Chavez M, Schwartz D, George N, Hugueville L, Kahn A, Dupont S, Bassett D, De F, Corsi M, Chavez M, Schwartz D, George N, Hugueville L. 2021. BCI learning induces core-periphery reorganization in M/EEG multiplex brain networks. *J Neural Eng* **18**. doi:10.1088/1741-2552/abef39

Corsi MC, Chavez M, Schwartz D, Hugueville L, Khambhati AN, Bassett DS, De Vico Fallani F. 2019. Integrating EEG and MEG Signals to Improve Motor Imagery Classification in Brain-Computer Interface. *Int J Neural Syst* **29**:1–12. doi:10.1142/S0129065718500144

Corsi MC, Sorrentino P, Schwartz D, George N, Gollo LL, Chevallier S, Hugueville L, Kahn AE, Dupont S, Bassett DS, Jirsa V, De Vico Fallani F. 2024. Measuring neuronal avalanches to inform brain-computer interfaces. *iScience* **27**:108734. doi:10.1016/j.isci.2023.108734

Coscia M, Wessel MJ, Chaudary U, Millán J del R, Micera S, Guggisberg A, Vuadens P, Donoghue J, Birbaumer N, Hummel FC. 2019. Neurotechnology-aided interventions for upper limb motor rehabilitation in severe chronic stroke. *Brain* **142**:2182–2197. doi:10.1093/brain/awz181

Crell MR, Müller-Putz GR. 2024. Handwritten character classification from EEG through continuous kinematic decoding. *Comput Biol Med* **182**:109132. doi:10.1016/j.compbiomed.2024.109132

da Silva FHL. 2010. Electrophysiological Basis of MEG SignalsMEG: An Introduction to Methods. Oxford University Press. pp. 1–23. doi:10.1093/acprof:oso/9780195307238.003.0001

Daly JJ, Wolpaw JR. 2008. Brain-computer interfaces in neurological rehabilitation. *Lancet Neurol* **7**:1032–1043. doi:10.1016/S1474-4422(08)70223-0

Darvas F, Scherer R, Ojemann JG, Rao RP, Miller KJ, Sorensen LB. 2010. High gamma mapping using EEG. *Neuroimage* **49**:930–938. doi:10.1016/j.neuroimage.2009.08.041

Davare M, Andres M, Cosnard G, Thonnard JL, Olivier E. 2006. Dissociating the role of ventral and dorsal premotor cortex in precision grasping. *J Neurosci* **26**:2260–2268. doi:10.1523/JNEUROSCI.3386-05.2006

Davare M, Kraskov A, Rothwell JC, Lemon RN. 2011. Interactions between areas of the cortical grasping network. *Curr Opin Neurobiol* **21**:565–570. doi:10.1016/j.conb.2011.05.021

de Cheveigné A. 2020. ZapLine: A simple and effective method to remove power line artifacts. *Neuroimage* **207**. doi:10.1016/j.neuroimage.2019.116356

Decety J. 1996. The neurophysiological basis of motor imagery. *Behav Brain Res* **77**:45–52.

Donoghue T. 2024. Aperiodic-History Aperiodic-History. *PsyArXiv* 1–20.

Donoghue T, Haller M, Peterson EJ, Varma P, Sebastian P, Gao R, Noto T, Lara AH, Wallis JD, Knight RT, Shestyuk A, Voytek B. 2020. Parameterizing neural power spectra into periodic and aperiodic components. *Nat Neurosci* **23**:1655–1665. doi:10.1038/s41593-020-00744-x

Donoghue T, Schaworonkow N, Voytek B. 2021. Methodological considerations for studying neural oscillations. *Eur J Neurosci* 1–26. doi:10.1111/ejn.15361

Dreyer P, Roc A, Pillette L, Rimbert S, Lotte F. 2023. A large EEG database with users' profile information for motor imagery brain-computer interface research. *Sci Data* **10**:1–14. doi:10.1038/s41597-023-02445-z

Echeverria-Altuna I, Quinn AJ, Woolrich MW, Nobre AC, Ede V. 2022. Transient beta activity and cortico-muscular connectivity during sustained motor behaviour. *Prog Neurobiol* 102281. doi:10.1016/j.pneurobio.2022.102281

Eder M, Xu J, Grosse-Wentrup M. 2024. Benchmarking brain-computer interface algorithms: Riemannian approaches vs convolutional neural networks. *J Neural Eng*. doi:10.1088/1741-2552/ad6793 Manuscript

Enz N, Ruddy KL, Rueda-Delgado LM, Whelan R. 2021. Volume of β-bursts, but not their rate, predicts successful response inhibition. *J Neurosci* **41**:5069–5079. doi:10.1523/JNEUROSCI.2231-20.2021

Fabus MS, Quinn AJ, Warnaby CE, Woolrich MW. 2021. Automatic decomposition of electrophysiological data into distinct nonsinusoidal oscillatory modes. *J Neurophysiol* **126**:1670–1684. doi:10.1152/jn.00315.2021

Farwell LA, Donchin E. 1988. Talking off the top of your head: toward a mental prosthesis utilizing event-related brain potentials. *Electroencephalogr Clin Neurophysiol* 510–523. doi:10.1080/15562948.2011.567142

Fatourechi M, Bashashati A, Ward RK, Birch GE. 2007. EMG and EOG artifacts in brain computer interface systems: A survey. *Clin Neurophysiol* **118**:480–494. doi:10.1016/j.clinph.2006.10.019

Fattori P, Breveglieri R, Marzocchi N, Filippini D, Bosco A, Galletti C. 2009. Hand orientation during reach-to-grasp movements modulates neuronal activity in the medial posterior parietal area V6A. *J Neurosci* **29**:1928–1936. doi:10.1523/JNEUROSCI.4998-08.2009

Fattori P, Kutz DF, Breveglieri R, Marzocchi N, Galletti C. 2005. Spatial tuning of reaching activity in the medial parieto-occipital cortex (area V6A) of macaque monkey. *Eur J Neurosci* **22**:956–972. doi:10.1111/j.1460-9568.2005.04288.x

Fattori P, Raos V, Breveglieri R, Bosco A, Marzocchi N, Galletti C. 2010. The dorsomedial pathway is not just for reaching: Grasping neurons in the medial parieto-occipital cortex of the macaque monkey. *J Neurosci* **30**:342–349. doi:10.1523/JNEUROSCI.3800-09.2010

Feingold J, Gibson DJ, Depasquale B, Graybiel AM. 2015. Bursts of beta oscillation differentiate postperformance activity in the striatum and motor cortex of monkeys performing movement tasks. *Proc Natl Acad Sci U S A* **112**:13687–13692. doi:10.1073/pnas.1517629112

Fox J, Weisberg S. 2019. An R Companion to Applied Regression, Third. ed. Sage.

Freudenburg Z V., Branco MP, Leinders S, Vijgh BH va. der, Pels EGM, Denison T, Berg LH va. den, Miller KJ, Aarnoutse EJ, Ramsey NF, Vansteensel MJ. 2019. Sensorimotor ECoG Signal Features for BCI Control: A Comparison Between People With Locked-In Syndrome and Able-Bodied Controls. *Front Neurosci* **13**:1–18. doi:10.3389/fnins.2019.01058

Friston K, Henson R, Phillips C, Mattout J. 2006. Bayesian estimation of evoked and induced responses. *Hum Brain Mapp* **27**:722–735. doi:10.1002/hbm.20214

Gaetz W, Liu C, Zhu H, Bloy L, Roberts TPL. 2013. Evidence for a motor gamma-band network governing response interference. *Neuroimage* **74**:245–253. doi:10.1016/j.neuroimage.2013.02.013

Gallego-Carracedo C, Perich MG, Chowdhury RH, Miller LE, Gallego JÁ. 2022. Local field potentials reflect cortical population dynamics in a region-specific and frequency-dependent manner. *Elife* **11**:1–24. doi:10.7554/eLife.73155

Gallego JÁ, Perich MG, Chowdhury RH, Solla SA, Miller LE. 2020. Long-term stability of cortical population dynamics underlying consistent behavior. *Nat Neurosci* **23**:260–270. doi:10.1038/s41593-019-0555-4

Gallego JA, Perich MG, Miller LE, Solla SA. 2017. Neural Manifolds for the Control of Movement. *Neuron* **94**:978–984. doi:10.1016/j.neuron.2017.05.025

Gallego JA, Perich MG, Naufel SN, Ethier C, Solla SA, Miller LE. 2018. Cortical population activity within a preserved neural manifold underlies multiple motor behaviors. *Nat Commun* **9**:1–13. doi:10.1038/s41467-018-06560-z

Gallese V. 1994. Deficit of hand preshaping after muscimol injection in monkey parietal cortex. *Neuroreport* **5**:1525–1529.

Galletti C, Fattori P. 2018. The dorsal visual stream revisited: Stable circuits or dynamic pathways? *Cortex* **98**:203–217. doi:10.1016/j.cortex.2017.01.009

Gao R, Peterson EJ, Voytek B. 2017. Inferring synaptic excitation/inhibition balance from field potentials. *Neuroimage* **158**:70–78. doi:https://doi.org/10.1016/j.neuroimage.2017.06.078

Georgopoulos AP, Kalaska JF, Caminiti R, Massey JT. 1982. On the relations between the direction of two-dimensional arm movements and cell discharge in primate motor cortex. *J Neurosci Off J Soc Neurosci* **2**:1527–1537. doi:10.1523/JNEUROSCI.02-11-01527.1982

Gerster M, Waterstraat G, Litvak V, Lehnertz K, Schnitzler A, Florin E, Curio G, Nikulin V. 2022. Separating Neural Oscillations from Aperiodic 1/f Activity: Challenges and Recommendations. *Neuroinformatics* **20**:991–1012. doi:10.1007/s12021-022-09581-8

Ghez C, Gordon J, Ghilardi MF. 1995. Impairments of reaching movements in patients without proprioception. II. Effects of visual information on accuracy. *J Neurophysiol* **73**:361–372. doi:10.1152/jn.1995.73.1.361

Giehl J, Noury N, Siegel M. 2021. Dissociating harmonic and non-harmonic phase-amplitude coupling in the human brain. *Neuroimage* **227**. doi:10.1016/j.neuroimage.2020.117648

Giehl J, Siegel M. 2024. Spectral waveform analysis dissociates human cortical alpha rhythms 1–11.

Gordon EM, Chauvin RJ, Van AN, Rajesh A, Nielsen A, Newbold DJ, Lynch CJ, Seider NA, Krimmel SR, Scheidter KM, Monk J, Miller RL, Metoki A, Montez DF, Zheng A, Elbau I, Madison T, Nishino T, Myers MJ, Kaplan S, Badke D'Andrea C, Demeter D V., Feigelis M, Ramirez JSB, Xu T, Barch DM, Smyser CD, Rogers CE, Zimmermann J, Botteron KN, Pruett JR, Willie JT, Brunner P, Shimony JS, Kay BP, Marek S, Norris SA, Gratton C, Sylvester CM, Power JD, Liston C, Greene DJ, Roland JL, Petersen SE, Raichle ME, Laumann TO, Fair DA, Dosenbach NUF. 2023. A somato-cognitive action network alternates with effector regions in motor cortex. *Nature* **617**:351–359. doi:10.1038/s41586-023-05964-2

Grafton ST. 2010. The cognitive neuroscience of prehension: Recent developments. *Exp Brain Res* **204**:475–491. doi:10.1007/s00221-010-2315-2

Gramfort A, Luessi M, Larson E, Engemann DA, Strohmeier D, Brodbeck C, Goj R, Jas M, Brooks T, Parkkonen L, Hämäläinen M. 2013. MEG and EEG data analysis with MNE-Python. *Front Neurosci*. doi:10.3389/fnins.2013.00267

Graziano MSA. 1999. Where is my arm? The relative role of vision and proprioception in the neuronal representation of limb position. *Proc Natl Acad Sci U S A* **96**:10418–10421. doi:10.1073/pnas.96.18.10418

Grosse-Wentrup M, Liefhold C, Gramann K, Buss M. 2009. Beamforming in Noninvasive Brain–Computer Interfaces. *IEEE Trans Biomed Eng* **56**:1209–1219. doi:10.1109/TBME.2008.2009768

Guillot A, Collet C, Nguyen VA, Malouin F, Richards C, Doyon J. 2009. Brain activity during visual versus kinesthetic imagery: An fMRI study. *Hum Brain Mapp* **30**:2157–2172. doi:10.1002/hbm.20658

Hagihira S, Takashina M, Mori T, Mashimo T, Yoshiya I. 2001. Practical issues in bispectral analysis of electroencephalographic signals. *Anesth Analg* **93**:966–970. doi:10.1097/00000539-200110000-00032

Hämäläinen M, Hari R. 2002. Magnetoencephalographic (MEG) characterization of dynamic brain activationBrain Mapping: The Methods. pp. 227–254.

Hanakawa T, Dimyan MA, Hallett M. 2008. Motor planning, imagery, and execution in the distributed motor network: A time-course study with functional MRI. *Cereb Cortex* **18**:2775–2788. doi:10.1093/cercor/bhn036

Hanakawa T, Immisch I, Toma K, Dimyan MA, Van Gelderen P, Hallett M. 2003. Functional properties of brain areas associated with motor execution and imagery. *J Neurophysiol* **89**:989–1002. doi:10.1152/jn.00132.2002

Hannah R, Muralidharan V, Sundby KK, Aron AR. 2020. Temporally-precise disruption of prefrontal cortex informed by the timing of beta bursts impairs human action-stopping. *Neuroimage* **222**. doi:10.1016/j.neuroimage.2020.117222

Hariz MI. 2002. Complications of deep brain stimulation surgery. *Mov Disord* **17**:162–166. doi:10.1002/mds.10159

Harris CR, Millman KJ, van der Walt SJ, Gommers R, Virtanen P, Cournapeau D, Wieser E, Taylor J, Berg S, Smith NJ, Kern R, Picus M, Hoyer S, van Kerkwijk MH, Brett M, Haldane A, del Río JF, Wiebe M, Peterson P, Gérard-Marchant P, Sheppard K, Reddy T, Weckesser W, Abbasi H, Gohlke C, Oliphant TE. 2020. Array programming with NumPy. *Nature* **585**:357–362. doi:10.1038/s41586-020-2649-2

Hatem SM, Saussez G, della Faille M, Prist V, Zhang X, Dispa D, Bleyenheuft Y. 2016. Rehabilitation of motor function after stroke: A multiple systematic review focused on techniques to stimulate upper extremity recovery. *Front Hum Neurosci* **10**:1–22. doi:10.3389/fnhum.2016.00442

Hatsopoulos NG, Donoghue JP. 2009. The Science of Neural Interface Systems. *Annu Rev Neurosci* **32**:249–266. doi:10.1146/annurev.neuro.051508.135241

Hazrati MK, Erfanian A. 2010. An online EEG-based brain-computer interface for controlling hand grasp using an adaptive probabilistic neural network. *Med Eng Phys* **32**:730–739. doi:10.1016/j.medengphy.2010.04.016

He S, Everest-Phillips C, Clouter A, Brown P, Tan H. 2020. Neurofeedback-linked suppression of cortical B bursts speeds up movement initiation in healthy motor control: A double-blind sham-controlled study. *J Neurosci* **40**:4021–4032. doi:10.1523/JNEUROSCI.0208-20.2020

Herman P, Prasad G, McGinnity TM, Coyle D. 2008. Comparative analysis of spectral approaches to feature extraction for EEG-based motor imagery classification. *IEEE Trans Neural Syst Rehabil Eng* **16**:317–326. doi:10.1109/TNSRE.2008.926694

Hervault M, Zanone PG, Buisson JC, Huys R. 2021. Cortical sensorimotor activity in the execution and suppression of discrete and rhythmic movements. *Sci Rep* **11**:1–15. doi:10.1038/s41598-021-01368-2

Hill RM, Boto E, Rea M, Holmes N, Leggett J, Coles LA, Papastavrou M, Everton SK, Hunt BAE, Sims D, Osborne J, Shah V, Bowtell R, Brookes MJ. 2020. Multi-channel whole-head OPM-MEG: Helmet design and a comparison with a conventional system. *Neuroimage* **219**. doi:10.1016/j.neuroimage.2020.116995

Hillebrand A, Barnes GR. 2011. Practical constraints on estimation of source extent with MEG beamformers. *Neuroimage* **54**:2732–2740. doi:10.1016/j.neuroimage.2010.10.036

Hochberg LR, Bacher D, Jarosiewicz B, Masse NY, Simeral JD, Vogel J, Haddadin S, Liu J, Cash SS, Van Der Smagt P, Donoghue JP. 2012. Reach and grasp by people with tetraplegia using a neurally controlled robotic arm. *Nature* **485**:372–375. doi:10.1038/nature11076

Hong KS, Khan MJ. 2017. Hybrid brain-computer interface techniques for improved classification accuracy and increased number of commands: A review. *Front Neurorobot* **11**. doi:10.3389/fnbot.2017.00035

Horki P, Bauernfeind G, Klobassa DS, Pokorny C, Pichler G, Schippinger W, Müller-Putz GR. 2014. Detection of mental imagery and attempted movements in patients with disorders of consciousness using EEG. *Front Hum Neurosci* **8**:1–9. doi:10.3389/fnhum.2014.01009

Hughes C, Herrera A, Gaunt R, Collinger J. 2020. Bidirectional brain-computer interfaces, 1st ed, Handbook of Clinical Neurology. Elsevier B.V. doi:10.1016/B978-0-444-63934-9.00013-5

Iivanainen J, Zetter R, Grön M, Hakkarainen K, Parkkonen L. 2019. On-scalp MEG system utilizing an actively shielded array of optically-pumped magnetometers. *Neuroimage* **194**:244–258. doi:10.1016/j.neuroimage.2019.03.022

Iturrate I, Chavarriaga R, Millán J del R. 2020. General principles of machine learning for brain-computer interfacing. *Handb Clin Neurol* **168**:311–328. doi:10.1016/B978-0-444-63934-9.00023-8

Janssen P, Scherberger H. 2015. Visual Guidance in Control of Grasping. *Annu Rev Neurosci* **38**:69–86. doi:10.1146/annurev-neuro-071714-034028

Jas M, Engemann DA, Bekhti Y, Raimondo F, Gramfort A, Gramfort A, Automated A, Engemann DA. 2017. Autoreject : Automated artifact rejection for MEG and EEG data. *Neuroimage* **159**:417–129. doi:10.1016/j.neuroimage.2017.06.030

Jayaram V, Barachant A. 2018. MOABB: Trustworthy algorithm benchmarking for BCIs. *J Neural Eng* **15**. doi:10.1088/1741-2552/aadea0

Jeannerod M. 1995. Mental imagery in the motor context. *Neuropsychologia* **33**:1419–1432. doi:10.1016/0028-3932(95)00073-C

Jeunet C, Glize B, McGonigal A, Batail JM, Micoulaud-Franchi JA. 2019. Using EEG-based brain computer interface and neurofeedback targeting sensorimotor rhythms to improve motor skills: Theoretical background, applications and prospects. *Neurophysiol Clin* **49**:125–136. doi:10.1016/j.neucli.2018.10.068

Jeunet C, Lotte F, Batail JM, Philip P, Micoulaud Franchi JA. 2018. Using Recent BCI Literature to Deepen our Understanding of Clinical Neurofeedback: A Short Review. *Neuroscience* **378**:225–233. doi:10.1016/j.neuroscience.2018.03.013

Jochumsen M, Khan Niazi I, Taylor D, Farina D, Dremstrup K. 2015. Detecting and classifying movement-related cortical potentials associated with hand movements in healthy subjects and stroke patients from single-electrode, single-trial EEG. *J Neural Eng* **12**:56013. doi:10.1088/1741-2560/12/5/056013

Jones SR. 2016. When brain rhythms aren’t ‘rhythmic’: implication for their mechanisms and meaning. *Curr Opin Neurobiol* **40**:72–80. doi:10.1016/j.conb.2016.06.010

Kachenoura A, Albera L, Senhadji L, Comon P. 2008. ICA: A potential tool for BCI systems. *IEEE Signal Process Mag* **25**:57–68. doi:10.1109/MSP.2008.4408442

Kandel ER. 2013. Principles of Neural Science, Fifth Edition, McGraw-Hill’s AccessMedicine. McGraw-Hill Education.

Kaongoen N, Choi J, Woo Choi J, Kwon H, Hwang C, Hwang G, Kim BH, Jo S. 2023. The future of wearable EEG: a review of ear-EEG technology and its applications. *J Neural Eng* **20**. doi:10.1088/1741-2552/acfcda

Karabanov AN, Madsen KH, Krohne LG, Siebner HR. 2021. Does pericentral mu-rhythm “power” corticomotor excitability? – A matter of EEG perspective. *Brain Stimul* **14**:713–722. doi:10.1016/j.brs.2021.03.017

Kawala-Sterniuk A, Browarska N, Al-Bakri A, Pelc M, Zygarlicki J, Sidikova M, Martinek R, Gorzelanczyk EJ. 2021. Summary of over fifty years with brain-computer interfaces—a review. *Brain Sci* **11**:1–41. doi:10.3390/brainsci11010043

Kehnemouyi YM, Wilkins KB, Anidi CM, Anderson RW, Afzal MF, Bronte-stewart HM. 2021. Modulation of beta bursts in subthalamic sensorimotor circuits predicts improvement in bradykinesia. doi:10.1093/brain/awaa394

Khawaldeh S, Tinkhauser G, Shah SA, Peterman K, Debove I, Khoa Nguyen TA, Nowacki A, Lenard Lachenmayer M, Schuepbach M, Pollo C, Krack P, Woolrich M, Brown P. 2020. Subthalamic nucleus activity dynamics and limb movement prediction in Parkinson’s disease. *Brain* **143**:582–586. doi:10.1093/brain/awz417

Kilavik BE, Ponce-Alvarez A, Trachel R, Confais J, Takerkart S, Riehle A. 2012. Context-related frequency modulations of macaque motor cortical LFP beta oscillations. *Cereb Cortex* **22**:2148–2159. doi:10.1093/cercor/bhr299

Kilavik BE, Zaepffel M, Brovelli A, MacKay WA, Riehle A. 2013. The ups and downs of beta oscillations in sensorimotor cortex. *Exp Neurol* **245**:15–26. doi:10.1016/j.expneurol.2012.09.014

Kim JA, Davis KD. 2021. Magnetoencephalography: Physics, techniques, and applications in the basic and clinical neurosciences. *J Neurophysiol* **125**:938–956. doi:10.1152/jn.00530.2020

Kobler RJ, Almeida I, Sburlea AI, Müller-Putz GR. 2020. Using machine learning to reveal the population vector from EEG signals. *J Neural Eng* **17**. doi:10.1088/1741-2552/ab7490

Koles ZJ. 1991. The quantitative extraction and topographic mapping of the abnormal components in the clinical EEG. *Electroencephalogr Clin Neurophysiol* **79**:440–447. doi:10.1016/0013-4694(91)90163-X

Kotte S, Kumar Dabbakuti JRK. 2020. Methods for removal of artifacts from EEG signal: A review. *J Phys Conf Ser* **1706**. doi:10.1088/1742-6596/1706/1/012093

Krusienski DJ, Grosse-Wentrup M, Galan F, Coyle D, Miller KJ, Forney E, Anderson CW. 2011. Critical issues in state-of-the-art brain-computer interface signal processing. *J Neural Eng* **8**. doi:10.1088/1741-2560/8/2/025002

Kurzweil R. 2014. The Singularity is Near In: Sandler RL, editor. Ethics and Emerging Technologies. London: Palgrave Macmillan UK. pp. 393–406. doi:10.1057/9781137349088_26

Kwon OY, Lee MH, Guan C, Lee SW. 2020. Subject-Independent Brain-Computer Interfaces Based on Deep Convolutional Neural Networks. *IEEE Trans Neural Networks Learn Syst* **31**:3839–3852. doi:10.1109/TNNLS.2019.2946869

Langford ZD, Procyk E, Wilson CRE. 2023. Frontal oscillatory beta bursts have rhythmically distinct regimes with differing functional relevance. *bioRxiv* 1–19. doi:/doi.org/10.1101/2023.11.13.566594

Lecaignard F, Bertrand O, Caclin A, Mattout J. 2021. Empirical Bayes evaluation of fused EEG-MEG source reconstruction: Application to auditory mismatch evoked responses. *Neuroimage* **226**. doi:10.1016/j.neuroimage.2020.117468

Lecaignard F, Mattout J. 2015. Forward Models for EEG/MEG. *Brain Mapp An Encycl Ref* **1**:549–555. doi:10.1016/B978-0-12-397025-1.00330-4

Lee SY, Kozalakis K, Baftizadeh F, Campagnola L, Jarsky T, Koch C, Anastassiou CA. 2024. Cell-class-specific electric field entrainment of neural activity. *Neuron* **112**:2614-2630.e5. doi:10.1016/j.neuron.2024.05.009

Leeb R, Lee F, Keinrath C, Scherer R, Bischof H, Pfurtscheller G. 2007. Brain-computer communication: motivation, aim, and impact of exploring a virtual apartment. *IEEE Trans neural Syst Rehabil Eng a Publ IEEE Eng Med Biol Soc* **15**:473–482. doi:10.1109/TNSRE.2007.906956

Lemm S, Blankertz B, Dickhaus T, Müller KR. 2011. Introduction to machine learning for brain imaging. *Neuroimage* **56**:387–399. doi:10.1016/j.neuroimage.2010.11.004

Lennon O, Tonellato M, Felice A Del, Di Marco R, Fingleton C, Korik A, Guanziroli E, Molteni F, Guger C, Otner R, Coyle D. 2020. A systematic review establishing the current state-of-the-art, the limitations, and the desired checklist in studies of direct neural interfacing with robotic gait devices in stroke rehabilitation. *Front Neurosci* **14**:1–18. doi:10.3389/fnins.2020.00578

Lenth R V. 2023. emmeans: Estimated Marginal Means, aka Least-Squares Means.

Li C-SR, Padoa-Schioppa C, Bizzi E. 2001. Neuronal Correlates of Motor Performance and Motor Learning in the Primary Motor Cortex of Monkeys Adapting to an External Force Field. *Neuron* **30**:593–607. doi:https://doi.org/10.1016/S0896-6273(01)00301-4

Lin Z, Zhang C, Wu W, Gao X. 2006. Frequency recognition based on canonical correlation analysis for SSVEP-based BCIs. *IEEE Trans Biomed Eng* **53**:2610–2614. doi:10.1109/TBME.2006.886577

Lisman J, Buzsáki G. 2008. A neural coding scheme formed by the combined function of gamma and theta oscillations. *Schizophr Bull* **34**:974–980. doi:10.1093/schbul/sbn060

Little S, Bonaiuto J, Barnes G, Bestmann S. 2019. Human motor cortical beta bursts relate to movement planning and response errors. *PLoS Biol* **17**:1–30. doi:10.1371/journal.pbio.3000479

Liu H, Wei P, Wang H, Lv X, Duan W, Li M, Zhao Y, Wang Q, Chen X, Shi G, Han B, Hao J. 2024. An EEG motor imagery dataset for brain computer interface in acute stroke patients. *Sci Data* **11**:1–10. doi:10.1038/s41597-023-02787-8

Llera A, Gomez V, Kappen HJ. 2014. Adaptive Multiclass Classification for Brain Computer Interfaces. *Neural Comput* **26**:1108–1127. doi:10.1162/NECO

Lofredi R, Neumann WJ, Bock A, Horn A, Huebl J, Siegert S, Schneider GH, Krauss JK, Kuühn AA. 2018. Dopamine-dependent scaling of subthalamic gamma bursts with movement velocity in patients with Parkinson's disease. *Elife* **7**:1–22. doi:10.7554/eLife.31895

Lopes da Silva F. 2013. EEG and MEG: Relevance to neuroscience. *Neuron* **80**:1112–1128. doi:10.1016/j.neuron.2013.10.017

Lotte F. 2014. A Tutorial on EEG Signal Processing Techniques for Mental State Recognition in Brain-Computer InterfacesGuide to Brain-Computer Music Interfacing. p. 32.

Lotte F, Bougrain L, Cichocki A, Clerc M, Congedo M, Rakotomamonjy A, Yger F. 2018a. A review of classification algorithms for EEG-based brain-computer interfaces: A 10 year update. *J Neural Eng* **15**. doi:10.1088/1741-2552/aab2f2

Lotte F, Jeunet C. 2018. Defining and quantifying users' mental imagery-based BCI skills: a first step. *J Neural Eng* **15**. doi:10.1088/1741-2552/aac577

Lotte F, Jeunet C, Mladenovic J, N'Kaoua B, Pillette L. 2018b. A BCI challenge for the signal processing community : considering the user in the loopSignal Processing and Machine Learning for Brain-Machine Interfaces. pp. 1–33.

Lotte F, Nam CS, Nijholt A. 2018c. Introduction : Evolution of Brain-Computer InterfacesTechnological and Theoretical Advance, Taylor & Francis (CRC Press). pp. 1–11.

Lotte F, Rimbert S. 2022. How ERD modulations during motor imageries relate to users ' traits and BCI performances44th International Engineering in Medicine and Biology Conference. Glasgow, United Kingdom.

Lozano AM, Lipsman N, Bergman H, Brown P, Chabardes S, Chang JW, Matthews K, McIntyre CC, Schlaepfer TE, Schulder M, Temel Y, Volkmann J, Krauss JK. 2019. Deep brain stimulation: current challenges and future directions. *Nat Rev Neurol* **15**:148–160. doi:10.1038/s41582-018-0128-2

Lu J, McFarland DJ, Wolpaw JR. 2013. Adaptive laplacian filtering for sensorimotor rhythm-based brain-computer interfaces. *J Neural Eng* **10**. doi:10.1088/1741-2560/10/1/016002

Luauté J, Morlet D, Mattout J. 2015. BCI in patients with disorders of consciousness: Clinical perspectives. *Ann Phys Rehabil Med* **58**:29–34. doi:10.1016/j.rehab.2014.09.015

Luiz P, Rodrigues C, Jutten C, Congedo M. 2019. Riemannian Procrustes Analysis : Transfer Learning for Brain-Computer Interfaces. *IEEE Trans Biomed Eng* **66**:2390–2401. doi:10.1109/TBME.2018.2889705

Lundqvist M, Herman P, Warden MR, Brincat SL, Miller EK. 2018. Gamma and beta bursts during working memory readout suggest roles in its volitional control. *Nat Commun* **9**:1–12. doi:10.1038/s41467-017-02791-8

Lundqvist M, Miller EK, Nordmark J, Liljefors J, Herman P. 2024. Beta : bursts of cognition. *Trends Cogn Sci* **xx**:1–15. doi:10.1016/j.tics.2024.03.010

Lundqvist M, Rose J, Herman P, Brincat S, Buschman T, Miller E. 2016. Gamma and beta bursts underlie working memory. *Neuron* **90**:152–164. doi:10.1016/j.neuron.2016.02.028

MacEira-Elvira P, Popa T, Schmid AC, Hummel FC. 2019. Wearable technology in stroke rehabilitation: Towards improved diagnosis and treatment of upper-limb motor impairment. *J Neuroeng Rehabil* **16**. doi:10.1186/s12984-019-0612-y

Makeig S, Enghoff S, Jung TP, Sejnowski TJ. 2000. A natural basis for efficient brain-actuated control. *IEEE Trans Rehabil Eng* **8**:208–211. doi:10.1109/86.847818

Malouin F, Richards CL, Jackson PL, Lafleur MF, Durand A, Doyon J. 2007. The kinesthetic and visual imagery questionnaire (KVIQ) for assessing motor imagery in persons with physical disabilities: A reliability and construct validity study. *J Neurol Phys Ther* **31**:20–29. doi:10.1097/01.NPT.0000260567.24122.64

Mane R, Wu Z, Wang D. 2022. Poststroke motor, cognitive and speech rehabilitation with brain-computer interface: A perspective review. *Stroke Vasc Neurol* **7**:541–549. doi:10.1136/svn-2022-001506

Mcdermott EJ, Raggam P, Kirsch S, Belardinelli P, Ziemann U. 2021. Artifacts in EEG-based BCI therapies : friend or foe ? Introduction Motivation.

McDermott EJ, Raggam P, Zrenner C, Kirsch S, Belardinelli P, Ziemann U. 2022. Artifacts in EEG-based BCI therapies: Friend or foe? *Sensors* **22**:1–18. doi:10.3390/s22010096

Mcfarland DJ. 2021. Brain-computer interfaces for amyotrophic lateral sclerosis Dennis. *Muscle Nerve* **61**:702–707. doi:10.1002/mus.26828.Brain-computer

McFarland DJ, Daly J, Boulay C, Parvaz MA. 2017. Therapeutic applications of BCI technologies. *Brain-Computer Interfaces* **4**:37–52. doi:10.1080/2326263X.2017.1307625

McFarland DJ, McCane LM, David S V., Wolpaw JR. 1997. Spatial filter selection for EEG-based communication. *Electroencephalogr Clin Neurophysiol* **103**:386–394. doi:10.1016/S0013-4694(97)00022-2

Medeiros de Freitas A, Sanchez G, Lecaignard F, Maby E, Barbosa Soares A, Mattout J. 2020. EEG artifact correction strategies for online trial-by-trial analysis. *J Neural Eng* **17**. doi:10.1088/1741-2552/ab581d

Medvedovsky M, Taulu S, Bikmullina R, Paetau R. 2007. Artifact and head movement compensation in MEG. *Neurol Neurophysiol Neurosci* **2007**:1–10.

Meng HJ, Pi YL, Liu K, Cao N, Wang YQ, Wu Y, Zhang J. 2018. Differences between motor execution and motor imagery of grasping movements in the motor cortical excitatory circuit. *PeerJ* **2018**:1–12. doi:10.7717/peerj.5588

Menz VK, Schaffelhofer S, Scherberger H. 2015. Representation of continuous hand and arm movements in macaque areas M1, F5, and AIP: A comparative decoding study. *J Neural Eng* **12**. doi:10.1088/1741-2560/12/5/056016

Meyer SS, Bonaiuto J, Lim M, Rossiter H, Waters S, Bradbury D, Bestmann S, Brookes M, Callaghan MF, Weiskopf N, Barnes GR. 2017. Flexible head-casts for high spatial precision MEG. *J Neurosci Methods* **276**:38–45. doi:10.1016/j.jneumeth.2016.11.009

Micera S, Caleo M, Chisari C, Hummel FC, Pedrocchi A. 2020. Advanced Neurotechnologies for the Restoration of Motor Function. *Neuron* **105**:604–620. doi:10.1016/j.neuron.2020.01.039

Michaels JA, Schaffelhofer S, Agudelo-Toro A, Scherberger H. 2020. A goal-driven modular neural network predicts parietofrontal neural dynamics during grasping. *Proc Natl Acad Sci U S A* **117**:32124–32135. doi:10.1073/pnas.2005087117

Miller KJ, Schalk G, Fetz EE, Den Nijs M, Ojemann JG, Rao RPN. 2010. Cortical activity during motor execution, motor imagery, and imagery-based online feedback. *Proc Natl Acad Sci U S A* **107**:4430–4435. doi:10.1073/pnas.0913697107

Mladenović J. 2021. Standardization of protocol design for user training in EEG-based brain-computer interface. *J Neural Eng* **18**. doi:10.1088/1741-2552/abcc7d

Mladenović J, Frey J, Pramij S, Mattout J, Lotte F. 2022. Towards Identifying Optimal Biased Feedback for Various User States and Traits in Motor Imagery BCI. *IEEE Trans Biomed Eng* **69**:1101–1110. doi:10.1109/TBME.2021.3113854

Mladenović J, Mattout J, Lotte F. 2019. A Generic Framework for Adaptive EEG-Based BCI Training and Operation. *Brain–Computer Interfaces Handb* 595–612. doi:10.1201/9781351231954-31

Moca V V., Bârzan H, Nagy-Dăbâcan A, Mureșan RC. 2021. Time-frequency super-resolution with superlets. *Nat Commun* **12**:1–18. doi:10.1038/s41467-020-20539-9

Mohan H, Verhoog MB, Doreswamy KK, Eyal G, Aardse R, Lodder BN, Goriounova NA, Asamoah B, B Brakspear ABC, Groot C, van der Sluis S, Testa-Silva G, Obermayer J, Boudewijns ZSRM, Narayanan RT, Baayen JC, Segev I, Mansvelder HD, de Kock CPJ. 2015. Dendritic and Axonal Architecture of Individual Pyramidal Neurons across Layers of Adult Human Neocortex. *Cereb Cortex* **25**:4839–4853. doi:10.1093/cercor/bhv188

Mondini V, Sburlea AI, Müller-Putz GR. 2024. Towards unlocking motor control in spinal cord injured by applying an online EEG-based framework to decode motor intention, trajectory and error processing. *Sci Rep* **14**:1–19. doi:10.1038/s41598-024-55413-x

Mueller-Putz G, Scherer R, Brunner C, Leeb R, Pfurtscheller G. 2008. Better than random: A closer look on BCI results. *Int J Bioelectromagn* **10**:52–55.

Müller-Gerking J, Pfurtscheller G, Flyvbjerg H. 1999. Designing optimal spatial filters for single-trial EEG classification in a movement task. *Clin Neurophysiol* **110**:787–798. doi:10.1016/S1388-2457(98)00038-8

Müller-Putz G, Leeb R, Tangermann M, Höhne J, Kübler A, Cincotti F, Mattia D, Rupp R, Müller KR, Millán JDR. 2015. Towards noninvasive hybrid brain-computer interfaces: Framework, practice, clinical application, and beyond. *Proc IEEE* **103**:926–943. doi:10.1109/JPROC.2015.2411333

Müller-Putz GR, Zimmermann D, Graimann B, Nestinger K, Korisek G, Pfurtscheller G. 2007. Event-related beta EEG-changes during passive and attempted foot movements in paraplegic patients. *Brain Res* **1137**:84–91. doi:10.1016/j.brainres.2006.12.052

Mumtaz W, Rasheed S, Irfan A. 2021. Review of challenges associated with the EEG artifact removal methods. *Biomed Signal Process Control* **68**:102741. doi:10.1016/j.bspc.2021.102741

Muralidharan A, Chae J, Taylor DM. 2011. Extracting attempted hand movements from eegs in people with complete hand paralysis following stroke. *Front Neurosci* **5**:1–7. doi:10.3389/fnins.2011.00039

Murata A, Gallese V, Luppino G, Kaseda M, Sakata H. 2000. Selectivity for the shape, size, and orientation of objects for grasping in neurons of monkey parietal area AIP. *J Neurophysiol* **83**:2580–2601. doi:10.1152/jn.2000.83.5.2580

Nalborczyk L, Alario FX, Longcamp M. 2025. Motor inhibition prevents motor execution during typing imagery: Evidence from an action-mode switching paradigm. *Cognition* **254**:105997. doi:10.1016/j.cognition.2024.105997

Naseer N, Hong KS. 2015. fNIRS-based brain-computer interfaces: A review. *Front Hum Neurosci* **9**:1–15. doi:10.3389/fnhum.2015.00003

Natraj N, Silversmith DB, Chang EF, Ganguly K. 2022. Compartmentalized dynamics within a common multi-area mesoscale manifold represent a repertoire of human hand movements. *Neuron* **110**:154-174.e12. doi:10.1016/j.neuron.2021.10.002

Neuper C, Wörtz M, Pfurtscheller G. 2006. Chapter 14 ERD/ERS patterns reflecting sensorimotor activation and deactivation. *Prog Brain Res* **159**:211–222. doi:10.1016/S0079-6123(06)59014-4

Nicolas-Alonso LF, Gomez-Gil J. 2012. Brain computer interfaces, a review. *Sensors* **12**:1211–1279. doi:10.3390/s120201211

Onton J, Westerfield M, Townsend J, Makeig S. 2006. Imaging human EEG dynamics using independent component analysis. *Neurosci Biobehav Rev* **30**:808–822. doi:10.1016/j.neubiorev.2006.06.007

Ottenhoff MC, Verwoert M, Goulis S, Colon AJ, Wagner L, Tousseyn S, van Dijk JP, Kubben PL, Herff C. 2023. Decoding executed and imagined grasping movements from distributed non-motor brain areas using a Riemannian decoder. *Front Neurosci* **17**:1–8. doi:10.3389/fnins.2023.1283491

Paek AY, Kilicarslan A, Korenko B, Gerginov V, Knappe S, Contreras-Vidal JL. 2020. Towards a Portable Magnetoencephalography Based Brain Computer Interface with Optically-Pumped

Magnetometers. *Proc Annu Int Conf IEEE Eng Med Biol Soc EMBS* **2020**-**July**:3420–3423. doi:10.1109/EMBC44109.2020.9176159

Papadopoulos S, Bonaiuto J, Mattout J. 2022. An Impending Paradigm Shift in Motor Imagery Based Brain-Computer Interfaces. *Front Neurosci* **15**. doi:10.3389/fnins.2021.824759

Papadopoulos S, Szul MJ, Congedo M, Bonaiuto JJ, Mattout J. 2024. Beta bursts question the ruling power for brain–computer interfaces. *J Neural Eng* **21**:16010. doi:10.1088/1741-2552/ad19ea

Park MC, Belhaj-Saïf A, Gordon M, Cheney PD. 2001. Consistent features in the forelimb representation of primary motor cortex in rhesus macaques. *J Neurosci* **21**:2784–2792. doi:10.1523/jneurosci.21-08-02784.2001

Pedregosa F, Varoquaux G, Gramfort A, Michel V, Thirion B, Grisel O, Blondel M, Prettenhofer P, Weiss R, Bubourg V, Vanderplas J, Passos A, Cournapeau D, Brucher M, Perrot M, Duchesnay E. 2011. Scikit-learn: Machine Learning in Python. *J Mach Learn Res* **12**:2825–2830.

Penfield W, Rasmussen T. 1950. The Cerebral Cortex of Man: A Clinical Study of Localization of Function, Macmillan.

Pfurtscheller G. 2010. The hybrid BCI. *Front Neurosci* **4**:1–11. doi:10.3389/fnpro.2010.00003

Pfurtscheller G. 1981. Central beta rhythm during sensorimotor activities in man. *Electroencephalogr Clin Neurophysiol* **51**:253–264. doi:10.1016/0013-4694(81)90139-5

Pfurtscheller G, Berghold A. 1989. Patterns of cortical activation during planning of voluntary movement. *Electroencephalogr Clin Neurophysiol* **72**:250–258. doi:10.1016/0013-4694(89)90250-2

Pfurtscheller G, Brunner C, Schlögl A, Lopes da Silva FH. 2006. Mu rhythm (de)synchronization and EEG single-trial classification of different motor imagery tasks. *Neuroimage* **31**:153–159. doi:10.1016/j.neuroimage.2005.12.003

Pfurtscheller G, Flotzinger D, Kalcher J. 1993. Brain-Computer Interface-a new communication device for handicapped persons. *J Microcomput Appl*. doi:10.1006/jmca.1993.1030

Pfurtscheller G, Lopes da Silva FH. 1999. Event-relared EEG/MEG synchronization and desynchronization: basic principles. *Clin Neurophysiol* **110**:1842–1857. doi:10.1016/S1388-2457(99)00141-8

Pfurtscheller G, Neuper C. 2001. Motor imagery direct communication. *Proc IEEE* **89**:1123–1134. doi:10.1109/5.939829

Pfurtscheller G, Neuper C. 1997. Motor imagery activates primary sensorimotor area in humans. *Neurosci Lett* **239**:65–68. doi:10.1016/S0304-3940(97)00889-6

Pfurtscheller G, Neuper C, Flotzinger D, Pregenzer M. 1997. EEG-based discrimination between imagination of right and left hand movement. *Electroencephalogr Clin Neurophysiol* **103**:642–651. doi:10.1016/S0013-4694(97)00080-1

Pfurtscheller G, Stancák A, Neuper C. 1996. Post-movement beta synchronization. A correlate of an idling motor area? *Electroencephalogr Clin Neurophysiol* **98**:281–293. doi:10.1016/0013-4694(95)00258-8

Pichiorri F, Mattia D. 2020. Brain-computer interfaces in neurologic rehabilitation practice, 1st ed, Handbook of Clinical Neurology. Elsevier B.V. doi:10.1016/B978-0-444-63934-9.00009-3

Pillette L, N'kaoua B, Sabau R, Glize B, Lotte F. 2021. Multi-Session Influence of Two Modalities of Feedback and Their Order of Presentation on MI-BCI User Training. *Multimodal Technol Interact MDPI* **5**:12. doi:10.3390/mti5030012

Preston C, Newport R. 2014. Noisy visual feedback training impairs detection of self-generated movement error: Implications for anosognosia for hemiplegia. *Front Hum Neurosci* **8**:1–6. doi:10.3389/fnhum.2014.00456

Purves. 2017. Neuroscience 6th Edition. Oxford University Press, Incorporated.

Putzolu M, Samogin J, Bonassi G, Cosentino C, Mezzarobba S, Botta A, Avanzino L, Mantini D, Vato A, Pelosin E. 2024. Motor imagery ability scores are related to cortical activation during gait imagery. *Sci Rep* **14**:1–10. doi:10.1038/s41598-024-54966-1

Quinn AJ, Lopes-Dos-Santos V, Huang N, Liang WK, Juan CH, Yeh JR, Nobre AC, Dupret D, Woolrich MW. 2021. Within-cycle instantaneous frequency profiles report oscillatory waveform Dynamics. *J Neurophysiol* **126**:1190–1208. doi:10.1152/jn.00201.2021

Raffin E, Hummel FC. 2017. Restoring Motor Functions After Stroke: Multiple Approaches and Opportunities. *Neuroscientist* **24**:400–416. doi:10.1177/1073858417737486

Raffin E, Mattout J, Reilly KT, Giraux P. 2012. Disentangling motor execution from motor imagery with the phantom limb. *Brain* **135**:582–595. doi:10.1093/brain/awr337

Ramadan RA, Vasilakos A V. 2017. Brain computer interface: control signals review. *Neurocomputing* **223**:26–44. doi:10.1016/j.neucom.2016.10.024

Raos V, Umiltá MA, Gallese V, Fogassi L. 2004. Functional properties of grasping-related neurons in the dorsal premotor area F2 of the macaque monkey. *J Neurophysiol* **92**:1990–2002. doi:10.1152/jn.00154.2004

Raos V, Umiltá MA, Murata A, Fogassi L, Gallese V. 2006. Functional properties of grasping-related neurons in the ventral premotor area F5 of the macaque monkey. *J Neurophysiol* **95**:709–729. doi:10.1152/jn.00463.2005

Rayson H, Szul MJ, El-Khoueiry P, Debnath R, Gautier-Martins M, Ferrari PF, Fox N, Bonaiuto JJ. 2023. Bursting with potential: How sensorimotor beta bursts develop from infancy to adulthood. *J Neurosci* **43**:8487–8503. doi:10.1523/JNEUROSCI.0886-23.2023

Rhodes E, Gaetz W, Marsden J, Hall SD. 2024. Post-Movement Beta Synchrony Inhibits Cortical Excitability. *Brain Sci* **14**. doi:10.3390/ brainsci14100970

Rieger M, Dahm SF, Koch I. 2017. Inhibition in motor imagery: a novel action mode switching paradigm. *Psychon Bull Rev* **24**:459–466. doi:10.3758/s13423-016-1095-5

Rienzo F Di, Collet C, Hoyek N, Guillot A. 2014. Impact of neurologic deficits on motor imagery: A systematic review of clinical evaluations. *Neuropsychol Rev* **24**:116–147. doi:10.1007/s11065-014-9257-6

Roberts G, Holmes N, Alexander N, Boto E, Leggett J, Hill RM, Shah V, Rea M, Vaughan R, Maguire EA, Kessler K, Beebe S, Fromhold M, Barnes GR, Bowtell R, Brookes MJ. 2019. Towards OPM-MEG in a virtual reality environment. *Neuroimage* **199**:408–417. doi:10.1016/j.neuroimage.2019.06.010

Roc A, Pillette L, Mladenovic J, Benaroch C, N'Kaoua B, Jeunet C, Lotte F. 2021. A review of user training methods in brain computer interfaces based on mental tasks. *J Neural Eng* **18**. doi:10.1088/1741-2552/abca17

Rodriguez-Larios J, Haegens S. 2023. Genuine beta bursts in human working memory: controlling for the influence of lower-frequency rhythms. *bioRxiv* 2023.05.26.542448.

Ronca V, Capotorto R, Flumeri G Di, Giorgi A, Vozzi A, Germano D, Virgilio V Di, Borghini G, Cartocci G, Rossi D, Inguscio BMS, Babiloni F, Aric P. 2024. Optimizing EEG Signal Integrity : A Comprehensive Guide to Ocular Artifact Correction.

Rosenfeld J V., Wong YT. 2017. Neurobionics and the brainecomputer interface: Current applications and future horizons. *Med J Aust* **206**:363–368. doi:10.5694/mja16.01011

Roy AM. 2022. An efficient multi-scale CNN model with intrinsic feature integration for motor imagery EEG subject classification in brain-machine interfaces 1–37.

Roy Y, Banville H, Albuquerque I, Gramfort A, Falk TH, Faubert J. 2019. Deep learning-based electroencephalography analysis: A systematic review. *J Neural Eng* **16**. doi:10.1088/1741-2552/ab260c

Sabio J, Lucia S. 2022. A scoping review on the use of consumer-grade EEG devices for research.

Sadeghi S, Maleki A. 2019. Accurate estimation of information transfer rate based on symbol occurrence probability in brain-computer interfaces. *Biomed Signal Process Control* **54**:101607. doi:10.1016/j.bspc.2019.101607

Sadeghi S, Maleki A. 2018. Recent advances in hybrid brain-computer interface systems: A technological and quantitative review. *Basic Clin Neurosci* **9**:373–388. doi:10.32598/bcn.9.5.373

Saeedi S, Chavarriaga R, Millan JDR. 2017. Long-Term Stable Control of Motor-Imagery BCI by a Locked-In User Through Adaptive Assistance. *IEEE Trans Neural Syst Rehabil Eng* **25**:380–391. doi:10.1109/TNSRE.2016.2645681

Safaie M, Chang JC, Park J, Miller LE, Dudman JT, Perich MG, Gallego JA. 2023. Preserved neural dynamics across animals performing similar behaviour. *Nature* **623**:765–771. doi:10.1038/s41586-023-06714-0

Schaworonkow N, Voytek B. 2021. Enhancing oscillations in intracranial electrophysiological recordings with data-driven spatial filters. *PLoS Comput Biol* **17**:e1009298. doi:10.1371/journal.pcbi.1009298

Scherberger H. 2021. Distributed yet compartmentalized neural dynamics of hand actions. *Neuron* **110**:10–11. doi:10.1016/j.neuron.2021.12.021

Scherer R, Faller J, Friedrich EVC, Opisso E, Costa U, Kübler A, Müller-Putz GR. 2015. Individually adapted imagery improves brain-computer interface performance in end-users with disability. *PLoS One* **10**:1–14. doi:10.1371/journal.pone.0123727

Schirrmeister RT, Springenberg JT, Fiederer LDJ, Glasstetter M, Eggensperger K, Tangermann M, Hutter F, Burgard W, Ball T. 2017. Deep learning with convolutional neural networks for EEG decoding and visualization. *Hum Brain Mapp* **38**:5391–5420. doi:10.1002/hbm.23730

Schmidt R, Ruiz MH, Kilavik BE, Lundqvist M, Starr PA, Aron AR. 2019. Beta oscillations in working memory, executive control of movement and thought, and sensorimotor function. *J Neurosci* **39**:8231–8238. doi:10.1523/JNEUROSCI.1163-19.2019

Schmidt SL, Peters JJ, Turner DA, Grill WM. 2020. Continuous deep brain stimulation of the subthalamic nucleus may not modulate beta bursts in patients with Parkinson's disease. *Brain Stimul* **13**:433–443. doi:10.1016/j.brs.2019.12.008

Schwarz A, Ofner P, Pereira J, Sburlea AI, Müller-Putz GR. 2018. Decoding natural reach-and-grasp actions from human EEG. *J Neural Eng* **15**. doi:10.1088/1741-2552/aa8911

Scott SH. 2003. The role of primary motor cortex in goal-directed movements: insights from neurophysiological studies on non-human primates. *Curr Opin Neurobiol* **13**:671–677. doi:https://doi.org/10.1016/j.conb.2003.10.012

Seeber M, Scherer R, Müller-Putz GR. 2016. EEG oscillations are modulated in different behavior-related networks during rhythmic finger movements. *J Neurosci* **36**:11671–11681. doi:10.1523/JNEUROSCI.1739-16.2016

Seeber M, Scherer R, Wagner J, Solis-Escalante T, Müller-Putz GR. 2015. High and low gamma EEG oscillations in central sensorimotor areas are conversely modulated during the human gait cycle. *Neuroimage* **112**:318–326. doi:10.1016/j.neuroimage.2015.03.045

Seedat ZA, Quinn AJ, Vidaurre D, Liuzzi L, Gascoyne LE, Hunt BAE, O'Neill GC, Pakenham DO, Mullinger KJ, Morris PG, Woolrich MW, Brookes MJ. 2020. The role of transient spectral 'bursts' in functional connectivity: A magnetoencephalography study. *Neuroimage* **209**. doi:10.1016/j.neuroimage.2020.116537

Segev I, Rall W. 1998. Excitable dendrites and spines: Earlier theoretical insights elucidate recent direct observations. *Trends Neurosci* **21**:453–460. doi:10.1016/S0166-2236(98)01327-7

Séguin P, Maby E, Fouillen M, Otman A, Luauté J, Giraux P, Morlet D, Mattout J. 2024. The challenge of controlling an auditory BCI in the case of severe motor disability. *J Neuroeng Rehabil* **21**:1–15. doi:10.1186/s12984-023-01289-3

Sergio LE, Hamel-Pâquet C, Kalaska JF. 2005. Motor Cortex Neural Correlates of Output Kinematics and Kinetics During Isometric-Force and Arm-Reaching Tasks. *J Neurophysiol* **94**:2353–2378. doi:10.1152/jn.00989.2004

Sherman MA, Lee S, Law R, Haegens S, Thorn CA, Hämäläinen MS. 2016. Neural mechanisms of transient neocortical beta rhythms : Converging evidence from humans, computational modeling, monkeys, and mice. doi:10.1073/pnas.1604135113

Shimazu H, Maier MA, Cerri G, Kirkwood PA, Lemon RN. 2004. Macaque Ventral Premotor Cortex Exerts Powerful Facilitation of Motor Cortex Outputs to Upper Limb Motoneurons. *J Neurosci* **24**:1200–1211. doi:10.1523/JNEUROSCI.4731-03.2004

Shin H, Law R, Tsutsui S, Moore CI, Jones SR. 2017. The rate of transient beta frequency events predicts impaired function across tasks and species. *Elife*. doi:10.7554/eLife.29086

Shlens J. 2014. A Tutorial on Principal Component Analysis. *arXiv*.

Sigl JC, Chamoun NG. 1994. AN INTRODUCTION TO BISPECTRAL ANALYSIS FOR THE ELECTROENCEPHALOGRAM. *J Clin Monit* **10**:392–404.

Singh Malan N, Sharma S. 2021. Time window and frequency band optimization using regularized neighbourhood component analysis for Multi-View Motor Imagery EEG classification. *Biomed Signal Process Control* **67**:102550. doi:10.1016/j.bspc.2021.102550

Sisti HM, Beebe A, Bishop M, Gabrielsson E. 2022. A brief review of motor imagery and bimanual coordination. *Front Hum Neurosci* **16**:1–7. doi:10.3389/fnhum.2022.1037410

Soh C, Hynd M, Rangel BO, Wessel JR. 2021. Adjustments to proactive motor inhibition without effector-specific foreknowledge are reflected in a bilateral upregulation of sensorimotor β-burst rates. *J Cogn Neurosci* **33**:784–798. doi:10.1162/jocn_a_01682

Song X, Yoon SC, Perera V. 2013. Adaptive Common Spatial Pattern for single-trial EEG classification in multisubject BCI. *Int IEEE/EMBS Conf Neural Eng NER* **19013**:411–414. doi:10.1109/NER.2013.6695959

Spruston N. 2008. Pyramidal neurons: dendritic structure and synaptic integration. *Nat Rev Neurosci* **9**:206–221. doi:10.1038/nrn2286

Spruston N, Kath WL. 2004. Dendritic arithmetic. *Nat Neurosci* **7**:567–569. doi:10.1038/nn0604-567

Steyrl D, Scherer R, Faller J, Müller-Putz GR. 2016. Random forests in non-invasive sensorimotor rhythm brain-computer interfaces: A practical and convenient non-linear classifier. *Biomed Tech* **61**:77–86. doi:10.1515/bmt-2014-0117

Steyrl D, Scherer R, Oswin F, Gernot RM. 2014. Motor Imagery Brain-Computer Interfaces : Random Forests vs Regularized LDA - Non-linear Beats Linear. *Proc 6th Int Brain-Computer Interface Conf* 8–11. doi:10.3217/978-3-85125-378-8-61

Sugata H, Hirata M, Yanagisawa T, Matsushita K, Yorifuji S, Yoshimine T. 2016. Common neural correlates of real and imagined movements contributing to the performance of brain-machine interfaces. *Sci Rep* **6**:1–11. doi:10.1038/srep24663

Szul MJ, Papadopoulos S, Alavizadeh S, Daligaut S, Schwartz D, Mattout J, Bonaiuto JJ. 2023. Diverse beta burst waveform motifs characterize movement-related cortical dynamics. *Prog Neurobiol* 165187. doi:10.1016/j.pneurobio.2023.102490

Takahashi K, Best MD, Huh N, Brown KA, Tobaa AA, Hatsopoulos NG. 2017. Encoding of both reaching and grasping kinematics in dorsal and ventral premotor cortices. *J Neurosci* **37**:1733–1746. doi:10.1523/JNEUROSCI.1537-16.2016

Tam W, Wu T, Zhao Q, Keefer E, Yang Z. 2019. Human motor decoding from neural signals: a review. *BMC Biomed Eng* **1**:1–22. doi:10.1186/s42490-019-0022-z

Tangermann M, Müller KR, Aertsen A, Birbaumer N, Braun C, Brunner C, Leeb R, Mehring C, Miller KJ, Müller-Putz GR, Nolte G, Pfurtscheller G, Preissl H, Schalk G, Schlögl A, Vidaurre C, Waldert S, Blankertz B. 2012. Review of the BCI competition IV. *Front Neurosci* **6**:1–31. doi:10.3389/fnins.2012.00055

Tayeb Z, Fedjaev J, Ghaboosi N, Richter C, Everding L, Qu X, Wu Y, Cheng G, Conradt J. 2019. Validating deep neural networks for online decoding of motor imagery movements from eeg signals. *Sensors (Switzerland)* **19**. doi:10.3390/s19010210

Tharwat A, Gaber T, Ibrahim A, Hassanien AE. 2017. Linear discriminant analysis: A detailed tutorial. *AI Commun* **30**:169–190. doi:10.3233/AIC-170729

Tinkhauser G, Pogosyan A, Little S, Beudel M, Herz DM, Tan H, Brown P. 2017a. The modulatory effect of adaptive deep brain stimulation on beta bursts in Parkinson's disease. *Brain* **140**:1053–1067. doi:10.1093/brain/awx010

Tinkhauser G, Pogosyan A, Tan H, Herz DM, Kühn AA, Brown P. 2017b. Beta burst dynamics in Parkinson's disease off and on dopaminergic medication. *Brain* **140**:2968–2981. doi:10.1093/brain/awx252

Todorov E. 2000. Direct cortical control of muscle activation in voluntary arm movements: a model. *Nat Neurosci* **3**:391–398. doi:10.1038/73964

Torrecillos F, Tinkhauser G, Fischer P, Green AL, Aziz TZ, Foltynie T, Limousin P, Zrinzo L, Ashkan K, Brown P, Tan H. 2018. Modulation of beta bursts in the subthalamic nucleus predicts motor performance. *J Neurosci* **38**:8905–8917. doi:10.1523/JNEUROSCI.1314-18.2018

Townsend BR, Subasi E, Scherberger H. 2011. Grasp movement decoding from premotor and parietal cortex. *J Neurosci* **31**:14386–14398. doi:10.1523/JNEUROSCI.2451-11.2011

Troebinger L, López JD, Lutti A, Bestmann S, Barnes G. 2014a. Discrimination of cortical laminae using MEG. *Neuroimage* **102**:885–893. doi:10.1016/j.neuroimage.2014.07.015

Troebinger L, López JD, Lutti A, Bradbury D, Bestmann S, Barnes G. 2014b. High precision anatomy for MEG. *Neuroimage* **86**:583–591. doi:10.1016/j.neuroimage.2013.07.065

Umilta MA, Brochier T, Spinks RL, Lemon RN. 2007. Simultaneous recording of macaque premotor and primary motor cortex neuronal populations reveals different functional contributions to visuomotor grasp. *J Neurophysiol* **98**:488–501. doi:10.1152/jn.01094.2006

Unterweger J, Seeber M, Zanos S, Ojemann JG, Scherer R. 2020. ECoG Beta Suppression and Modulation During Finger Extension and Flexion. *Front Neurosci* **14**:1–10. doi:10.3389/fnins.2020.00035

van Bree S, Levenstein D, Krause MR, Voytek B, Gao R. 2025. Processes and measurements: a framework for understanding neural oscillations in field potentials. *Trends Cogn Sci*. doi:10.1016/j.tics.2024.12.003

Van Caenegem EE, Hamoline G, Waltzing BM, Hardwick RM. 2022. Consistent under-reporting of task details in motor imagery research. *Neuropsychologia* **177**. doi:10.1016/j.neuropsychologia.2022.108425

Van Schie HT, Mars RB, Coles MGH, Bekkering H. 2004. Modulation of activity in medial frontal and motor cortices during error observation. *Nat Neurosci* **7**:549–554. doi:10.1038/nn1239

Vidaurre C, Blankertz B. 2010. Towards a cure for BCI illiteracy. *Brain Topogr* **23**:194–198. doi:10.1007/s10548-009-0121-6

Vidaurre C, Kawanabe M, Von Bünau P, Blankertz B, Müller KR. 2011. Toward unsupervised adaptation of LDA for brain-computer interfaces. *IEEE Trans Biomed Eng* **58**:587–597. doi:10.1109/TBME.2010.2093133

Vigué-Guix I, Soto-Faraco S. 2023. Using occipital α-bursts to modulate behavior in real-Time. *Cereb Cortex* **33**:9465–9477. doi:10.1093/cercor/bhad217

Vilela M, Hochberg LR. 2020. Applications of brain-computer interfaces to the control of robotic and prosthetic arms, 1st ed, Handbook of Clinical Neurology. Elsevier B.V. doi:10.1016/B978-0-444-63934-9.00008-1

Virtanen P, Gommers R, Oliphant TE, Haberland M, Reddy T, Cournapeau D, Burovski E, Peterson P, Weckesser W, Bright J, van der Walt SJ, Brett M, Wilson J, Millman KJ, Mayorov N, Nelson ARJ, Jones E, Kern R, Larson E, Carey CJ, Polat İ, Feng Y, Moore EW, VanderPlas J, Laxalde D, Perktold J, Cimrman R, Henriksen I, Quintero EA, Harris CR, Archibald AM, Ribeiro AH, Pedregosa F, van Mulbregt P, Vijaykumar A, Bardelli A Pietro, Rothberg A, Hilboll A, Kloeckner A, Scopatz A, Lee A, Rokem A, Woods CN, Fulton C, Masson C, Häggström C, Fitzgerald C, Nicholson DA, Hagen DR, Pasechnik D V., Olivetti E, Martin E, Wieser E, Silva F, Lenders F, Wilhelm F, Young G, Price GA, Ingold GL, Allen GE, Lee GR, Audren H, Probst I, Dietrich JP, Silterra J, Webber JT, Slavič J, Nothman J, Buchner J, Kulick J, Schönberger JL, de Miranda Cardoso JV, Reimer J, Harrington J, Rodríguez JLC, Nunez-Iglesias J, Kuczynski J, Tritz K, Thoma M, Newville M, Kümmerer M, Bolingbroke M, Tartre M, Pak M, Smith NJ, Nowaczyk N, Shebanov N, Pavlyk O, Brodtkorb PA, Lee P, McGibbon RT, Feldbauer R, Lewis S, Tygier S, Sievert S, Vigna S, Peterson S, More S, Pudlik T, Oshima T, Pingel TJ, Robitaille TP, Spura T, Jones TR, Cera T, Leslie T, Zito T, Krauss T, Upadhyay U, Halchenko YO, Vázquez-Baeza Y. 2020. SciPy 1.0: fundamental algorithms for scientific computing in Python. *Nat Methods* **17**:261–272. doi:10.1038/s41592-019-0686-2

Waldert S, Preissl H, Demandt E, Braun C, Birbaumer N, Aertsen A, Mehring C. 2008. Hand movement direction decoded from MEG and EEG. *J Neurosci* **28**:1000–1008. doi:10.1523/JNEUROSCI.5171-07.2008

Wallstrom GL, Kass RE, Miller A, Cohn JF, Fox NA. 2004. Automatic correction of ocular artifacts in the EEG: A comparison of regression-based and component-based methods. *Int J Psychophysiol* **53**:105–119. doi:10.1016/j.ijpsycho.2004.03.007

Wang L, Xu G, Wang J, Yang S, Yan W. 2008. Application of Hilbert-Huang transform for the study of motor imagery tasks. *Proc 30th Annu Int Conf IEEE Eng Med Biol Soc EMBS'08 - "Personalized Healthc through Technol* 3848–3851. doi:10.1109/iembs.2008.4650049

Wellmer J, Von Der Groeben F, Klarmann U, Weber C, Elger CE, Urbach H, Clusmann H, Von Lehe M. 2012. Risks and benefits of invasive epilepsy surgery workup with implanted subdural and depth electrodes. *Epilepsia* **53**:1322–1332. doi:10.1111/j.1528-1167.2012.03545.x

Wessel JR. 2020. B-Bursts Reveal the Trial-To-Trial Dynamics of Movement Initiation and Cancellation. *J Neurosci* **40**:411–423. doi:10.1523/JNEUROSCI.1887-19.2019

West TO, Duchet B, Farmer SF, Friston KJ, Cagnan H. 2023. When do bursts matter in the primary motor cortex? Investigating changes in the intermittencies of beta rhythms associated with movement states. *Prog Neurobiol* **221**:102397. doi:10.1016/j.pneurobio.2022.102397

West TO, Duchet B, Farmer SF, Friston KJ, Cagnan H. 2022. When do bursts matter in the primary motor cortex? Investigating changes in the intermittencies of beta rhythms associated with movement states. *Prog Neurobiol*. doi:10.1016/j.pneurobio.2022.102397

Willett FR, Avansino DT, Hochberg LR, Henderson JM, Shenoy K V. 2021. High-performance brain-to-text communication via handwriting. *Nature* **593**:249–254. doi:10.1038/s41586-021-03506-2.High-performance

Wilson LE, Da J, Castanheira S, Kinder BL, Baillet S. 2024. Model selection for spectral parameterization. *bioRxiv* 2024.08.01.606216.

Wittevrongel B, Holmes N, Boto E, Hill R, Rea M, Libert A, Khachatryan E, Van Hulle MM, Bowtell R, Brookes MJ. 2021. Practical real-time MEG-based neural interfacing with optically pumped magnetometers. *BMC Biol* **19**:1–15. doi:10.1186/s12915-021-01073-6

Wolpaw JR. 2002. Brain Computer Interfaces for communication and control. *Front Neurosci* **4**:767–791. doi:10.3389/conf.fnins.2010.05.00007

Wolpaw JR, McFarland DJ, Neat GW, Forneris CA. 1991. An EEG-based brain-computer interface for cursor control. *Electroencephalogr Clin Neurophysiol* **78**:252–259. doi:10.1016/0013-4694(91)90040-B

Wolpaw JR, Millán J del R, Ramsey NF. 2020. Brain-computer interfaces: Definitions and principles. *Handb Clin Neurol* **168**:15–23. doi:10.1016/B978-0-444-63934-9.00002-0

World Health Organization. 2011. Summary World Report On Disability, World Health.

Xu L, Xu M, Ke Y, An X, Liu S, Ming D. 2020. Cross-Dataset Variability Problem in EEG Decoding With Deep Learning. *Front Hum Neurosci* **14**:1–10. doi:10.3389/fnhum.2020.00103

Xu P, Liu T, Zhang R, Zhang Y, Yao D. 2014. Using particle swarm to select frequency band and time interval for feature extraction of EEG based BCI. *Biomed Signal Process Control* **10**:289–295. doi:10.1016/j.bspc.2013.08.012

Yeh CH, Al-Fatly B, Kühn AA, Meidahl AC, Tinkhauser G, Tan H, Brown P. 2020. Waveform changes with the evolution of beta bursts in the human subthalamic nucleus. *Clin Neurophysiol* **131**:2086–2099. doi:10.1016/j.clinph.2020.05.035

Yi W, Qiu S, Wang K, Qi H, Zhang L, Zhou P, He F, Ming D. 2014. Evaluation of EEG oscillatory patterns and cognitive process during simple and compound limb motor imagery. *PLoS One* **9**:1–19. doi:10.1371/journal.pone.0114853

Yoo PE, Oxley TJ, Hagan MA, John S, Ronayne SM, Rind GS, Brinded AM, Opie NL, Moffat BA, Wong YT. 2020. Distinct Neural Correlates Underlie Inhibitory Mechanisms of Motor Inhibition and Motor Imagery Restraint. *Front Behav Neurosci* **14**:1–10. doi:10.3389/fnbeh.2020.00077

Zarei R, He J, Siuly S, Zhang Y. 2017. A PCA aided cross-covariance scheme for discriminative feature extraction from EEG signals. *Comput Methods Programs Biomed* **146**:47–57. doi:10.1016/j.cmpb.2017.05.009

Zhang S, Szul MJ, Papadopoulos S, Massera A, Rayson H, Bonaiuto JJ. 2024. Multi-scale parameterization of neural rhythmicity with lagged Hilbert autocoherence. *bioRxiv*. doi:10.1101/2024.12.05.627017

Zhou B, Wu X, Lv Z, Zhang L, Guo X. 2016. A fully automated trial selection method for optimization of motor imagery based Brain-Computer interface. *PLoS One* **11**:1–20. doi:10.1371/journal.pone.0162657

Zich C, Quinn AJ, Bonaiuto JJ, O'Neill G, Mardell LC, Ward NS, Bestmann S. 2023. Spatiotemporal organization of human sensorimotor beta burst activity. *Elife* **12:e80160**. doi:10. 7554/ eLife. 80160

Chapter 6 - Appendix

6.1 List of abbreviations

AIP.....Anterior intraparietal area

AP.....Action potential

ASR.....Artifact subspace reconstruction

AUC.....Area under the curve

BCI.....Brain-computer interface

CNS.....Central nervous system

CSP.....Common spatial pattern

ECoG.....Electrocorticography

EEG.....Electroencephalography

ERD.....Event-related desynchronization

ERS.....Event-related synchronization

fMRI.....Functional magnetic resonance imaging

fNIRS.....Functional near infrared spectroscopy

FWHM.....Full width at half maximum

GP(e).....Globus pallidus (external)

hpMEG.....High-precision magnetoencephalography

ICA.....Independent component analysis

ITR.....Information transfer rate

LDA.....Linear discriminant analysis

LFP.....Local field potential

M1.....Primary motor cortex

MEG.....Magnetoencephalography

MI.....Motor imagery

MI-BCI.....Motor imagery brain computer interface

OPM.....Optically pumped magnetometers

PCA.....Principal component analysis

PM(d/v).....Premotor cortex (dorsal/ventral)

PSD.....Power spectral density

(E/I)PSP.....(Excitatory/Inhibitory) Post-synaptic potential

ROC.....Receiver operating characteristic

S(1/2).....(Primary/Secondary) Sensory area

SMA.....Supplementary motor area

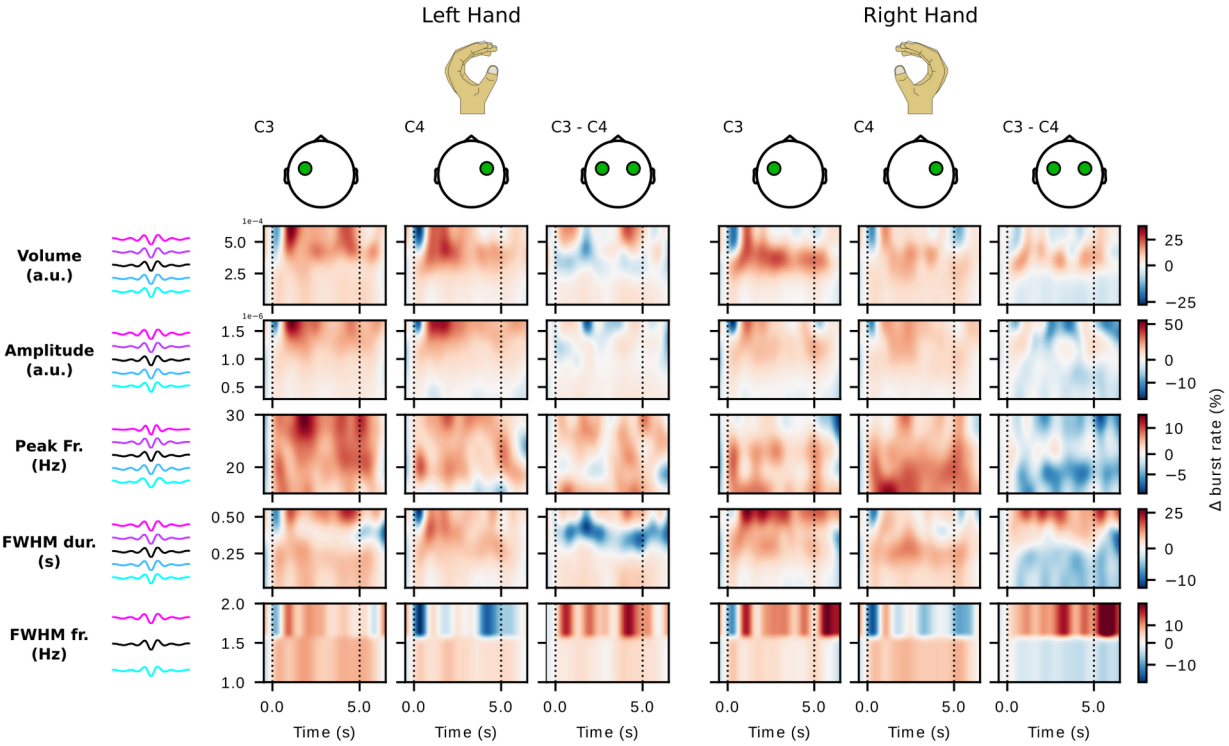
SNR.....Signal-to-noise ratio

STN.....Subthalamic nucleus

TF.....Time-frequency

V6A.....Sixth visual (dorsomedial) area

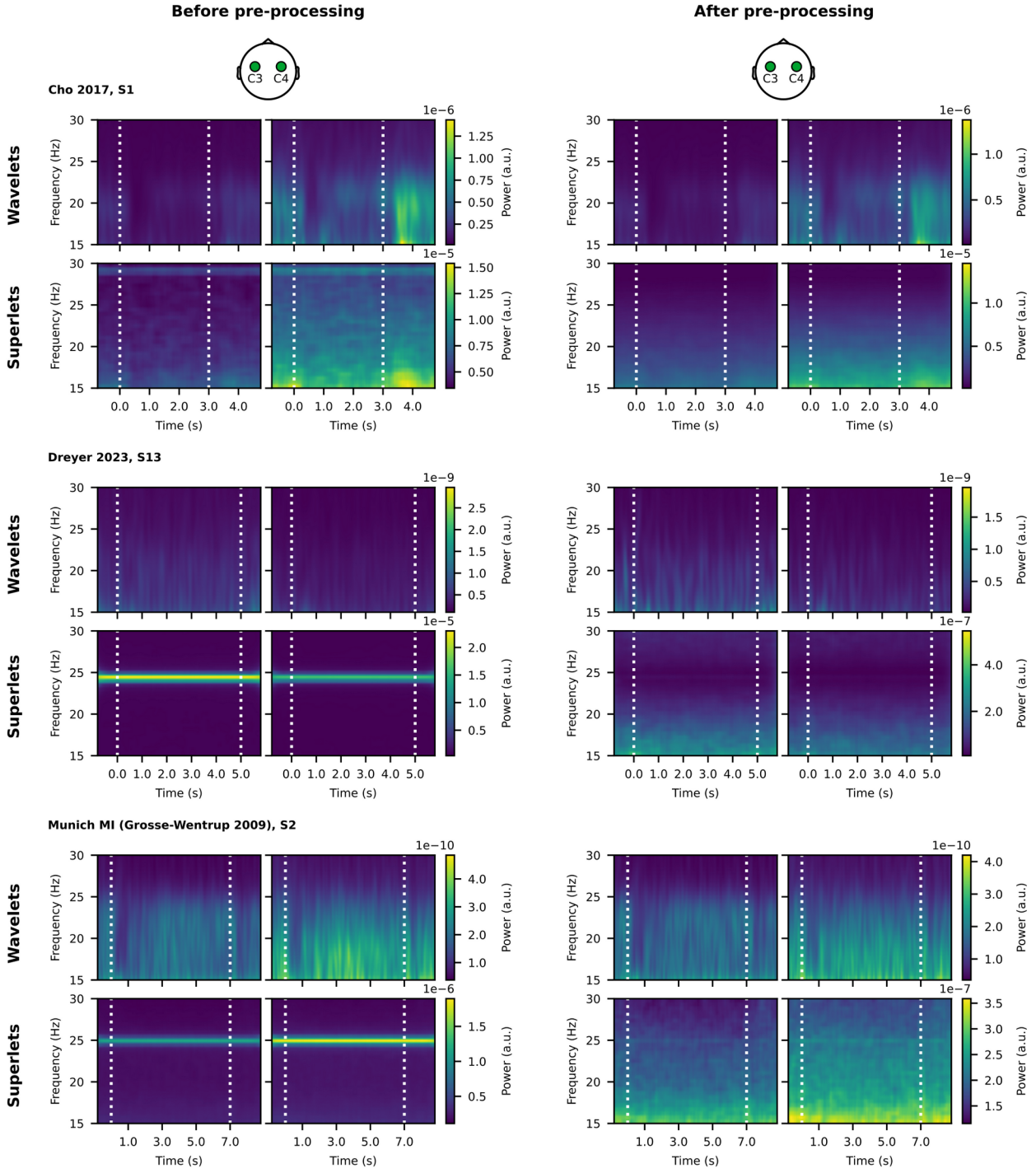
6.2 Supplementary material



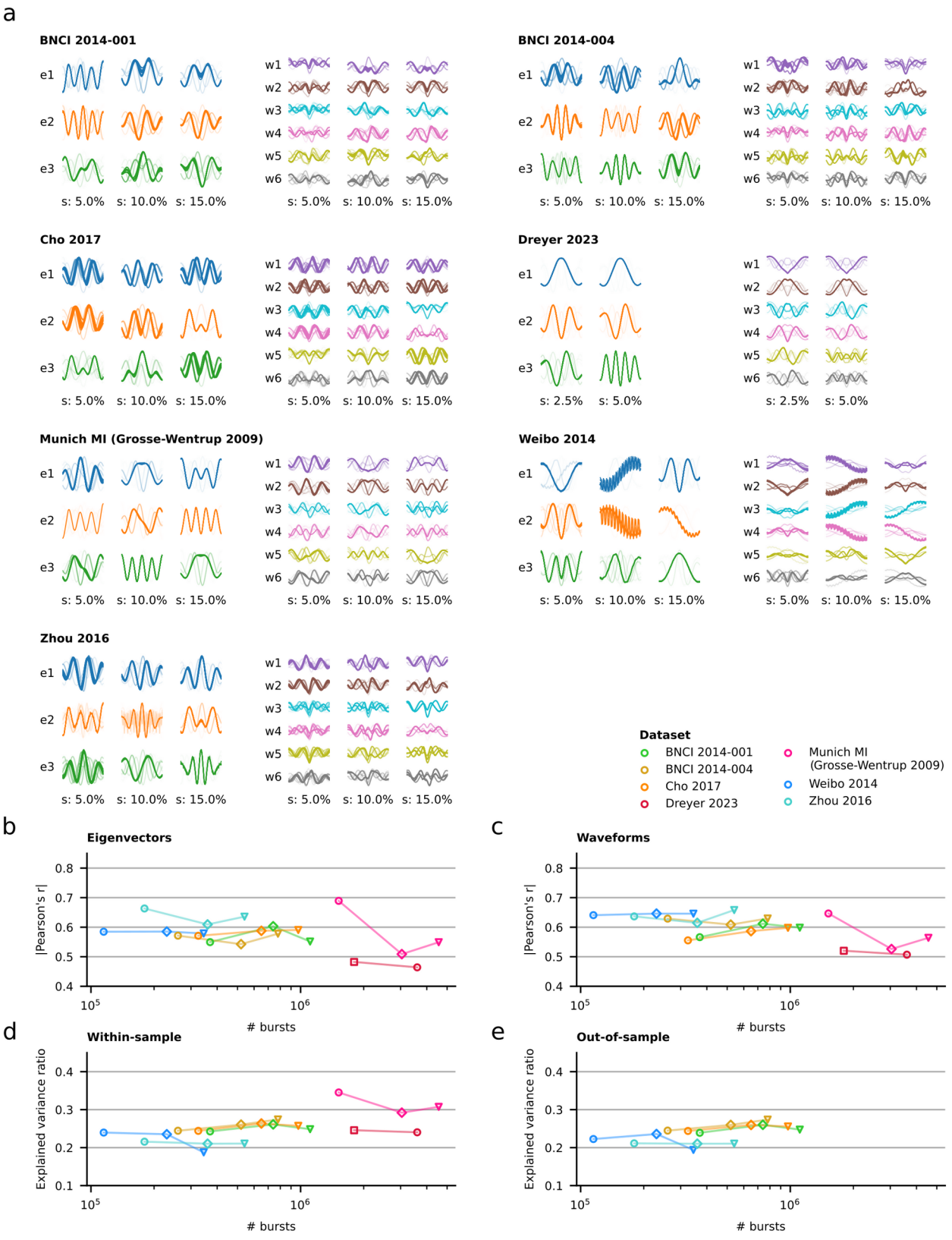
Sup. Figure 3.1.1: Trial-averaged, baseline-corrected burst rate along different TF-derived features for a representative subject (Zhou 2016 dataset, S1).



Sup. Figure 3.1.2: Results for binary “left hand” vs “right hand” classification for all subjects of each dataset included in the analysis. Color code as in figure 3.1.6.

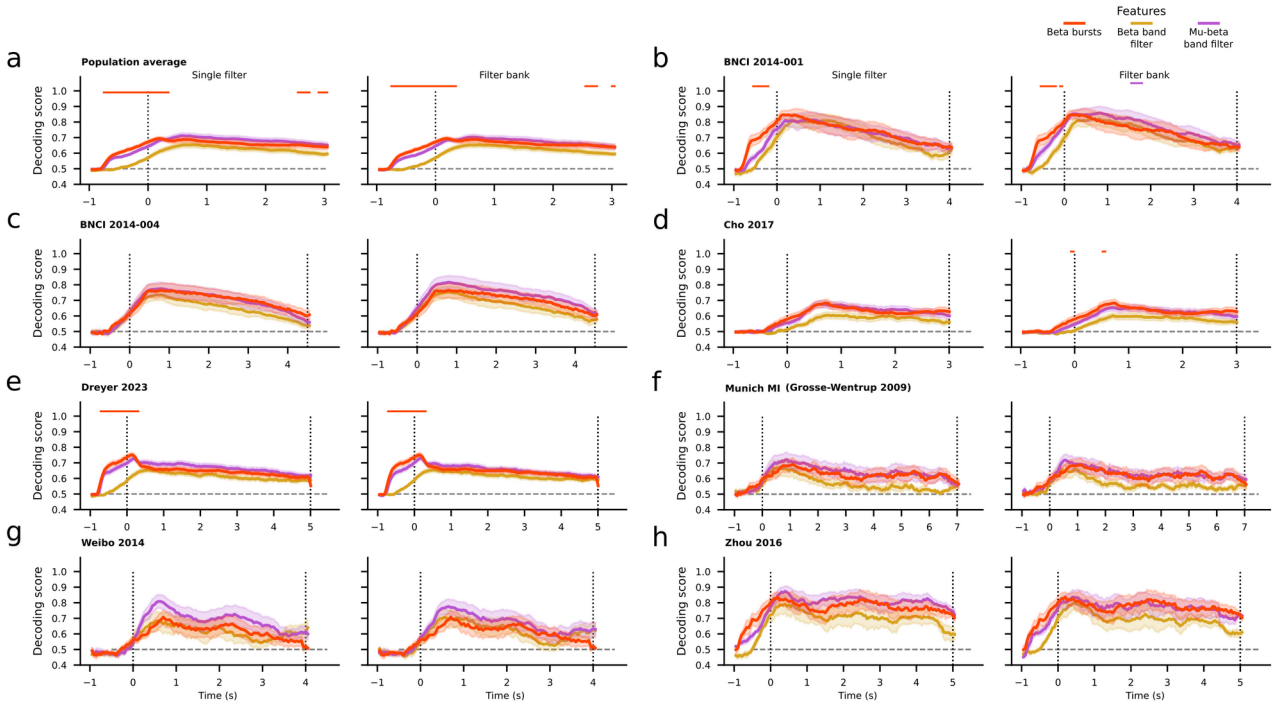


Sup. Figure 3.2.1: Three examples of trial-averaged data contaminated by noise in the frequency range of 24 – 30 Hz. The first column shows contaminated data in channels C3 and C4. The narrow-band, high-amplitude oscillation is present in both hemispheres and is not modulated by task demands (task onset and end are indicated by the dotted, vertical lines). In every example, a wavelet-based, time-frequency transformation does not reveal the underlying noise, unlike the superlets transformation which offers better time and frequency resolution. The second column showcases that the pre-processing pipeline effectively cleans the recordings allowing for detection of the underlying burst activity.

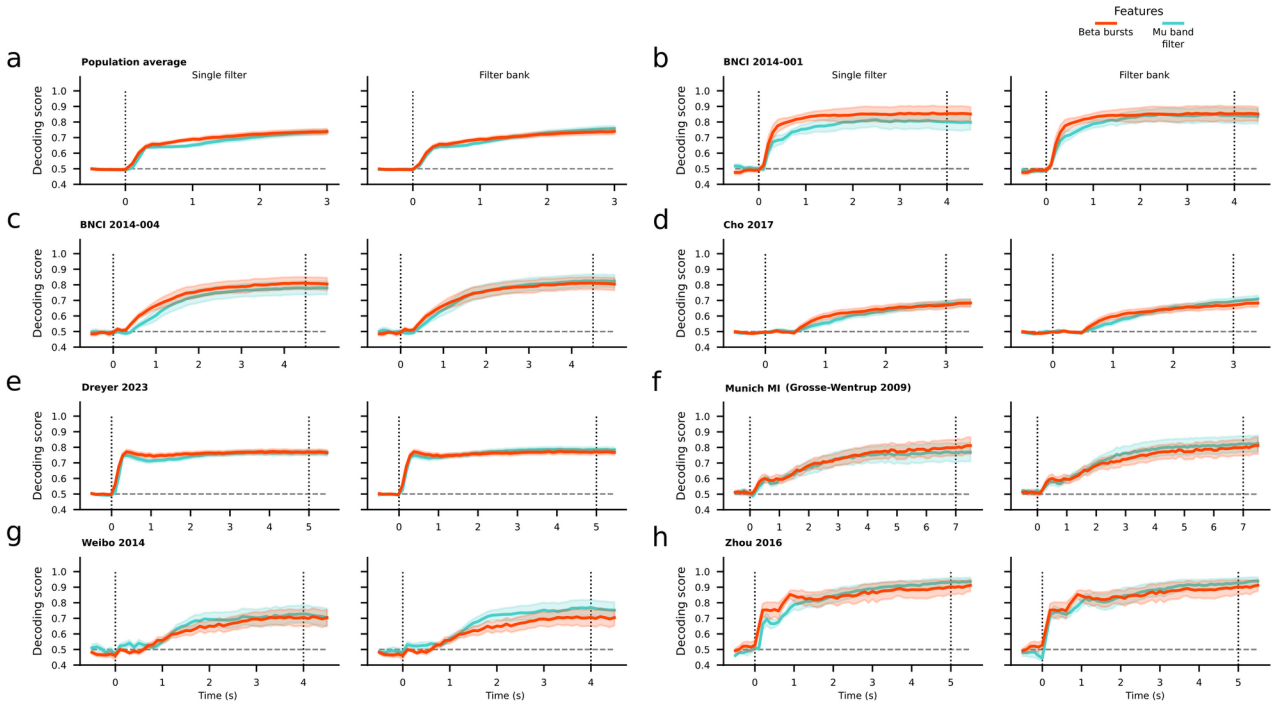


Sup. Figure 3.2.2: Collection of PCA eigenvectors and corresponding waveforms used as kernels, selected using the modulation index. **(a)** For each dataset each column shows the eigenvectors (e1-3) and waveforms (w1-6) corresponding to a different sample size (s). The random sampling per sample size is repeated thirty

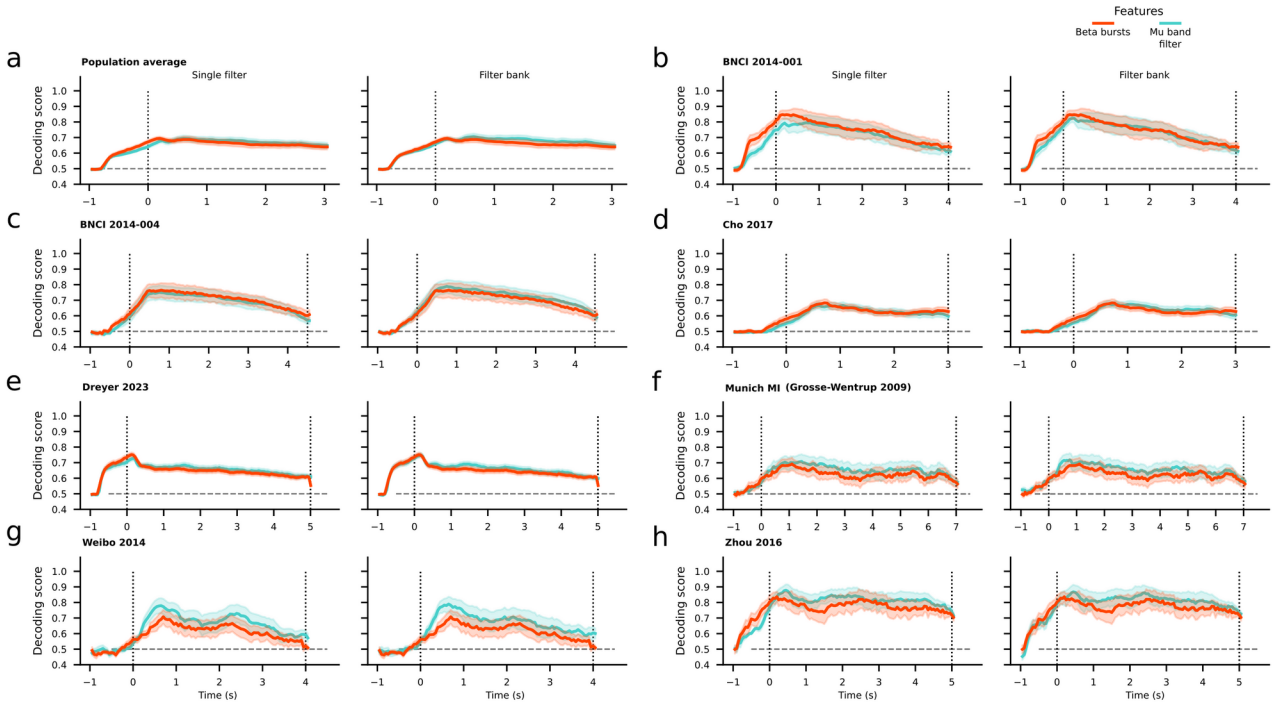
(← continues from previous page) times. Within each subplot, Pearson's correlation coefficients are used to rank the selected eigenvectors and waveforms per iteration of the random resampling. The shape with the maximum absolute correlation to the corresponding shape of the first iteration is plotted. Transparency levels of the depicted shapes equal the corresponding absolute correlation coefficients. The polarity of the depicted shapes is determined based on the signed correlation coefficients and matches the polarity of the first iteration's shapes. Smaller sample sizes are often characterized by greater variability in the shape of the selected eigenvectors and waveforms. The shapes of the selected eigenvectors and waveforms are more consistent when the sample size increases. High-frequency noise remaining in the data after pre-processing may affect some of the selected eigenvectors and waveforms, most prominently in the case of the Weibo 2014 dataset. **(b)** Sum of absolute Pearson's correlation coefficients across all selected eigenvectors, averaged over all random samples. Different sample sizes are quantified in terms of the number of bursts used for fitting the PCA algorithm. Higher values imply higher reproducibility of selected eigenvectors. A value of 1 corresponds to identical eigenvectors and a value of 0 to orthogonal eigenvectors. Within each dataset values remain stable regardless of the increase in the number of bursts included in the PCA, especially for datasets with fewer number of detected bursts. **(c)** Average of maximum absolute Pearson's correlation coefficients across all selected waveforms, averaged over all random samples. Higher values imply higher reproducibility of selected waveforms. The sample size used in this study offers consistent results in kernel selection. **(d)** Variance ratio of randomly sampled bursts explained by the selected eigenvectors, averaged over all random samples. **(e)** Variance ratio of all detected bursts explained by the selected eigenvectors, averaged over all random samples. The amount of data for two of the datasets included in this study was too large to perform this evaluation. The selected eigenvectors explain approximately the same amount of data variability irrespective of the tested sample size. Markers indicate the sample size as percentage of the total available trials (□ : 2.5%, o : 5%, ♦ : 10%, ᵛ : 15%). The values on the abscissa are plotted on a logarithmic scale. Each dataset is color-coded with a distinct color as indicated in the legend.



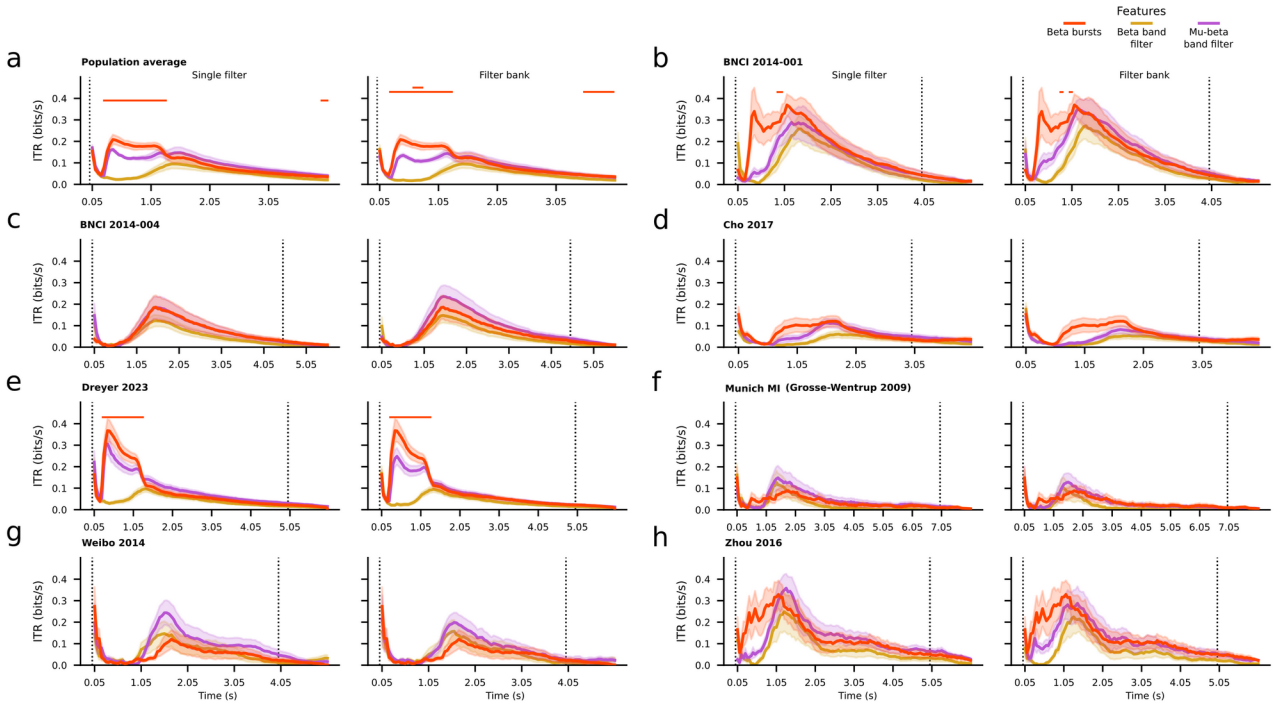
Sup. Figure 3.2.3: (a) Population average, time-resolved decoding score and standard error for the beta burst convolution (red), beta band (yellow) and mu-beta band (purple) filtering pipelines using a sliding window. Due to the different duration of the task for each dataset we restricted the time to the minimum trial period corresponding to 3 seconds. **(b – h)** Average, time-resolved decoding score and standard error per dataset of the same features using a sliding window. For each panel, the left subplot depicts the decoding results obtained using a single filter, while the right subplot depicts the results based on a filter bank technique. The beta burst results are the same for the pair of each panel. The horizontal dashed line corresponds to the expected chance level. Vertical dotted lines represent the onset and end of the trial period of each dataset. The two horizontal lines on the top of each subplot show the results of the two pair-wise permutation cluster tests, that is, between the beta bursts and the beta band (bottom line) or mu-beta band (top line) filtering technique respectively, with correction for multiple comparisons at significance level of 0.05. At any time point, each line is color-coded so as to indicate which feature produces, on average, better results. A lack of color at any given time point indicates no statistically significant differences between the compared features.



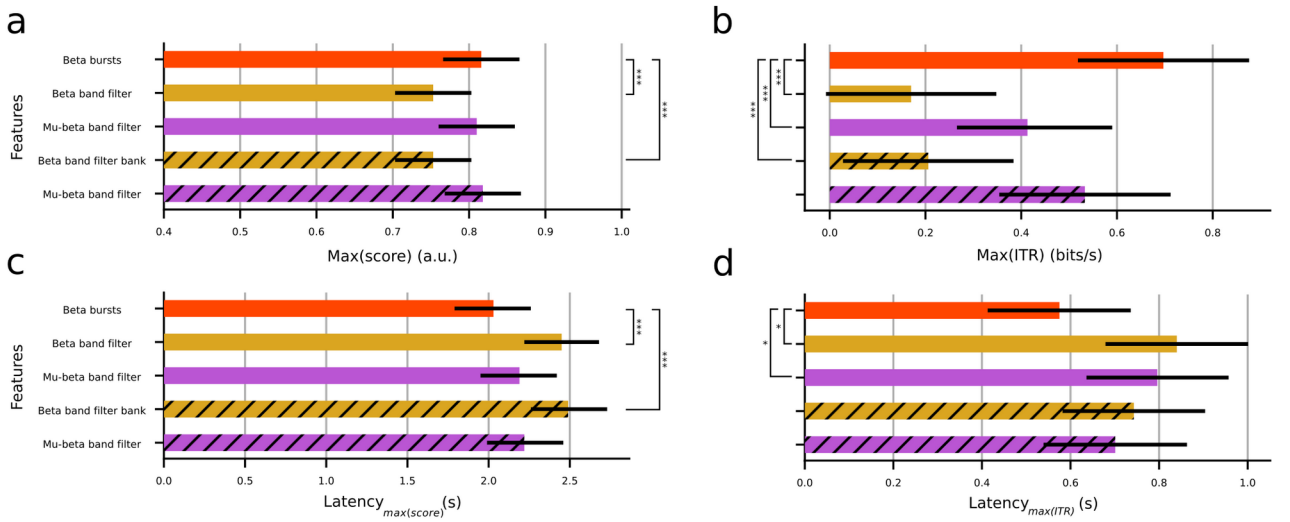
Sup. Figure 3.2.4: (a) Population average, time-resolved decoding score and standard error for the beta burst convolution (red) and mu band (turquoise) filtering pipelines using an incremental window. Due to the different duration of the task for each dataset we restricted the time to the minimum trial period corresponding to 3 seconds. **(b – h)** Average, time-resolved decoding score and standard error per dataset of the same features using an incremental window. For each panel, the left subplot depicts the decoding results obtained using a single filter, while the right subplot depicts the results based on a filter bank technique. The beta burst results are the same for the pair of each panel. The horizontal dashed line corresponds to the expected chance level. Vertical dotted lines represent the onset and end of the trial period of each dataset. The horizontal line on the top of each subplot shows the results of the pair-wise permutation cluster tests that is, between the beta bursts and the mu band filtering technique, with correction for multiple comparisons at significance level of 0.05. At any time point, each line is color-coded so as to indicate which feature produces, on average, better results. A lack of color at any given time point indicates no statistically significant differences between the compared features.



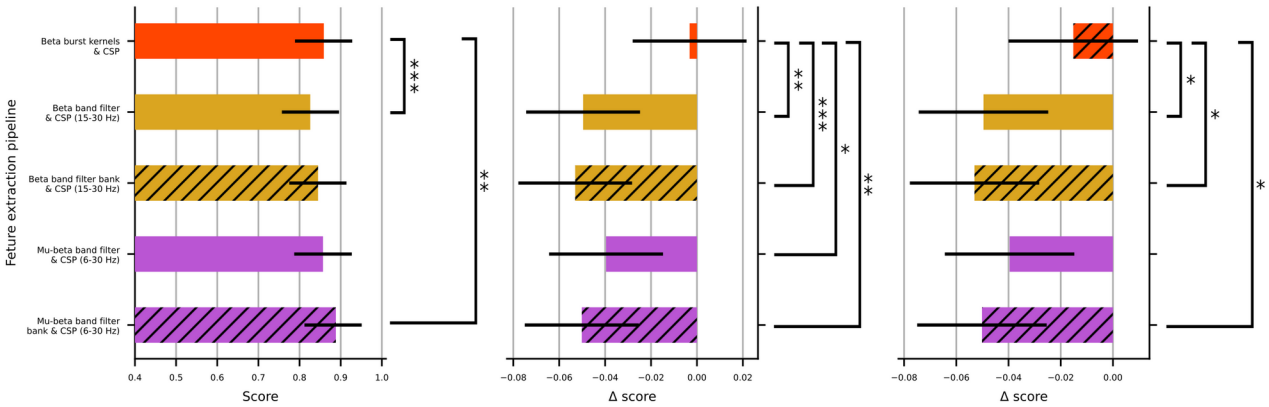
Sup. Figure 3.2.5: (a) Population average time-resolved decoding score and standard error for the beta burst convolution (red) and mu band (turquoise) filtering pipelines using a sliding window. Due to the different duration of the task for each dataset we restricted the time to the minimum trial period corresponding to 3 seconds. **(b – h)** Average, time-resolved decoding score and standard error per dataset of the same features using a sliding window. For each panel, the left subplot depicts the decoding results obtained using a single filter, while the right subplot depicts the results based on a filter bank technique. The beta burst results are the same for the pair of each panel. The horizontal dashed line corresponds to the expected chance level. Vertical dotted lines represent the onset and end of the trial period of each dataset. The horizontal line on the top of each subplot shows the results of the pair-wise permutation cluster tests that is, between the beta bursts and the mu band filtering technique, with correction for multiple comparisons at significance level of 0.05. At any time point, each line is color-coded so as to indicate which feature produces, on average, better results. A lack of color at any given time point indicates no statistically significant differences between the compared features.



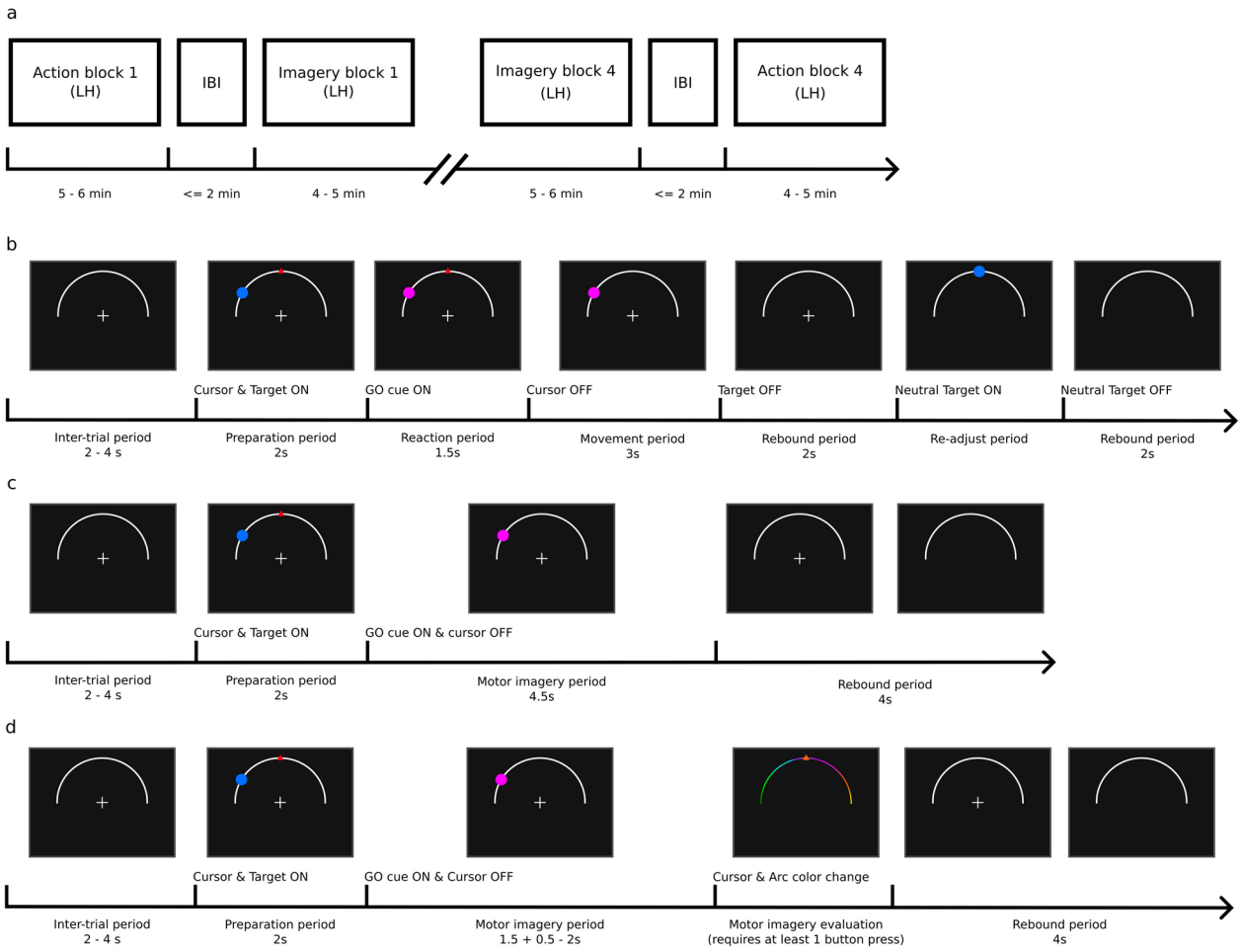
Sup. Figure 3.2.6: (a) Population average, time-resolved information transfer rate (ITR) and standard error for the beta burst convolution (red), beta band (yellow) and mu-beta band (purple) filtering pipelines using a sliding window. Due to the different duration of the task for each dataset we restricted the time to the minimum trial period corresponding to 3 seconds. **(b – h)** Average, time-resolved information transfer rate (ITR) and standard error per dataset of the same features using a sliding window. For each panel, the left subplot depicts the ITR results obtained using a single filter, while the right subplot depicts the results based on a filter bank technique. The beta burst results are the same for the pair of each panel. Vertical dotted lines represent the onset and end of the trial period of each dataset. The two horizontal lines on the top of each subplot show the results of the two pair-wise permutation cluster tests, that is, between the beta bursts and the beta band (bottom line) or mu-beta band (top line) filtering technique respectively, with correction for multiple comparisons at significance level of 0.05. At any time point, each line is color-coded so as to indicate which feature produces, on average, better results. A lack of color at any given time point indicates no statistically significant differences between the compared features.



Sup. Figure 3.2.7: Population-level statistical analysis based on linear mixed models when using a sliding window per feature. **(a)** Average maximum decoding score. **(b)** Average maximum ITR. **(c)** Average latency to reach the maximum decoding score. **(d)** Average latency to reach the maximum ITR. Error bars show 95% confidence intervals. Hatches indicate the use of a filter bank technique. Asterisks indicate statistically significant differences among pairwise comparisons of the beta bursts and the rest of the features (* : $p < 0.05$. ** : $p < 0.01$, *** : $p < 0.001$). A lack of asterisks implies no statistically significant differences. Note that the log transform of the maximum ITR and latency to maximum ITR were used for the statistical analysis (see 3.2.3 Methods), but panels **b** and **d** depict results before applying the transformation for ease of comparisons with panels **a** and **c** respectively.



Sup. Figure 3.3.1: Population average decoding score and transfer learning decoding loss using the trial period of each dataset, assessed with different features. Beta bursts significantly improve decoding score compared to beta band power, but result in statistically significant score loss compared to a filter bank approach that analyzes mu and beta band activity. Transfer of beta burst waveforms significantly minimizes classification score loss in across-session transfer learning approaches compared to transferring CSP filters estimated using processed eeg signals. Similar results are observed when transferring CSP filters estimated using waveform-resolved burst rate compared to filters estimated using eeg signals (* : $p < 0.05$. ** : $p < 0.01$, *** : $p < 0.001$).



Sup. Figure 4.3.1: Design of experimental paradigm. **(a)** Each run consists of multiple, pseudo-randomized blocks of trials. Blocks may correspond to one of two conditions “Action” or “Imagery” during which participants are asked to either perform wrist movements or practice kinesthetic motor imagery of wrist movements. Each block lasts approximately 5 minutes and a short break is administered between consecutive blocks. **(b)** An “Action” trial starts with the appearance of a fixation cross and a white, semicircular path for a variable period of 2 to 4 seconds. Following, the triangular, red cursor and the circular, blue target appear on the screen for a period of 2 seconds, after which the target’s color changes to magenta serving as a cue for the execution of the movement. The red cursor disappears once the participant is moving their wrist. The trial is aborted if the movement does not start within 1.5 seconds following cue onset. After the completion of the movement or alternatively after 4.5 seconds following cue onset the cue disappears and the participant is asked to keep their hand still for 2 seconds. Then, the fixation cross disappears and a target appears on the screen, asking participants to re-position their hand before proceeding to the next trial. Finally, following hand re-positioning the fixation cross stays off for a period of 2 seconds. **(c)** An “Imagery” trial is organized in phases similar to an “Action” trial. Two main differences are that the cursor disappears automatically once the cue is on with no possibility to abort the trial early and that no readjustment of the hand is required at the end of imagery. An “Imagery” will be aborted if the participant moves their hand at any time point. **(d)** A small portion of trials in an “Imagery” block correspond to catch trials. During catch trials the fixation cross disappears and the arc path changes color following a random interval of 2 to 4 seconds following the cue onset. A new cursor appears on screen and the participant is asked to approximately indicate where it would have landed based on a self-evaluation of the motor imagery they have produced in the time they were given. This evaluation is compared to real movements’ metrics and the participant is encouraged to adjust their imagery if the reported movement is too small or too large in

(← continues from previous page) amplitude, or else the fixation cross and the white arc path reappear as in “Imagery trials”. A short period is provided before the next trial starts.

6.3 List of contributions

6.3.1. Peer-reviewed articles

S Papadopoulos, L Darmet, M J Szul, M Congedo, J J Bonaiuto and J Mattout, Surfing beta burst waveforms to improve motor imagery-based BCI Imaging Neuroscience 2024; https://doi.org/10.1162/imag_a_00391.

Papadopoulos S, Szul M J, Congedo M, Bonaiuto J J and Mattout J, Beta bursts question the ruling power for brain-computer interfaces J. Neural Eng., 2024, 21 (1), pp.016010. https://doi.org/10.1088/1741-2552/ad19ea.

M J Szul, **S Papadopoulos**, S Alavizadeh, S Daligaut, D Schwartz, J Mattout, J J Bonaiuto, Diverse beta burst waveform motifs characterize movement-related cortical dynamics Progress in Neurobiology 2023 102490, https://doi.org/10.1016/j.pneurobio.2023.102490.

S Papadopoulos, J Bonaiuto, and J Mattout, An Impending Paradigm Shift in Motor Imagery Based Brain-Computer Interfaces, Front. Neurosci., vol. 15, 2022, https://doi.org/10.3389/fnins.2021.824759.

6.3.2. Peer-reviewed conference articles

S L Cernera, T Gemicioglu, J Berezutskaya, R Csaky, M Verwoert, D Polyakov, **S Papadopoulos**, V Spagnolo, J Gonzalez-Astudillo, S Kuma et al., Master classes of the tenth international brain-computer interface meeting: showcasing the research of BCI trainees, J. Neural Eng., 2025, https://doi.org/10.1088/1741-2552/adb335.

S Papadopoulos, L Darmet, M J Szul, M Congedo, J Bonaiuto, J Mattout, Improved motor imagery decoding with spatiotemporal filtering based on beta burst kernels, Proceedings of the 9th Graz BCI Conference 2024, Graz, Austria, September 09-12, 2024. https://doi.org//10.3217/978-3-99161-014-4-042.

6.3.3. Pre-prints

S Zhang, M J Szul, **S Papadopoulos,** A Massera, H Rayson, J J Bonaiuto, Multi-sclae parameterization of neural rhythmicity with lagged Hilbert autocoherence bioRxiv 2024.12.05.627017, https://doi.org/10.1101/2024.12.05.627017.

6.3.4. Peer-reviewed conference abstracts with oral presentation

S Papadopoulos, L Darmet, M J Szul, M. Congedo, J Bonaiuto, J Mattout, “Fast and reliable hand motor imagery decoding based on beta burst rate modulations”, Corticodays 2024, Nancy, France, May 22-23, 2024.

S Papadopoulos, L Darmet, M J Szul, M Congedo, J Bonaiuto, J Mattout, “Fast and reliable hand motor imagery decoding based on beta burst rate modulations”, Neural Traces 2024, Berlin, Germany, April 10-12, 2024.

S Papadopoulos, M J Szul, M Congedo, J Bonaiuto, J Mattout, “What is the exact relationship between beta band activity and hand motor imagery?”, BCI Meeting 2023, Sonian Forest, Brussels, Belgium, June 06-09, 2023.

S Papadopoulos, M J Szul, M Congedo, J Bonaiuto, J Mattout, “Exploring distinct beta band activity representations during hand motor imagery”, Corticodays 2023, Paris, France, May 09-10, 2023.

S Papadopoulos, M Congedo, J Bonaiuto, J Mattout, “Improving Classification Accuracy of Motor Imagery Tasks with Novel Neurophysiological Markers”, IEEE international conference on metrology for extended reality, artificial intelligence and neural engineering, Rome, Italy, October 26-28, 2022.

S Papadopoulos, M Congedo, J Bonaiuto, J Mattout, “Refining Neurophysiological Markers for Motor Imagery Based Brain Computer Interfaces”, Corticodays 2022, Autrans, France, March 16-18, 2022. sciencesconf.org:corticodays:394569.

6.3.5. Peer-reviewed conference abstracts with poster presentation

M Bergeron, **S Papadopoulos**, J Mattout, J Bonaiuto, “Characterization of mu waveforms during motor imagery”, Corticodays 2025, Lyon, France, May 12-13, 2025.

D Agrawal, **S Papadopoulos**, P Seguin, E Maby, J Bonaiuto, J Mattout, “Using beta bursts to decode covert actions in severely motor impaired patients”, Corticodays 2025, Lyon, France, May 12-13, 2025.

S Papadopoulos, M J Szul, M Congedo, J Bonaiuto, J Mattout, “Exploring distinct beta band activity representations during hand motor imagery for improved brain-computer interfaces”, NeuroFrance 2023, Lyon, France, May 24-26, 2023.